Reductive scavenging of reactive oxygen species in prokaryotes

Rubrerythrin and Superoxide Reductase

Ana Filipa Pinto

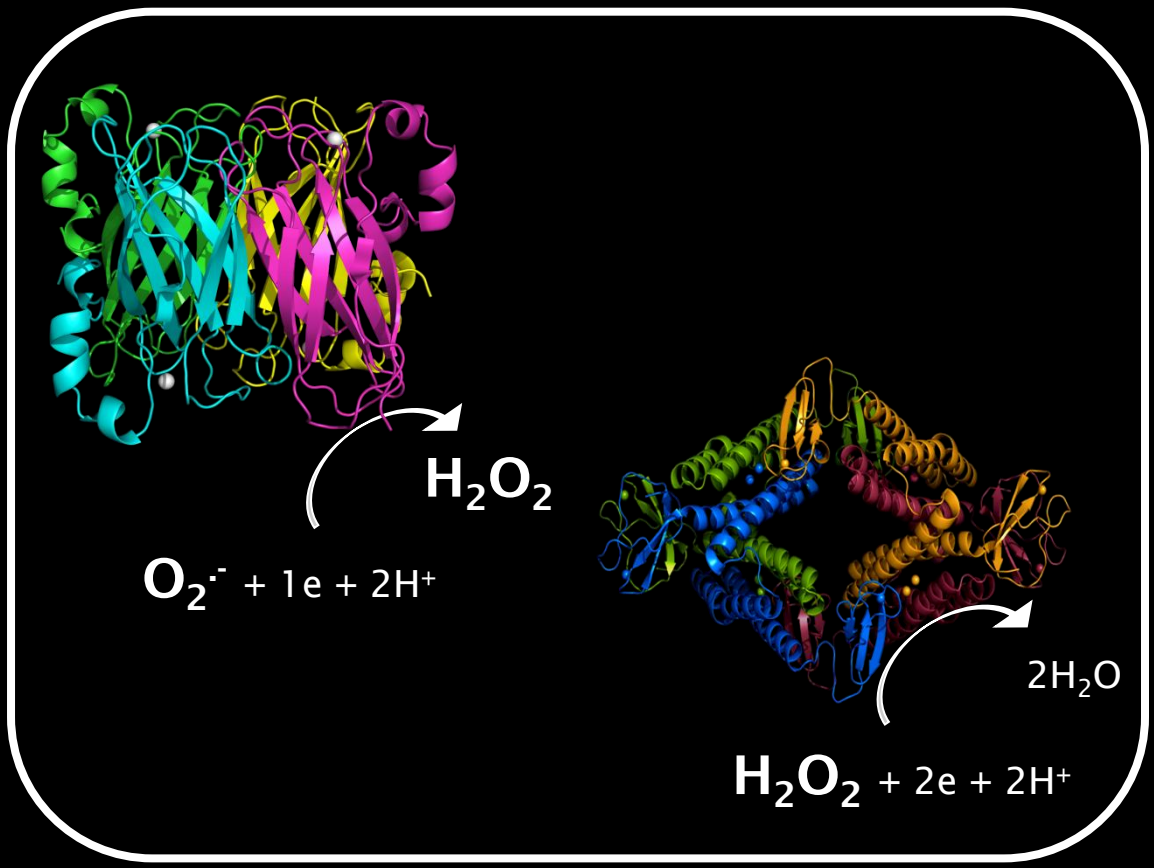

Dissertation presented to obtain the Ph.D degree in Biochemistry

Instituto de Tecnologia Química e Biológica | Universidade Nova de Lisboa

Oeiras,
July, 2012

INSTITUTO
DE TECNOLOGIA
QUÍMICA E BIOLÓGICA
/UNL

Knowledge Creation

ITQB-UNL | Av. da República, 2780-157 Oeiras, Portugal
Tel (+351) 214 469 100 | Fax (+351) 214 411 277

www.itqb.unl.pt

Reductive scavenging of reactive oxygen species in prokaryotes

Rubrerythrin and Superoxide Reductase

Ana Filipa Carapinha Pinto

Supervisors: Prof. Miguel S. Teixeira and Dr. Célia V. Romão

Dissertation presented to obtain the PhD degree in Biochemistry

Instituto de Tecnologia Química e Biológica
Universidade Nova de Lisboa

Oeiras, June 2012

Apoio financeiro da Fundação para a Ciência e Tecnologia e do Programa Operacional Potencial Humano do Fundo Social Europeu POPH/FSE no âmbito do Quadro Comunitário de apoio (Bolsa de Doutoramento SFRH/ BD/ 41355/ 2007)

From left to right: Fernando Antunes, Cláudio Soares, Alessandro Giuffrè, Ana Filipa Pinto, João Vicente, Claudina Roudrigues-Pousada, Célia Romão and Miguel Teixeira

Second Edition, July 2012

Cover: 3D crystal structures of Superoxide reductase from *Ignicoccus hospitalis* (left) and Desulforubrerythrin from *Campylobacter jejuni* (right).

Metalloproteins and Bioenergetics Unit
-Metalloenzymes and Molecular Bioenergetics Laboratory
Instituto de Tecnologia Química e Biológica
Universidade Nova de Lisboa
Av. da República
Estação Agronómica Nacional
2780-157 Oeiras
Portugal
Tel. +351- 214 469 323

Foreword

This dissertation is the result of research work for four years at the Metalloenzymes and Molecular Bioenergetics Laboratory integrated in the Metalloproteins and Bioenergetics Unit at the *Instituto de Tecnologia Química e Biológica* from *Universidade Nova de Lisboa*, under the supervision of Prof. Miguel Teixeira and Célia Romão. The work here described concerns the study of two systems involved in the scavenging of Reactive Oxygen Species widely distributed in Prokaryotes: Rubrerythrins and Superoxide Reductases. A rubrerythrin-like protein from *Campylobacter jejuni*, Desulforubrerythrin, was studied by biochemical, spectroscopic and structural methods and a NADH-linked H_2O_2 reductase activity was measured. Superoxide detoxification in *Ignicoccus hospitalis* was studied by characterizing a non-canonical superoxide reductase by biophysical and structural methods.

This thesis is divided in four parts: Part I, organized in three chapters, comprising a general introduction to oxygen biochemistry (Chapter 1), to the two families of proteins concerning this thesis (Chapter 2) and to the pathogenic and hyperthermophilic organisms encoding for the proteins studied (Chapter 3). Part II concerns the experimental results obtained for desulforubrerythrin, a multidomain protein from *Campylobacter jejuni,* namely the biochemical and spectroscopic characterization of the protein (Chapter 4) and the analysis of its 3D crystal structure obtained by X-ray crystallography in two different redox states (Chapter 5). Part III (Chapters 6 and 7) focus on the study of a superoxide reductase enzyme from *Ignicoccus hospitalis* (wild-type and two site-directed mutants) and on the analysis of the 3D crystal structure obtained by X-ray crystallography.

Finally this dissertation closes with a Part IV, a discussion chapter that integrates the results obtained.

Acknowledgements

I would like to acknowledge the following people for being indispensable for the work presented here:

Prof. Miguel Teixeira - My supervisor, for giving the opportunity to work in his lab and develop the work presented here, for the fruitful discussions and advices, for his knowledge and judgemental critics in every subject that definitely made my critical “eye” grow.

Dra. Célia Romão - My co-supervisor who has been there in the more “poltergeisty” moments and helped me go through. For all the discussions and advices and for always pushing me forward.

Dra. Diane Cabelli - For receiving me at the Brookhaven National Laboratory, for her essential collaboration on the pulse radiolysis studies on superoxide reductases, for the discussions and advices.

Dra. Lígia Saraiva - For supervising and supporting all the molecular biology work on superoxide reductases, performed in her lab and for the helpful advices.

Dr. Smilja Todorovic - For her resonance Raman studies on rubrerythrins and superoxide reductases and for many helpful discussions and advices throughout the work presented here.

Prof. Peter Hilderbrandt - For his discussions and advices throughout the four years of research work presented here.

Dr. João Rodrigues - For passing me on his heritage of the superoxide reductases, his knowledge and helpful advices.

Dr. João Vicente - For being my “tutor” in the early stages of my research work in the lab still as a university student. For his patience, knowledge and valuable advices.

Dr. Pedro Matias - For his strong collaboration in the X-ray structures determination of all the proteins involved in this thesis and also for the fruitful discussions as part of my thesis commission.

Dr. Tiago Bandeiras - For the work on the superoxide reductases crystallization and 3D structure determination.

Prof. Fernando Antunes - For allowing me visit his lab (FCUL) in order to perform some assays on rubrerythrins activity and for helpful discussions as part of my thesis commission.

Prof. Harald Huber - For providing us with genomic DNA of *Nanoarchaeum equitans* and *Ignicoccus hospitalis.*

Metalloproteins and Bioenergetics Unit - For all the fun, knowledge, friendship, work discussions, gossip, not exactly in this order: the Metalloenzymes and Molecular Bioenergetics Laboratory Célia Romão, Sandra Santos, Liliana Pinto, Vera Gonçalves, Miguel Ribeiro, Cecília Miranda, Joana Carrilho and the Biological Energy Transduction Laboratory Manuela Pereira, Ana Paula Batista, Patrícia Refojo, Lara Paulo, Bruno Marreiros and Afonso Duarte. The previous members of this unit Andreia Veríssimo, Filipa Sousa, João Rodrigues, João Vicente and Fabrizio Testa.

Molecular Genetics of Microbial Resistance Laboratory - For the availability and help on the molecular biology work on superoxide reductases and for the good environment in the lab.

Family and Friends

A special acknowledgement to my friends and family for all the support.

FCT

Fundação para a Ciência e Tecnologia is acknowledged for financial support to: PDTC/BiaPro/67263/2006 (MT), PDTC/BiaPro/67240/2006 (CVR) and PEst-OE/EQB/LA0004/2011; and for the PhD grant SFRH/BD/41355/2007.

Thesis publications

In this thesis a list of original publications is included:

- "Desulforubrerythrin from *Campylobacter jejuni*, a novel multidomain protein", **Pinto AF**, Todorovic S, Hildebrandt P, Yamazaki M, Amano F, Igimi S, Romão CV, Teixeira M. 2011 J Biol Inorg Chem.;16(3):501-10
- "Thermofluor-based optimization strategy for the stabilization and crystallization of *Campylobacter jejuni* Desulforubrerythrin" Santos SP, Bandeiras TM, **Pinto AF**, Teixeira M, Romão CV. 2012 Protein Expr Purif.;81(2):193-200
- "Reductive elimination of superoxide: Structure and mechanism of superoxide reductases", **Pinto AF**, Rodrigues JV, Teixeira M, 2010 Biochim Biophys Acta.; 1804(2):285-97
- "Cloning, purification, crystallization and X-ray crystallographic analysis of *Ignicoccus hospitalis* neelaredoxin", Pinho FG, Romão CV, **Pinto AF**, Saraiva LM, Huber H, Matias PM, Teixeira M, Bandeiras TM. 2010 Acta Crystallogr Sect F Struct Biol Cryst Commun.;66 (Pt 5):605-7
- "Superoxide reductase from *Nanoarchaeum equitans*: expression, purification, crystallization and preliminary X-ray crystallographic analysis", Pinho FG, **Pinto AF**, Pinto LC, Huber H, Romão CV, Teixeira M, Matias PM, Bandeiras TM. 2011 Acta Crystallogr Sect F Struct Biol Cryst Commun.;67(Pt 5):591-5

Three manuscripts are in preparation, based on studies presented in Chapters 5, 6 and 7:

- "Three dimensional structure of the multidomain desulforubrerythrin from *Campylobacter jejuni*", **Pinto AF**, Matias P, Carrondo MA, Teixeira M., Romão CV, manuscript under preparation

- “Superoxide reduction in the crenarchaeon *Ignicoccus hospitalis*” **Pinto AF**, Romão CV, Pinto LC, Huber H, Saraiva LM, Cabelli D, Teixeira M, manuscript under preparation
- “Insights on the superoxide reductase structures from the two symbiotic organism: *Ignicoccus hospitalis* and *Nanoarchaeum equitans* reveal differences on the catalytic site”, Romão CV, **Pinto AF**, Pinho FG, Barradas AR, Matias PM, Teixeira M, Bandeiras T, manuscript under preparation.

Summary

The purpose of this thesis is to contribute to a better understanding of systems involved in the scavenging of reactive oxygen species. The work focuses on an enzyme from the Rubrerythrin family that reduces hydrogen peroxide and one from the Superoxide Reductase family that reduces the superoxide anion. Both of these families are distributed widely across the three domains of life, Archaea, Bacteria and Eukarya, but are mainly found in anaerobic and microaerophilic prokaryotes.

The target enzymes were a new multidomain rubrerythrin-like protein from the pathogenic bacterium *Campylobacter jejuni*, and a superoxide reductase from the hyperthermophilic archaeon *Ignicoccus hospitalis*. The objectives were to further understand these enzymes by establishing the nature and properties of their metal/catalytic centers and elucidate the reduction mechanisms of these two proteins at the molecular level, by biophysical methods and through the determination of their 3D structures by X-ray crystallography.

In the genome of *Campylobacter jejuni* NCTC 11168 the gene *cj0012c* encodes a rubrerythrin-like protein. Using homology analysis, this protein has been proposed by Yamasaki and co-workers (Yamasaki, M., *et al.*, FEMS Microbiol Lett, 2004. 235(1): p. 57-63) to have domains homologous to rubredoxin oxidoreductase and to rubrerythrin. The amino acid sequence revealed three iron binding domains: an N-terminal desulforedoxin-like domain, followed by a four-helix-bundle domain harbouring a non-sulfur diiron center, and a rubredoxin-like domain at the C-terminus.

In this work, the protein was overexpressed in *Escherichia coli*, purified, and biochemically and structurally characterized. In solution the protein is a homotetramer of 24 kDa monomers. Each of the iron binding sites was identified and its electronic and redox properties determined by a combination of UV-visible, electron paramagnetic resonance and resonance Raman spectroscopies.

The protein was shown to indeed contain two $FeCys_4$ centers with reduction potentials of +240 mV (desulforedoxin-like center) and +185 mV (rubredoxin-like center). These centers are in the high-spin configuration in the as-isolated ferric form and are the main spectral contributors to its UV-visible spectrum. The protein further accommodates a diiron site with reduction potentials of +270 and +235 mV for the two sequential redox transitions Fe(III)-Fe(III)→(FeIII)-Fe(II) and Fe(III)-Fe(II)→Fe(II)-Fe(II). Resonance Raman spectroscopy combined with isotope labelling (D_2O and H_2O^{18}) shows that the diiron in the diferric state is probably bridged by a μ-oxo species. The protein is rapidly reoxidized by hydrogen peroxide but only slowly by oxygen. It has a significant NADH-linked hydrogen peroxide reductase activity of 3.9 ± 0.5 μmol H_2O_2 $min^{-1}mg^{-1}$, determined using two non-physiological electron transfer proteins from *Escherichia coli* (a NADH oxidoreductase and a rubredoxin). The reduction of hydrogen peroxide has been the most reproducible activity observed *in vitro* for the rubrerythrin family.

With its unique set of component domains, the protein is a novel example within the overall large diversity of domain organizations exhibited by this enzyme family. Given its component domains and homology to the rubrerythrin family, the protein was named by us as desulforubrerythrin (DRbr). To understand this unique domain architecture, the determination of its 3D structure by X-ray crystallography was carried out.

A thermofluor study was used to screen buffer components, pH and salt concentration and to select a buffer condition that allowed successful crystallization of the *Campylobacter jejuni* desulforubrerythrin protein. Desulforubrerythrin was seen to be stabilized by lower pH and high salt concentration, and was dialyzed against the selected buffer (100 mM MES pH 6.2 and 500 mM NaCl). Good quality crystals were obtained, which allowed the X-ray crystal structure of DRbr to be determined to 2.0 Å resolution. This is the first crystal structure of a rubrerythrin-like protein with this arrangement of domains. The protein crystallizes as a

tetramer, having an intricate domain-swapped configuration. The 3D structure was obtained in two different redox states. The arrangement of the rubredoxin and the diiron sites is such that electron transfer occurs from an external donor to the rubredoxin site, which then transfers the electron to the diiron center at *c.a.* 13 Å. In contrast, the desulforedoxin-like centers are located far away from the other metal sites *(c.a.* 34 Å between the Dx iron center and the diiron centers) and, despite the structure being now available, their function remains unclear. The 3D structure showed a diiron center in two different redox states with a redox-linked ligand and iron movement, a characteristic feature of the diiron site in rubrerythrins.

Superoxide reductases (SOR) reduce superoxide to hydrogen peroxide. In many organisms, this system appears to be the only route for superoxide detoxification, as their genomes do not encode for other superoxide scavenging enzymes, the SODs.

The catalytic site is known to be composed of an iron bound to four histidines and a cysteine in a square pyramidal geometry. In the oxidized state a sixth ligand, a glutamate residue, is present in most SORs. However, several issues still remained to be explained, namely the number of catalytic intermediates of the reaction cycle and the role of specific amino acid residues close to the catalytic site.

A superoxide reductase from *Ignicoccus hospitalis* has been shown to lack the positively charged lysine residue (Lys 24, in *Archaeoglobus fulgidus*), conserved in the majority of SORs; this natural variation is also observed in other SORs from several *Crenarchaeota*. This residue is thought to have a relevant role for attracting the superoxide anion into the active site and stabilizing the first catalytic intermediate.

In this work, the wild-type (wt) protein and two site-directed mutants were expressed, purified and studied: mutant E23A where the glutamate residue that acts as a sixth ligand to the iron centre in the ferric-SOR was changed to alanine, and T24K where the lysine residue was reintroduced in the same position as found for other SORs. The

ferric-SORs were found to share the same spectral characteristics as found for other SORs. A pH induced wavelength shift at the visible band was also associated with the change of the Glu/H_2O-SOR form to a hydroxide bound species, with an associated pK_a of 10.5 for the wild-type protein, and 10.7 and 6.5 for the T24K and E23A mutants, respectively. The reduction potentials were determined to be E'_0 (wt) = +235, E'_0 (E23A) = +283, E'_0 (T24K) = +195 mV *vs.* SHE at pH 7. The reduction potential was found to be pH independent for both the wt protein and the T24K mutant from pH 5 to 8.5. The E23A mutant is pH dependent in the pH range of 5 to 7.5 with an associated pK_a of 6.3.

The reaction mechanism was studied by pulse radiolysis where the enzyme is exposed to known amounts of the superoxide anion and the electronic changes of the active site followed by visible absorption spectroscopy on a fast (microsecond to millisecond) timescale. The results show that the first intermediate detected is similar to those of the canonical enzymes and that the rate of its formation, 0.7×10^9 $M^{-1}s^{-1}$ for the wt protein, is also within the range for the other enzymes; *i.e.,* the lysine residue seems to be not essential for the mechanism of superoxide reduction. Similar studies on the two mutants revealed no significant differences on the rates for the formation of the first intermediate.

In the case of *Ignicoccus hospitalis* SOR, the data only reveals the formation of a single intermediate. In comparison with the results obtained for other SORs it was possible to establish that there are two types of apparent mechanisms, with one or two intermediates, independent of both the type of SOR, with one iron or two iron atoms, and its thermophilicity.

The 3D X-ray crystal structure of the wt *Ignicoccus hospitalis* SOR (determined at 1.85 Å resolution) reveals that the homotetramer protein has positively charged residues, such as arginine and lysine residues positioned around the active site. These appear to be sufficient to attract and guide the superoxide anion into the active site. For the E23A

mutant the 3D structure revealed that in the absence of the glutamate and thus resembling a catalytic ferric intermediate, a lysine (Lys 21) side chain is directed towards the iron site. The role of this type of residue of attracting the substrate into the active site and stabilizing an intermediate species is then maintained in this SOR. A comparison of the 3D structures obtained in this work and from the databank suggests that indeed in all SORs a lysine close to the active iron center plays a role in the enzyme mechanism, most probably through stabilizing the hydroperoxide intermediate.

Sumário

O objectivo desta tese de doutoramento é contribuir para uma melhor percepção dos sistemas envolvidos na desintoxicação das espécies reactivas de oxigénio. O trabalho desenvolvido centraliza-se no estudo de uma enzima pertencente à família das Rubreritrinas que reduz o peróxido de hidrogénio e no estudo de uma enzima que reduz o anião superóxido da família das Superóxido Reductases. Ambas as famílias estão extensamente distribuídas nos três domínios da vida: Archaea, Bacteria e Eucaria; contudo estas proteínas são mais abundantes em procariotas anaeróbios e microaerofilicos.

As enzimas estudadas são: desulforubreritrina (DRbr), uma proteína com multi-domínios tipo-rubreritrina da bactéria patogénica *Campylobacter jejuni*, e uma superóxido reductase (SOR) do archaeon hipertermófilo *Ignicoccus hospitalis*. O objectivo deste estudo é promover uma melhor compreensão destas enzimas, estabelecendo a natureza e propriedades dos seus centros metálicos/catalíticos, elucidando ao nível molecular os mecanismos de redução e a determinação da estrutura cristalina 3D por cristalografia de raios-X.

No genoma de *Campylobacter jejuni* NCTC 11168 o gene *cj0012c* codifica para uma proteína tipo-rubreritrina. Pela análise de homólogos desta proteína, foi proposto por Yamasaki e coautores (Yamasaki, M., *et al.*, FEMS Microbiol Lett, 2004. 235 (1): 57-63) como tendo domínios homólogos a uma rubredoxina oxidoreductase e a uma rubreritrina. A sequência de aminoácidos revelou a presença de três domínios com centros de ferro: um domínio N-terminal do tipo-desulforedoxina (Dx), seguido de um domínio de quatro-hélices contendo um centro binuclear de ferro não-sulfuroso, e no C-terminal um domínio tipo-rubredoxina (Rd). Nesta tese a proteína foi sobre expressa em *Escherichia coli*, purificada e caracterizada bioquímica e estruturalmente. Em solução a proteína é um homotetrâmero de monómeros de 24 kDa. Cada centro de ferro foi identificado e as suas propriedades redox e electrónicas

foram determinadas por uma combinação de espectroscopias de UV-visível, Ressonância Paramagnética Electrónica e Ressonância de Raman.

Foram determinados experimentalmente os potenciais de redução para os dois centros de $FeCys_4$, +240 mV (centro do tipo-desulforedoxina) e +185 mV (centro do tipo-rubredoxina). Estes centros de ferro estão numa configuração de alto-spin na forma férrica e são os que mais contribuem espectralmente na região do UV-Visível. Para além destes dois centros, a proteína acomoda também um centro binuclear de ferro com potenciais de redução de +270 e +235 mV para as duas transições redox sequenciais Fe(III)-Fe(III) → Fe(III)-Fe(II) e Fe(III)-Fe(II) → Fe(II)-Fe(II). A espectroscopia de Ressonância de Raman acoplada à marcação isotópica (D_2O e H_2O^{18}) revelou que os átomos de ferro do centro binuclear no estado diférrico estão provavelmente ligados em ponte por uma espécie μ-oxo. A proteína é rapidamente reoxidada por peróxido de hidrogénio mas lentamente por oxigénio. A redução do peróxido de hidrogénio é a actividade enzimática *in vitro* mais reprodutível registada para a família das rubreritrinas. Tem uma actividade significativa de reductase de peróxido de hidrogénio associada à oxidação de NADH de 3.9 ± 0.5 μmol H_2O_2 min^{-1} mg^{-1}, determinada pelo uso de duas proteínas de *Escherichia coli* que transferem electrões do NADH para uma rubredoxina e desta para a DRbr. Devido à composição única de domínios, esta proteína é um novo exemplo dentro da enorme diversidade relativa à organização de domínios exibida por esta família de enzimas. A homologia com a família das rubreritrinas e a presença de um domínio na região do N-terminal esta proteína foi designada por nós de desulforubreritrina (DRbr). De modo a perceber esta arquitectura até agora única, foi determinada a estrutura cristalina 3D por cristalografia de raios-X.

O estudo pela técnica de termofluor contemplou o varrimento de várias condições de estabilização da proteína, incluindo componentes da solução tampão, pH e concentração de sal, tendo sido possível

selecionar a condição da solução tampão que permitiu com sucesso a cristalização da desulforubreritrina de *Campylobacter jejuni*. Verificou-se que esta proteína era estável a pH 6.2 e em concentrações de sal elevado, e por isso foi dialisada para a solução tampão selecionada (100 mM MES pH 6.2 e 500 mM NaCl). Cristais de elevada qualidade foram obtidos, permitindo a determinação da estrutura cristalina por difracção de raios-X da DRbr com uma resolução de 2.0 Å. Esta é a primeira estrutura cristalina de uma proteína do tipo rubreritrina, com esta arquitectura de domínios. A proteína cristalizou na forma tetramérica e tem uma configuração de domínios trocados. A estrutura cristalina 3D foi obtida em dois estados de redução diferentes. O arranjo estrutural do centro de ferro do domínio rubredoxina e do centro binuclear de ferro é tal que a transferência electrónica ocorre de um dador de electrões externo para o centro de ferro da rubredoxina, que por sua vez transfere os electrões para o centro binuclear que se encontra a uma distância de 13 Å aproximadamente. Em contraste, os centros de ferro dos domínios Dx estão muito distantes dos outros centros metálicos (34 Å, aproximadamente, entre o centro de ferro da Dx e o centro binuclear) e apesar de estruturalmente caracterizados, a sua função ainda não é conhecida. As estruturas 3D em diferentes estados de redução demonstram ainda que há um movimento de um átomo de ferro e de um ligando do mesmo no centro binuclear que é dependente do estado de redução, e é característico do centro binuclear em rubreritrinas.

As SOR reduzem superóxido a peróxido de hidrogénio. Em muitos organismos, este sistema aparece como o único mecanismo directo para a desintoxicação do superóxido, uma vez que os seus genomas não codificam para outras enzimas que eliminam o superóxido, como as superóxido dismutases (SOD).

O centro catalítico das SOR é composto por um ferro ligado a quatro resíduos de histidinas e um resíduo de cisteína numa geometria pirâmide quadrangular. No estado oxidado um sexto ligando do centro

de ferro, um resíduo de glutamato, está presente na maioria das SORs. Existem no entanto, várias questões a estudar, nomeadamente o número de intermediários catalíticos do ciclo da reacção e o papel de determinados resíduos de aminoácidos perto do centro catalítico.

Para a superóxido reductase de *Ignicoccus hospitalis* verificou-se a ausência de um resíduo carregado positivamente, a lisina 24 (numeração da SOR de *Archaeoglobus fulgidus*), conservado na maioria das SORs; esta variação natural é também observada em outras SORs de vários organismos *Crenarchaeota*. Este resíduo é sugerido como tendo um papel relevante para atracção do anião superóxido para o centro activo e de estabilizar o primeiro intermediário catalítico.

Neste trabalho, a proteína nativa e dois mutantes dirigidos foram expressos, purificados e caracterizados: o mutante E23A, onde o resíduo glutamato que actua como sexto ligando do centro de ferro na forma férrica da SOR foi mutado para uma alanina, e o mutante T24K, onde o resíduo de lisina foi reintroduzido na mesma posição em que é encontrado noutras SORs. As formas férrica das SORs de *Ignicoccus hospitalis* partilham as mesmas características espectrais encontradas em outras SORs. A variação do espectro eletrónico induzido pela variação do pH foi também observada, resultando na transformação da forma Glu/(H_2O)-SOR para a forma da SOR ligada ao grupo hidróxido, com um pK_a associado de 10.5 para a proteína nativa, e 10.7 e 6.5 para os mutantes T24K e E23A, respectivamente. Os potenciais de redução foram também determinados: E'_0 (nativa) = +235, E'_0 (E23A) = +283, E'_0 (T24K) = +195 mV *vs.* SHE a pH 7. O potencial de redução revelou-se independente dos valores de pH para a proteína nativa e o mutante T24K no intervalo de valores de pH de 5 a 8.5. O mutante E23A é dependente do pH no intervalo de valores de pH 5 a 7.5, com um pK_a associado de 6.3.

O mecanismo de reacção foi estudado por radiólise de pulso onde a enzima é exposta a quantidades conhecidas de anião superóxido e as

alterações electrónicas do centro activo são seguidas por espectroscopia de absorção na região do visível numa rápida escala de tempo (microssegundos a milissegundos). Os resultados obtidos demonstraram que o primeiro intermediário detectado é semelhante ao obtido para enzimas canónicas, e a constante de velocidade da sua formação, 0.7×10^9 $M^{-1}s^{-1}$ para a proteína nativa, está também dentro dos valores encontrados para outras enzimas; conclui-se assim que o resíduo de lisina ausente (lisina 24) parece não ser essencial no mecanismo de redução do superóxido. Estudos semelhantes para os dois mutantes não revelaram diferenças significativas, relativas à constante de velocidade de formação do primeiro intermediário.

Para a SOR de *Ignicoccus hospitalis*, os dados revelaram apenas a formação de uma espécie intermediária. Em comparação com os resultados obtidos para outras SORs foi possível estabelecer a existência de dois tipos de mecanismo aparente, com um ou dois intermediários, independentemente do tipo de SOR (com um ou dois ferros) e da termofilicidade do organismo.

A estrutura 3D obtida por cristalografia de raios-X, da SOR nativa de *Ignicoccus hospitalis* revelou que a proteína homotetramerica tem resíduos carregados positivamente, como por exemplo resíduos de arginina e lisina, localizados perto do centro activo. Esta análise sugere que estes resíduos poderão estar envolvidos na atracção do anião superóxido para o centro activo. Para o mutante E23A a estrutura 3D revelou que a ausência do resíduo de glutamato, e por isso semelhante a um intermediário catalítico na forma férrica, a cadeia lateral de uma lisina (lisina 21) está direccionada para o centro de ferro. O papel deste tipo de resíduo em atrair o substrato para o centro activo e de estabilizar uma espécie intermediária, é mantido nesta SOR.

A comparação das várias estruturas 3D obtidas neste estudo e com outras disponíveis nas bases de dados sugerem que de facto em todas as SORs um resíduo de lisina algures ao redor do centro activo tem um

papel no mecanismo enzimático, mais provavelmente ao estabilizar um intermediário hidroperóxido.

Abbreviations

Å	Angstrom (10^{-10} meters)
BCA	Bicinchoninic acid
Bfr	Bacterioferritin (hemoferritin)
bp	base pairs
Da	Dalton
Dfx	Desulfoferrodoxin
DNA	Deoxyribonucleic acid
Dps	DNA protecting protein under starved conditions
Dx	Desulforedoxin
e	electron
EDTA	Ethylenediaminetetraacetic acid
E'_0	Conditional Reduction potential
ε	Molar absortivity
EPR	Electron Paramagnetic Resonance
FMN	Flavin monucleotide
FTIR	Fourier transform infrared spectroscopy
Fur	Ferric uptake regulator
g	EPR g-factor
H^+	proton
HTH	Helix-turn-Helix
IPTG	Isopropylthiogalactoside
LB	Luria Bertani
M	Molar
MES	2-(N-morpholino) ethanesulphonic acid
Mm	Molecular mass
MW	Molecular weight
NAD^+	Nicotinamide adenine dinucleotide
NADH	Reduced nicotinamide adenine dinucleotide
$NADP^+$	Nicotinamide adenine dinucleotide phosphate
NADPH	Reduced nicotinamide adenine dinucleotide phosphate
OD	optical density
PAGE	polyacrylamide gel electrophoresis
PCR	Polymerase Chain Reaction

PDB	Protein Data Bank
PMSF	phenylmethylsulfonyl fluoride
Rbr	Rubrerythrin
Rd	Rubredoxin
ROS	Reactive Oxygen Species
RR	Resonance Raman
S	Spin quantum number
SDS	sodium dodecyl sulfate
SHE	Standard hydrogen electrode
SOD	Superoxide dismutase
SOR	Superoxide reductase
TPTZ	2,4,6-tripyridyl-triazine
Tris	Tris (hydroxymethyl)-aminomethane
UV	Ultraviolet
Vis	Visible
wt	wild-type

Latin abbreviations

i.e.	id est, that is to say
e.g.	exempli gratia, for example
et al.	et alia, and other people
c.a.	circa, approximately

Aminoacid abbreviations

A	Ala	Alanine
C	Cys	Cysteine
D	Asp	Aspartate
E	Glu	Glutamate
F	Phe	Phenylalanine
G	Gly	Glycine
H	His	Histidine
I	Ile	Isoleucine
K	Lys	Lysine

L	Leu	Leucine
M	Met	Methionine
N	Asn	Asparagine
P	Pro	Proline
Q	Gln	Glutamine
R	Arg	Arginine
S	Ser	Serine
T	Thr	Threonine
V	Val	Valine
W	Trp	Tryptophan
Y	Tyr	Tyrosine

Table of Contents

Part I – General Introduction

Chapter 1

1 – Oxygen

Molecular oxygen or dioxygen (O_2) discovery has been considered the most important event in the history of chemistry, but at the same time it has been controversial. Three scientists in the 18th century made important contributions to the field and to the discovery of oxygen (*1*). The first report of discovery and isolation of O_2 belongs to Joseph Priestley in 1774 (Figure 1.1) when, by heating the red mineral mercuric oxide in a sealed glass chamber, a new gas was liberated and a candle burned furiously. Priestley also showed that this released element was responsible for a mouse to live longer and that this element was regenerated by a sprig of mint left in the same chamber where the mouse had died, in a process later called oxygenic photosynthesis (*1*). Due to the existing phlogiston theory (*2*), Priestley named this element as "dephlogisticated air" and described his methods and discoveries to a group of scientists in Paris, where a famous French Chemist was present, Antoine Lavoisier (Figure 1.1).

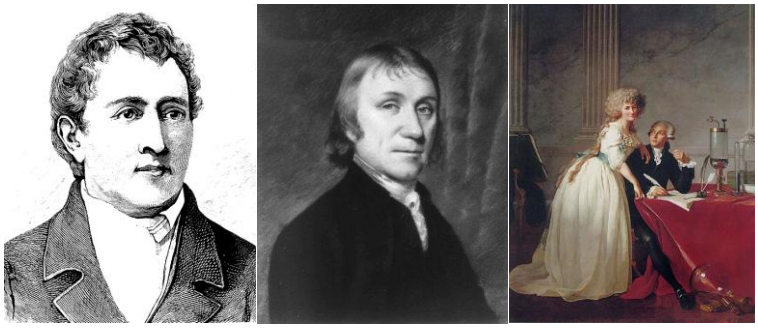

Figure 1.1 – The three discoverers of oxygen. From left to right: Carl Wilhem Scheel (1742-1789) from *The Popular science monthly in 1887*, Joseph Priestley (1733-1804), portrait of Joseph Priestley by Ellen Sharples, and Antoine Lavoisier (1743-1794), portrait of Monsieur de Lavoisier and his Wife, chemist Marie-Anne Pierrette Paulze by Jacques-Louis David.

Lavoisier at the time of Priestley visit had been also involved in experiments with the red mercuric oxide and realized that upon heating, the metallic liquid was restored, with the release of a gas, which he assumed to be carbon monoxide (*1*). Knowing the experiments of Priestley allowed Lavoisier to discover that this gas was present in the atmospheric air. After nine months of Priestley publication Lavoisier published also his discovery, without any credit to Priestley work. In 1777 he named it oxygen, as part of all acids (oxy in Greek means acid and "gene" former). Lavoisier further established oxygen as an oxidant, in the combustion process and that it is essential for biological respiration (*3*). In spite of Priestley and Lavoisier contributions and discoveries, Carl Scheele, a Swedish chemist, should be the one to be given the first credits on O_2 discovery (*4*) (Figure 1.1). Probably in 1771, Scheele made its first attempt by discovering a "fire air", which supported combustion but he failed to publish his findings, probably by not understanding its breakthrough (*1*). Scheele was also exchanging correspondence with Lavoisier and by Spring of 1774, described him ways of preparing the "fire air". Later on, Lavoisier denied knowing this letter sent by Scheele. Only by 1777 he was able to publish his findings but at that time Priestley and Lavoisier had already published their discoveries, that led to new interpretations of chemical theory (*1*).

In the end of 18^{th} century it was established that oxygen comprises 21% of Earth's atmosphere and is fundamental for aerobic life and toxic in high concentrations, and also the essential oxidant for the combustion of organic molecules.

Regarding the deleterious effects of oxygen and its derivatives, the reactive oxygen species (ROS), they were not understood until 1954, when Gerschman *et al.* (*5*) discovered that oxygen poisoning and X-ray irradiation generated oxygen-derived free radicals.

The significant oxygen presence in Earth´s atmosphere dated from *c.a.* 1×10^9 years ago (*3*), but in the beginning of life on Earth, there was a reducing atmosphere and ferrous iron was present in abundance (*6*).

Oxygen started to be introduced as a product of photosynthetic oxidation of water by prokaryotes (cyanobacteria). The transformation of Earth's atmosphere to an oxidizing environment took about 750 million years, and during that adaption period, transition metals that were present in the anaerobic systems in the reduced forms were oxidized and precipitated as metal oxides, *e.g.*, $Fe^{2+} \rightarrow Fe_2O_3$, Fe_3O_4 and $Mn^{2+} \rightarrow MnO_2$ (*7*). With an increasing oxidizing atmosphere revolutionary consequences for the anaerobic life occurred and some species adapted and evolved to oxygen-utilizing aerobic life forms, while others were retreated to oxygen-free environments (*8*).

The decreased bioavailability of iron by its oxidation was concomitant with the oxidation of copper (I) to soluble copper (II) (*6*) ideally used as a metal redox active center in enzymes with higher reduction potentials (0 to 0.8 V *vs.* SHE) in comparison with the generally lower reduction potentials of iron–containing enzymes in anaerobic organisms (*9*). The high concentrations of atmospheric oxygen also turned possible the formation of ozone (O_3) by solar radiation, generating a protective shield against UV light, which allowed the establishment of terrestrial life (*3*).

The duality of oxygen concerns in one hand its fundamental role in bioenergetics, as it allows extracting maximal energy from the reduced organic compounds associated with its reduction to water and, on the other hand, the reduction of oxygen, in a stepwise non-controlled way that leads to the formation of ROS, such as the superoxide anion or hydrogen peroxide.

1. 1 - Oxygen Chemistry

The oxygen molecule (O_2) has a great oxidizing power, and its four-electron reduction to water has a reduction potential of +0.815 V (*vs.* SHE, pH 7, 25ºC) (*10*). O_2 is very stable and kinetically inert, due to its electronic configuration. It has a triplet ground state, whose antibonding molecular orbitals ($\pi^*_{y,z}$) have two unpaired electrons (total spin S =1), giving the molecule its paramagnetism (*3*) (Figure 1.2).

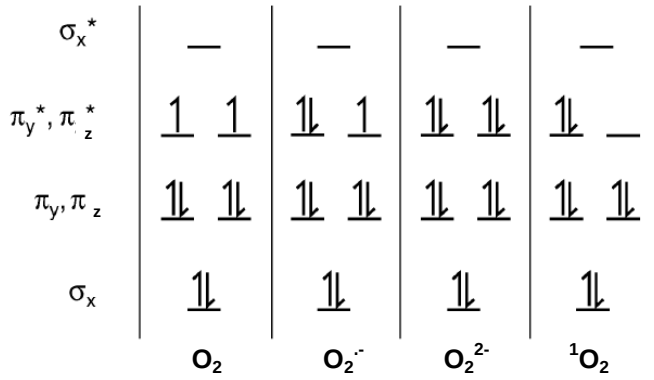

Figure 1.2 – Simplified molecular orbital diagrams of molecular oxygen (O_2), superoxide ($O_2^{\cdot-}$), peroxide (O_2^{2-}) and singlet oxygen ($^1O_2$). Adapted from (*11*).

Due to the conservation of spin rule, the O_2 molecule reacts only in a process in which the total spin of the system does not change. This important restriction on oxidation by O_2, is only overcome by spin inversion, or when the reductant is also a paramagnetic species, *e.g.*, a transition metal ion or a radical species (Figure 1.3) (*3*).

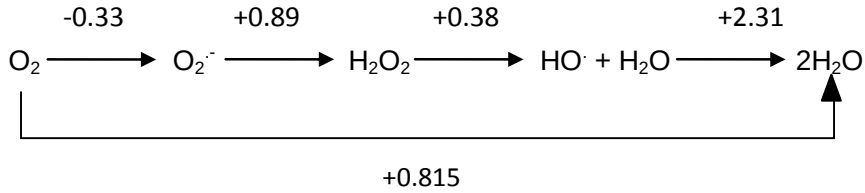

Figure 1.3 – Oxygen one-electron reduction steps and respective reduction potentials, adapted from (*3*). The reduction potentials are in Volts at pH 7 and 25ºC, *vs* SHE.

1.1.1 - Oxygen Reduction

The reduction of O_2 can occur upon one electron reaction with a paramagnetic species, radical species or by previous formation of singlet oxygen (Scheme 1.1).

Scheme 1.1 – Dioxygen reduction

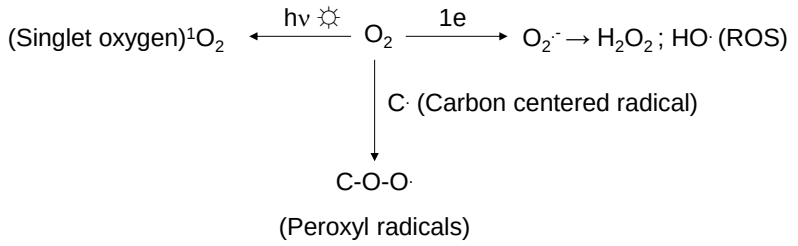

a) One electron reaction

The one electron reduction of molecular oxygen, which has a low reduction potential (E'_0 = -0.33 V) generates the superoxide radical, and may occur only in the presence of reactants with a lower reduction potential (Figure 1.3), and with a spin state that may allow to overcome the kinetic barrier imposed by the spin restriction (*12*).

b) Quenching of carbon-centered radicals by O_2

Molecular oxygen can react with carbon radicals (*e.g.,* benzyl and alkyl groups) to generate peroxyl radicals that will then initiate a radical chain reaction, where secondary peroxyl radicals will be produced (*3*).

c) Formation of singlet molecular oxygen, $^1O_2$

The singlet molecular oxygen is a very reactive species since the spin restriction is overcome (Figure 1.2). This singlet state can be generated by excitation of the ground triplet state upon photosensitization reactions (*12*).

1.1.2 - Reactive Oxygen Species

1.1.2.1 - Superoxide

The superoxide anion ($O_{2^{\cdot-}}$) has a pK_a of 4.8 and at low pH values forms $HOO^{\cdot}$, the perhydroxyl species.

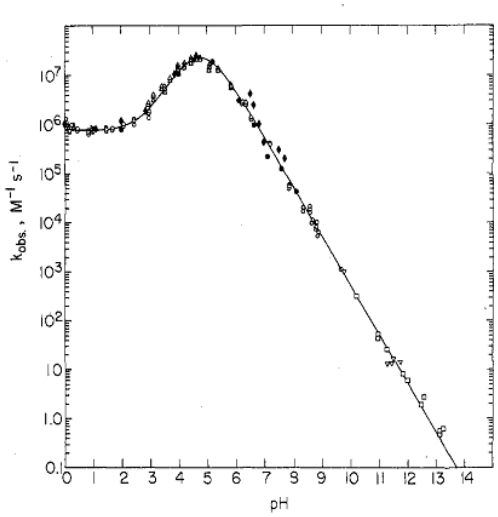

Figure 1.4 – Second-order rate constant for the decay of superoxide *vs.* pH. Observed rates obtained from stopped-flow (o), pulse radiolysis (Δ), continuous flow (V) and γ rays (□) analysis. From (*12*) .

The kinetics of protonation and deprotonation in water for superoxide was studied by pulse radiolysis (*10*) (Figure 1.4). Its disproportionation is a second-order and pH dependent spontaneous process (eq 1.1-1.2), (Figure 1.4) and has a maximum rate (k ~10^7 $M^{-1}s^{-1}$) at a pH that corresponds to the pK_a for $HOO^{\cdot}/O_2^{\cdot -}$. The kinetics of disproportionation of $HOO^{\cdot}$ are described by the following equations (*10*):

$HOO^{\cdot} + O_2^{\cdot -} \rightarrow HOO^{-} + O_2$, $k = 1.0 \times 10^8$ M^{-1} s^{-1} (eq 1.1)

$HOO^{\cdot} + HOO^{\cdot} \rightarrow H_2O_2 + O_2$, $k = 8.6 \times 10^5$ M^{-1} s^{-1} (eq 1.2)

$O_2^{\cdot -} + O_2^{\cdot -} + 2H^+ \rightarrow O_2 + H_2O_2$, $k < 0.3$ M^{-1} s^{-1} (eq 1.3)

At pH 7, the equilibrium in aqueous media favours the disproportionation of $O_2^{\cdot -}$ with $K = 4 \times 10^{20}$ (*13*).

Superoxide anion in aqueous solutions can act as a reducing agent for multiple species, such as hemes in cytochromes or Cu^{2+} in copper proteins, *e.g.* plastocyanins (*14-15*). As an oxidant, it can oxidize

ascorbate (k= 2.7 x10 ^{5} M^{-1} s^{-1}), generating H_2O_2 (*12*). The species $HOO^{\cdot}$ can abstract protons from allylic carbons in fatty acids, being the initiator of a lipid peroxidation chain reaction, but at neutral pH these reactions are no longer relevant. So, the reactivity of the superoxide anion in biological (aqueous) solutions at neutral pH involves mainly the reaction with other radicals and metal ions/metalloproteins (see section 1.2).

1.1.2.2 - Hydrogen peroxide

Hydrogen peroxide (H_2O_2) is electronically a non-radical, having no unpaired electrons, being its reactivity basically dependent on its low energy bonds (H-OOH, 376 kJ/mol; HO-OH, 213 kJ/mol) as compared with the bond energies of 493 kJ/mol for O_2 and 393 kJ/mol for $O_2^{\cdot -}$ (*3*). In water it behaves as a very weak acid with a pK_a = 11.8, and may be formed by dimerization of hydroxyl radicals (*12*),

$$2HO^{\cdot} \rightarrow H_2O_2,\ k = 5 \times 10^{9}\ M^{-1}s^{-1} \qquad \text{(eq 1.4)}$$

by proton-induced disproportionation of superoxide ions (*3*),

$$O_2^{\cdot -} + O_2^{\cdot -} + 2H^{+} \rightarrow O_2 + H_2O_2 \qquad \text{(eq 1.5)}$$

and by the consecutive reduction of O_2 by 2 electrons (*3*)

$$O_2 + 2H^{+} + 2e \rightarrow H_2O_2 \qquad \text{(eq 1.6)}$$

H_2O_2 may participate in some known reactions that will generate the most reactive oxygen species, hydroxyl radical ($OH^{\cdot}$), by the Haber-Weiss reaction (*12*):

$$O_2^{\cdot -} + H_2O_2 \rightarrow OH^{\cdot} + OH^{-} + O_2 \qquad \text{(eq 1.7)}$$

However, in the presence of a metal ion, such as ferrous iron, the reactivity is much faster, through the Fenton reaction, where a reduced metal reduces H_2O_2, generating the hydroxyl radical (*12*):

$$Fe^{2+} + H_2O_2 \rightarrow Fe^{3+} + OH^{\cdot} + OH^{-},\ k = 76\ M^{-1}s^{-1} \qquad \text{(eq 1.8)}$$

This rate is related to the ferrous iron in solution, whereas for Fe^{2+}-citrate this rate increases to $4.9 \times 10^3\ M^{-1}s^{-1}$ (*12*).
This process may be potentiated since the superoxide anion reacts with ferric iron, regenerating the ferrous ion that may continue the production of hydroxyl, until hydrogen peroxide is exhausted.

1.1.2.3 - Hydroxyl Radical

In aqueous solutions $OH^{\cdot}$ species is the most powerful oxidant among the ROS, having a standard reduction potential $E'_0\ (OH^{\cdot}/H_2O) = 2.31$ V. It ionizes at very high pH values:

$$OH^{\cdot} \rightarrow O^{-} + H^{+},\ (pK_a = 11.9) \qquad \text{(eq 1.9)}$$

The dimerization of hydroxyl will generate H_2O_2 at near diffusion-controlled rates, $k = 5 \times 10^9\ M^{-1}s^{-1}$, although *in vivo* it is unlike to occur because the steady state concentration of $OH^{\cdot}$ is nearly zero. The reactivity of this radical is so high, that will react with any component in its vicinity with high rate constants ($\sim 10^9\ M^{-1}s^{-1}$), diffusing only 5-10 molecular diameters from its site of formation (*12*).
Hydroxyl can be generated by biologically relevant reactions such as the Fenton reaction (eq 1.8), or UV-induced homolytic cleavage of the O-O bond of H_2O_2 (eq 1.10).

$$H\text{-}O\text{-}O\text{-}H \rightarrow 2OH^{\cdot} \qquad \text{(eq 1.10)}$$

Hydroxyl radical reactions may occur by hydrogen abstraction, as in lipid peroxidation, or by hydrogen addition, generating guanine or thymine radicals in DNA molecules (*16-17*).

1.2 - Oxygen Toxicity

1.2.1 - ROS generation in biological systems

Oxygen toxicity in biological systems is believed to derive mainly from superoxide formed from the one-electron reduction of oxygen by components of the mitochondrial electron transfer chain and consequently generating H_2O_2 and $OH^{\cdot}$ (*12, 18*). Superoxide dismutase (SOD) is an enzyme responsible for scavenging superoxide by dismutation. The study of the phenotypes of SOD deletion mutants from *Escherichia* (*E.*) *coli*, by Carlioz and Touati, in 1986 (*19*) indicated defects in catabolism, biosynthesis and DNA replication, that could be reverted by complementation with SOD. This evidenced that superoxide is formed inside the cell and damages cell components if not scavenged by SOD. Along the years it has been proven that multiple *E. coli* reduced enzymes may be oxidized unspecifically by oxygen at a significant rate, such as complex I (NADH: ubiquinone oxidoreductase), alternative or Type II NADH dehydrogenase, succinate: quinone oxidoreductase (SQR), quinol: fumarate oxidoreductase (QFR), sulfite reductase and aspartate oxidase (*20-26*), among many others. The common features of these enzymes are that they contain redox cofactors, such as flavin or metal centers, for one-electron-transfer reactions. The rate at which these enzymes reduce oxygen depends on the degree of solvent exposure of the flavin or metal center, on the stability of the flavosemiquinone, the intermediate radical form that will transfer one electron to oxygen, and the reduction potential of the flavin or metal cofactors. Due to these reasons, the oxidation rates of these enzymes by oxygen vary by several orders of magnitude and the final product can be $O_2^{\cdot-}$ or H_2O_2 (*27*).

The rate of superoxide production in the cell was proposed to be around 3 μMs^{-1}, under standard aerobic growth conditions (*28*), corresponding to no more than 1% of the total oxygen consumption by respiring aerobic cells. But due to the scavenging system of superoxide (SOD in *E. coli*), the steady state concentration of $O_2^{\cdot -}$ is only 10^{-10} M, two fold lower than the necessary amount to inhibit cell growth (*29*).

Hydrogen peroxide is produced at a rate of 4 μMs^{-1} and steady state concentrations in the cell have been estimated to be about 10^{-7} M in the exponential cell growth state, the concentration limit for toxicity being *c.a.* 10^{-5} M (*12, 30*). The concentration of hydrogen peroxide inside the cell is also very dependent on its concentration in the culture medium, since, in contrast with superoxide, it is able to diffuse across the membrane.

1.2.1.1 - Superoxide and Hydrogen peroxide

Studies done by Boehme *et al.* in 1976 (*31*) revealed that high pressures of oxygen created a specific phenotype in *E. coli*, where cells lost the ability to grow without supplements of nicotinamide, branched-chain aminoacids and sulfurous aminoacids; the same phenotype was displayed by *sod*$^-$ mutants (*19*). The growth failure registered is usually due to the loss of activity of specific enzymes such as dihydroxyacid dehydratases, involved in branched chain aminoacid synthesis, and aconitase, a tricarboxylic acid (TCA) cycle enzyme, in the presence of $O_2^{\cdot -}$, as shown *in vitro* and in *sod*$^-$ mutants (*32-35*). These enzymes have a solvent-exposed [4Fe-4S] $^{2+/1+}$ cluster, which has been proposed to be responsible for the high oxygen and superoxide sensitivity of these enzymes, which become inactive due to release of iron ions (*36*).

For studying H_2O_2 reactivity, the use of *E. coli* catalase (*kat*) mutants, an enzyme able to scavenge this species by dismutation, is the best approximation for evaluating the cell damages by H_2O_2. The amount of 1µM of H_2O_2 was found to inhibit the growth of an *E. coli* strain MG1655 (*37*). This growth impairment can be due to the reaction of H_2O_2 with

cysteine residues generating sulfenic acid adducts or even sulfinic acid. at a rate of 10^6 $M^{-1}s^{-1}$ (*11*) as well as to the oxidation of many metalloproteins, by the Fenton reaction (eq. 1.8).

1.2.1.2 - Fenton Reaction and Hydroxyl

The iron available in the cell is to be used for heme synthesis, for iron incorporation into iron-dependent enzymes and ferritin, an iron storage protein, and is also suspected of being responsible for ROS generation (*36*).

DNA damage by Fenton reaction products (eq 1.8) as hydroxyl, includes oxidative lesions and mutagenesis. DNA being a negatively charged phosphate molecule may associate Fe^{2+} and the H_2O_2-dependent Fenton reaction occurs at its surface, affecting the DNA bases. As a consequence, by hydrogen abstraction, it may lead to strand breakage and base release (*17*). At physiological pH the Fenton reaction, that depends upon the coordination environment of the iron atom, an open coordination site or a readily dissociable ligand such as water (*38*), has a rate ranging from 10^3- 10^4 $M^{-1}s^{-1}$ (*12*). The Fenton reaction was demonstrated *in vivo* using *sod*$^-$ mutants, which lead to an increase of superoxide concentration in the cell and as a consequence 100 fold higher mutations; studies performed with a *fur* (ferric uptake regulator) mutant, which leads to increased iron content showed a 2.5 fold higher mutation rate (*39*) (Figure 1.5).

The extent of DNA damage may be counterbalanced by the action of several transcriptional regulators that respond to several types of oxidative stress, such as, elevated concentrations of iron, H_2O_2 or superoxide anion.

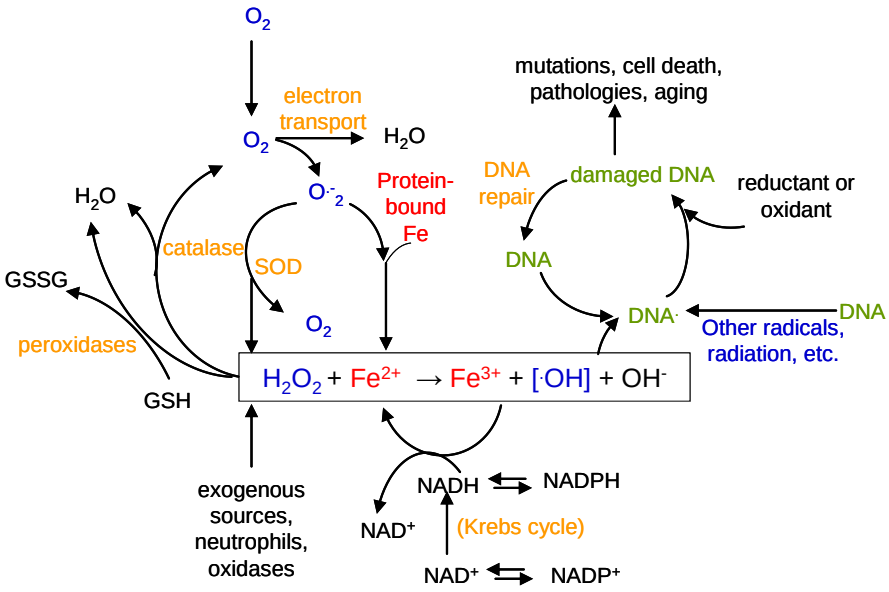

Figure 1.5 – Oxidative stress in the cell and DNA damage via Fenton reaction. H_2O_2 is generated exogenously or by endogenous metabolism; $O_2^{\cdot -}$ is produced by one electron reduction of oxygen by flavoproteins, metalloproteins; Superoxide dismutase (SOD) can scavenge $O_2^{\cdot -}$, producing H_2O_2 which will react with the released Fe, in a Fenton reaction producing $OH^{\cdot}$, that will react with DNA, damaging and generating mutations and other harmful processes. Scavenging systems like catalase and peroxidases can diminish the content of H_2O_2 in the cell. Adapted from (*17*).

1.2.2 - Cellular responses to ROS

Modulations of protein activity or redox regulation are important mechanisms for controlling the oxidative stress and avoid harmful consequences to the cell. Transcription factors containing redox centers sense elevated levels of reactive species like superoxide and hydrogen peroxide, as well as iron concentration, activating the expression of a varied number of proteins. The description of these regulatory transcription factors in prokaryotes will focus on those responding to superoxide (SoxR(S)), hydrogen peroxide (OxyR and PerR) and iron (FuR).

1.2.2.1 - SoxR(S), two component regulatory system

The SoxR(S) system responds to superoxide or nitric oxide (NO) stress and is activated in two transcriptional steps (*40*). The discovery of this system occurred when Hassan and Fridovich (*41*) exposed *E. coli* to redox-cycling antibiotics and verified that the expression of MnSOD (manganese containing superoxide dismutase) was strongly induced. Some years later, two proteins, SoxR, a sensor protein that responds to oxidative stress and SoxS, a transcriptional activator that positively regulates a wide number of genes, were found out to be responsible for the high MnSOD expression in *E. coli* (*42*). The activation of this regulon is governed by the two proteins SoxR and SoxS that will trigger consecutive stages of transcription.

SoxR is a 17kDa protein containing a helix-turn-helix motif (HTH; DNA binding motif) in the N-terminal domain. It is a homodimer and each monomer contains one redox-active $[2Fe\text{-}2S]^{2+/1+}$ cluster (*43*). $O_2^{\cdot -}$ and NO will oxidize the active center or nitrosylate it (*44*), respectively, causing a conformational change in the dimer (Figure 1.6). The redox switch of the cluster is the key for activation in this process. The active form will bind the promoter region of the *soxS* gene, inducing the transcription of *sox*S. SoxS is a 13kDa protein related to the transcriptional regulator family AraC/XylS (*45*) and it interacts with RNA polymerase to promote transcription of multiple genes, including *sod* (superoxide dismutase), *zwf* (glucose-6-phosphate dehydrogenase), *fpr* (NADH:flavodoxin oxidoreductase), *fldA* (flavodxin 1), *fumC* (fumarase C), *acnA* (aconitase), *nfo* (endonuclease IV) and *micF* (a regulatory RNA) (*30*). The expression of these genes will have a protective role against superoxide and also to maintain the metabolism and the reduced state of the cell.

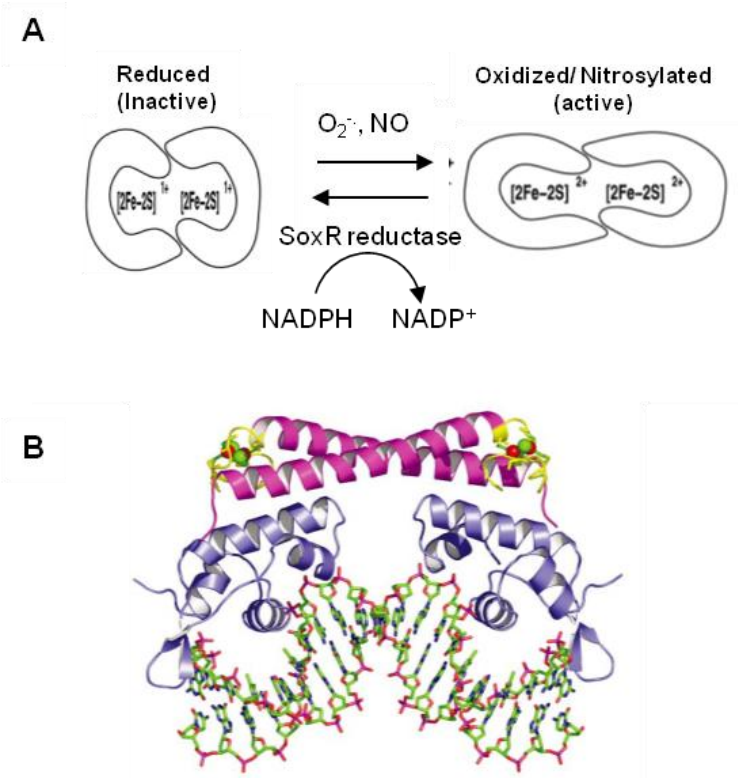

Figure 1.6 – A) SoxR activation and deactivation model (From (*46*)). B) Overall structure of the SoxR–DNA complex. The SoxR dimer is in the oxidized/active state. The SoxR protein is shown in a ribbon representation and the DNA fragment appears in a stick model. The DNA-binding domain, dimerization helix, and Fe-S cluster binding domain are shown in blue, magenta, and yellow, respectively. The [2Fe-2S] cluster is represented with brown and green spheres (pdb 2ZHG; from (*47*)).

The reduction potential of SoxR $[2Fe\text{-}2S]^{2+/1+}$ center, -285 mV (*46*), suggests that the reduction of this protein to its inactive, predominant redox state, is linked to the $NAD(P)H/NAD(P)^+$ concentration ratio (E'_0 = -340 mV) (Figure 1.6). Since the majority of expressed genes induced by SoxS, will replenish the NAD(P)H pool in the cell, this two regulatory system, SoxR(S) is then autoregulated (*48*).

1.2.2.2 - OxyR regulator

The bacterial *oxyR* regulator responds to peroxide stress and is governed by OxyR. This protein has a molecular mass of 34kDa and belongs to the LysR family of transcription factors (*50*), with a HTH motif in the N-terminal region. OxyR forms a tetramer in solution and its active form occurs upon oxidation by hydrogen peroxide, which will trigger the formation of a disulfide bond, between Cys199 and Cys208 (*E. coli* numbering) (*43*). This active state, suffers a conformational shift that allows its binding to the promoter region of several genes, through direct contact with RNA polymerase (Figure 1.7).

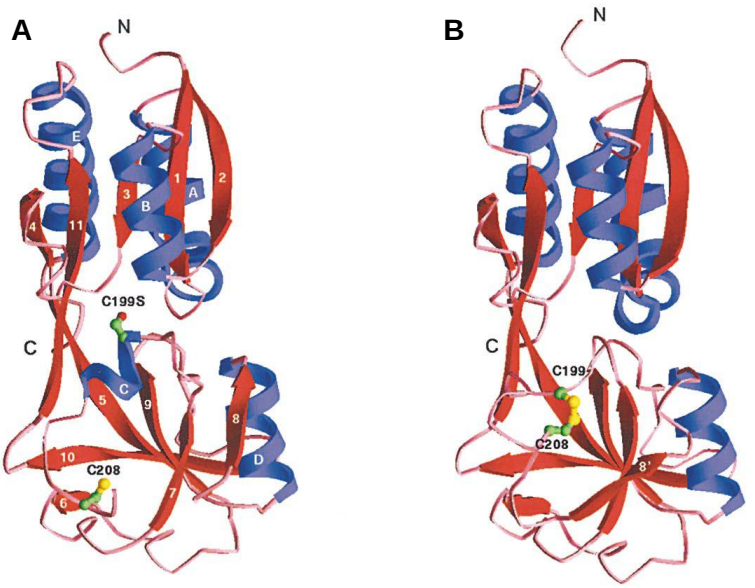

Figure 1.7 – Structure of the OxyR regulatory domain from *E. coli*. OxyR monomers in the reduced (pdb 1I69) (A) and oxidized (pdb 1I6A) (B) forms are shown with the redox-active cysteines Cys-199 and Cys-208 (From (*49*)).

In *E. coli*, OxyR activates the expression of several genes involved in H_2O_2 stress, such as *katG* (catalase), *ahpCF* (alkyl hydroperoxide reductase), *oxyS* (transcription regulator that belongs to the SoxR(S) regulon), *dps* (DNA binding protein from starved cells), *fur* (ferric uptake regulator, see 1.2.2.3), *gorA* (glutathione reductase) and *grxA*

(glutaredoxin). The deactivation of OxyR is dependent on disulfide reducing systems such as glutathione together with glutaredoxin and thioredoxin reductase with thioredoxin. *In vivo* studies showed that glutathione and glutaredoxin are the major systems responsible for reducing the disulfide bond, which means that this protein is also autoregulated. The low reduction potential of the redox Cys center (-185 mV) means that OxyR is in the dithiol form in the cell and is the predominating form (*46*).

1.2.2.3 - Fur and PerR regulators

Fur-like proteins (Ferric uptake regulator) coordinate the regulation of iron assimilation. Fur acts as a positive transcriptional repressor; it represses transcription upon interaction with Fe^{2+} (Figure 1.8). Fur protein is a homodimer composed by two 17kDa subunits. Each subunit can be divided in two domains, an N-terminal DNA-binding domain with a regulatory binding site and a C-terminal domain rich in histidine residues which has a structural binding site and is involved in the dimerization (*51-52*). A divalent cation (ferrous iron *in vivo*) binds to the regulatory binding site allowing the protein to bind to the promoter region of iron-regulated genes, repressing gene transcription. The regulatory binding site can bind other divalent metal ions instead of Fe(II), such as Mn(II), Co(II), Zn(II) and Ni(II). The structural metal binding site has a very high affinity to Zn (II) (*52-53*) (Figure 1.8).

The dimer active form binds the -35 and -10 promoter region of Fur-repressed genes. Fur-binding sites were originally found to form a 19-bp palindromic consensus sequence known as the 'Fur box'.

The activation of Fur will repress iron acquisition genes when high levels of iron are present in the cell, such as genes expressing iron transport systems, *exbBC* and *tonB* (siderophore iron transport) and *sodA* (MnSOD). Other genes are also known to be induced by iron in a Fur-dependent manner, although they do not have a typical Fur box: *acnA* (aconitase), *bfr* (bacterioferritin), *ftnA* (ferritin), *fumA* (fumarase),

sodB (FeSOD) (*54-56*).

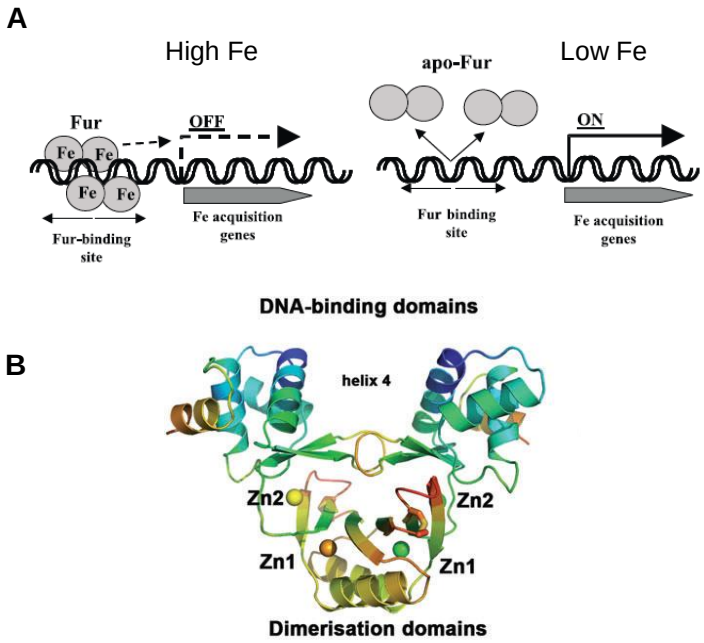

Figure 1.8 – A) Model of Fur-mediated gene repression (From (*57*)); B) The 3D structure of Zn bound Fur from *Vibrio cholerae* (pdb 2W57; from (*52*)). Zinc ions are represented in spheres (yellow (Zn1) and orange (Zn2) from one monomer and green (Zn1 and Zn2) from the other monomer).

The regulation of Fur is part of an important link between redox stress management and iron homeostasis. In *E. coli* the *fur* gene is part of an operon with *fdA* (flavodoxin), which is able to maintain the ferrous ion pool in the cell, helping the activation of the Fur protein (*58*). This operon is induced by the SoxR(S) system and the *fur* gene has its own promoter, which is induced by OxyR (*58*).

Fur-like proteins able to sense signals other than iron have been found in gram positive and gram negative bacteria, such as Zur (Zinc uptake regulator), Mur (Manganese uptake regulator), Nur (Nickel uptake regulator), PerR (Peroxide regulator) and Irr (Iron responsive regulator) (*51*). In PerR, peroxide-regulon repressor, firstly characterized in

Bacillus (*B.*) *subtilis*, the iron-binding site has new functions such as metal-based sensor for peroxides (*59*). This regulator is the major one of the peroxide stress response in *B. subtilis*, but several other genomes were found to encode for a PerR-like protein, such as *Campylobacter* (*C.*) *jejuni* (*60*). This protein contains a structural Zn^{2+} site and can be activated to bind DNA by either Fe^{2+} or Mn^{2+} as co-repressors, bound to the regulatory binding site (Figure 1.9). In the active form with Fe^{2+}/ Mn^{2+} bound to protein, H_2O_2 will oxidize the iron atom, as in a Fenton reaction, generating a hydroxyl or ferryl species. This reactive species will oxidize one of the metal-coordinating histidines, facilitating the dissociation of Fe^{3+} and blocking the access to Fe^{2+} ions (*51*). As a consequence, these results in lack of DNA-binding activity, allowing the induction of the genes whose transcription was blocked. These genes will encode for, *e.g.*, Dps like protein (MrgA), catalase (KatA), alkyl hydroperoxide reductase (AhpCF), enzymes of heme biosynthesis (HemAXCDBL) and Zinc uptake ATPase (ZosA) (*61*).

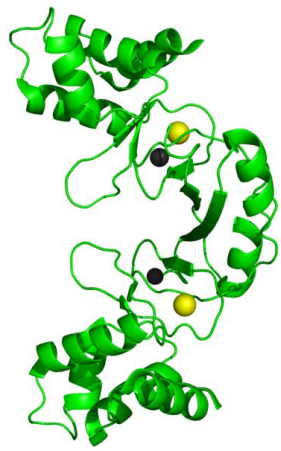

Figure 1.9 - Representation of the PerR-Zn-Mn crystal structure (*62*) (pdb 3F8N). Ribbon structure in green, the structural Zn^{2+} ions are in black and the Mn^{2+} regulatory ions are in yellow. Picture created with PyMOL (*63*).

1.2.3 - ROS and pathogens

Some organisms, including anaerobes or microaerobes are pathogenic, invading and colonizing a host. To counteract this invasion the host uses many strategies, including the generation of ROS to kill the pathogenic organisms. The immune system of the host comprises specialized cells, *e.g.,* macrophages and neutrophils, that are able to internalize the pathogen (phagocytosis) and by an intense oxidative burst, will produce ROS and destroy the invading organism (*64*). Cells like macrophages and neutrophiles use NADPH oxidase (Nox), a multicomponent enzyme, to generate superoxide and to initiate the ROS production. Nox enzymes constitute a family of transmembrane proteins comprising seven isoforms Nox 1-5 and Duox 1-2 (*65*). The structure of all these isoforms consists of six transmembrane domains and a cytosolic C-terminus (Figure 1.10). The III and IV transmembrane domains bind two prosthetic heme groups and the C-terminus contains two domains that bind the cofactor flavin adenine nucleotide (FAD) and the electron donor, NADPH (*65*).

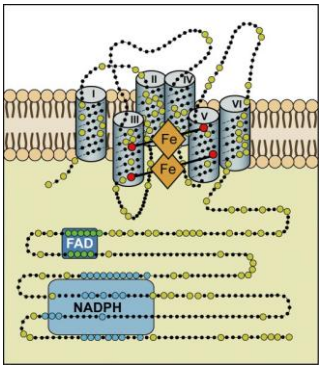

Figure 1.10 – Proposed structure of the core region of NADPH oxidase (NOX) enzymes. From (*65*).

Nox use these cofactors to transfer electrons from the cytosolic donor, NADPH to FAD and then sequentially to each heme group and finally to the molecular oxygen on the opposite side of the membrane to generate $O_2^{\cdot -}$ (*65*) (eq 1.11).

$$NADPH + 2O_2 \rightarrow NADP^+ + 2O_2^{-\cdot} + H^+ \quad \text{(eq 1.11)}$$

NADPH is provided by the induced pentose phosphate pathway and the superoxide is generated to the extracellular space. The engulfed pathogens are wrapped in a plasma membrane vesicle that will be exposed to high fluxes of superoxide. In acidic pH the superoxide will be as the more reactive and membrane-permeable $HOO^{\cdot}$ species or can also generate H_2O_2, which can cross the membrane easily.

The generation of $OH^{\cdot}$ is also possible inside the phagocytic vacuole, since neutrophiles generate both superoxide and hypochlorous acid (HOCl) (eq 1.12).

$$HOCl + O_2^{\cdot -} \rightarrow O_2 + OH^{\cdot} + Cl^- \quad \text{(eq 1.12)}$$

Hypochlorous acid generation is catalyzed by myeloperoxidase, an enzyme that in neutrophiles, is secreted into the vacuole. It is a heme-containing enzyme with a non-specific peroxidase activity, oxidizing a varied number of substrates (*66*). The oxidation of highly concentrated Cl^- anions in the vacuole, allows the generation of the hypochlorous acid that besides reacting with $O_2^{\cdot -}$, can oxidize many biological samples (*66*).

Another reactive species generated in macrophages and neutrophiles is nitric oxide (NO). This species is highly reactive and can react with $O_2^{\cdot -}$, forming peroxynitrite ($ONOO^-$) that can oxidize iron-sulfur proteins, among many others. In macrophages, the enzyme inducible nitric oxide synthase (iNOS) is responsible for catalyzing the generation of NO, using NADPH and oxygen (*67*).

In summary, the oxidative stress produced by oxygen and its reduced intermediates is significantly interrelated with nitric oxide stress and iron homeostasis, involving a plethora of regulatory systems networks. The knowledge of these processes is particularly important to further

understand the molecular basis of pathogenesis, namely how pathogens counteract the human immune system.

Chapter 2

This Chapter includes material published in

"Reductive elimination of superoxide: Structure and mechanism of superoxide reductases", **Pinto AF**, Rodrigues JV, Teixeira M., 2010 Biochim Biophys Acta.; 1804 (2):285-97.

2 - ROS detoxification enzymes

Oxidative stress in aerobic and anaerobic (facultative and strict) organisms has different impacts and responses, but shares some pathways for scavenging and reacting with ROS.

In aerobes the ROS production has its main origin in the aerobic electron transfer chain associated with the respiratory chain, which links NADH oxidation to O_2 reduction to H_2O, and is composed of several complexes containing flavins, quinones and iron-sulfur centers which are prone to oxidation by O_2, producing $O_2^{\cdot -}$ and H_2O_2 (see Section 1.2.1). Exogenous sources of ROS occur upon colonization of a host, whose immune system produces $O_2^{\cdot -}$ and H_2O_2, as mentioned in Chapter 1. For these reasons, organisms have to regulate the steady-state concentration of these species using scavenging systems consisting of enzymes and antioxidant compounds. The goal is to maintain a balance of ROS formation and elimination and its concentration below toxic levels.

The most ubiquitous enzymatic systems involved in the scavenging of ROS among aerobic organisms, but also in anaerobic and facultative organisms, are superoxide dismutases (SOD) and peroxidases, of which catalase is a particular case.

2.1 - Scavenging Systems: SOD and Peroxidases

Superoxide Dismutase (SOD)

Superoxide dismutases constitute a family of enzymes able to catalyze the disproportionation of superoxide by redox-cycling of the metal in the active site (*68*). The disproportionation of superoxide is accomplished by SODs in two-steps (eq 2.1 and 2.2), which are both first-order in respect to $O_2^{\cdot -}$ and with kinetic rate constants in the range of 10^9 M^{-1} s^{-1} (*69*), close to the diffusion limit rate and also competitive in comparison with the rate for autodisproportionation (~10^7 $M^{-1}s^{-1}$) (Chapter 1).

$M^{(n+1)+} + O_2^{\cdot -} + H^+ \rightarrow M^{n+}(H^+) + O_2$ (eq 2.1)

$M^{n+}(H^+) + O_2^{\cdot -} + H^+ \rightarrow M^{(n+1)+} + H_2O_2$ (eq 2.2)

$2O_2^{\cdot -} + 2H^+ \rightarrow O_2 + H_2O_2$ (eq 2.3)

The dismutation of superoxide follows a ping pong mechanism, where two $O_2^{\cdot -}$ will bind in two steps, the first coupled to uptake of a proton which will facilitate substrate reduction and binding for the second $O_2^{\cdot -}$ substrate molecule (*69-72*).

According to the metal cofactor each SOD harbors, they can be classified into three groups: Cu and Zn-containing superoxide dismutase (Cu,Zn-SOD), SODs specific for Fe, Mn or for either of the two metals (Fe-SOD, Mn-SOD or Fe/Mn-SOD) and the SODs that use Ni (Ni-SOD) (*68*). Although sharing the same function the overall structure differs for the three types of SODs (Figure 2.1).

Fe-SOD and Mn-SOD aminoacid sequences are extremely conserved namely on what concerns the residues of the active site and some nearby residues. The active site contains one Fe/Mn ion coordinated in a trigonal bipyramid geometry by three histidines, an aspartate and a molecule of OH^-/H_2O (*69*). Fe-SODs are considered the most primitive SODs due to the Fe prevalence in a reducing environment as in the primitive atmosphere. Consistent with the diminished bioavailability of Fe and appearance of O_2, the MnSOD and CuZnSOD evolved (*71*).

Distinct from Mn or Fe-SOD is Cu,Zn-SOD which has an active site with one copper and one zinc atoms bridged by a histidine. The Cu ion is bound by three histidines in a distorted square planar structure and an additional water molecule, while the zinc ion is bound by two histidines and an aspartate. Cu,Zn-SODs are most abundant in the cytosol of eukaryotic cells, periplasm of gram-negative bacteria, in chloroplasts and extracellular space of mammals (*69*).

The Ni-SODs enzymes were only recently found in *Streptomyces* bacteria and in cyanobacteria. The active site has a Ni ion bound in a square planar geometry to two thiolates from two cysteines and two backbone nitrogens from histidine and cysteine residues (*73*).

In *E. coli* Fe-SOD is synthesized to almost 20 µM and $O_2^{\cdot -}$ is maintained at 0.1 nM (*28*), which shows that the catalytic efficiency of SODs and the abundance of protein in the cytosol leads to a low level of $O_2^{\cdot -}$, non-hazardous to cell metabolites.

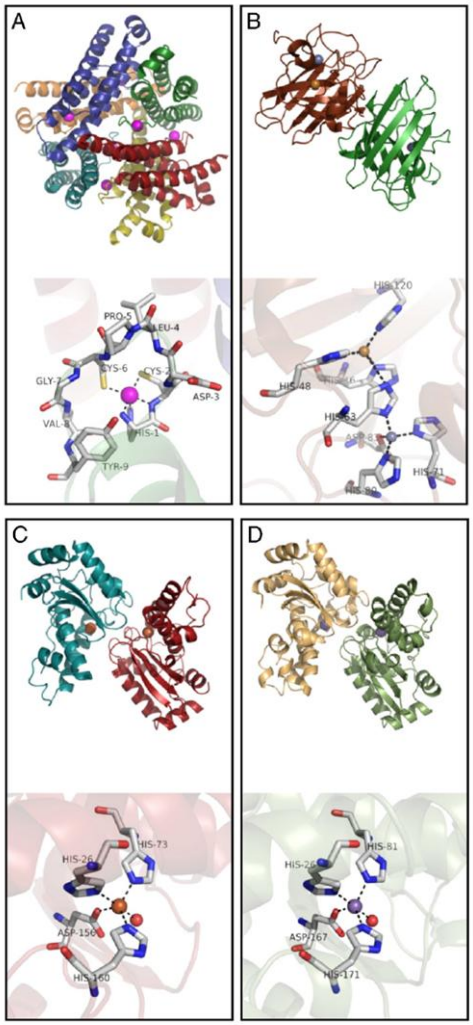

Figure 2.1 - A comparison of the enzyme structures and active sites for the four SODs, (A) *Streptomyces coelicolor* NiSOD (pdb: 1T6U), (B) human CuZnSOD (pdb: 1PU0), (C) *E. coli* FeSOD (pdb: 1ISA) and (D) *E. coli* MnSOD (pdb: 1VEW). From (71).

Peroxidases

Hydrogen peroxide is mainly scavenged by two types of enzymes. Peroxidases scavenge H_2O_2 by using it to oxidize other substrates (eq 2.4) and catalases directly catalyse the dismutation of H_2O_2 to O_2 and H_2O (eq 2.5):

$$RH_2 + H_2O_2 \rightarrow R + 2H_2O \quad \text{(eq 2.4)}$$

$$H_2O_2 + H_2O_2 \rightarrow O_2 + 2H_2O \quad \text{(eq 2.5)}$$

Peroxidases are a large family of enzymes that have a wide range of substrates/electron donors. There are heme and non-heme peroxidases and in this last group the most important enzymes are thiol-specific peroxidases, glutathione peroxidases (Gpx) and peroxiredoxins (Prx) (*74*). Glutathione peroxidase encompasses a family of multiple isozymes, which catalyze the reduction of H_2O_2 or organic hydroperoxides to water or corresponding alcohols using reduced glutathione. Some of these isozymes have selenium-dependent glutathione peroxidase activity (*75*). Peroxiredoxins are a ubiquitous family of antioxidant enzymes. Alkyl hydroperoxide reductase (AhpC) is a 2 Cys-peroxiredoxin and is the most studied enzyme from Prxs and is identified in a variety of prokaryotes (*76*). It is able to reduce a large number of substrates from H_2O_2 to organic compounds (*76*).

Catalases are among the most studied of enzymes. Three classes of proteins with no aminoacid sequence and structure similarity but with catalase activity have been defined (*77*). The class that is most widespread in nature and which has been most extensively characterized is composed of mono functional, tetrameric heme-catalases subdivided on large (> 75 kDa) or small (< 60 kDa) subunits enzymes (*77*). The second, less widespread class is composed of bifunctional, heme-containing catalase-peroxidases that are closely related by sequence and structure to plant peroxidases and are widely distributed among prokaryotes and protozoa (*77*). The third class

includes the non-heme or Mn-containing catalases, which have only been found in prokaryotes (*77*).

The mechanism of H_2O_2 dismutation by heme-catalases occurs in two stages. The first substrate molecule is reduced to water, oxidizing catalase to an oxyferryl porphyrin cation species, named compound I. A second H_2O_2 molecule can complete the catalytic cycle reducing compound I back to Fe^{3+} along with the generation of water and O_2 (eq 2.6; E for enzyme and Por for porphyrin) (*78*).

$$E(Por\text{-}Fe^{3+}) + H_2O_2 \rightarrow \text{Compound I } (Por^{+}\text{-}Fe^{4+}{=}O) + H_2O$$
$$\text{Compound I } (Por^{+}\text{-}Fe^{4+}{=}O) + H_2O_2 \rightarrow E(Por\text{-}Fe^{3+}) + H_2O + O_2 \qquad \text{(eq 2.6)}$$

Catalases do not follow Michaelis-Menten kinetics except at very low substrate concentrations, and different enzymes are affected differently at higher substrate concentrations. Turnover rates range from 54 000 s^{-1} to 833 000 s^{-1}, which are considered the highest turnover rates for an enzymatic system (*78*).

McCord and Fridovich in 1971 (*79*) proposed a correlation between oxygen tolerance and the content of SOD and catalase enzymes, so that anaerobic organisms unable to cope with oxygen would not need to express these scavenging enzymes. This hypothesis led to misleading assumptions, that in anaerobes the presence of O_2 would impair growth and lead to death of these microorganisms, preventing its growth in the aerobic world. This proposal was found to be wrong when it became clear that anaerobic organisms can synthesize SODs and catalases, or even other types of oxidative stress protective enzymes, such as peroxidases and superoxide reductases (see 2.3 section), as well as by the multiple observations reporting a wide scale of oxygen sensitivity of the so-called anaerobic organisms. For example, within sulfate-reducing bacteria, *Desulfovibrio* (*D.*) *gigas* and *D. vulgaris* Hildenborough that were considered strict anaerobes, have been found to be aero-tolerant (*80-82*) and *D. desulfuricans* ATCC 27774 has even been reported to

grow at nearly atmospheric oxygen levels (~21%) (*83*). Studies on *Clostridium* (*C.*) *acetobutylicum* (*84*), a strict anaerobe, showed that in its genome it is encoded a homologue to a PerR protein. In a *perR* mutant strain, the viability upon aeration increased in comparison to the wild type (wt). It was found that the *perR* mutant synthesizes enzymes involved in oxidative stress response, such as an NADH oxidase and a rubrerythrin (see section 2.2). Nowadays it is perfectly established, mainly due to the huge number of microbial genomes sequenced, that even organisms still considered strict anaerobes, in the sense of being incapable of growing in the presence of oxygen, contain the most diverse oxygen and/or ROS detoxifying enzymes (Figure 2.2).

Superoxide reductases and Rubrerythrins are the two families of proteins that are the scope of this thesis, which will be now described in detail (Figure 2.2).

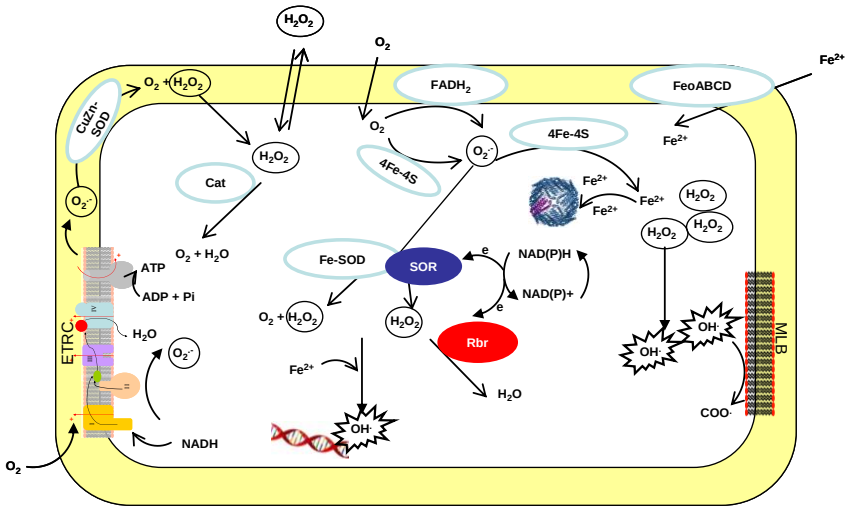

Figure 2.2 – Scheme of ROS generation and ROS scavenging enzymes inside a Gram-negative cell. Cat - catalase, Fd - ferrodoxin, FeoABCD - ferrous iron transporter, $FADH_2$ - flavoprotein, 4Fe-4S - four-iron four-sulfur cluster containing enzyme (*e.g.,* aconitase), Rbr - Rubrerythrin, Fe-SOD - Iron Superoxide Dismutase, CuZn-SOD - Copper Zinc Superoxide Dismutase and SOR - Superoxide Reductase. The reactive oxygen species, superoxide ($O_2^{\cdot-}$) and hydrogen peroxide (H_2O_2) have a black circle and the highly reactive hydroxyl ($OH^{\cdot}$) species is star shaped. ETRC – electron transfer respiratory chain and MLB – membrane lipid bilayer.

2.2 – Rubrerythrin

Rubrerythrins are proteins which in general comprise two types of iron sites: a non sulfur diiron center of the μ-oxo bridged histidine/carboxylate family located in a four-helix bundle structural domain, and a rubredoxin-type [$FeCys_4$] center, located at the C-terminal domain in most rubrerythrins. These proteins received these trivial name due to the presence of the rubredoxin and hemerythrin-like diiron centers (*85-86*). Hemerythrin is an oxygen carrying enzyme from worms which received this name due to its color (erythrin for red, in Greek, and heme by functional analogy with hemoglobin). This hemerythrin-like domain is also referred as an erythrin domain.
Since the identification of the first rubrerythrin in the sulfate reducing bacterium *D. vulgaris* (*85*), they have been found in the most diverse organisms of the three life domains, Archaea, Bacteria and Eukarya (*87-95*). Several *in vitro* activities have been assigned to rubrerythrin, such as pyrophosphatase (*96*), ferroxidase (*97*) and superoxide dismutase (*98*), but H_2O_2 reductase, linked to NADH oxidation by another partner enzyme, has been considered the most probable *in vivo* activity of rubrerythrins (*99-102*).

2.2.1 - Aminoacid sequence analysis

The family of rubrerythrins (Rbr) was thought to be exclusive of prokaryotes, but recently the genomes of three protozoa *Entamoeba histolytica*, *Trichomonas vaginalis* (*92*) and *Cyanophora* (*C.*) *paradoxa* (*88*) were found to contain genes encoding rubrerythrins. The *C. paradoxa* enzyme, symerythrin, has only conserved the four-helix bundle structural domain and presents a high internal sequence similarity (see section 2.2.3) and thus was given that name (*88*). The other eukaryotic rubrerythrins have the C- terminal rubredoxin domain conserved. In rubrerythrins the conserved ligands for the metal ions of the diiron site, $E\text{-}(X)_{29\text{-}37}\text{-}E\text{-}(X)_2\text{-}H_n\text{-}(X)_n\text{-}E\text{-}(X)_2\text{-}E\text{-}(X)_{29\text{-}37}\text{-}E\text{-}(X)_2\text{-}H$,

correspond to a pair of two carboxylates plus an histidine residue (EX_nEX_2H) and an additional carboxylate. This motif is conserved as seen in the selected aminoacid sequences in Figure 2.3; furthermore, a pair of strictly conserved tyrosine residues is hydrogen-bonded to the two terminal glutamate ligands of the diiron site (Y27 and Y102 for Rbr from *D.vulgaris*) (*103-104*). The most divergent aminoacid sequence is that of the *C. paradoxa* symerythrin (in comparison to Rbr from *D. vulgaris*, 34% of similarity and 18% of identity). The average similarity of the aminoacid sequences of rubrerythrins in figure 2.3 is about 60%.

2.2.2 – Physiological studies

The biochemical and biophysical characterization of rubrerythrins, namely the two iron centers and the *in vitro* assays for different functions preceded for more than a decade the *in vivo* approaches to unravel their function. Only in 2001, Lumppio and coauthors (*90*) used a catalase-deficient *E. coli* strain for complementation assays with a plasmid harboring the gene for *D. vulgaris* rubrerythrin or nigerythrin[1]. They showed that after 30 min exposure to 2.5 mM H_2O_2 the strains expressing nigerythrin or rubrerythrin increased their viability as compared to the mutant strain. For *D. vulgaris*, upon exposure to oxygen for one hour, cell cultures were analyzed and their proteomic content and RNA levels, revealed that rubrerythrin protein levels and gene transcripts were decreased (*105*).

The level of protein content was seen to decrease as well for H_2O_2 exposed cell cultures of *Campylobacter* (*C.*) *jejuni*, which encodes for a rubrerythrin-like protein ((*106*), Chapter 4).

1 - The name ‘nigerythrin’ (niger, black) was given to a rubrerythrin analogue present in *D. vulgaris* (*96*).

Helix 1
Helix 2
Helix 3
Helix 4
C.butyricum
C.acetobutylicum
D.vulgaris
M.thermoacetica
P.gingivalis
T.bacterium
F.magna
C.perfringens
Ngr.D.vulgaris
T.vaginalis
Eukarya
E.histolytica
C.paradoxa
A.fulgidus
M.jannaschii
Archaea
S.acidocaldarius
S.tokodaii
S.elongatus
P.furiosus

Figure 2.3 – Amino acid sequence alignment of the four-helix bundle domain of rubrerythrins from Bacteria, Eukarya and Archaea: *Campylobacter jejuni subsp. jejuni* NCTC 11168 (gi|218561705|); *Clostridium butyricum* 5521 (gi|182419666|); *Clostridium acetobutylicum* DSM 1731 (gi|336292356|); *Desulfovibrio vulgaris* Hildenborough (gi|46581497|); *Moorella thermoacetica* ATCC 39073 (gi|6449424|); *Porphyromonas gingivalis* ATCC 33277 (gi|188994166|); uncultured termite group 1 bacterium (gi|189485275|); *Finegoldia magna* ATCC 29328 (gi|169825293|); *Clostridium perfringens* str.13 (gi|18309117|); nigerythrin from *Desulfovibrio vulgaris* Hildenborough (gi|46578436|); *Trichomonas vaginalis* G3 (gi|15442078|); *Entamoeba histolytica* HM-1:IMSS (gi|67472683|); *Cyanophora paradoxa* (gi|1016189|); *Methanocaldococcus jannaschii* DSM 2661 (gi|15668915|); *Sulfolobus acidocaldarius* DSM 639 (gi|70607981|); *Sulfolobus tokodaii* str.7 (gi|342306703|); *Synechococcus elongatus* PCC 6301(gi|56687405|) and *Pyrococcus furiosus* DSM 3638 (gi|18977655|). Black boxes represent strictly conserved residues and dark grey boxes represent highly conserved residues. The "*" are for the ligands involved on the di-iron site plus the two tyrosine residues that are strictly conserved and are hydrogen bonded to the glutamates labelled by **.

A *Porphyromonas* (*P.*) *gingivalis* rubrerythrin-mutant strain, a pathogenic prokaryote lacking a catalase and heme-peroxidases, was revealed to be more oxygen and H_2O_2 sensitive than the wt strain (*93*). A particularly interesting work with *P. gingivalis*, using an animal model, showed that the rubrerythrin played an important role for the pathogen survival in the presence of a fully functional host immune response. Surprisingly, the authors showed that rubrerythrin was not associated with the neutrophils oxidative burst but with the generation of reactive nitrogen species (RNS) by iNOS in macrophages (*107*). This was, so far, the first and only work correlating rubrerythrin and reactive nitrogen species. Upregulation of rubrerythrin expression was also seen for *Methanothermobacter thermoautotrophicus* (*108*) under oxidative stress conditions and in a *perR* mutant in *C. acetobutylicum* (*84*).

2.2.3 - Structural domains

There is a large diversity of rubrerythrin-like proteins due to the combination of several types of structural domains. This variety

comprises: the presence of the rubredoxin-like domain in the N-terminal and/or the C-terminal domain of the protein; the size of this domain; and the presence of other redox sites in the N-terminus, as a desulforedoxin-like domain. Some examples of this diversity are depicted in Figure 2.4.

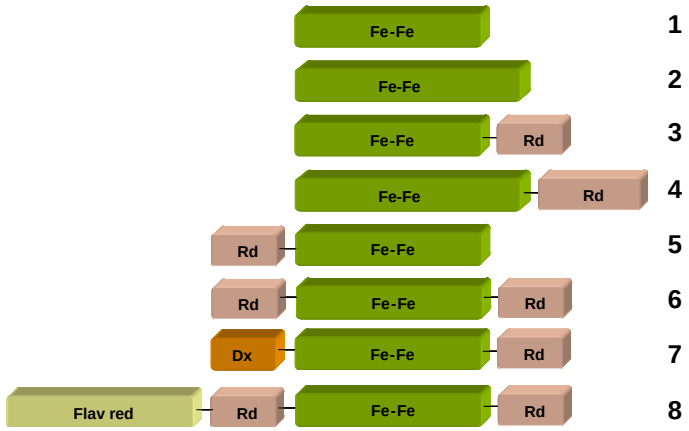

Figure 2.4 – Representation of domain arrangements found in Rbr family. Examples given for each example are in order of appearance: 1) Sulerythrin from *Sulfolobus tokodaii* str. 7 (gi|342306703), 2) *Spirillum volutans* (gi|3372506|), 3) *Desulfovibrio vulgaris subsp. vulgaris* DP4 (gi|120601988|), 4) *Synechococcus sp.* RS9917 (gi|87123471|), 5) Rubperoxin from *Clostridium acetobutylicum* (gi|81775388), 6) *Clostridium ramosum* DSM 1402 (gi|167754543|), 7) Desulforubrerythrin from *Campylobacter jejuni subsp. jejuni* NCTC 11168 (gi|218561705|), 8) *Dorea longicatena* DSM 13814 (gi|153853488|). Each box corresponds to different domains: Fe-Fe – Erythrin/Four helix bundle (green), Rd – Rubredoxin (pink), Dx – Desulforedoxin (orange) and Flav red – Flavin reductase (yellow).

2.2.3.1 - Rubredoxin domain

Rubredoxins are small proteins (*c.a.* 50 aminoacid residues in general) with a redox site composed of one iron atom coordinated to the sulfur atoms of four cysteines, in a tetrahedral geometry, which is considered the simplest example of an iron-sulfur center (Figure 2.5) (*109*). These proteins are found mainly in anaerobic prokaryotes, but also in unicellular eukaryotes, such as the alga *Guillardia theta* (*110*). According to the ligand binding motifs, rubredoxins were classified in type I and II (*111*). In type I rubredoxins, the most abundant, the

coordinating cysteines appear in two pairs, having in between each cysteine two aminoacid residues, and each pair being separated by *c.a.* 30 residues. In type II rubredoxins, found so far only in sulfate reducing bacteria (*109, 111*), the first two cysteines are separated by four residues, $CX_4CX_nCX_2C$. A rubredoxin-like protein is desulforedoxin (Dx), which is one of the smallest metalloproteins known, with *c.a.* 35 aminoacids, that received this name because it was first isolated from a *Desulfovibrio* species (*112*). In this protein, the binding motif is CX_2CX_nCC (Figure 2.5), which results in a slightly more distorted tetrahedral geometry (*113*). Dx was so far only isolated from *D. gigas* (*112*), but its presence has also been detected in the genomes of *Dehalococcoides sp.* and of the methanogenic archaeon *Methanoregula boonei*.

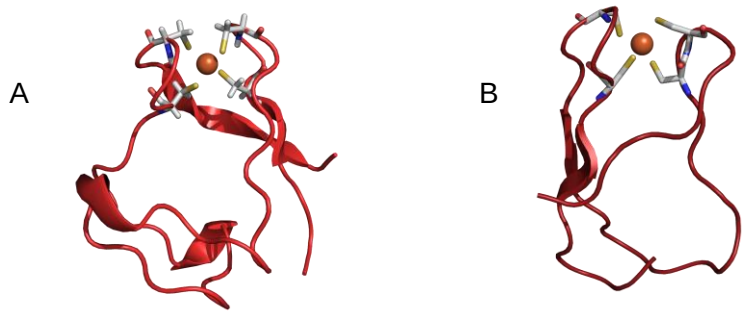

Figure 2.5 – 3D crystal structure of A) Rubredoxin from *Desulfovibrio vulgaris* (pdb 1RB9) and B) Desulforedoxin from *Desulfovibrio gigas* (pdb 1DXG). The proteins are shown in a cartoon representation and the iron ligands are in the stick model with each atom colored by element: carbon (gray), oxygen (red), nitrogen (blue) and sulfur (yellow). Iron ion is represented in an orange sphere. Figure prepared using PyMOL (*63*).

In Rbrs and flavorubredoxins (FlRd) (a flavodiiron protein of class B) (*114*), a rubredoxin-like domain is present at the N or C-terminus, with the ligand motif of Type I rubredoxins. However, in most rubrerythrins, the spacing between the two cysteine pairs is about 12 residues. Desulforedoxin domains may be found in multidomain proteins as in rubrerythrins ((*115*); Chapter 4) and in 2Fe-SORs (*116*) (see section 2.3). In 2003, Radu Silaghi-Dumitrescu *et al.*, characterized a 25 kDa

rubredoxin-like protein, named as High molecular weight rubredoxin (Hrb), from *Morella thermoacetica.* This protein was shown to be reduced by NADH and to transfer electrons to a flavodiiron protein (*117*), being composed of a NADH: flavin oxidoreductase-like and rubredoxin domains. These Hrbs are mostly found in the phylum of firmicutes, namely in the clostridia class.

The iron site of rubredoxins in the oxidized ferric form is in a paramagnetic high-spin state and its UV-Visible spectrum is dominated by cysteine-Fe^{3+} charge transfer transitions with absorption maxima at 490 and 380 nm (ε_{493} = 7 $mM^{-1}cm^{-1}$) (*109*). The EPR spectrum has resonances characteristic of an S=5/2 spin ground state, with a rhombicity E/D=0.33, yielding a low intensity resonance at g~9.4 (|S=1/2> doublet) and a strong resonance at g=4.3, due to the |S=3/2> middle doublet (*109*). The UV-visible spectrum of desulforedoxins is slightly different (see chapter 4).

Rubredoxins have reduction potentials ranging from -100 to +150 mV, acting as electron carriers in diverse metabolic pathways (*109*); in rubrerythrins the potential is much higher (above +180 mV), while in *E. coli* Flrd it is -65 mV (*85, 118*). Rubredoxin was shown to act as an electron donor to membrane-bound alkane hydroxylases (*119*), and to a bacterioferritin (*120*), but the most common function, so far, appears to be in ROS scavenging electron transfer chains, as electron donors to rubrerythrins (*101*), superoxide reductases (*121*) and flavodiiron proteins (*122*). Desulforedoxin also acts as an electron donor to the superoxide reductase from *D. gigas* (*112*).

Rubredoxins are in general reduced by NAD(P)H oxidoreductases from several families (*e.g.,* (*123-125*)).

2.2.3.2 - Four-helix bundle domain

The conserved non-heme, non-sulfur carboxylate-bridged diiron site is in a structural motif designed as a four-helix bundle that consists of four helices packed in a coiled-coil arrangement (*103*). This is characteristic

of several O_2-activating enzymes such as the R2 subunit of ribonucleotide reductase (RNR-R2), methane monooxygenase (MMOH), stearoyl-ACP Δ^9 desaturase and of the O_2-carrying enzyme, hemerythrin (Figure 2.6). These proteins share some properties (*126*):

1) two iron atoms at the dinuclear site which are separated at least by 4 Å, in the reduced form;
2) the two iron ions are in a stable high-spin state in the oxidized and reduced forms;
3) each iron is bound to one histidine, one or two carboxylate residues (Asp or Glu), with the exception for hemerythrin in which iron ligands are only histidine residues, one to two bridging glutamates and a solvent based bridge (hydroxo or oxo species, in the oxidized form).

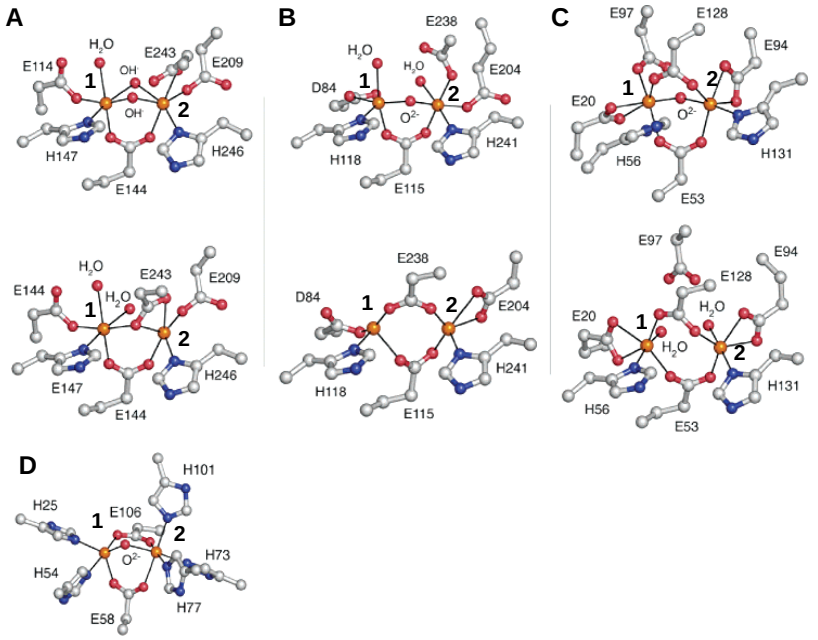

Figure 2.6 - Dioxygen-utilizing carboxylate-bridged diiron centers. Top- oxidized states; Bottom- reduced states. (A) Methane Monooxygenase from *Methylococcus capsulatus*. (B) Ribonucleotide reductase R2 from *Chlamydia trachomatis*. (C) Rubrerythrin from *D. vulgaris*. (D) Methemerythrin from *Themiste dyscrita.* Fe1 is on the left, and Fe2 is on the right. All atoms and side chains are in a ball and stick model and are colored by atom type [carbon (gray), oxygen (red), nitrogen (blue) and iron (orange). Adapted from (*127*).

A characteristic spectroscopic feature for this family of proteins is due to the anti ferromagnetic coupling of the two irons in the mixed-valence state (Fe^{2+}-Fe^{3+}), resulting in a S=½ spin state which gives rise to a rhombic EPR resonance with g< 2 (*85*).

In rubrerythrins the diiron center, depending on the redox state, is coordinated differently. In the oxidized form, the Fe1 (Figure 2.6C) is coordinated by four glutamate residues whereas the Fe2 is coordinated by one histidine and three glutamate residues (Figure 2.6C). The two iron atoms are bridged by two of the coordinating glutamates and a solvent species that can be a hydroxo or peroxo, which is still not known. In the reduced form, the Fe1 is coordinated by one histidine, three glutamate residues and one water molecule; the Fe2 is also coordinated by one histidine, three glutamate residues and one water molecule (Figure 2.6C). The two iron atoms are still bridged by two glutamate residues but the solvent bridge is no longer present, as it happens in the other diiron enzymes (Figure 2.6). The X-ray crystal structure of the oxidized (all-ferric) and reduced (all-ferrous) *D.vulgaris* Rbr (Figure 2.6C and Figure 2.7) (*104*) shows that the Fe1 undergoes an appreciable redox-induced movement, which does not happen with the other diiron enzymes. The ferric Fe1 atom is coordinated by the Glu97 residue that upon reduction unbinds and the iron moves ~2 Å towards the His56 residue. The distance between the two irons increases from 3.3 to 4 Å.

In the reduced form, each pair of helices contributes with three diiron coordinating residues (see Figure 2.3 and 2.7). The flexibility and symmetry of the diiron center, in the reduced form, is characteristic of rubrerythrins. Recently a review by S.C. Andrews (*128*) proposed, due to this symmetry, that rubrerythrin-like proteins originated via gene duplication or fusion of two α-helices.

Rubrerythrins are at least homodimers, with a “head-to-tail” arrangement, where the N-terminal four-helix bundle is followed by a C-terminal beta structure, the rubredoxin-like domain (Figure 2.7). This

arrangement is functionally important, as it allows the diiron site from one monomer to be at 12-13 Å from the [Fe(Cys)$_4$] center from the other monomer (*103*), a distance suitable for efficient electron transfer; on the contrary, the distance between the diiron and the [Fe(Cys)$_4$] centers from the same monomer is too large for that purpose, *c.a.* 30 Å.

Besides the 3D crystal structure from *D. vulgaris* rubrerythrin (*103-104, 129-130*), there are 3D crystal structures determined by X-ray crystallography for other rubrerythrins, such as those from *P. furiosus* (Structural Genomics, (*131*)), *Sulfolobus tokodaii* (*132*), *Burkholderia pseudomallei* (Structural Genomics) and *Campylobacter jejuni* (Chapter 5).

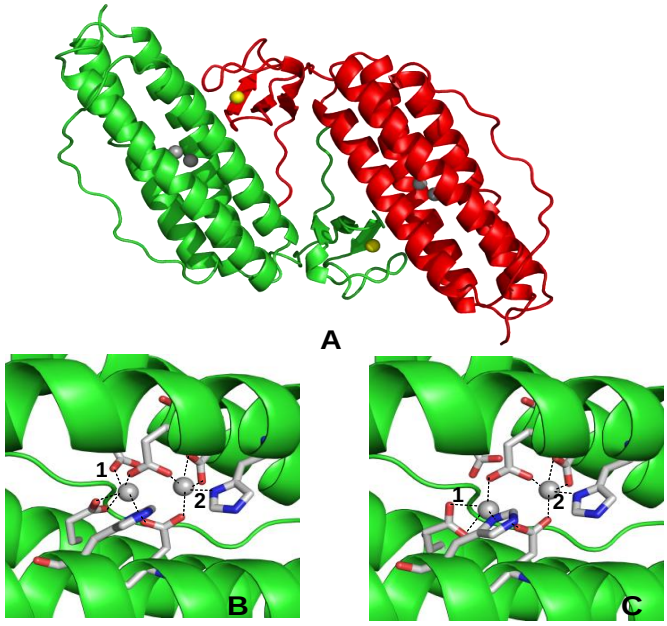

Figure 2.7 – 3D crystal structure of Rubrerythrin from *Desulfovibrio vulgaris* (A) homodimer pdb 1RYT, (B) All-ferric diiron center pdb 1LKM and (C) All-ferrous diiron center pdb 1LKO. Iron atoms from the diiron center are represented in gray spheres and the iron atoms from Rd domain are represented in yellow spheres. Picture created with PyMOL (*63*).

Some differences have been reported among the crystal structures of rubrerythrins. In *P. furiosus* Rbr and *Sulfolobus tokodaii* sulerythrin, a Rbr-like protein, the four-helix bundle is domain swapped within the homodimer (*132-133*) where each pair of helices comes from two different monomers. The metal content of the binuclear center of rubrerythrins has also been controversial. A native rubrerythrin isolated from *D.vulgaris* was shown to contain a Zn atom in position 1 (*130, 134*). Interestingly, the same redox-induced metal movement was observed. The enzyme from *S. tokodaii*, contains also a heterometallic site, but in this case the Zn atom was at position 2 (*132*). The different metal contents of the binuclear center, of these native or recombinant rubrerythrins, can account for the different activities reported for this family of proteins and its physiological relevance is still under discussion.

2.2.4 - Hydrogen peroxide reduction mechanism

Rubrerythrins are involved in oxidative stress protection and have been proposed to reduce hydrogen peroxide, receiving electrons from a NAD(P)H dependent chain (*90, 100-102, 124*).

The peroxidase activity is reported to have a turnover number around 2 x 10^3 min^{-1} for reduction of hydrogen peroxide using as an electron donor a rubredoxin (*99*); however, this activity is very low in comparison with canonical peroxidases, such as that of horseradish peroxidase (1.7 x 10^5 min^{-1}), which may be mainly due to the fact that the peroxidase activity assays for rubrerythrins are usually performed with non-physiological electron transfer proteins (*100*).

The reduction of H_2O_2 occurs at the diiron site, being the Rd site, used as an electron transfer center. A mechanism was proposed based on the 3D crystallographic structures and stopped-flow kinetic data, by Kurtz et al (*135*) (Figure 2.8). The active enzyme starts in its diferrous state and is thought to reduce H_2O_2 via a two-electron reaction, forming a diferrous-dihydroperoxo intermediate, which is stabilized by a

glutamate residue (E97 in *D. vulgaris* Hildenborough numbering). This glutamate may act as a proton acceptor of oxygen of the peroxo species, promoting the release of a water molecule (Figure 2.8); the diferric site is then re-reduced by consecutive electron transfer steps. Upon reduction of the mixed-valence state, the iron moves away (in red in Figure 2.8) concomitantly with the binding to a histidine residue (H56) and the unbinding to a glutamate residue (E97). These intermediate steps still lack experimental verification.

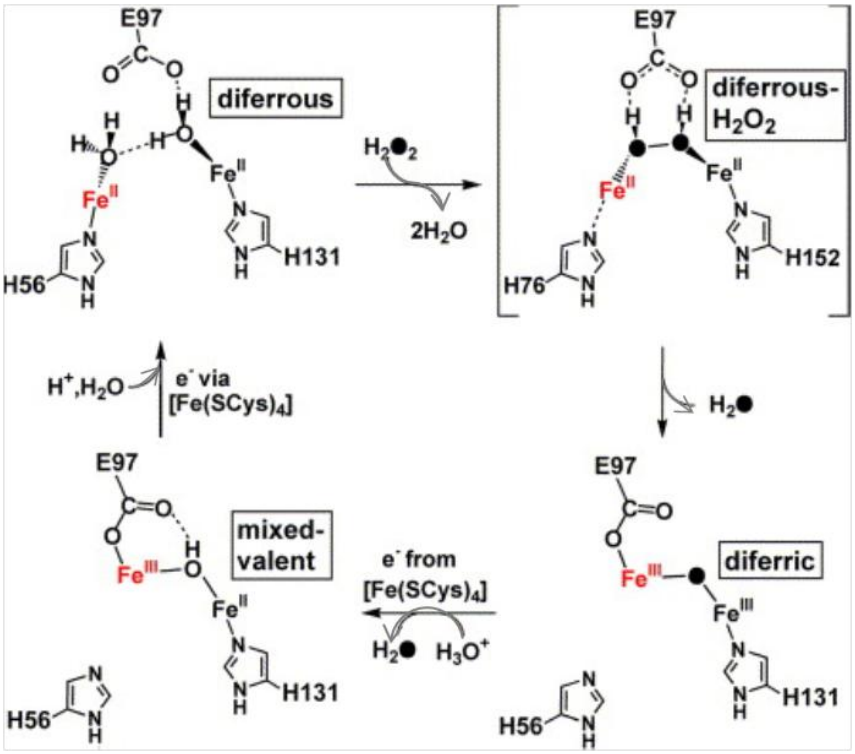

Figure 2.8 – Proposed mechanism for H_2O_2 reduction at the active site of rubrerythrin from *D. vulgaris* (*104*). Oxygens originating from H_2O_2 are in black circles. The iron that moves ("toggling" iron) is in red. Figure from (*86*).

2.2.5 - Physiological electron donors

It has been assumed that rubredoxins are the physiological electron donors for rubrerythrins. These proteins have been found in a wide

variety of genomic organizations. For example in *D. vulgaris* Hildenborough its gene is part of a cluster with genes coding for a rubredoxin and a PerR-like protein (*99*), while in *C. thermoaceticum* there is a five-gene cluster encoding for several enzymes involved in oxidative stress response, for example, superoxide reductase, a flavodiiron protein, a rubredoxin and a high-molecular-weight rubredoxin (*90, 136-137*). Similar organizations occur in other organisms, but also in many cases *rbr*-genes appear to be monocistronic (*90*) (database: Genome Protmap in NCBI (*138*)). It is worth mentioning that rubrerythrins also exist in organisms that appear not to contain any rubredoxin, suggesting that other electron donors have to exist. Furthermore, in almost all cases, the NAD(P)H oxidoreductases which presumably donate electrons to the rubredoxin are not known.

2.3 - Superoxide Reductase

Superoxide reductases (SORs) were first isolated from sulfate reducing bacteria of the *Desulfovibrio* genus (*116, 139*). In 1990 I. Moura and coworkers, reported the isolation and characterization of a novel protein from *D. desulfuricans* (ATCC 27774) and from *D. vulgaris Hildenborough*, containing two iron sites: center I, similar to that of desulforedoxin, and center II, a new type of iron site, which in that preparation was in the ferrous form; for these reasons the protein was named desulfoferrodoxin, Dfx (a contraction of desulforedoxin, ferrous and redoxin).

According to the number of metal centers, there are two types of superoxide reductases: 1) neelaredoxins, or 1Fe-SORs, given their trivial name for their blue color (*neela* in Sanskrit language, as at that time their function was unknown) associated with the iron center II, and 2) desulfoferrodoxins, or 2Fe-SORs (Figure 2.9). Both iron sites are close to the molecular surface and exposed to the solvent. This situation is different from that of superoxide dismutases, in which the

metal centers are embedded inside the protein, at the end of a substrate channel (*70*).

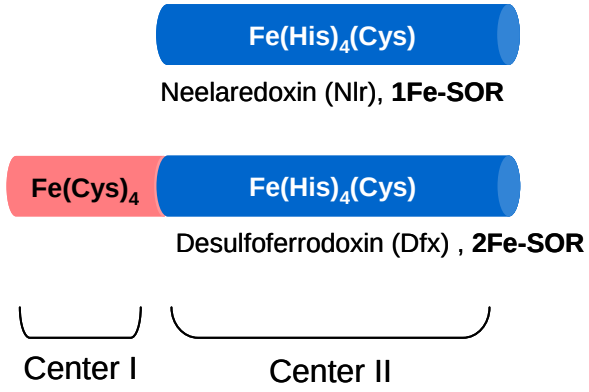

Figure 2.9 – Domain arrangement for 1Fe-SOR and 2Fe-SOR.

In the 2Fe-SORs, center I has an iron coordinated by four cysteines, in a distorted tetrahedral geometry, similarly to desulforedoxins (Figure 2.10-B1) (*113, 140*); however, there is a putative 2Fe-SOR from an uncultured termite group 1 bacterium phylotype Rs-D17 in which center I is of the rubredoxin type (Figure 2.11). The common iron site for the two types of SOR, called center II in 2Fe-SORs, is in the ferrous state coordinated in a square-pyramidal geometry by four nitrogens (three N^{ε} and one N^{δ}) from histidine-imidazoles in the equatorial plane, and the fifth axial position (at the inner side of the protein) is occupied by a cysteine-sulfur (Figure 2.10 B3). It has been generally assumed that no solvent molecule occupies the sixth axial position. The structure of the ferric form has been unambiguously determined only for the 1Fe enzymes from *P. furiosus* (*141*) and *P. horikoshii,* which show that the ferric ion becomes bound to a monodentate carboxylate from a glutamate residue, establishing an octahedral geometry around the iron ion (Figure 2.10 B2). This change in iron-coordination upon oxidation/reduction is accompanied by a significant movement of two

loop regions (Gly9-Lys15 and Gly36-Pro40, in *P. furiosus* 1Fe-SOR), which affects the accessibility to the ferrous iron site.

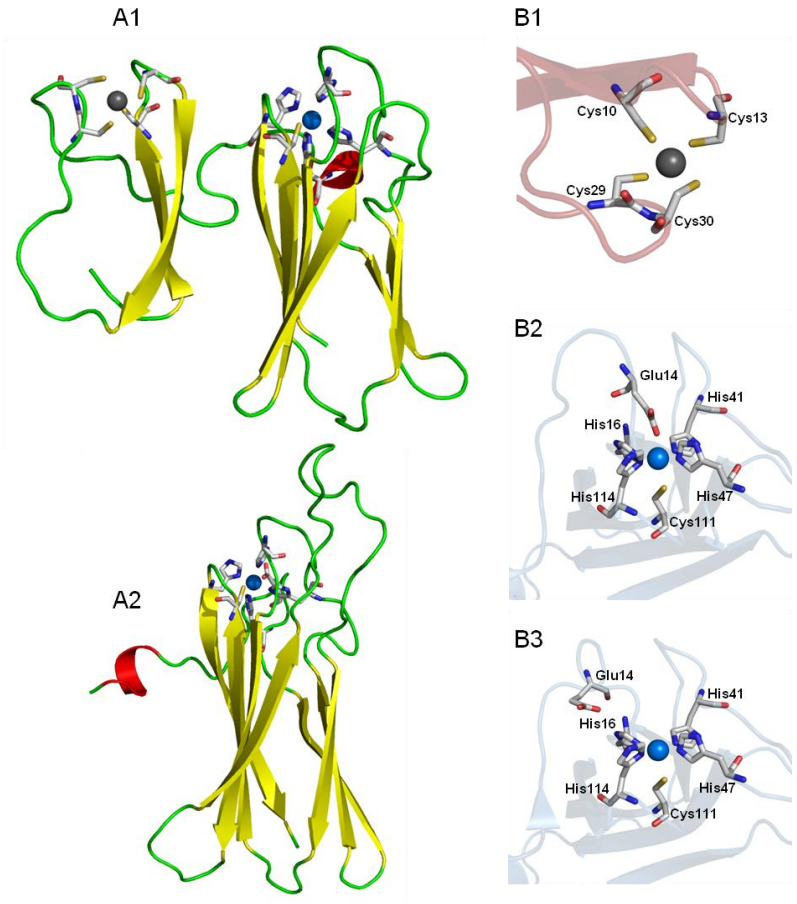

Figure 2.10 – 3D crystal structures of superoxide reductases. A1) *D. desulfuricans* desulfoferrodoxin, 2Fe-SOR (pdb 1DFX); A2) *P. furiosus* neelaredoxin, 1Fe-SOR (pdb 1DO6); B1) structure of Dfx $FeCys_4$ center I; B2, 3) 1Fe-SOR oxidized and reduced center, respectively. Iron ion is represented in a silver (center I) and in blue (center II) spheres. Figure adapted from (*142*).

2.3.1 - Amino acid sequence analysis

It was initially thought that SORs were restricted to anaerobic prokaryotes, but this is not the case: they are also present in facultative microorganisms and in eukaryotes, *e.g.*, from the microaerophilic

protozoan *Giardia intestinalis* (*94*) and from the anaerobic diatom *Thalassiosira pseudonana* (*143*). Superoxide reductases coexist in many organisms with the other superoxide detoxifying enzymes, *i.e.*, superoxide dismutases of the Fe/Mn and/or CuZn types, while other organisms appear to rely solely on SORs for superoxide detoxification. It seems that the superoxide reductases are an example of the evolutionary diversity in nature rather than being a specific type of enzymes designed for protection of particular anaerobes.

It is remarkable that very few amino acid residues are strictly conserved (Figure 2.11); these are 1) the metal ligands - the cysteines of the $FeCys_4$ center (in the 2Fe-SORs), and the four histidines and the cysteine bound to the catalytic center; and 2) the proline at the characteristic motif -(E)(K)H(V)P- and an isoleucine after the third histidine ligand. Other residues that were considered strictly conserved and catalytically important are not at all conserved, such as the above mentioned glutamate residue bound to center II in several oxidized SORs, or the lysine residue, also at the -(E)KHVP- motif, and located close to the catalytic site. The low amino acid conservation establishes the minimal requisites for the catalytic mechanism, as will be discussed later.

2.3.2 - Physiological studies

The first evidence for a possible function of these enzymes came from the observation by D. Touati and coworkers that a DNA fragment of the sulfate reducing bacterium *Desulfoarculus baarsii* was able to complement an *E. coli* superoxide dismutases deletion mutant (*144*). It came as a surprise that this fragment encoded not a superoxide dismutase, but a 2Fe-SOR. These authors further established that site II was the catalytic one, as expression of the 2Fe-SOR first domain was not able to complement the *E. coli* mutant strain (*145*). Later, other SORs (1Fe- or 2Fe-) were also shown to complement the same *E. coli* deletion strain (*e.g.*, (*146-147*)).

Pyrococcus furiosus
Desulfovibrio gigas
Archaeoglobus fulgidus
Nanoarchaeum equitans
Thermofilum pendens
Methanosarcina acetivorans
Clostridium phytofermentans
Desulfovibrio vulgaris
Desulfovibrio desulfuricans
Desulfoarculus Baarsii
Geobacter uraniireducens
Archaeoglobus fulgidus
Treponema pallidum
uncultured bacterium

Figure 2.11 - Amino acid sequence alignment of SORs, using ClustalX (*148*). Residues that bind the catalytic center are indicated by an *; the cysteines binding center I of 2Fe-SORs are encircled by boxes. Strictly conserved residues are shaded in black and residues conserved in majority are shaded in grey; the lysine of the (E)(K)H(V)P(V) motif is marked with an arrow. 1Fe-SORs (Neelaredoxins): *Pyrococcus furiosus* DSM 3638 (gi|18977653|); *Desulfovibrio gigas* (gi|4235394|); *A. fulgidus* (gi|11497956|); *Nanoarchaeum equitans* (gi|41614807|); *Thermofilum pendens* Hrk 5 (gi|119720733|); *Methanosarcina acetivorans* C2A (gi|20092535|). 2Fe-SORs (Desulfoferrodoxins): *Clostridium phytofermentans* ISDg (gi|160880064|); *Desulfovibrio vulgaris* Hildenborough (gi|46581585|); *Desulfovibrio desulfuricans* ATCC 27774 (gi|157830815|); *Desulfoarculus baarsii* (gi|3913458|); *Geobacter uraniireducens* Rf4 (gi|148264558|); *Archaeoglobus fulgidus* (gi|11498439|). Neelaredoxin from *Treponema pallidum subsp. pallidum* str. Nichols (gi|15639809|) and a 2Fe-SOR with a Rd-like domain from an uncultured termite group 1 bacterium phylotype Rs-D17 (gi|189485274|).

Fridovich and coworkers (*149*) proposed that the activity observed for these enzymes was not of dismutation, but of superoxide reduction, leading to elimination of superoxide and formation of hydrogen peroxide, which then led to the now accepted superoxide reductase activity. Apart from the heterologous complementation assays, very few *in vivo* studies have been performed for these enzymes. A *D.* vulgaris mutant strain with increased resistance to oxygen was found to have *dfx* transcriptional levels higher than those of the wt strain (*150*); in agreement with those results, a *D. vulgaris dfx* deletion mutant had a higher sensitivity to oxygen (*150*). An up-regulation of the transcriptional level of SORs encoding genes was also observed in *C. acetobutylicum* (*151*), in *Thermotoga maritima* (*152*) and in *Treponema denticola* (*153*) upon oxygen stress. In contrast, these levels apparently do not change in *D. vulgaris* and *P. furiosus*, under oxidative stress, what may indicate a constitutive expression of the SOR genes (*154-155*).

2.3.3 - Properties of the iron sites

Superoxide reductases have been extensively studied using a wide range of spectroscopic tools, namely UV-Visible, Resonance Raman, EPR, Mössbauer and Fourier Transform Infrared (FTIR). Both iron sites

are in a high spin state in the oxidized (S = 5/2) and reduced (S = 2) forms. Therefore, both exhibit characteristic EPR resonances in the ferric state with variable rhombicities (E/D ~0.1 or ~0.3) (*139, 156-157*). This fact, together with the considerable overlap of the resonances from each center, complicates considerably the EPR spectra of SORs. Therefore, EPR is not a good technique to unambiguously distinguish the two sites in 2Fe-SORs, or to monitor changes at the catalytic site and differentiate active and inactive forms of the enzymes. In contrast, the two sites are easily discernible by electronic absorption (Figure 2.12): center I has the characteristic features of a desulforedoxin, $FeCys_4$ site, with maxima at 375 and 495 nm and a broad shoulder at 560 nm; center II has a broad absorption band at ~ 660 nm, which is responsible for the blue color of 1Fe-SORs, or the grey color (the mixture of pink and blue) for the oxidized 2Fe-SORs, and a shoulder at ca 330 nm. The 660 nm band has been attributed to a sulfur to iron charge transfer transition (*157*). In the fully reduced state both types of SORs are colorless, while the half-reduced (center I oxidized, center II reduced) 2Fe-SORs are pink. These features have been essential to elucidate the catalytic mechanism of SORs, coupling absorption spectroscopy to fast kinetics methods (pulse radiolysis and stopped-flow).The two centers have quite distinct reduction potentials: center I close to 0 mV and center II between 190 and 365 mV, at neutral pH. This large difference has also been important to study in detail the events at the catalytic center II without interference of center I. The potentials for the catalytic center are similar to those reported for superoxide dismutases, and perfectly adequate for superoxide reduction (E'_0 ($O_2^{\cdot-}/H_2O_2$) = 890 mV, at pH 7).

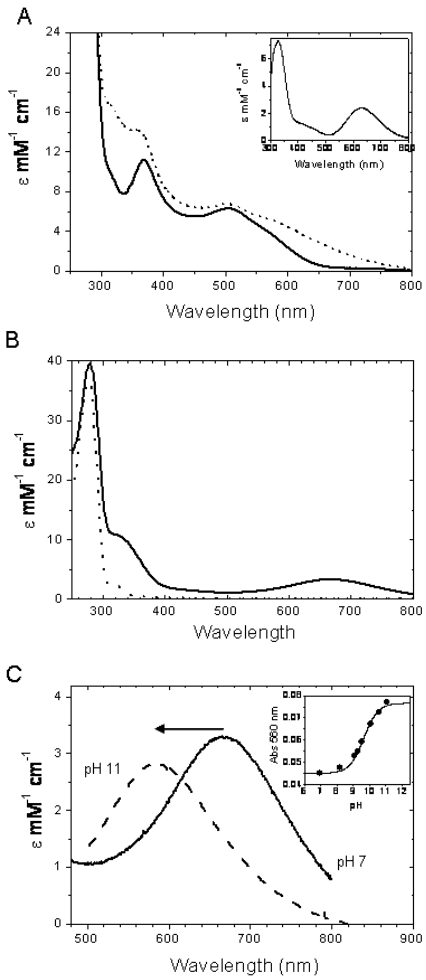

Figure 2.12 - Characteristic UV-visible spectra of superoxide reductases. A) Spectra of *Archaeoglobus fulgidus* 2Fe-SOR in the half-reduced state (center I oxidized, center II reduced in a solid line) and fully oxidized (both centers oxidized, dashed line); inset shows the difference spectrum of those two, *i.e.*, the features of center II. B) Spectra of *A. fulgidus* 1Fe-SOR in the oxidized (solid line) and reduced states (dotted line). C) pH-induced spectral changes of the characteristic absorbance band at 660 nm, of *A. fulgidus* 1Fe-SOR; inset shows the pH-titration followed by visible spectroscopy. From (*142*).

2.3.4 - Superoxide reduction mechanism

Since the isolation of the first 1Fe-SOR from *D. gigas* (*139*), there has been increasing evidence for pH dependent equilibria at or near the catalytic site, some of which are of mechanistic relevance. In fact, the reductase reaction involves also the consumption of two protons (eq 2.6) since at physiological pH values the superoxide anion is in the basic, deprotonated form (pK_a ~4.8) (Chapter 1).

$$Fe^{2+} + O_2^{\cdot-} + 2H^+ \rightarrow Fe^{3+} + H_2O_2 \qquad \text{(eq 2.6)}$$

At pH above 9, the glutamate (sixth iron ligand) containing enzymes, (in the oxidized state), exhibit a drastic change of the electronic absorption spectra, with the absorption band shifting to ~590 nm (Figure 2.12C). This transition has an apparent pK_a of ~9.5. The chemical identity of the basic form was established by Resonance Raman spectroscopy. A vibrational band was detected at 466-471 cm^{-1}, characteristic of a high-spin Fe^{3+}-OH stretching mode vibration, in the wt 2Fe-SOR from *D. baarsii*, and its E47A and K48I mutants, which disappears at acidic pH values and exhibits a clear shift when the samples were prepared in $H_2{}^{18}O$ or D_2O, establishing it as an iron-hydroxide form (*158*). The same observation was reported for the enzymes from *Archaeoglobus* (*A.*) *fulgidus* and *Nanoarchaeum* (*N.*) *equitans* (*159*). Therefore, this transition corresponds in fact to a ligand-exchange, the glutamate ligand being substituted by a hydroxide anion, and the value of the apparent pK_a gives an indication of the relative affinities of the iron ion for each ligand, *i.e.*, the pK_a is not a true proton ionization constant for the glutamate-bound enzymes. This ligand exchange has been also observed by EPR spectroscopy (a rhombic EPR spectrum, with E/D~0.25 appears at high pH (*139, 157, 160*)), and by FTIR (*161*). In site-directed mutants of the glutamate ligand, as well as for the *N. equitans* enzyme (a natural glutamate "mutant" (*162*)), a pH dependent equilibrium is also observed, but with a much lower apparent pK_a, *c.a.* 2 units lower (*160, 163*). Again, Resonance Raman data has shown that the basic form corresponds to a hydroxide-bound iron. However, in these cases, the pH dependence can be attributed to a true protonic equilibrium due to the protonation of the hydroxide ligand at acidic pH values. These processes are essential to understand the reactivity of these enzymes with superoxide. The same pH dependent processes were shown to affect (decrease) the reduction potentials of center II from the *D. baarsii* 2Fe-SOR, but not that of center I (*160*) (see chapter 6).

The mechanism of superoxide reduction has been scrutinized mainly using pulse radiolysis. This approach allows the production of defined amounts of the superoxide anion in a very fast time scale (superoxide is formed in the first microseconds after pulsing an air-saturated solution with electrons (*164*)), and in a rather "clean" way, and was essential to establish the oxidative part of the catalytic mechanism of these enzymes (reduction of superoxide to hydrogen peroxide and concomitant oxidation of the ferrous enzyme to the ferric, resting state). The reaction is initiated with the enzyme in the reduced state (colorless, as there is no electronic absorption in the visible region). The enzyme solution is then pulsed with an electron beam generating substoichiometric superoxide and the reaction is monitored by single wavelength optical spectroscopy. The spectral features of each intermediate are obtained through measurements at a sufficient number of wavelengths (which enables to reconstruct the electronic spectrum) and for a sufficiently long time range (up to seconds). Using this method and a sufficiently large concentration of enzyme, the same sample can be pulsed several times, and the amount of protein that reacted may be quantified, from which the extinction coefficients of each species can be determined.

The first step of the reaction appears to be common to all enzymes so far studied (Figure 2.13): upon the superoxide pulse, a first intermediate, T1, is formed, with an absorption maximum at *ca* 620 nm (*163*). This process occurs with a second order rate constant of ~10^9 $M^{-1}s^{-1}$, *i.e.*, at diffusion-limited rate. The observation of the visible absorption of T1 indicates immediately that at this stage the iron is already in a ferric form, Fe (III), which implies that the superoxide anion was concomitantly reduced to peroxide, and there is a general agreement that T1 corresponds to a ferric-(hydro) peroxo species (*165-168*). This intermediate, in the *A. fulgidus* enzyme, subsequently decays in a pH dependent pseudo first order, unimolecular process, to another species T2, with an associated pK_a of 6.5 and optical properties

identical to those observed for a species to which a hydroxide is bound (*158*), for pH values above 6.5. This observation establishes that at this stage the product was already released from the enzyme. For the enzyme, the transient state T2 decays further to the resting, oxidized state (k_3), again in a unimolecular process, presumably re-binding the glutamate ligand, displacing the H_2O or the OH-bound ligand, depending on the pH. For the glutamate mutants, as for the *N. equitans* enzyme, T2 is the final state of the oxidative part of the catalytic cycle, with the typical associated pK_a of 6.5. For the 2Fe-SOR from *D. baarsii* and the 1Fe-SOR from *Treponema pallidum*, two intermediates are also detected, while for the *D. vulgaris* and *Giardia intestinalis* enzymes, T1 decays directly to the resting form or glutamate-bound form, also in a unimolecular process *i.e.*, no intermediates could be detected (Figure 2.13).

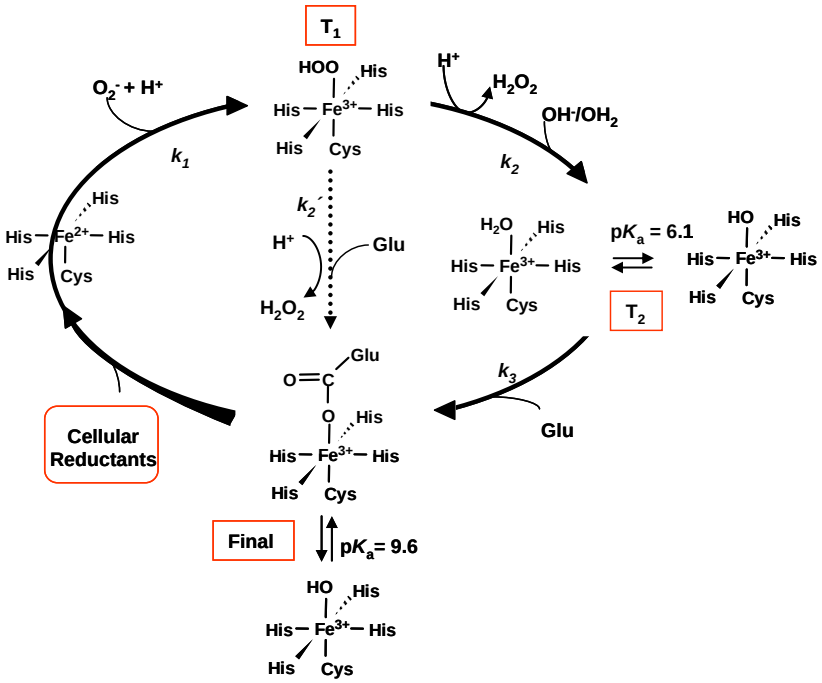

Figure 2.13 – Mechanism of the catalytic reduction of superoxide, evidencing the detected intermediates. Adapted from (*142*).

2.3.5 - Role of specific aminoacid residues

Two particular amino acid residues have been considered important for the mechanism of superoxide reduction, apart from the metal ligands: the glutamate ligand (E12 in *A. fulgidus* 1Fe-SOR, E47 in *D. vulgaris* 2Fe-SOR), and the lysine of the motif –EKHVP- (K13 in *A. fulgidus* 1Fe-SOR) (Figure 2.11). The glutamate was proposed to assist the release of the product from the catalytic site, or to be involved in some proton transfer event. The lysine residue was considered either to provide a positive surface charge near the active site, thereby contributing to increase the rate constant for binding of the anionic substrate, or to provide a proton and/or to stabilize through an hydrogen-bond the hydroperoxide ligand (T1).

2.3.6 - Physiological electron donors – Reductive path

It has been generally assumed that rubredoxins are the direct electron donors to superoxide reductases, which was initially suggested due to the genomic organization of the respective genes in *D. vulgaris* (*169*). The analysis of the complete genomes also reveals that the genes coding for SORs are found in quite diverse genetic *loci*; only in a few cases they are found together with genes encoding either their electron donors (rubredoxins, as in *D. vulgaris,* (*99*)), or other oxidative stress responsive genes.

Indeed, it has been demonstrated that for 1Fe- and 2Fe-SORs, reduced rubredoxins are quite efficient electron donors to center II, with second order rate constants in the order of ~10^6-10^7 $M^{-1}s^{-1}$ (*121, 170-171*). These rubredoxins are in turn reduced by NAD(P)H dependent oxidoreductases. In addition to rubredoxin, it was also demonstrated, by steady-state kinetics, that desulforedoxin is able to function as an electron donor to *D. gigas* SOR (*172*). However, it is now quite clear that other physiological electron donors must exist as a large number of organisms having genes encoding SORs do not contain genes coding for rubredoxins.

Chapter 3

3 - Microaerobes, anaerobes and hyperthermophiles: response to oxidative stress

3.1 - *Campylobacter jejuni*

Campylobacter (*C.*) *jejuni* from the delta-epsilon group of proteobacteria is a microaerophilic, gram-negative, flagellate and spiral pathogenic bacterium (Figure 3.1). It is related to the *Helicobacter pylori* pathogenic bacteria and colonizes the small bowel and the colon, where it finds a more microaerophilic environment. Worldwide infection by this pathogenic bacterium causes food-borne diarrhoeal disease and has been linked to reactive arthritis and Guillain-Barré syndrome (*173-174*). This syndrome is a neurologic disease that causes ascending paralysis and is triggered by a preceding bacterial infection. These infections are associated with the consumption of contaminated poultry, meat products and water. Due to the socioeconomical importance and to its pathogenicity it has been the scope of many studies.

Figure 3.1 – Electron Microscopy image of *Campylobacter jejuni* cells (*175*).

The re-annotation of *C. jejuni* NCTC 11168 genome (*176*), after the prior genomic study in the year 2000 (*177*), revealed a small genome with 1,641,481 base pairs (30.6% G+C) predicted to encode 1,643 proteins. It is one of the densest bacterial genomes sequenced with 94.3% of the genome encoding for proteins. It contains hypervariable sequences, which consists in polymers of nucleotides that comprise clusters for biosynthesis or modification of surface structures, as lipooligosaccharide and extracellular polysaccharide biosynthesis and flagellar modification (*177*). These homopolymeric structures may be

related to a survival strategy of *C. jejuni* for host colonization (*177*). The capsule is important for serum resistance, for the adherence and invasion of epithelial cells and virulence (*174*). *C. jejuni* invades intestinal epithelial cells, as an intracellular bacterium, leading to the induction of cytokines such as IL-8 and CLXCL20, that are proposed to initiate a pro-inflammatory response from dendritic cells, macrophages and neutrophiles (*174*) (Figure 3.2).

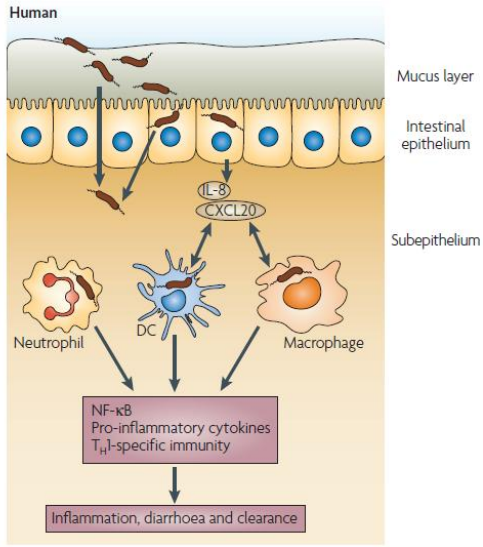

Figure 3.2 – Innate immune response to *C. jejuni* in humans. The bacterial cells interact with the epithelial cells from the intestine causing a production of cytokines. *C. jejuni* cells bind to it and are internalized by the epithelial cells. IL-8 and CXCL20 cytokines will induce the action of dendritic cells (DC), macrophages and neutrophiles, initiating a massive pro-inflammatory response (From (*174*)).

C. jejuni as a microaerophilic organism requires O_2 for growth only at low oxygen tensions of 2-10%, conditions that are found in the intestinal tract (*178*). Studies revealed that at higher oxygen levels (15-21%), the survival of *C. jejuni* was only enabled by the addition of superoxide dismutase, catalase, sodium dithionite or histidine to the growth medium (*179-181*), suggesting that this bacterium has a higher susceptibility to reactive oxygen species than aerobes. The microaerophilic lifestyle is made possible by the presence of oxygen-consuming enzymes such as

a cbb_3 type oxygen reductase (*182*) and oxidative-stress scavenging enzymes. Indeed, the genomes of *Campylobacter* species reveal the presence of genes encoding for several of the canonical proteins and enzymes involved in detoxification of reactive oxygen species, such as catalase (KatA), superoxide dismutase (Fe-SOD), alkyl hydroperoxide reductase (AhpC), truncated globin (Ctb), thiol peroxidase, Fur (Ferric iron uptake regulator) and ferredoxin (FdxA) (*177, 183-188*). An *ahpC* mutant in *C. jejuni* was shown to be less able to survive upon exposure to atmospheric oxygen levels (*184*), especially during the stationary phase. Upstream of *ahp*C, there is a gene encoding for a ferredoxin. Its expression is iron-induced and the mutation of the gene affected the aerotolerance of *C. jejuni* cells (*187*).

Table 3.1 – Example of proteins from *C. jejuni* with an up-regulated expression in response to iron limitation conditions in the growth medium. From (*189-190*).

Proteins in *C.jejuni* expressed under low iron condition	**Function**
PerR	Peroxide stress regulator
KatA	Catalase
AhpC	Alkyl hydroperoxide reductase
Thiol peroxidase	peroxidase
Fe-SOD	Fe-Superoxide Dismutase
Cft	Ferritin
CfrA	Ferric-enterobactin receptor
ChuABCD	Heme uptake system

In *C. jejuni* the absence of iron leads to an up-regulation of genes encoding for oxidative stress defense proteins and iron acquisition systems (Table 3.1). The best known iron capture systems are the ferric ion chelators. The enterobactin siderophore, CfrA in *C. jejuni* is regulated by Fur, and is up-regulated in its absence (*191*). Another iron uptake system, the heme uptake system ChuABCD (Table 3.1) was found in *C. jejuni* as a cluster of five genes *cj1613c-cj1617*. The utilization of iron occurs due to the degradation of the heme, performed

by the *cj1613c* gene product, that acts as a heme oxygenase (*192*). This system is used as an instrument of colonization and survival in the host.

In an enriched iron medium, the expression of genes involved in energy metabolism or encoding for proteins that require iron for their function, as cofactors, is up-regulated. Examples are, succinate: quinone oxidoreductase (SdhABC) and periplasmic nitrate reductase (NapABGH) (*189-190*). These studies further showed that a non-heme iron protein, Cj0012c, was up-regulated in these conditions; this protein was shown to be an oxidative stress-sensitive protein. It has three iron binding motifs and is a rubrerythrin-like protein (*106*), and was recently designated as desulforubrerythrin (DRbr; described later in Chapters 4 and 5).

3.2 - Hyperthermophiles: *Ignicoccus hospitalis* and *Nanoarchaeum equitans*

By definition, hyperthermophiles are organisms that do not propagate below 60ºC. Hyperthermophiles from the Archaea and Bacteria domains, grow optimally from 80ºC to 122ºC and were first discovered in 1981 (*193*); the highest growth temperature of 122ºC was recently reported for *Methanopyrus kandleri* (*194*).

Hyperthermophiles are found within high temperature environments, such as hot terrestrial and deep-sea hydrothermal vents of volcanic origin. In the ribosomal 16S rRNA based-phylogenetic tree, hyperthermophiles occupy all the short deep branches closer to the root (Figure 3.3). The earliest archaeal phylogenetic lineage is represented by the members of the novel phylum of *Nanoarchaeota*. Due to their position in the universal phylogenetic tree and due to their characteristics, hyperthermophiles have been proposed to be the present day life forms closest to the last common ancestor (*193*).

A large number of hyperthermophilic organisms gain energy by inorganic redox reactions and use CO_2 as a carbon source to build-up organic cell material, and so behave as chemolithoautotrophs. Electron donors can be molecular hydrogen as well as sulfide, sulfur and iron. Anaerobic respiration will have as final electron acceptors nitrate, sulfate, sulfur and carbon dioxide.

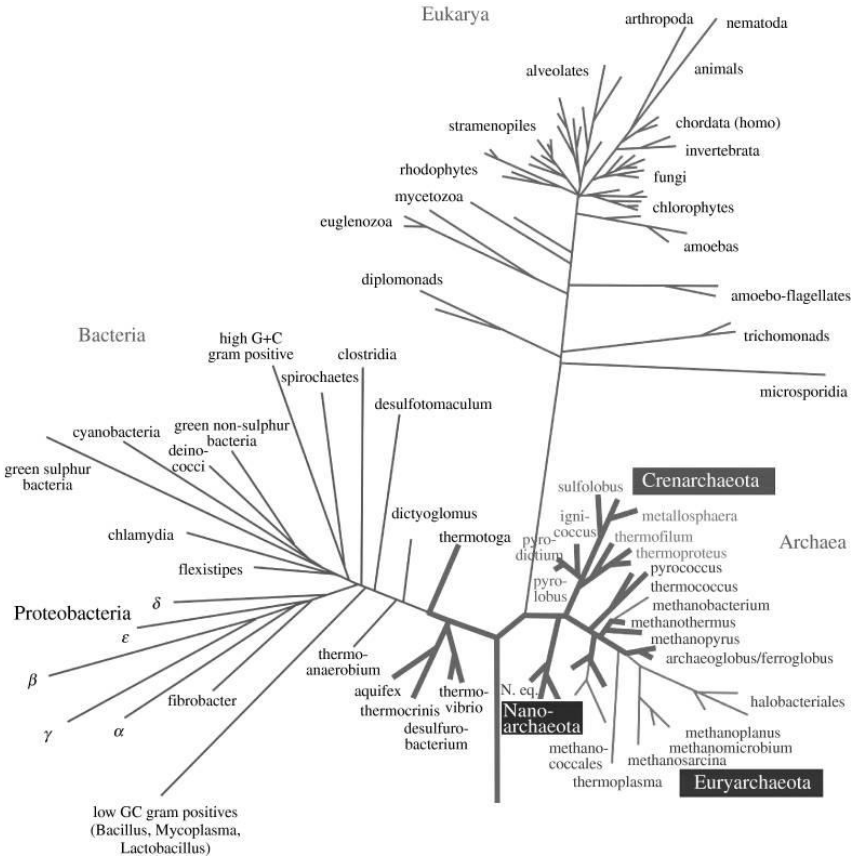

Figure 3.3 – 16S rRNA-based phylogenetic tree (the thick lines represent hyperthermophilic organisms). From (*193*).

Hyperthermophiles are so far found in the Bacterial phyla of *Thermotogae* and *Aquificae*, and in all phyla of Archaea,

Crenarchaeota, *Eukyarchaeota* and *Nanoarchaeota*. Within the *Crenarchaeota* phylum there is the genus *Ignicoccus*, which comprises a chemolithoautotrophic organism named *Ignicoccus hospitalis* KIN4/I^T, isolated in 2007 from a submarine hydrothermal system at the Kolbeinsey Ridge (*195*). This archaeon is an anaerobic organism that has an optimum growth temperature of 90ºC and an optimum pH of 5.5. This species couples CO_2 fixation with sulfur respiration using molecular hydrogen as electron donor. CO_2 fixation is done through a newly discovered pathway called the dicarboxylate/4-hydroxybutyrate cycle (*195*). The genome of *I. hospitalis* consists of a single circular chromosome with almost 1.4 Mbp and a 56.6% of G+C content with 96.6% of genes encoding for proteins (*195*). This organism and the other *Ignicoccus* species (*I. islandicus* and *I. pacificus*) show a cell envelope with particular features, lacking any rigid cell component as S-layer or pseudomurein as currently found for other Archaea and Bacteria (*196*). Transmission electron microscopy (*197*) revealed that the cells have two membranes, a cytoplasmatic membrane with an irregular shape, surrounded by vesicles transferred from the cytoplasm to the periplasm (Figure 3.4A). This periplasmic space has 20 up to 500 nm of width and the outer membrane that envelopes the cell consists of archaeal isoprenyl diether lipids and of million copies of a themostable oligomeric pore-forming protein (*197*).

I.hospitalis forms an intimate association with *Nanoarchaeum* (*N.*) *equitans*, unique among the Archaea domain (Figure 3.4). *N. equitans* cells can only grow in the presence of and in contact with *I. hospitalis* cells. This “parasite” has a very compact genome of only 0.49 Mbp (94% protein encoding genes), being the smallest genome of all known Archaea, and lacks genes for the biosynthesis of lipids, aminoacids, nucleotides and cofactors. Therefore this association looks like an essential way of obtaining the components for maintaining cell viability. In *I. hospitalis* small vesicles that engulf cytoplasmatic material will migrate through the large periplasm to the outer membrane and pore-

forming proteins, that are formed at the point of contact of the two organisms, will allow the transfer of cellular components between the two organisms (*197*). There is probably a concerted mechanism that supplies *N. equitans* cells as revealed by ultra-structural investigations (Figure 3.4B-G). The mechanisms that enable this association are still under study.

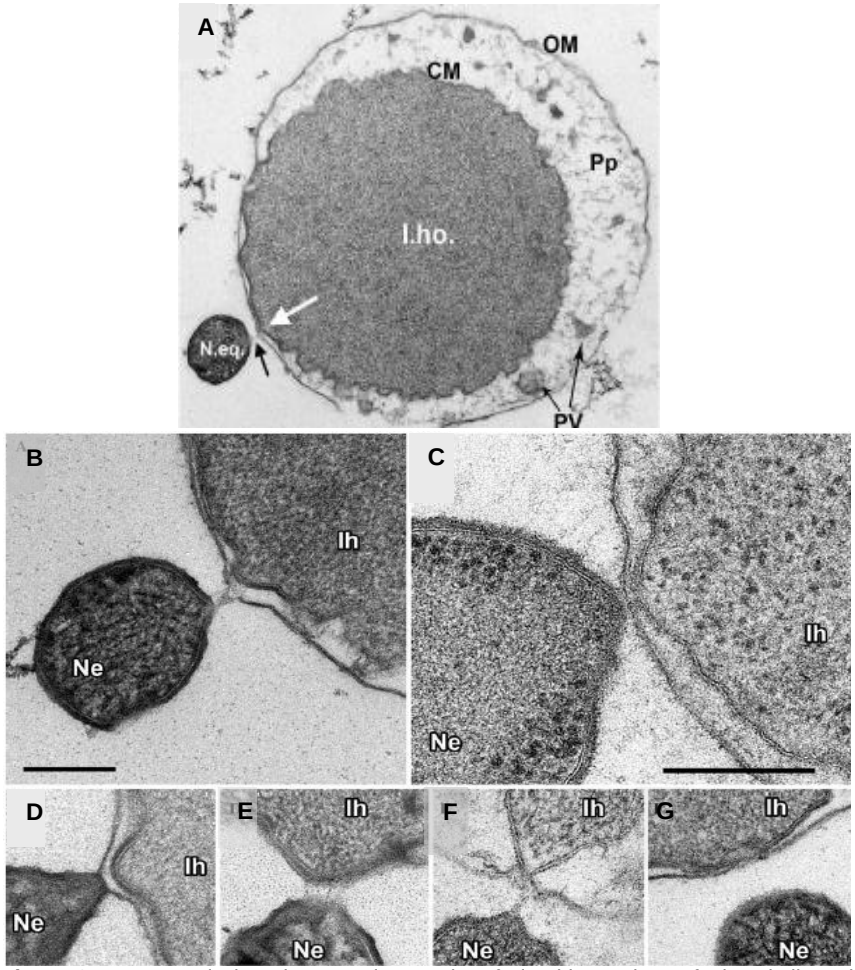

Figure 3.4 – Transmission electron micrographs of ultrathin sections of *I.hospitalis* and *N.equitans* A) *Iho*, *I.hospitalis* cell; CM, cytoplasmatic membrane; Pp, periplasm; OM, outer membrane; PV, periplasmic vesicles; *N.eq*, *N.equitans* cell, from (*198*); B) *Ih* (*I. hospitalis*) and *Ne* (*N. equitans*) connected by fibrous material; C) Outer membrane of *Ih* in direct contact with the membrane of *Ne*; D) to G) Examples of the variation of contact sites between *Ih* and *Ne.* B to D from (*197*).

Proteomic analysis of a co-culture of these organisms revealed that the presence of *N. equitans* increases the expression of proteins from *I. hospitalis* involved in energy generation, including the constituents of ATP synthase, [Ni-Fe] hydrogenase and polysulfide reductase (*199*). The increased rate of respiration and ATP synthesis suggests a higher energy demand resulting from the metabolic needs of *N.equitans* (*199*). Both *I. hospitalis* and *N.equitans* have mechanisms to deal with the toxicity of reactive oxygen species. In *I. hospitalis* a gene encoding for a superoxide reductase (SOR) is present (Igni_1348) as well as an alkyl hydroperoxide reductase (Igni_0459). Another small protein is encoded and expressed in high amounts and is a erythrin-like protein (Igni_0095) (*199*). In *N.equitans* most ROS scavenging systems are also absent; its genome encodes only for a SOR (*162*) and a thioredoxin peroxidase (Table 3.2).

Table 3.2 – *I.hospitalis* and *N.equitans* genes that encode proteins involved in oxidative stress (*199*).

Oxidative stress related genes from *I. hospitalis*	**Protein name**
Igni_0095	erythrin-like protein
Igni_0459	Alkyl hydroperoxidase
Igni_1348	Superoxide reductase
Igni_1363	Heat-shock protein
Oxidative stress related genes from *N. equitans*	
NEQ011	Superoxide reductase
NEQ344	Heat-shock protein
NEQ459	Thioredoxin peroxidase

The analysis of the aminoacid sequence of the two SORs from these two organisms revealed that they lacked two aminoacid residues, conserved among the majority of SORs, a lysine in *I. hospitalis* SOR and a glutamate in *N. equitans* SOR, placed in the motif **EK**HVP and enrolled in the superoxide reduction mechanism of these enzymes. The

SOR from *I. hospitalis* is within the scope of this thesis in Chapter 6 and 7 and the SOR from *N. equitans* was studied previously (*162*) (see also Chapter 7).

Part II –

Desulforubrerythrin:

Experimental Results

Introduction

Campylobacter (*C.*) *jejuni* is a Gram-negative pathogenic proteobacterium of the delta-epsilon group. It is the leading cause of food-borne diarrheal disease worldwide, having an infection dose as low as 500-800 bacteria; about two million cases/year of *C. jejuni* associated gastroenteritis are estimated to occur just in the United States, and more severe sequelae may occur subsequently to *C. jejuni* infection (*174, 200*). *C. jejuni* colonizes the small bowel and the colon, where it finds a microaerophilic environment. In fact, *C. jejuni* is only able to grow at low oxygen partial pressures (*201-202*). The microaerobic lifestyle is made possible by a concerted interplay of oxygen-consuming enzymes (namely the cbb_3 type oxygen reductase (*203*), which has a high oxygen affinity (*204*)) and oxidative-stress responsive enzymes: microaerophiles like *C. jejuni* are particularly vulnerable to the detrimental effects of oxidative stress and need to have efficient mechanisms to eliminate oxygen and its toxic species. Indeed, the genomes of *Campylobacter* species reveal the presence of genes coding for several of the canonical enzymes and proteins involved in detoxification of reactive oxygen species, such as catalase, superoxide dismutase, alkyl hydroperoxide reductase, hemoglobin Ctb, thiol peroxidase, DNA-binding proteins from starved cells (Dps) and Ferritin (*177, 184-185, 205*). Some of these enzymes have been shown to be important for the colonization and persistence within macrophages (*e.g.,* (*206-207*)). Apart from those enzymes, in recent years several novel systems involved in oxidative stress response have been described in anaerobes and microaerobes. Among those are the superoxide reductases (SORs) and rubrerythrins (*e.g.,* (*86, 208*)) (see Chapter 2). Rubrerythrins constitute a family of proteins with two types of iron sites: a non-sulfur diiron center of the μ-oxo bridged histidine/carboxylate family, located in a four-helix bundle structural domain, and a rubredoxin-type [$FeCys_4$] center, located at the C-

terminal in most rubrerythrins. This protein family received this trivial name due to the presence of the rubredoxin and hemerythrin-like diiron centers (*85, 209*). Since the identification of the first rubrerythrin in the sulfate reducing bacterium *Desulfovibrio* (*D.*) *vulgaris* (*85*), they have been found in the most diverse organisms of the three life domains, Archaea, Bacteria and Eukarya (*92, 102, 128*). Several physiological roles were proposed for these proteins, but the most consensual is hydrogen peroxide reduction, linked to NAD(P)H oxidation (*90, 100*). Rubrerythrins have been found to complement catalase null strains, and rubrerythrin deletion mutants are more sensitive to oxygen and hydrogen peroxide (*93*). In the genome of *C. jejuni* NCTC 11168 there is a gene, *cj0012c*, that encodes for a rubrerythrin-like protein (*106*). This protein was identified by Yamasaki M. and co-workers and they verified that the exposure of *C. jejuni* cell extracts to different concentrations of H_2O_2 led to the degradation of Cj0012c, suggesting that it is involved in H_2O_2 oxidative stress response (*106*). A preliminary analysis of the deduced amino acid sequence suggested the presence of an additional domain at the N-terminus, apart from the rubrerythrin ones, namely, a putative desulfoferrodoxin-like domain, which led to the initially proposed name for this protein: **R**ubredoxin oxidoreductase (rbo, the previous designation for desulfoferrodoxins) – **R**ubrerythrin-like protein from ***C****ampylobacter* (Rrc) (*106*). Desulfoferrodoxins are 2Fe superoxide reductases (see Chapter 2), which have at the N-terminus a non-catalytic desulforedoxin-like domain (*208*). Quite importantly, it had been shown that the *cj0012c* gene was regulated by PerR, (*207*) as well as by Fur (*189-190*), which suggests its involvement in oxidative stress response as previously proposed (*106*). Bacterial factors that combat reactive species enable the organisms to persist inside host cells, including macrophages, *i.e.*, elucidation of oxidative stress responses is critical to understand pathophysiology (*e.g.* (*202*)). Therefore, we set to extensively characterize this novel protein from *C. jejuni*, identifying its three metal sites, and establishing its *in vitro* function as a NADH-linked hydrogen peroxide reductase (Chapter 4). Furthermore, due to the

unambiguous identification of each protein domain we have renamed the protein to desulforubrerythrin (DRbr).

DRbr is to date the only studied example from the rubrerythrin family containing a third domain, namely a N-terminal desulforedoxin module, and no structural information is available. Analyzing all the known crystallographic structures of rubrerythrin family members, it is known that for the cases where the protein is composed of a four helix bundle and a rubredoxin domain, this domain is always close (*c.a.* 13 Å) to the diiron center (*103, 130, 133*). The structural fold of the Dx domain is known from the crystallographic structure of desulforedoxin itself and also from the Dx domain of the 2Fe superoxide reductases (*113, 140*). Although structural information is known for each individual domain of DRbr, the lack of a complete structural model for DRbr is still limiting our understanding of the structural arrangement of the different domains and their role in the reaction mechanism with hydrogen peroxide. The X-ray structure of this rubrerythrin-like protein is here reported (Chapter 5) and represents the first structure of a rubrerythrin protein with these domains.

Chapter 4

Summary

A novel multidomain metalloprotein from *Campylobacter jejuni* was overexpressed in *Escherichia coli*, purified and extensively characterized. This protein is isolated as a homotetramer of 24 kDa monomers. According to the amino acid sequence, each monomer was predicted to contain three structural domains: an N-terminal desulforedoxin-like domain, followed by a four-helix-bundle domain harboring a non-sulfur µ-oxo diiron center, and a rubredoxin-like domain at the C-terminus. The three predicted iron sites were shown to be present and were studied by a combination of UV-Visible, EPR and Resonance Raman spectroscopies, which allowed the determination of the electronic and redox properties of each site. The protein contains two $FeCys_4$ centers with reduction potentials of +240 mV (desulforedoxin-like center) and +185 mV (rubredoxin-like center). These centers are in high-spin configuration in the as-isolated ferric form. The protein further accommodates a µ-oxo bridged diiron site with reduction potentials of +270 and +235 mV for the two sequential redox transitions. The protein is rapidly reoxidized by hydrogen peroxide and has a significant NADH-linked hydrogen peroxide reductase activity of 3.9 ± 0.5 µmol H_2O_2 $min^{-1}mg^{-1}$. Due to its building blocks and its homology to the rubrerythrin family, the protein is named desulforubrerythrin (DRbr). It represents a novel example of the large diversity of the organization of domains exhibited by this family of enzymes.

This Chapter includes material published in

"Desulforubrerythrin from *Campylobacter jejuni*, a novel multidomain protein", **Pinto AF**, Todorovic S, Hildebrandt P, Yamazaki M, Amano F, Igimi S, Romão CV, Teixeira M. 2011J Biol Inorg Chem.;16(3):501-10

Pinto AF is responsible for the experimental work and paper preparation presented, with the exceptional collaboration from:

Yamazaki M, Amano F and Igimi S that cloned the gene *cj0012c* into the pMAL vector and generously sent to us the plasmid transformed into JM109 *E. coli* cells.

Todorovic, S and Hildebrandt, P were responsible for the Resonance Raman spectroscopic data and fruitful discussions.

4 - Desulforubrerythrin, a novel multidomain protein

4.1 - Experimental Procedures

Expression of recombinant DRbr

The pMAL system (New England Biolabs) (*210*) was used for cloning the gene *cj0012c* from *C. jejuni* NCTC11168 as previously described (*106*) and transformed into *E. coli* strain BL21DE3 cells. Overexpression of DRbr was performed by growing this strain aerobically at 37 ˚C in M9 minimal medium, with 20 mM glucose, 400 µM $FeSO_4$ and 100 µg/mL ampicilin. When the optical density at 600 nm reached 0.3, isopropyl-1-thio-β-D-galactopyranoside (IPTG) was added (250 µM final concentration), and after *c.a.* 16 h the cells were harvested by centrifugation, resuspended in a buffer containing 50 mM Tris-HCl pH 8, 100 mM NaCl, 1 mM $MgCl_2$, 0.1 mg/mL lysozyme and 20 µg/mL DNase I, and stored at -80˚C. The high amount of iron was essential to obtain the protein with the correct amount of iron incorporated.

Purification of recombinant DRbr

All purification procedures were carried out under anaerobic conditions at 4˚C, in a Coy glove box, with an O_2-free atmosphere constituted by a mixture of 95% argon and 5% hydrogen; all buffers were degassed and flushed with argon. The DRbr was followed throughout the purification procedure by SDS-PAGE (*211*) and UV/Visible spectroscopy. The soluble cellular extract was obtained after passing the cell suspension three times through a French press (35000 psi), followed by ultracentrifugation at 125 000 g for 1 h at 4˚C. It was subsequently applied onto a Q-Sepharose Fast Flow column (XK 26/10, GE Healthcare) previously equilibrated with 20 mM Tris-HCl (pH 7.2), and eluted at 2 mL/min with a linear gradient from 0 to 1 M NaCl in the same buffer. The DRbr fraction eluted at *c.a.* 0.2 M NaCl was then dialyzed overnight against 10 mM potassium phosphate (KP_i) pH 7.0 buffer and loaded onto a Bio-gel hydroxyapatite type II column (XK16/40, GE

Healthcare), equilibrated with the same buffer. The protein was eluted with a linear gradient from 0 to 1 M KPi at pH 7.0. Fractions containing the protein eluted at ~0.3 M KPi and were concentrated in a Diaflo (Amicon) using a YM10 membrane and applied to a molecular filtration column, Sephadex 75 (XK 26/60, GE Healthcare), equilibrated with 20 mM Tris-HCl (pH 7.2) and 150 mM NaCl. The final fraction was concentrated and its purity was verified by SDS-PAGE.

Determination of protein concentration, metal content and molecular mass

The protein concentration was assayed by the bicinchoninic acid method (BCA) (*212*), and the iron content was determined using 2, 4, 6-tripyridyl -1, 2, 3-triazine (TPTZ) (*213*) and by inductively coupled plasma emission spectrometry (ICP); the zinc content was also evaluated by ICP. The molecular mass of the protein was determined by size-exclusion chromatography on a Superdex 200 column (XK 10/300, GE Healthcare), using appropriate molecular mass standards.

Sequence alignment and dendogram

Amino acid sequence alignments were performed with ClustalX (*148*) and Genedoc (*214*).

Spectroscopies

UV/Visible spectra were acquired with a Shimadzu UV-1603 spectrophotometer; EPR spectra were collected by a Bruker EMX spectrometer, equipped with an ESR 900 continuous-flow helium cryostat from Oxford Instruments.

For Resonance Raman studies, about 2 µL of 3 mM protein (in 20 mM Tris-HCl, pH 7.2) were introduced into a liquid nitrogen-cooled cryostat (Linkam THMS600) mounted on a microscope stage and cooled down to 83 K. Spectra of the frozen sample were collected in backscattering geometry using a confocal microscope coupled to the Raman

spectrometer (Jobin Yvon U1000), and the 413 nm excitation line from a krypton ion laser (Coherent Innova 302). For isotopic labeling experiments, the protein was lyophilized and then re-dissolved in $H_2{}^{18}O$ or D_2O, and measured as described above. Typically, spectra were accumulated for 60 seconds with a laser power at sample of 8 mW. After polynomial background subtraction, the frequencies and line-widths of the Raman bands were determined.

Redox titrations

Redox titrations followed by EPR spectroscopy were performed anaerobically in 50 mM Tris-HCl (pH 7.2) at 25 °C, by stepwise addition of buffered (250 mM Tris-HCl at pH 9.0) sodium dithionite as reductant or H_2O_2 as oxidant. A 100 µM protein solution, a platinum and a Ag/AgCl electrodes and the following redox mediators (40 µM each) were used: potassium ferricyanide (E'_0 = +430 mV), N,N dimethyl-p-phenylenediamine (E'_0 = +340 mV), tetramethyl-p-phenylenediamine (E'_0 = +260 mV), 1,2-naphtoquinone-4-sulphonic acid (E'_0 = +215 mV), 1,2-naphtoquinone (E'_0 = +180 mV), trimethylhydroquinone (E'_0 = +115 mV), 1,4-naphtoquinone (E'_0 = +60 mV), menadione (E'_0 = 0 mV), plumbagin (E'_0 = -40 mV), indigo trisulphonate (E'_0 = -70 mV), phenazine (E'_0 = -125 mV), 2-hydroxy-1,4-naphtoquinone (E'_0 = -152 mV) and anthraquinone-2-sulphonate (E'_0 = -225 mV). The electrodes were calibrated with a saturated quinhydrone solution at pH 7.0. The reduction potential values are reported with the standard hydrogen electrode as reference. All experimental data were analyzed using Nernst equations for non-interacting redox centers considering single one-electron transitions for the rubredoxin and desulforedoxin domains, and two consecutive one-electron processes for the diiron center.

Peroxidase activities with artificial electron donors (o-dianisidine and guaiacol)

H_2O_2-dependent oxidation of *o*-dianisidine and guaiacol was followed at 460 and 470 nm, respectively, at room temperature as a function of time

in anaerobic conditions. For the two assays, a buffer of 50 mM Tris-HCl, pH 7.2 degassed under an argon flux was used and the final concentrations were: DRbr 1 µM, H_2O_2 250 µM, 1 mM of *o*-dianisidine (ε_{460} = 11.3 $mM^{-1}cm^{-1}$) or 5 mM of guaiacol (ε_{470} = 26.6 $mM^{-1}cm^{-1}$) 5 mM.

NADH-linked hydrogen peroxide reductase activity

As an artificial electron donating system, a mixture of NADH:flavorubredoxin oxidoreductase (Flrd-Red) and the rubredoxin domain (Rd-Flrd) of flavorubredoxin (*215*), both from *E. coli,* were used. The *E. coli* proteins were purified as described in (*114, 215*). The enzyme activity was measured anaerobically (under argon atmosphere) at room temperature in 50 mM Tris-HCl (pH 7.2) in a closed spectrophotometric cell containing 200 µM NADH and optimum concentrations found for a maximum activity: 2 µM Flrd-Red, 4 µM Rd-Flrd, 500 nM DRbr and 100 µM of H_2O_2. The NADH oxidation, initiated by addition of DRbr, was monitored by the decrease in absorbance at 340 nm (ε = 6220 $mM^{-1}cm^{-1}$).

Protein degradation upon H_2O_2 exposure

SDS-PAGE was used to follow DRbr protein degradation upon incubation with different amounts of H_2O_2 (0-10 mM), in turnover conditions. DRbr (10µM) was incubated for 15 minutes with 150 µM of NADH, 125 nM of Flrd-Red and 250 nM of Rd-Flrd. The samples after incubation were loaded into the gel.

Stopped-flow kinetics of NADH: H_2O_2 electron transfer following DRbr oxidation

Oxidation of reduced DRbr by H_2O_2 was followed in a SF-61 DX2 stopped-flow apparatus (Hi-Tech Scientific) placed inside an anaerobic Glove Box MB150, MBRAUN (<2 ppm O_2). Protein solutions were made anaerobic by repeated cycles of vacuum and equilibration with argon. Prior to the experiments, the stopped-flow apparatus was incubated with degassed water and buffer. The solutions were loaded in two drive

syringes. One syringe contained reduced DRbr, previously prepared by incubation of 80 µM of DRbr with 2 µM Flrd-Red, 4 µM Rd-Flrd and 200 µM NADH; the second syringe contained H_2O_2 at different concentrations (10 to 200 µM). The reaction mixture was 1:1. Reduction of DRbr was verified by its UV-Visible spectrum, mixing it with degassed buffer.

4.2 - Results and Discussion

Biochemical characterization

The desulforubrerythrin was overexpressed in *E. coli*, grown in minimal medium supplemented with iron, and purified anaerobically through a three-step chromatographic process; from one liter of culture medium *c.a.* 60 mg of pure protein were obtained. The quantification of iron and zinc per mol of monomer gave 3.5 ± 0.2 and 0.17 ± 0.1, respectively, confirming that DRbr has *c.a.* 4 iron atoms per monomer and virtually no zinc atoms. By SDS-PAGE a single band at ~25 kDa was detected (Figure 4.1A), in agreement with the molecular mass deduced from the amino acid sequence, 24526 Da. The elution profile in a gel filtration column revealed that the protein in solution is mainly in a form with a molecular mass of ≈ 97 KDa, *i.e.*, it forms a tetramer (Figure 4.1B). Note that, in general, rubrerythrins are isolated as homodimers in solution (*133, 136*) while the X-ray structures of those proteins suggest either a dimeric or a tetrameric quaternary structure (*e.g.*, (*104, 132-133*)).

UV/Visible spectra

The UV/Vis spectrum of (oxidized) DRbr (Figure 4.2A, trace a) shows bands at 370, 490 and 560 nm, with an absorbance ratio A_{280}/A_{489} of 3.7. These features are reminiscent of [$FeCys_4$] ferric sites; diiron sites have in general low molar absortivities such that they are difficult to detect when in the presence of other chromophores. Figure 4.2 displays the spectra of a desulforedoxin-like center (Figure 4.2B, trace a) and of a canonical rubredoxin (Figure 4.2B, trace b).

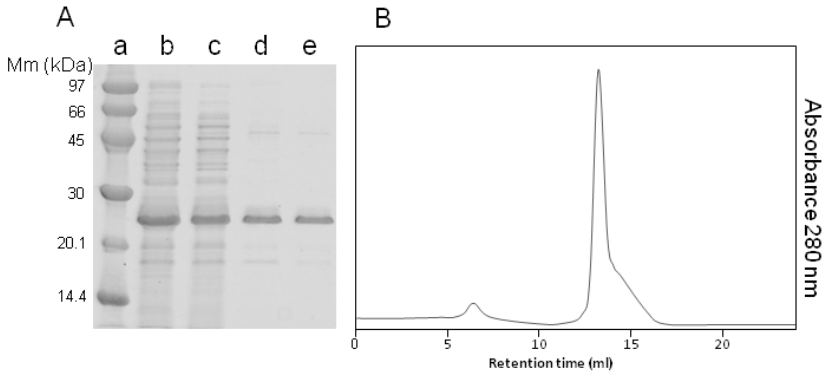

Figure 4.1 - A- SDS-Page: a – Low Molecular mass markers (GE Healthcare); b – soluble fraction; c – fraction eluted from Q-Sepharose Fast Flow column; d – fraction eluted from HTP column; e – final fraction eluted from Gel Filtration S75 column. B- DRbr elution profile from Superdex200 (HR3.2/300) column; the first peak (small) corresponds to blue dextran, the second peak corresponds to the protein with a retention time of 13.2mL (tetramer, according to the calibration); y-axis corresponds to absorbance at 280nm.

The addition of those two spectra in a 1:1 ratio (Figure 4.2B, trace c) generates a spectrum with features almost identical to those of oxidized DRbr (Figure 4.2B, trace d), including the relative absorbances at each maximum. In fact, the main difference between rubredoxin- and desulforedoxin-like sites resides in the relative absorbances of each main band: at 370 nm both iron centers have similar contributions whereas at 490 nm, the spectral contribution of the rubredoxin site is *c.a.* 50% higher than that of the desulforedoxin-site. A deconvolution of the components of the spectrum of the *C. jejuni* protein could be obtained after its partial reduction with sodium dithionite. Subtracting the spectrum of substoichiometrically reduced DRbr (Figure 4.2A, trace b) from the spectrum of the oxidized form (Figure 4.2A, trace a) reveals features identical to those of desulforedoxin (Figure 4.2A, inset) (*112*), which further corroborates the presence of a rubredoxin and a desulforedoxin site. Furthermore, the finding that the described subtraction yields the spectrum of a desulforedoxin indicates that this site has a reduction potential higher than that of the rubredoxin one.

Complete reduction leads to the full bleaching of the visible absorption (Figure 4.2A, trace c).

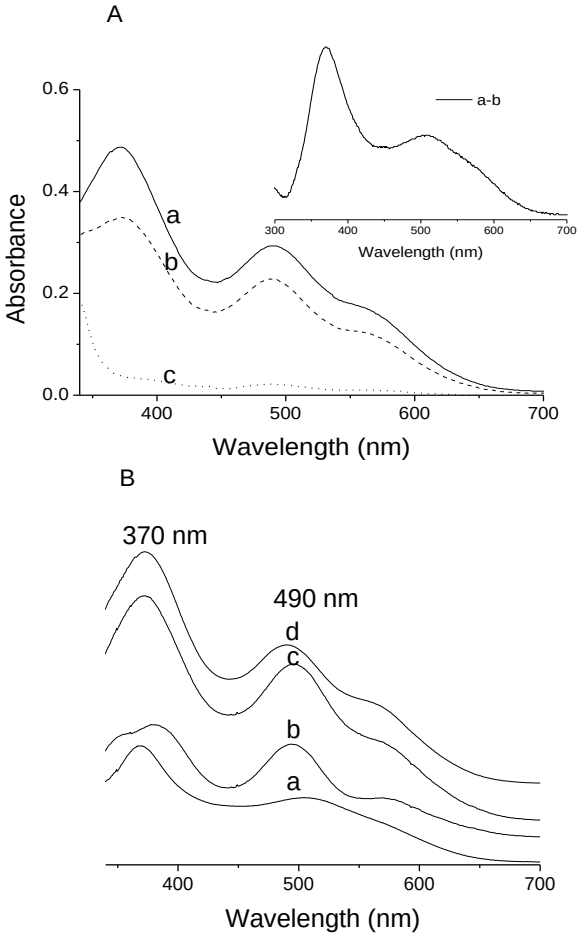

Figure 4.2 - UV/Visible absorption spectra of *C. jejuni* DRbr. A, Stepwise reduction of DRbr with sodium dithionite under anaerobic conditions: a) spectrum of the as-isolated protein (50 μM) in 20 mM Tris-HCl pH 7.2; b) partially reduced protein after addition of substoichiometric amounts of sodium dithionite; c) protein fully reduced by sodium dithionite; inset –Spectrum *a* minus spectrum *b*. B – a) Spectrum of partially reduced desulfoferrodoxin (Dx domain oxidized) from *Archaeoglobus* (*A.*) *fulgidus (171)*; b) spectrum of *A. fulgidus* rubredoxin 1 (*121*); c) the 1:1 sum of spectra a and b; d) spectrum of the as-isolated DRbr; the spectra are offset vertically and are displayed according to the respective molar extinction coefficients.

EPR Spectra

The EPR spectrum at 8 K of the as-isolated DRbr (Figure 4.3, trace a) displays several resonances at low-magnetic fields, characteristic of high-spin (S=5/2) ferric ions, and at g-values slightly lower than 2, due to an S=1/2 center. The resonances at low-field could be deconvoluted into three distinct components, differing by the ratio of the zero-field splitting terms (rhombicity, E/D). By comparison with the corresponding g-values of *D. gigas* desulforedoxin (*112*) and canonical rubredoxins (as well as of rubrerythrins) (*e.g.* (*109*)), the resonances due to the center with lower rhombicity (E/D = 0.1, g=8.0 and 3.6 from the |Ms=±1/2> doublet and g= 5.6 from the |Ms=±3/2> doublet) can be assigned to the desulforedoxin-like center, while those with g-values at 4.85 and 3.65 ($|M_S=\pm3/2>$ doublet), and g = 9.3 (ground or excited doublet), are attributed to the rubredoxin-like center (with a rhombicity E/D = 0.23).

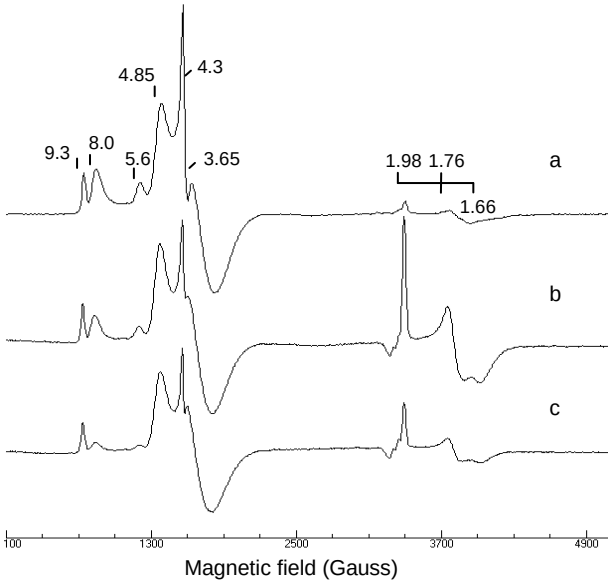

Figure 4.3 - EPR spectra of *C. jejuni* DRbr: a) DRbr as isolated; b) and c) are spectra of DRbr upon successive addition of substoichiometric amounts of sodium ascorbate. The protein concentration was 200 μM in 20 mM Tris-HCl (pH 7.2) and 150 mM NaCl. Experimental conditions: T = 7 K; microwave power, 2 mW; microwave frequency, 9.38 GHz; modulation amplitude, 1 mT.

This assignment is corroborated by the analysis of spectra obtained with partially reduced samples (Figure 4.3, traces b and c), and taking into account that the desulforedoxin-like center is the one with the higher reduction potential. In fact, the first set of resonances to disappear from the spectra upon partial reduction are those of the spin system with E/D=0.1. A third component is discernible in the spectra, with g = 4.3 and E/D = 0.33, which may be due to some heterogeneity at the ferric sites. The resonances with g-values of 1.98, 1.76 and 1.66, better observed in a partially reduced state (Figure 4.3, trace b), are detected up to *c.a.* 20 K and are characteristic of a S = 1/2 center with anti-ferromagnetically coupled iron atoms in a mixed valence (Fe^{III}-Fe^{II}) state (*85, 216*). In the fully oxidized and reduced states, these resonances vanish, as characteristic of diiron centers of the histidine/carboxylate family, which form di-ferric or di-ferrous states with null or even total spin (*216*). No signals could be detected with parallel mode EPR for either of those redox forms of the diiron center, which suggests either a total spin S = 0, or a large value for the zero field splitting.

Resonance Raman spectroscopy

The Resonance Raman spectrum of DRbr in the as-isolated state, obtained with 413-nm excitation, shows several bands in the low frequency region (Figure 4.4, trace a). The bands at 316, 366 and 383 cm^{-1} are attributed to modes involving the Fe-S coordinates originating from both rubredoxin and desulforedoxin centers (*216-217*). In addition, a broad band at 520 cm^{-1} indicates the presence of an oxygen bridged diiron center. This mode lies in the range of symmetric Fe-O-Fe stretching modes (ν_s) of µ-oxo bridged diiron centers found in proteins and model complexes, and exhibits a large bandwidth as previously observed (*218-219*). The ν_s band is well defined in the spectra of H_2O_2-oxidized DRbr (Figure 4.4, trace b). The assignment of the 520 cm^{-1} band is further supported by the results of isotopic labeling. For these experiments, the protein was lyophilized and then re-dissolved in $H_2{}^{18}O$

to substitute the bridging oxygen by ^{18}O (*219-221*). The UV-Vis absorption spectrum confirmed that the protein remained intact upon removal and subsequent addition of water. As a consequence of the isotopic substitution, the 520 cm^{-1} band undergoes a downshift by *c.a.* 17 cm^{-1} to 503 cm^{-1} (Figure 4.4, trace c). The magnitude of the $^{18}O/^{16}O$ shift of the ν_s mode ($\Delta\nu_s$) is characteristic of μ-oxo bridged diiron centers (*217, 219, 222-223*). In particular, both the energy of the Fe-O-Fe stretching and the $^{18}O/^{16}O$ shift observed in DRbr are identical to the respective values reported for the di-iron-oxo center in stearoyl–ACP desaturase (*219*). In that enzyme, the calculated Fe-O-Fe bond angle is 123^0. Therefore, a similar value should hold for the DRbr diiron center, since there is a direct correlation of ν_s and $\Delta\nu_s$ with the geometry of the center. The subtle downshift of the band observed after dissolving the lyophilized protein in D_2O might reflect hydrogen bonding interactions of the bridging oxygen but rules out the involvement of a hydroxyl ligand (Figure 4.4, trace d).

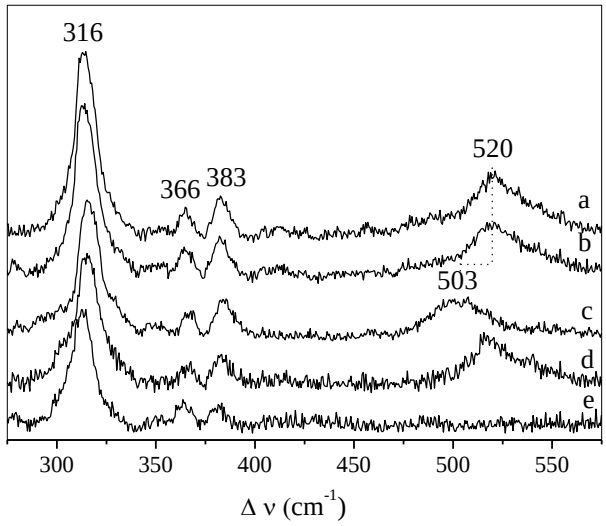

Figure 4.4 - Resonance Raman spectra of *C. jejuni* DRbr obtained with 413-nm excitation: a) DRbr in the as-isolated state; b) DRbr in the H_2O_2-oxidized state; c) DRbr in $H_2{}^{18}O$; d) DRbr in D_2O; and e) ascorbate-reduced DRbr. The spectra were measured at 83 K with an accumulation time of 60 seconds and a laser power at the sample of 8 mW.

Upon reduction of the protein with ascorbate the 520 cm^{-1} band disappears. This finding can be readily attributed to the lack of resonance enhancement due to the absence of an electronic transition in the ferrous form of the diiron center (Figure 4.4, trace e) as well as to the absence of the oxo bridge in the reduced centre, as commonly observed for diiron centers (*218*). Note that $^{18}O/^{16}O$ and D/H exchange as well as reduction by ascorbate affect the vibrational modes of the rubredoxin and desulforedoxin centers only within the experimental accuracy ($\pm$ 1 cm^{-1}).

Potentiometric characterization

The reduction potentials of each center were determined by redox titrations at pH 7.5 monitored by EPR spectroscopy. For the rubredoxin center (monitored at g = 4.85), a reduction potential of +185 ± 30 mV was determined, while for the desulforedoxin center (monitored at g=8.0 and g=5.6), a value of +240 ± 30 mV was obtained (Figure 4.5A). For the diiron center, the changes in intensity at the g=1.76 and g=1.66 resonances were monitored. The bell shaped data dependence was analyzed on the basis of a Nernst equation for two consecutive mono-electronic processes(see footnote 1), yielding reduction potentials of +270 ± 20 and +235 ± 20 mV for the first (E1: Fe^{III}-Fe^{III}/Fe^{III}-Fe^{II}) and second (E2: Fe^{III}-Fe^{II}/Fe^{II}-Fe^{II}) steps, respectively (Figure 4.5B). The reduction potentials for the diiron center are within the values reported for the equivalent sites in rubrerythrins (*e.g.* (*216*)). On the contrary, the value determined for the desulforedoxin-like site, +240 mV, is quite high, as compared to those of *D. gigas* desulforedoxin (-35 mV, (*113*)) and of the desulforedoxin-like centers in 2Fe-SORs (~0 to -60 mV, *e.g.*, (*156, 171*)). In turn, the value obtained for the rubredoxin site, +185 mV, is lower than those reported for the corresponding rubredoxin centers in rubrerythrins (+230 to +281 mV (*85, 96*)), but still much higher than those for isolated rubredoxins (generally, -100 to + 50 mV (*109*)).This observed difference may be partially explained by the presence of

several amino acid substitutions in DRbr close to the iron-binding cysteines (see later in Figure 4.12).

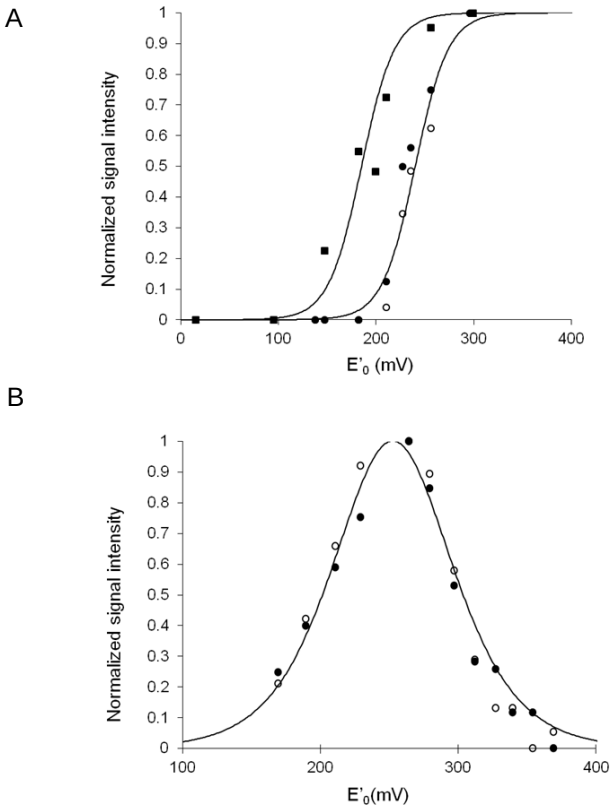

Figure 4.5 - Redox titration of DRbr, monitored by EPR spectroscopy. A) Rubredoxin center – intensity changes of the g = 9.3 resonance (■); Desulforedoxin center - intensity changes of the g = 5.6 (●) and g = 8.0 (○) resonances. The solid lines were calculated by Nernst equations for monoelectronic processes, with E'_0= +185 mV and E'_0 = +240 mV. B) Diiron center - intensity changes of the g = 1.76 (●) and g = 1.66 (○) resonances; the solid line corresponds to a Nernst equation for two consecutive one-electron processes (E'_0(1) = +270 and E'_0(2) = +235 mV). The EPR signals were normalized in relation to the maximum intensity of each resonance.

1- Nernst equation for two consecutive mono-electronic processes, considering the population of Fe^{III}-Fe^{II} species:

$[Fe^{III-II}] = e^{[(E1-E)/(RT/nF)]} / (e^{[(E1+E2-2E)/(RT/nF)]} + e^{[(E1-E)/(RT/nF)]} + 1)$; E– solution redox potential; E1,E2- reduction potential; n=1; F- Faraday constant; R– Universal gas constant; T- temperature

NADH: H_2O_2 reductase activity

Having established the presence of the initially proposed metal centers, and determined their redox properties, we addressed the physiological role of *C. jejuni* DRbr.

Assays for peroxidase activity using as electron donors *o*-dianisidine and guaiacol in anaerobic conditions gave no activity. As observed for some rubrerythrins, DRbr is only slowly oxidized by oxygen, but rapidly by hydrogen peroxide (Figure 4.6).

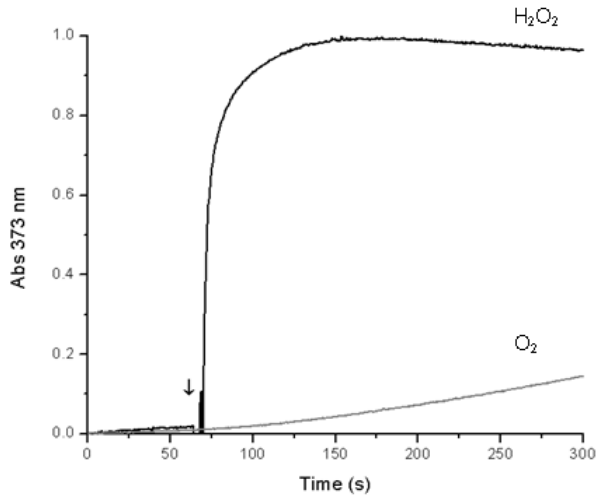

Figure 4.6 – Oxidation of DRbr by H_2O_2 or O_2 followed by UV/Visible spectroscopy. The anaerobic protein sample in 20 mM Tris-HCl pH 7.2, sodium dithionite and H_2O_2 solutions were degassed. A 50 µM DRbr solution was reduced stepwise by adding sodium dithionite. To the fully reduced DRbr was added H_2O_2 or O_2, in an amount equivalent to that of the reduced centers. The black arrow corresponds to the addition of H_2O_2 or aeration. The protein oxidation was followed by UV/Visible spectra and as a function of time at 373 nm.

The physiological electron donors of DRbr are not known, hampering a proper assay system for a NAD(P)H:H_2O_2 oxidoreductase activity. Nevertheless, it was found that *E. coli* NADH: flavorubredoxin oxidoreductase (Flrd-Red) was able to reduce DRbr in the presence of the rubredoxin-domain of *E. coli* flavorubredoxin (Rd-Flrd). Therefore, oxidation of NADH was monitored upon addition of H_2O_2, to a mixture

containing catalytic amounts of Flrd-Red, Rd-Flrd and DRbr (Figure 4.7). An activity of 3.9 ± 0.5 µmol H_2O_2 $min^{-1}mg^{-1}$ was obtained, which is in the same order of magnitude of the values reported for other rubrerythrins, that range from 0.12 µmol H_2O_2 $min^{-1}mg^{-1}$ for the *Entamoeba* (*E.) histolytica* enzyme (*224*) to 0.99 µmol H_2O_2 $min^{-1}mg^{-1}$ for the *Clostridium* (*C.*) *acetobutylicum* protein (*101*). Moreover, the DRbr activity assays the NADH: H_2O_2 ratio was found to be close to 1, in, which indicates that hydrogen peroxide was reduced to water. Therefore, we may suggest that, as rubrerythrins, *C. jejuni* DRbr has a role in detoxification of hydrogen peroxide.

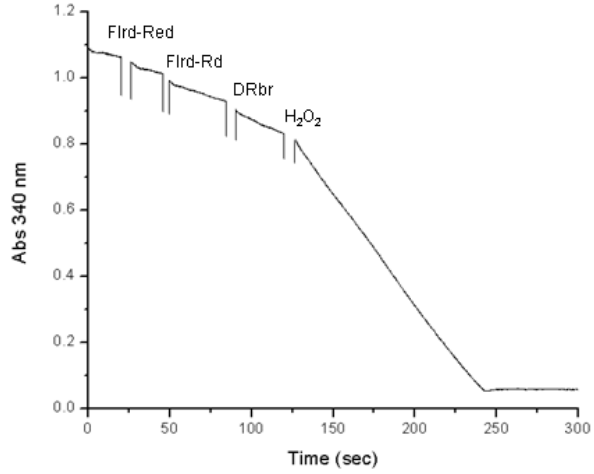

Figure 4.7 - H_2O_2 reductase activity followed by NADH oxidation at 340 nm; 100 µM of H_2O_2 added to: 500 nM of as isolated DRbr, 2 µM of Flrd-Red, 4 µM of Rd-Flrd and 200 µM of NADH. All solutions were degassed under argon in 50 mM Tris-HCl pH 7.2 at room temperature. Each component of the reaction was sequentially added as indicated in the figure. The NADH oxidation by each component of the assay, as control, was obtained and properly subtracted from the DRbr contribution.

Protein Degradation

During the redox titrations it was usually witnessed that protein stability was compromised after some reduction cycles, especially the Dx iron centre as the EPR resonances attributed to this iron site had diminished their amplitudes. Also the yield of protein production was only optimal

by performing the purification in anaerobic conditions. In addition to these observations, Yamazaki M *et al.*, (*106*), also showed that the exposure of *C. jejuni* cell extracts to different concentrations of H_2O_2 (0 to 1mM) led to the degradation of DRbr, more significantly above 0.2 mM of H_2O_2.

In order to verify this phenomenon *in vitro* with purified protein, we incubated the as isolated DRbr reduced with FlRd-Red, Rd-FlRd and NADH (*i.e.*, under turnover conditions) with different concentrations of H_2O_2 (0 to 10 mM). After a 15 minute period of incubation the assay mixtures were loaded in a SDS-PAGE (Figure 4.8). Above 0.4 mM of H_2O_2 concentration, it is evident the appearance of bands at smaller molecular masses and the decrease of the band at ~24 kDa (DRbr monomer) (Fig 4.8). The degradation of the monomer is concomitant with the increase of intensity of a lower molecular mass band at ~20 kDa, which is compatible with the break of one of the three domains, which can be assumed to be the Dx domain, due to the verified instability of this centre in redox cycles. The degraded monomer (~20 kDa) above higher concentrations of H_2O_2 (5 mM) also starts to disappear. Bands with even lower molecular masses start to appear at ~0.4 mM H_2O_2, suggesting a further degradation of the protein.

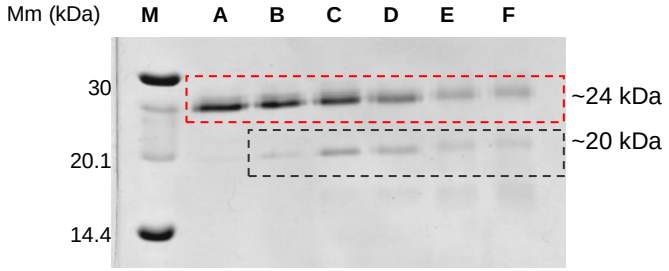

Figure 4.8 – SDS-PAGE of DRbr, after the reaction with H_2O_2: DRbr (10 µM) with Flrd-Red (125 nM), Rd-Flrd (250 nM) and NADH (150 µM) with various concentrations of H_2O_2 for 15 minutes. M – Low molecular weight SDS-PAGE markers, A - 0 mM H_2O_2 without Flrd-Red added, B – 0 mM H_2O_2, C – 0.4 mM H_2O_2, D – 1 mM H_2O_2, E – 5 mM H_2O_2, F – 10 mM H_2O_2.

Other experiments were performed in order to understand the degradation profile upon H_2O_2 incubation with DRbr. Incubating 83 µM DRbr with excess of H_2O_2, 1.6 mM and 3.6 mM, *i.e.,* around 20x and 40x times higher, and for 30 minutes, it was possible to follow by EPR and visible spectroscopies the degradation of an iron center (Figure 4.9). The degradation of the Dx iron center ($FeCys_4$) was confirmed by EPR, since the intensities at the g-values, g=8.0 and g= 5.6, characteristic of this center are diminishing in contrast with the other g-values attributed to Rd iron site (Figure 4.3). Furthermore, a resonance at g~4.3 starts appearing, suggesting the formation of "free iron" in solution. The visible spectrum d) also is different from the a) spectrum in Figure 4.9 corresponding to DRbr as purified, denoting the modification of the iron centers in the protein, namely the Dx iron center. These results support the idea of sensitivity upon H_2O_2 exposure.

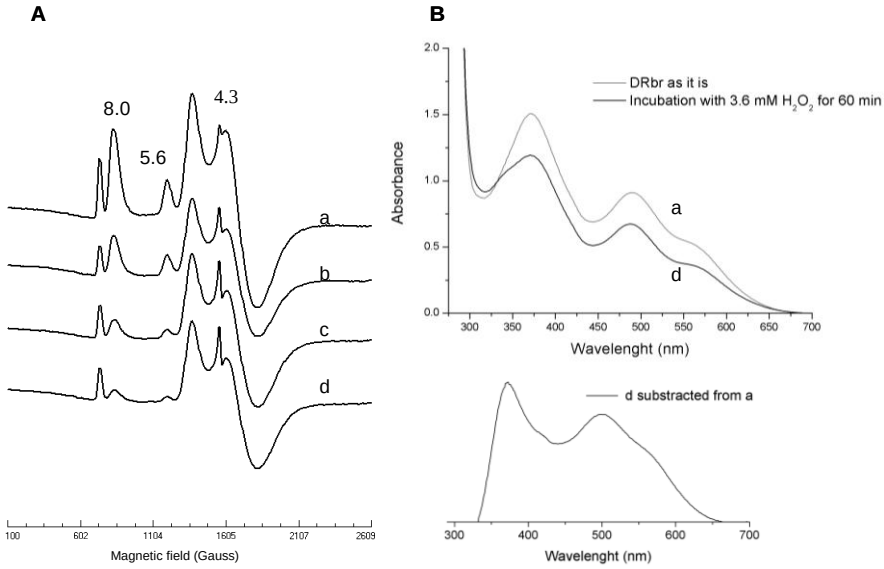

Figure 4.9 – Oxidation of oxidized as purified DRbr by H_2O_2 followed by EPR (A) and UV/Visible (B) spectroscopies. The sample of DRbr (83 µM) (a) was incubated with 1 mM of H_2O_2 (b), for 30 minutes with 3.6 mM H_2O_2 (c) and for 60 minutes with 3.6 mM H_2O_2 (d). Intensities at the g-values, g=8.0 and g= 5.6, correspond to the desulforedoxin-like center.

These preliminary data raises the puzzling question of which is the function of this redox center (Dx) and more importantly, the function of the protein itself.

Stopped-flow kinetics of NADH: H_2O_2 electron transfer following DRbr oxidation

The kinetics of DRbr oxidation was also studied by stopped-flow upon addition of H_2O_2. DRbr was previously reduced by mixing it with NADH and catalytic amounts of Flrd-Red and Rd-Flrd. By deconvolution of the UV-Visible spectra it is possible to determine the contribution of each $FeCys_4$ centre at each step of the oxidation process by different amounts of the substrate, H_2O_2. Since we are measuring the enzyme oxidation, it is not possible to have catalytic concentrations and the reaction already occurs in the dead time, the protein being more than 50% oxidized at the beginning of the measurements. In spite of these constraints, it is still possible to infer about the oxidation rates order and the intramolecular electron flow in DRbr.

In Figure 4.10A, visible spectra of the final species are presented after the oxidation of DRbr with different amounts of H_2O_2 and in the same time range, 450 milliseconds. The first step of oxidation occurs with the concomitant increase of absorbance at 490 nm and 373 nm, in the range from 10 to 80 µM of H_2O_2.

This increase is also revealed in Figure 4.11F, where the maximum absorbance at 490 nm is reached in ~200 msec, in agreement with the stoichiometry of the reaction (1 DRbr: 2 H_2O_2). The small increase of absorbance at 490 nm, between 80 and 200 µM H_2O_2 occurs with a higher increase in absorbance of the band at 373 nm that has its maximum after 500 msec (Figure 4.11E). By deconvolution of the visible spectra, we can say that the first oxidation step is relative to the $FeCys_4$ rubredoxin site (comparing Figures 4.10A and B with Figure 4.2). With higher concentrations of H_2O_2 the oxidation is faster and after ~500 msec we obtain a spectrum of the fully oxidized protein.

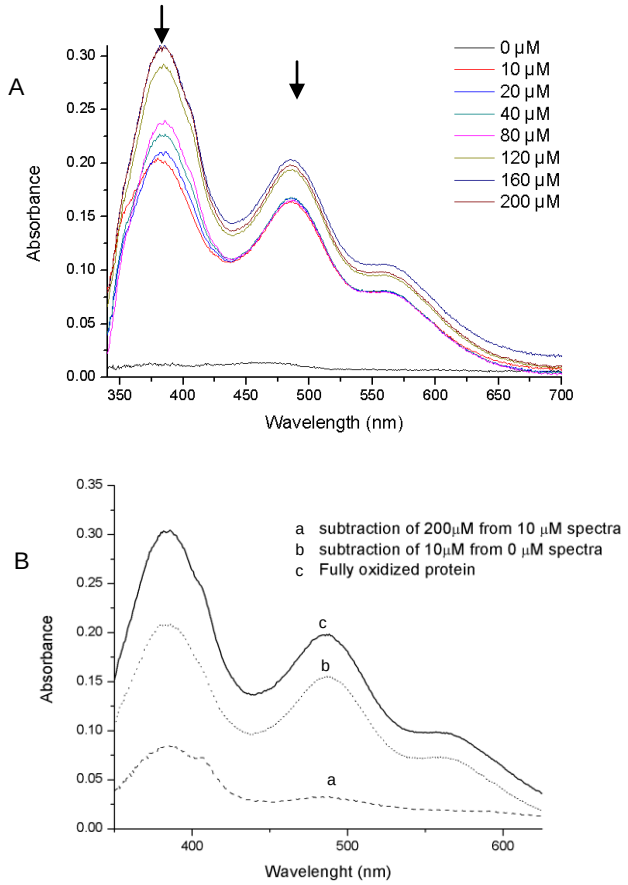

Figure 4.10 – Visible spectra obtained by stopped-flow assays of DRbr (40 µM) oxidation by H_2O_2. A) Visible spectra obtained after mixing the reduced DRbr with different concentrations of H_2O_2, from 0 to 200 µM, after 450 milliseconds. The first spectra of oxidized species correspond to H_2O_2 concentrations of 10 to 80 µM and the last spectra of oxidized species corresponds to H_2O_2 concentrations of 120 to 200 µM. B) Deconvolution of the spectra obtained by DRbr oxidation by H_2O_2: a) Subtraction of the spectrum at 10 µM of H_2O_2 from the reduced protein spectrum at 0 µM H_2O_2; b) from the final oxidized species (200 µM H_2O_2), subtracting the spectrum at 10 µM H_2O_2; c) the fully oxidized protein spectrum is obtained by subtracting the spectrum of the reduced species from the most oxidized spectrum at 200 µM H_2O_2.

The final spectrum at 200 µM H_2O_2 can be subtracted from the spectrum from the first step of oxidation (relative to 10 µM H_2O_2) and the spectrum obtained has a maximum at ~380 nm and a low intensity band at 490 (Figure 4.9B), which indicates that the major species

contributing to that increase is the $FeCys_4$ site of the desulforedoxin domain.

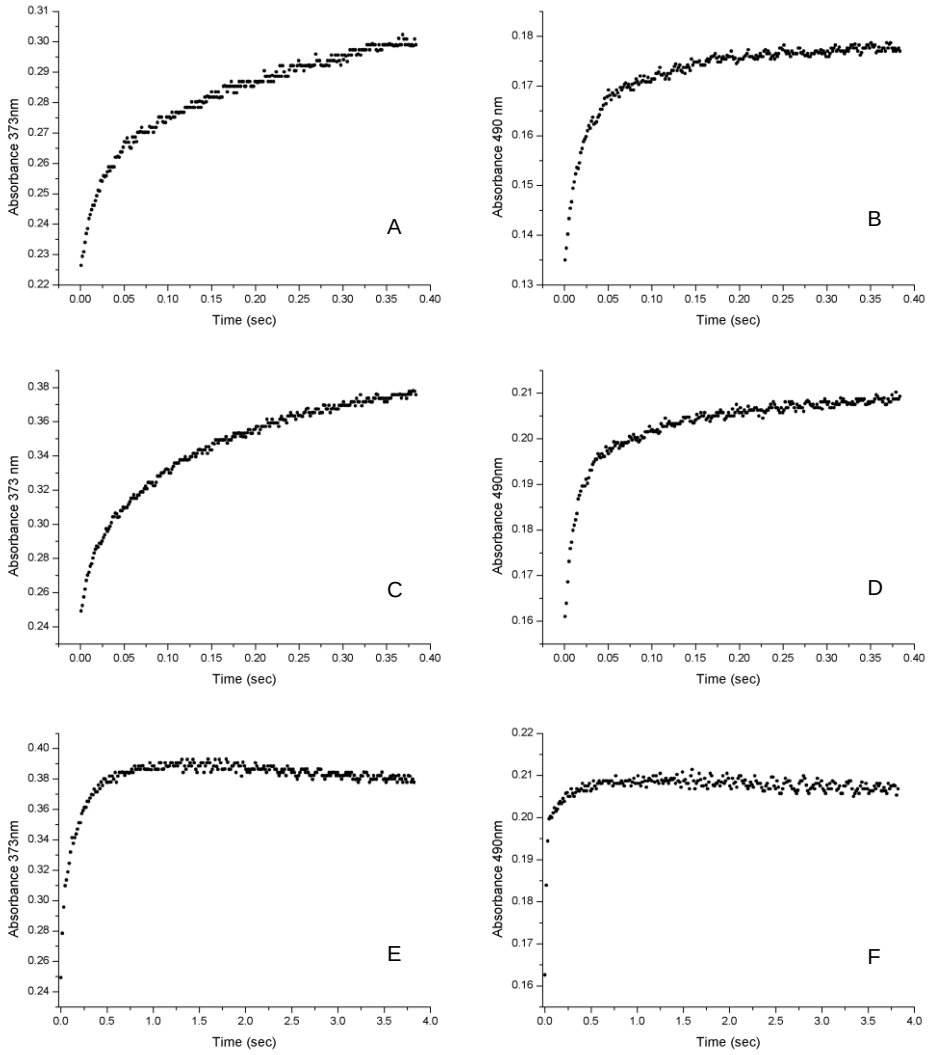

Figure 4.11 – Oxidation of DRbr followed at two wavelengths, 373 nm (A, C, E) and 490 nm (B, D, F), for 0.4 seconds (A-D) and 4 seconds (E-F). A and B) Reaction of 40 µM of reduced DRbr with 40 µM H_2O_2 in 0.4 seconds; C and D) Reaction of 40 µM of reduced DRbr with 200 µM H_2O_2 in 0.4 seconds; E and F) Reaction of 40 µM of reduced DRbr with 200 µM H_2O_2 in 4 seconds, DRbr totally oxidized in less than 1 second.

These results are in agreement with the reduction potential determination (Figure 4.5), which suggests that the rubredoxin site is the point of electrons entry, being oxidized firstly and in a faster time scale (< 200 msec). The diiron site (the catalytic site) has a higher reduction potential and should be the sink of the electrons entering from the rubredoxin iron site. Finally the desulforedoxin iron site has a similar reduction potential as the diiron site, but its oxidation occurs in a longer time scale (< 500 msec) (see Chapter 8 for further discussion).

DRbr domains and sequence analysis

Rubrerythrins are widespread in both prokaryotic domains, Archaea and Bacteria, in strictly anaerobic, facultative or aerobic microorganisms and were also found in the genomes of Eukaryotes such as the anaerobic protozoa *Entamoeba (E.) histolytica*, *E. dispar*, *Trichomonas vaginalis* and the photosynthetic protozoan *Cyanophora paradoxa*.

Genes encoding other orthologues of DRbr were also found in other proteobacteria: *Helicobacter* (*H.*) *winghamensis*, *Sulfurospirillum* (*S.*) *deleyianum*, *Sulforuvum sp*, *Wolinella* (*W.) succinogenes* and *Vibrio* (*V.*) *shilonii* (Figure 4.12). The highest amino acid sequence identities and similarities of *C. jejuni* DRbr are with the orthologues from the same genus (*c.a.* 90% identity) (Figure 4.12). The proteins from *W. succinogenes* DSM 1740, *H. winghamensis*, and *S. deleyianum*, organisms that belong to the same order as *Campylobacter*, present also high identities and similarities with *C. jejuni* DRbr (≈ 70-85% identity). The average identity with rubrerythrins is 45-55%, the lower similarities being with the “single domain” erythrin-like proteins.

It was concluded from the amino acid sequence alignment that all the amino acid residues involved as ligands of the binuclear center, on the four-helix bundle, and the four cysteines from the rubredoxin domain, in the rubrerythrin family are strictly conserved in the DRbr sequences (Figure 4.12). The ligands for the metal ions of the diiron site are: E52-$(X)_{32}$-E85-$(X)_2$-H88-$(X)_{30}$-E119-$(X)_2$-E122-$(X)_{30}$-E153-$(X)_2$-H156 (according to the *C. jejuni* DRbr numbering); two tyrosines, whose

homologues in the protein from *D. vulgaris* form hydrogen bonds to two glutamic ligands (*103-104*) - Y59 (H-bond to E119) and Y127 (H-bond to E52) are also conserved; the binding motif for the rubredoxin domain is C183-$(X)_2$-C186-$(X)_{12}$-C199-$(X)_2$-C202.

The analysis of the amino acid sequences of the rubredoxin domains suggests a possible explanation for the lower reduction potential of the rubredoxin center of the *C. jejuni* DRbr, in comparison with those from rubrerythrins. The high reduction potential of the rubredoxin site in rubrerythrins (E_0~+250 mV) was attributed to the presence of a few amino acid substitutions in the cysteines binding loops, as compared to canonical rubredoxins, such as the *C. pasteurianum* protein (E_0= -57mV): the motifs –CxVC- and -CpLCgV- of this rubredoxin are substituted by – CxNC- and -CpACgH- in *D. vulgaris* rubrerythrin (Figure 4.12) (*103*). The presence of the asparagine and histidine residues, changes the electrostatic environment near the iron ion, leading to an increase of the reduction potential (*103, 225*).The sequence of *C. jejuni* DRbr shows the motifs –CxVC- and -CpLCkA-, *i.e.*, it is more similar to that of the *C. pasteurianum* rubredoxin than to those of rubrerythrins. Interestingly, the motif found for the *C*. *jejuni* DRbr is also present in all other desulforubrerythrins.

DX-domain
Four-helix bundle domain - Helix 1
Four-helix bundle domain - Helix 2
Four-helix bundle domain - Helix 3
Four-helix bundle domain - Helix 4
Rd-domain
Campylobacter jejuni
Campylobacter coli
Campylobacter upsaliensis
Helicobacter winghamensis
Sulfurospirillum deleyianum
Wolinella succinogenes
Sulfurovum sp.
Vibrio shilonii
Desulfovibrio vulgaris_Rbr
Desulfovibrio vulgaris_Ngr

Figure 4.12– Amino acid sequence alignment of the DRbr from *Campylobacter* (*C.*) *jejuni* subsp. *jejuni* NCTC 11168 with DRbrs identified so far in other organisms (% identity with *Campylobacter jejuni* subsp. *jejuni* NCTC 11168, NCBI-GI): *C. jejuni* subsp. *jejuni* NCTC 11168 (218561705); *C. coli* RM2228 (97%, 57504610); *C. upsaliensis* RM3195 (91%, 57505768); *Helicobacter winghamensis* ATCC BAA-430 (85%, 229376137); *Sulfurospirillum deleyianum* DSM 6946 (77%, 229532747); *Wolinella succinogenes* (71%, 34483443); *Sulfurovum sp.* NBC37-1 (68%, 151423895); *Vibrio shilonii* AK1 (34%,148837950); rubrerythrin from *Desulfovibrio vulgaris* Hildenborough (30%, 46581497) and nigerythrin from *Desulfovibrio vulgaris* Hildenborough (26%, 46578436). Black boxes represent strictly conserved residues, dark grey boxes represent highly conserved residues, and light grey indicates conserved residues among the sequences presented. Further notations are: "+" - the N-terminal four cysteines corresponding to the Dx domain; "*" - the ligands involved on the di-iron site; "Δ"- tyrosine residues that form a H-bond with two glutamate ligands; "#"- the C-terminal four cysteines corresponding to the rubredoxin domain. The top numbering corresponds to DRbr *C. jejuni* sequence.

4.3 - Conclusions

In summary, we have characterized a novel protein from the pathogen *Campylobacter jejuni*. It contains a distinct combination of structural modules: a desulforedoxin-like, a four-helix bundle and rubredoxin-like domains. The presence of the latter two domains allows classifying the protein as a member of the large family of rubrerythrins. The combination of these three building blocks justifies the new name proposed for this protein, desulforubrerythrin. The spectroscopic data unequivocally show that the protein contains two $FeCys_4$ centers (desulforedoxin- and rubredoxin-like) and a diiron center of the histidine/carboxylate type, with a μ-oxo bridge in the oxidized state.

We further showed that the protein has a hydrogen peroxide reductase activity, which agrees well with the fact that it is regulated by PerR. However, the new experiments showing that the Dx iron sites are degraded in the presence of H_2O_2 raises challenging and still unanswered questions.

Acknowledgements

This work was financed by Fundação para a Ciência e Tecnologia projects PDTC/ BiaPro/67263/2006 (MT) and PDTC/BiaPro/67240/2006 (CVR). We thank the collaboration of Fay Mossel and João V. Rodrigues at earlier stages of this work. ICP analysis were performed at the Laboratório de Análises (523-A), Departamento de Química, CQFB/REQUIMTE, FCT/UNL.

Chapter 5

Summary

Desulforubrerythrin (DRbr) from *Campylobacter* (*C.*) *jejuni* was studied biochemically and spectroscopically, as described in Chapter 4 (*115*).
The X-ray structure of DRbr is here briefly reported, and represents the first structure of a rubrerythrin protein with this three-domain architecture. It has a swapped domain configuration as for the thermophilic enzymes from *Pyrococcus furiosus, Sulfolobus tokodaii* (*132-133*) and from *Burkholderia pseudomallei* (pdb 4di0). The 3D crystal structure was obtained at a 2.0 Å resolution in which the protein is in two states, differing in the oxidation state of the diiron center. The structure supports the electron transfer process proposed in Chapter 4, *i.e.*, the rubredoxin site is the electron entry point, transferring the electron to the diiron center, at ~13 Å. The function of the desulforedoxin center remains to be understood.

This Chapter includes material published and to be published in:

"Three-dimensional structure of the three-domain desulforubrerythrin from *Campylobacter jejuni*", **Pinto AF**, Matias P, Carrondo MA, Teixeira M, Romão CV, manuscript under preparation

"Thermofluor-based optimization strategy for the stabilization and crystallization of *Campylobacter jejuni* Desulforubrerythrin" Santos SP, Bandeiras TM, **Pinto AF**, Teixeira M, Romão CV. 2012 Protein Expr Purif.; 81(2):193-200

Pinto AF is responsible for protein purification and crystallization procedures and is involved in structural analysis, manuscript preparation and discussion.

5 - Desulforubrerythrin 3D Structure

5.1 Experimental Procedures

Thermofluor assay

The protein was purified as described in Chapter 4. The final buffer was 20 mM Tris–HCl pH 7.2, 150 mM NaCl and the protein concentration used in all the thermofluor assays was 0.05 mg/mL and for crystallization procedures was 25 mg/mL.

Protein melting temperature (T_m) determination was performed by monitoring protein unfolding using the fluoroprobe SYPRO Orange dye (Molecular Probes), which upon binding to the hydrophobic protein regions emits fluorescence that can be measured as a function of temperature. The thermal shift assay was performed on an iCycle iQ5 Real Time PCR Detection System (Bio-Rad), equipped with a charge-coupled device (CCD) camera and a Cy3 filter with excitation and emission wavelengths of 490 and 575 nm, respectively. This equipment can simultaneously detect the fluorescence changes in 96-well plates (low profile plate, Bio-Rad) and thus can be used for parallel thermal stability studies. In order to optimize the fluorescence signal to noise ratio an assay optimization was performed.

Typical assay volumes are 25 µl, and initially a signal strength optimization is required. Considering that the experimental volume is fixed, two remaining experimental parameters may influence the signal strength – protein and dye concentration. Using a fixed protein concentration of 0.05 mg/mL, increasing dye concentrations were tested (from 1- to 10-fold, diluted from the initial 5000-fold stock in 50 mM Hepes pH 8.0). The 96-well plates were sealed with Optical Quality Sealing Tape (Bio-Rad) and centrifuged at 2500 g for 2 min immediately before the assay to remove possible air bubbles. For the thermal denaturation tests the plates were heated from 20 to 90 ºC with stepwise increments of 1 ºC per minute and a 10 s hold step for every point, followed by the fluorescence reading. The best signal-to-noise

ratio was obtained using 0.05 mg/mL protein and 10-fold dye as final assay concentrations. Buffer formulation screening was prepared based on the Solubility kit from Jena Biosciences (100 mM buffer concentration and pH range 3–10) with the addition of increasing NaCl concentrations (0, 150 and 500 mM). The assay was prepared by adding 2.5 µl of protein–dye mixture solution previously prepared in 50 mM HEPES pH 8.0 to 22.5 µl of the different screening buffers. The reference experiment was prepared using the protein purification buffer (20 mM Tris–HCl pH 7.2, 150 mM NaCl).

The additive screening assay was performed by adding aliquots of 2.5 µl of each additive compound (Hampton Research) to 22.5 µl of the protein–dye mixture. In this screen the protein–dye mixture was prepared in the buffer yielding the highest Tm in the previous screening (100 mM MES pH 6.2, 500 mM NaCl). The control experiment was prepared by adding the protein buffer instead of the additive compound.

Protein crystallization

Following the thermofluor analysis, the protein was dialyzed into the new buffer (100 mM MES pH 6.2, 500 mM NaCl) and concentrated up to 25 mg/mL. Crystallization trials were done at the nanoliter (nL) scale with the Classic Screen (Nextal) using a Cartesian Crystallization Robot Dispensing System (Genomics Solutions) and round-bottom Greiner 96-well CrystalQuick™ plates (Greiner Bio-One). Taking into consideration the thermofluor results from the additive screen, two additional crystallization drops per condition screened were prepared with the same protein concentration, but adding for each condition 10 mM cadmium chloride (position b) or 10 mM zinc chloride (position c). Only one drop 100:100 (nL) was prepared, and drops were equilibrated against 100 µl of reservoir solution. Dark red colored crystals appeared in less than 1 h and only in (position a) for condition A5: 100 mM Hepes pH 7.5, 5% (v/v) isopropanol, 10% (w/v) PEG 4000.

Optimization of the crystallization procedure was carried out for improving the quality of crystals by the hanging-drop vapor diffusion

technique at 20 ºC, using the additive screen (Hampton Research) in 48-well plates (Hampton Research). Subsequently, crystals appeared using the following additives: 100 mM ammonium sulfate (B3), 10 mM sarcosine (D5), 10 mM adenosine-5-triphosphate disodium salt (D10), 10 mM Tris(2-carboxyethyl)phosphine (TCEP) hydrochloride (D11) (Figure 5.1b and c), 10 mM GSH-GSSG (D12), 3% 1,4-dioxane (G9), 3% methanol (G12).

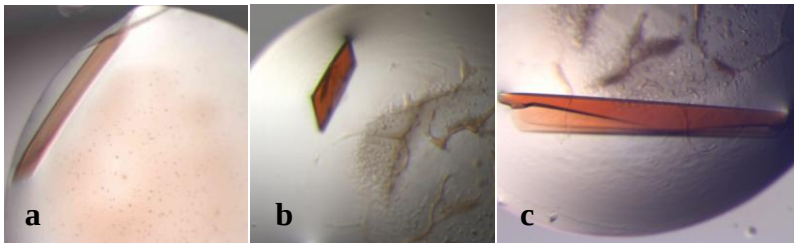

Figure 5.1 – *Campylobacter jejuni* DRbr crystals, a) Crystal obtained by streak seeding in 100 mM Hepes pH 7.5, 10% (v/v) glycerol and 18% (w/v) PEG 8000, b and c) crystals obtained by optimization from an additive screening using 1µl of DRbr plus 0.8 µl of the mixture 100 mM Hepes pH 7.5, 14% (w/v) PEG 8000, 10% (v/v) glycerol and 0.2 µl of 100 mM TCEP. The protein concentration was always 25 mg/mL.

Additional crystal optimization was performed by varying the type of polyethylene glycol (PEG) and the percentage used and the isopropanol was replaced by glycerol in the same percentage. A reproducible condition for crystal growth was achieved, 100mM Hepes pH 7.5, 10% glycerol, 18% PEG 8000. From a drop with multiple and small crystals, a streak seeding was done into three previous (15 minutes) pre-equilibrated drops with 100mM Hepes pH 7.5, 10% glycerol, 18% PEG 8000 in the reservoir solution (500 µl) and 100mM Hepes pH 7.5, 10% glycerol, 16% PEG 8000 in the drop with protein (25 mg/mL) in a 1:1 ratio. From the streak seeding protocol, a large crystal appeared with *c.a.* 1.4 mm in length (Figure 5.1a). The crystal was cryoprotected using the reservoir solution supplemented with 20 % glycerol prior to flash-cooling in liquid nitrogen.

Data Collection and Refinement

X-Ray diffraction data were collected at the European Synchrotron Radiation Facility, using the BM-16 beamline. A dataset was measured at a resolution of 2.0 Å; the data was then integrated using XDS (*226*). Scaling, merging and conversion to structure factors were carried out with SCALA and TRUNCATE (*227*). The crystal structure of DRbr was solved by the method MAD at iron K-edge energy, taking advantage of the content of four irons per monomer. Automatic chain tracing and building of side chains using the deduced aminoacid sequence were successfully conducted using the ARP/wARP program (*228*). Refinement was performed using REFMAC (*229*), and COOT (*230*) was used for model building during the refinement, to check the model against calculated $2|F_o|-|F_c|$ and $|F_o|-|F_c|$ electron density maps and make further corrections. The final model was validated using PROCHECK (*231*) and the Ramachandran plot, in which all the atoms are on the allowed regions. The final model had R_{factor} and $R\text{-}_{free}$ of 14.1 % and 18.2 %, respectively. Full details on data processing and refinement will be presented in the manuscript in preparation.

5.2 Results and Discussion

The protein was purified in three chromatographic steps under anaerobic conditions, as previously described (Chapter 4, (*115*)); in solution, the protein oligomeric state is a tetramer, as determined in the final purification step by size exclusion chromatography (Chapter 4, (*115*)). The purified protein was stored at -80 ºC in the buffer 20 mM Tris–HCl pH 7.2, 150 mM NaCl under anaerobic conditions. Although the protein was purified and stored under anaerobic conditions, the crystallization screens were performed aerobically; this change on the protein environment did not induce any protein degradation or precipitation during the experiment. Several aerobic crystallization screenings were carried out with the ‘‘as purified’’ protein, but always without success. Therefore, a thermofluor-based stability study was

performed, in order to find a different buffer formulation, where the protein would be more stable in solution, and thus increasing the likelihood of obtaining protein crystals. Considering the melting temperature and the protein-unfolding transient slope of DRbr, it can be concluded that the optimal condition is achieved by a 100 mM MES pH 6.2 buffer solution in the presence of of 500 mM NaCl (Figure 5.2).

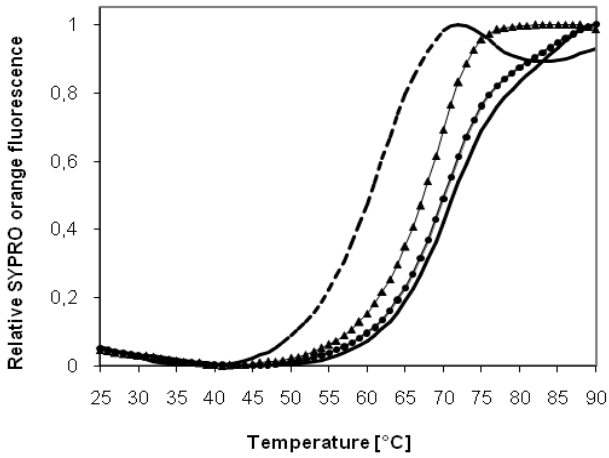

Figure 5.2 - Curves obtained from the fluorescence data, comparing the best buffer (100 mM MES pH 6.2) in combination with salt concentration, zero (solid line; Tm 71ºC and slope 5.8),150 mM (closed circles; Tm 70ºC and slope 6.2) and 500 mM (closed triangles; Tm 69ºC and slope 7.6) with the control experiment, 100 mM Tris–HCl pH 7.2, 150 mM NaCl (dotted line; Tm 62ºC and slope 6.7). Normalized variation of SYPRO Orange fluorescence with temperature.

In order to optimize DRbr protein crystals, a second crystallization screen was performed using the additive screen (Hampton Research). At this stage, protein crystals were observed with different additives: ammonium sulfate, sarcosine, 1,4-dioxane, methanol and TCEP hydrochloride, the latter being the one that gave the most promising crystals (Figure 5.1b and 5.1c). Although an improvement of crystal quality was obtained in the presence of additives, the X-ray diffraction measurements were done from the crystal obtained with no additives (Figure 5.1a).

Overall structure and domain swapping

The crystal structure of DRbr reveals four subunits in the asymmetric unit organized as a tetramer, which is in agreement with the previous data indicating a tetramer in solution (Chapter 4) (*115*). The DRbr monomer (Figure 5.3a) contains a N-terminal domain with a two-stranded-β-sheet, the desulforedoxin domain (Dx), followed by a four-helix bundle, composed by two pairs of helices (H1/H2 and H3/H4), separated by a linker; helix D is connected by another linker to the C-terminal domain, the rubredoxin domain (Rd), formed by a three-stranded-β-sheet.

The tetrameric configuration shows that the four-helix bundle domain is swapped, *i.e.,* two helices are from one monomer and the other two are from another monomer (Figure 5.3d). For monomer A, the N-terminal desulforedoxin (Dx) domain dimerizes with the N-terminal Dx domain from the monomer B; the four-helix bundle is swapped with the four-helix bundle domain from monomer B, and the C-terminal rubredoxin (Rd) domain is close to the swapped four-helix bundle domain of the monomers C and D (Figure 5.3).

Considering the swapping configuration of the two helix pairs from each monomer, the binuclear center is coordinated by ligands from two different monomers: the H1/H2 helices from monomer A contribute with coordinating ligands to the binuclear center together with H3/H4 helices from monomer B. This swapping domain configuration has been previously observed for rubrerythrin from *Pyrococcus furiosus* (*131, 133*) and for the erythrins from *Sulfolobus tokodaii* (*132*) and *Burkholderia pseudomallei* (pdb 4di0).

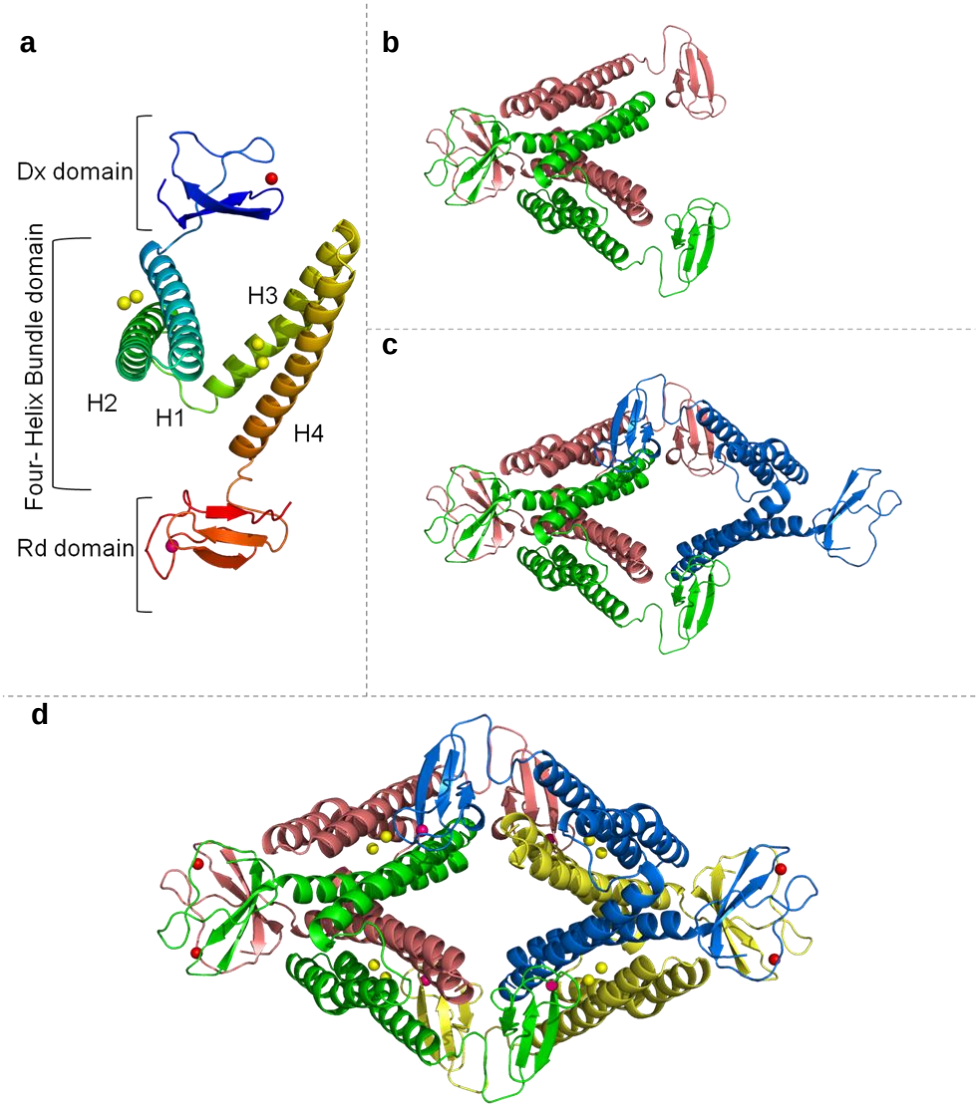

Figure 5.3 – Crystal structure of DRbr. a) Monomer structure is coloured from blue (N-terminal) to red (C-terminal); b) Dimer structure with monomer A (green) and monomer B (pink); c) Trimer structure with monomer A (green), monomer B (pink) and monomer C (blue); d) Tetramer structure with monomer A (green), monomer B (pink), monomer C (blue) and monomer D (yellow); Dx iron atoms are represented in red spheres, diiron atoms in yellow spheres and Rd iron atoms in pink spheres. H1 – helix 1, H2 – helix 2, H3 – helix 3, H4 – helix 4. Figure generated with PyMOL (*63*).

Iron sites

Each monomer accommodates three iron-binding sites, and four iron atoms. The N-terminal Dx domain has one solvent-exposed $Fe(Cys)_4$ iron site and the C-terminal Rd domain has another $Fe(Cys)_4$ iron center, also solvent-exposed but in close contact with the diiron center from the other pair of monomers.

The diiron center is represented in Figure 5.4a and b, in two configurations. It should be noticed that at this stage is not possible to accurately know to which redox states correspond the two forms observed. However, comparing with other structures we can suggest that upon reduction there is an iron movement going from the structure shown in Figure 5.4a (diferric or mixed-valence) to that in Figure 5.4b (mixed-valence or diferrous). The movement of the Fe1 of *c.a.* 2 Å is also accompanied by the increase of the distance between the two irons, from 3.27 to 3.83 Å (Figure 5.4, Table 5.1).

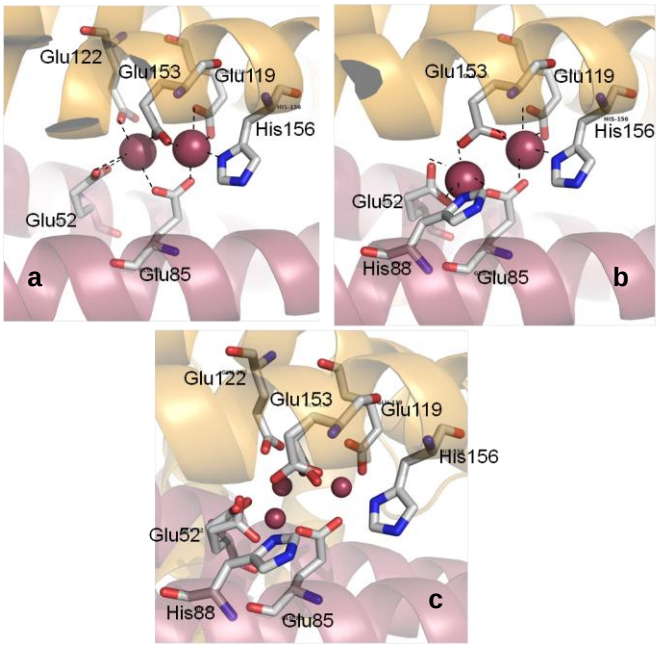

Figure 5.4 – Diiron center and coordinating ligands. a) Diferric or mixed-valence state, b) Mixed-valence or diferrous state, c) diiron center in the redox states determined, a and b overlapped. Iron ions in red. Fe1 is on the left and Fe2 is on the right. Iron ions are represented in red spheres. Figure generated with PyMOL (*63*).

The coordinating iron ligands are E52, E85 from one monomer and E119, E122, E153, H156 from the other monomer in the oxidized form (Figure 5.4a); in the reduced form E52, E85 and H88 from one monomer and E119, E153 and H156 from the other (Figure 5.4b) (see Table 5.1). The redox-dependent movement of Fe1 of *c.a.* 2 Å is accompanied by the unbinding of E122 and the binding of H88 to it, upon reduction (Figure 5.4). The same redox-dependent movement has been observed for the rubrerythrins from *D. vulgaris* and *P. furiosus* (*131, 135*) and for the erythrin from *S. tokodaii* (*132*). Both Fe1 and Fe2 in the more reduced state are square pyramidal coordinated. In the more reduced form each iron is ligated terminally by one bidentate glutamate, one histidine, a H_2O molecule and is bridged by two glutamate ligands. A H_2O molecule is proposed to be bound to each iron (*104*) in the reduced form and in the oxidized form to bridge the diiron atoms as a μ-oxo bridge, as seen by Resonance Raman data (Chapter 4), and by comparison with other Rbr structures.

Table 5.1 – Distances between the coordinating ligands and the diiron center in the two states. Position A corresponds to the more oxidized form and Position B to the more reduced one. The * corresponds to a change of conformation of the ligand Glu153. The type of bond of each ligand is also indicated.

Ligands of the diiron center	Fe1(position A) (distance in Å)	Fe1 (position B) (distance in Å)	Fe2 (distance in Å)
His156	-	-	2.17
Glu119 (bidentate)	-		2.32 2.33
Glu85 (bridging Fe1 and Fe2)	2.12	1.88	2.06
Glu153 (bridging Fe1 and Fe2)	1.87*	2.03	2.12 2.14*
Glu122	2.12	-	-
Glu 52 (bidentate)	2.25	2.06 2.29	-
His88	-	1.96	-

The strictly conserved residues in the vicinity of the diiron center Y59 and Y127 are hydrogen bonded to E119 and E52.

The diiron center is located 13 Å away from the nearest Rd iron site and 34 Å distant from the nearest Dx iron site, in another monomer (Table 5.2). This shows that Rd has to be the electron entry point, from an as yet unknown donor, passing the electron to the diiron center, located at a distance suitable for the electron transfer. The function of the Dx domain, apart from its possible contribution to the dimerization, remains unclear.

Table 5.2 – Distances between the iron centers in monomer A. The distances are relative to Fe1.

Iron centers		Distance (Å)
Fe1-Fe2 (A)	**Fe1**-F2 (B)	24
Fe1-Fe2 (A)	Rd (D)	13
Fe1-Fe2 (A)	Dx (B)	34
Fe1-Fe2 (A)	Rd (A)	33
Dx (A)	Dx (B)	16
Rd (A)	Dx (D)	43

Part III – Superoxide Reductase: Experimental Results

Introduction

Apart from the 1Fe-SOR from *Nanoarchaeum* (*N.*) *equitans*, which naturally lacks the glutamate residue that in many SORs binds the ferric ion, some SORs were also found lacking the Lys residue of the 'conserved' motif E_{23}**K**H**V**P_{27} (namely the 1Fe-SOR from the archaeon *Ignicoccus* (*I.*) *hospitalis*). In this enzyme, the lysine and valine residues are both replaced by threonine residues (Chapter 6, figures 6.1 and 6.2).

It has been generally reported for the catalytic cycle of SORs the existence of one or two intermediates (Figure III.I): one intermediate, T1, for the 2Fe-SOR from *Desulfovibrio* (*D.*) *vulgaris* and 1Fe-SOR from *Giardia*(*G.*) *intestinalis*; and two intermediates, T1 and T2, for 1Fe-SOR and 2Fe-SOR from *Archaeoglobus* (*A.*) *fulgidus*.

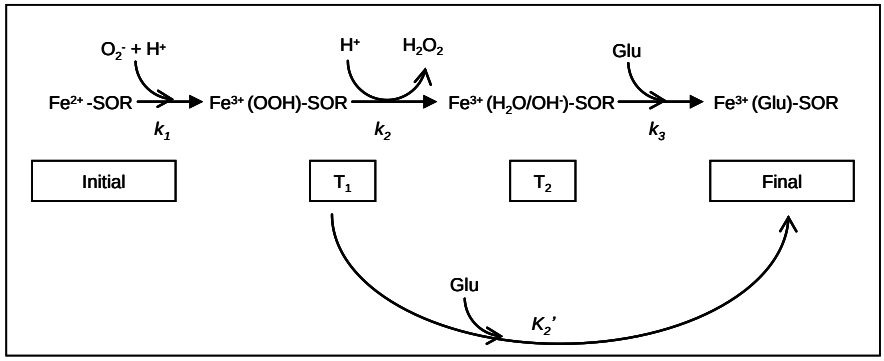

Figure III.I – Superoxide reduction mechanism and the different catalytic intermediates

To further clarify the number of intermediates in the catalytic cycle of SORs, in particular whether it is somehow related to thermophilicity, as well as the role of the "key" aminoacid residues lysine and glutamate (Lys13 and Glu12 in 1Fe-SOR from *A. fulgidus*, for residues numbering see Table 1) in the catalytic cycle and using preferentially wild-type (wt) enzymes instead of mutants, we decided to study the enzyme from *I. hospitalis*. Furthermore, we constructed a glutamate mutant E23A, thus simulating a double mutant in relation to the canonical enzymes, and a

revert mutant T24K, substituting the threonine residue by a lysine, in an attempt to “recover” the canonical enzyme.

Table III.I – Numbering of center II aminoacid ligands of the SORs represented in the sequence alignment in Chapter 6 (see Figure 6.1)
(-“residues not conserved “)

	Catalytic Fe ligands						
	Glu	Lys	His	His	His	Cys	His
1Fe-SOR							
P. furiosus	E14	K15	H16	H41	H47	C111	H114
D. gigas	E15	K16	H17	H45	H51	C115	H118
A. fulgidus	E12	K13	H14	H40	H46	C110	H113
N. equitans	-	K9	H10	H35	H41	C97	H100
I. hospitalis	E23	-	H25	H50	H56	C109	H112
2Fe-SOR							
D. vulgaris	E47	K48	H49	H69	H75	C116	H119
D. desulfuricans	E47	K48	H49	H69	H75	C116	H119
D. baarsii	E47	K48	H49	H69	H75	C116	H119
A. fulgidus	E47	K48	H49	H69	H75	C116	H119

The wt and mutant enzymes were extensively studied using pulse radiolysis, stopped flow techniques and potentiometric analysis (Chapter 6). The three dimensional structure was determined by X-ray crystallography for the SORs from *N. equitans* and *I. hospitalis*, as well as for the *I. hospitalis* SOR mutant, E23A (Chapter 7).

The results presented here provide a structural model for the interpretation of the properties and the mechanisms of superoxide reduction for this family of proteins.

Chapter 6

6 - Superoxide reduction in the crenarchaeon *Ignicoccus hospitalis*

Summary

Superoxide reductases (SORs) are the most recent superoxide detoxification systems identified in anaerobic and microaerophilic bacteria and archaea. SORs are metalloproteins characterized by a catalytic non-heme iron centre in the ferrous form, coordinated by four histidine and one cysteine ligands. A lysine residue (Lys24 in *Archaeoglobus fulgidus* numbering) near the active site is thought to confer a positive patch to attract the superoxide anion and to stabilize the intermediate of the reduction mechanism through an hydrogen bond. This residue is absent in *Ignicoccus hospitalis* 1Fe-SOR. Properties and catalytic mechanism of this SOR and two site-directed mutants were studied by a combination of spectroscopic methods and pulse radiolysis. Two mutants were studied: E23A in which the Glu residue, also conserved among the majority of SORs, was mutated; and T24K where the Lys residue was placed in the same position as for other SORs. The efficiency of the wt protein in reducing superoxide is comparable to other SORs, meaning that other positively charged residues should be assisting the reduction steps of superoxide anion. A lysine residue (number 21 in *Ignicoccus hospitalis* sequence) is found near the active site and is conserved among a group of SORs encoded in *Crenarchaeota*. This subgroup of archaea should have superoxide detoxification mechanisms as efficient as in other “canonical” SORs.

This Chapter includes material to be published in the manuscript:
"Superoxide reduction in the crenarchaeon *Ignicoccus hospitalis*" **Ana F. Pinto**, Célia V. Romão, Liliana C. Pinto, Harald Huber, Lígia M. Saraiva, Diane Cabelli, Miguel Teixeira

Ana F. Pinto is responsible for the experimental work and paper preparation.

Harald Huber generously cultivated and gave us genomic DNA from *Ignicoccus hospitalis*

Diane Cabelli is responsible for obtaining all the pulse radiolysis data and is a long-term collaborator in Superoxide Reductases studies

Lígia M. Saraiva hosted and supervisioned in the "Molecular Genetics of Microbial Resistance Laboratory", the molecular biology work on the superoxide reductase from *Ignicoccus hospitalis*

6 - Superoxide reduction in the crenarchaeon *Ignicoccus hospitalis*

6.1 - Experimental Procedures

Cloning and overproduction of recombinant wt and site-directed mutants of SOR from Ignicoccus hospitalis

Amplification of the complete gene (375 bp) encoding the wt 1Fe-SOR from *Ignicoccus* (*I.*) *hospitalis* was achieved by PCR using *I. hospitalis* genomic DNA and the oligonucleotides presented in Table 6.1. The obtained DNA fragment was cloned into vector pET24a (+) (Novagen) yielding pET241FeSOR, which was transformed into *Escherichia (E.) coli* XL2Blue cells and, once the correct sequence was confirmed by DNA sequencing, introduced into *E. coli* BL21(DE3)Gold cells for production of the recombinant wt protein.

For the modification of selected amino acid residues, we used plasmid pET241FeSOR and the appropriate pair of primers (Table 6.1) and followed the protocol described in the Quik Change TM Site-directed mutagenesis kit from Stratagene. The generated vectors pET241FeSORE23A and pET241FeSORT24K were next transformed into *E. coli* XL1Blue cells and, once confirmed the correct sequence and the absence of undesirable mutations, the vectors were transferred to the expression strain *E. coli* BL21 (DE3) Gold.

Protein production was achieved by growing the *E. coli* cells aerobically, at 37 ºC, in M9 minimal medium, supplemented with 30 µg mL^{-1} kanamycin and with 200 µM $FeSO_4.7H_2O$, until the OD_{600nm} reached 0.3. At this stage 400 µM isopropyl-1-thio-β-D-galactopyranoside (IPTG) was added, the temperature was lowered to 28 ºC and the growth continued for 20 h. The cells were then harvested by centrifugation at 10 000 g for 10 min at 4ºC, and used to isolate the SOR proteins.

Table 6.1 – Table of primers used for the amplification of Igni_1348 gene and the primers used for the mutagenesis protocol.

Gene	Primers	
Igni_1348		
Forward	5`-GAG GAC ACG GAC GAG **CAT ATG** AAG AG-3`	Nde I restriction site
Reverse	5`-GAG GGA GAA CG**A AGC TT**T TTC CTT TC-3`	Hind III restriction site
Igni_1348	(E23A mutant)	
Forward	5'-GCC ATA TCC AAG GCT **GCC** ACC CAT ACG CCC AAG A-3'	mutation for E23A in bold
Reverse	5'-TCT TGG GCG TAT GGG TG**G CA**G CCT TGG ATA TGG C-3'	mutation for E23A in bold
Igni_1348	(T24K mutant)	
Foward	5´- CCA AGG CTG AG**A AG**C ATA CGC CCA AGA -3'	mutation for T24K in bold
Reverse	5´- TCT TGG GCG TAT GC**T TC**T CAG CCT TGG -3'	mutation for T24K in bold

Purification

The cells collected were resuspended in a buffer containing 20 mM Tris-HCl pH 7.6, 1 mM phenylmethanesulphonyl fluoride (PMSF) and 20 µg mL^{-1} DNase I (Sigma) and broken in a minicell French press at 19 000 psi. All subsequent purification steps were done at pH 7.6 and 4 ºC. After centrifugation at 100 000 g for 2h, the soluble extract was dialyzed against 20 mM Tris-HCl pH 7.6 and 1 mM PMSF (buffer A). Before the chromatographic purification, the soluble fraction was heated for 20 min at 60 ºC and centrifuged for 20 min at 7000 g. The supernatant was then loaded onto an anionic exchange column, a Q-Sepharose fast flow column (XK 26/10) (GE Healthcare) previously equilibrated with buffer A; the column was eluted with a linear gradient of 0-1 M NaCl. The fraction containing the SOR was eluted around 0 mM of NaCl and was concentrated by ultra filtration (Amicon) and loaded onto a Superdex 75 column (XK 26/60) (GE Healthcare) previously equilibrated with 20 mM Tris-HCl pH 7.6 and 150 mM NaCl. The collected fractions were analyzed and judged to be pure on the basis of SDS-PAGE (*211*). The oligomerization state was determined by size-exclusion chromatography on a Superdex 200 column (XK 10/300, GE Healthcare), using

appropriate molecular mass standards. The protein concentration and total iron content were determined by the BCA assay (Pierce) (*212*) and the TPTZ method (*213*), respectively. The mutants were purified as the wt protein. The yield of pure protein was 17 mg /L of growth for the wt protein and E23A SOR mutant and 3 mg/L of growth for the T24K SOR mutant.

Spectroscopic Studies

All UV-Visible studies were performed at room temperature on a Shimadzu UV-1603 spectrophotometer.

pH studies by Stopped-Flow

For determining the pK_a of the oxidized form of *I. hospitalis* 1Fe-SOR (wt and mutants) a Bio-Logic stopped-flow SM300/S apparatus equipped with a TIDAS spectrometer was used. The change in pH was accomplished by mixing 145 µM of SOR, in 20mM Tris-HCl pH 7.6 and 150mM NaCl, with 100mM of Bis-tris propane and MES or CAPS with the desired pH, loaded in two separate syringes, with a volume ratio of 1:5. The spectra were recorded and the pH induced wavelength shifts were registered from *c.a.* 640 nm at high pH to *c.a.* 540 nm at low pH. The data was fitted to a single-protonation equilibrium $pH = pK_a^{ox} + \log([HA]/[A]$, HA and A being the protonated and deprotonated forms, respectively. The change in pH was confirmed by directly measuring the pH of a solution at 1:5 ratio of protein solution to buffer.

Redox titrations

Redox titrations followed by UV/Visible spectroscopy were performed anaerobically in 50 mM Tris-HCl, 50 mM Bis-tris propane or MES at the desired pH, by stepwise addition of sodium ascorbate as reductant and potassium hexachloroiridate (K_2IrCl_6) as oxidant. A 50 µM protein solution, a combined Ag/AgCl electrode and the following redox mediators (7 µM each) were used: ferrocene (E'_0 = +530 mV), N,N dimethyl-p-phenylenediamine (E'_0 = +340 mV), tetramethyl-p-

phenylenediamine (E'_0 = +260 mV), ρ- benzoquinone (E'_0 = +240 mV), 1,2-naphtoquinone (E'_0 = +180 mV), trimethylhydroquinone (E'_0 = +115 mV), 1,4-naphtoquinone (E'_0 = +60 mV) and duroquinone (E'_0 = +5 mV). The electrodes were calibrated with a saturated quinhydrone solution at pH 7.0. The reduction potentials values are reported against the standard hydrogen electrode (SHE). All experimental data were analyzed using Nernst equations considering a single one-electron transition for the iron center.

Reactivity towards Superoxide: Pulse Radiolysis assays

Pulse radiolysis experiments were performed at the Brookhaven National Laboratory (BNL) using a 2 MeV Van der Graaf accelerator as already described (*232*). Dosimetry was carried out using the $(SCN)_2^-$ dosimeter assuming a G value of 6.0 and a molar extinction coefficient of 7950 $M^{-1}cm^{-1}$ at 472 nm. Superoxide radicals (1-20 μM) were generated using doses of 100-2500 rads. Water radiolysis yields the following species, where the number in parentheses are G values, that is the number of molecules/100 eV of energy absorbed by the medium (*164*)

$H_2O \rightarrow e_{aq}$ (2.75), $^{\cdot}OH$ (2.65), H (0.65), H_2O_2 (0.7), H_2 (0.45)

The primary radicals e_{aq}, $^{\cdot}OH$ and H can be converted to $O_2^{\cdot -}$ radicals in the presence of formate (HCO_2^-) and oxygen (*233*)

$e_{aq} + O_2 \rightarrow O_2^{\cdot -}$ $pK_a(HO_2/O_2^{\cdot -}) = 4.8$

$^{\cdot}OH/H + HCO_2^- \rightarrow H_2O/H_2 + CO_2^{\cdot -}$

$CO_2^{\cdot -} + O_2 \rightarrow O_2^{\cdot -} + CO_2$

All pulse radiolysis samples were prepared using Millipore ultra purified distilled water. When needed, prior to the assay, the protein was

reduced with the addition of stoichiometric quantities of sodium ascorbate. The experiments were done at 25ºC and 65ºC in air-saturated solutions containing 4 to 8 µM of oxidized SOR for studies of the superoxide dismutation and 40 to 100 µM of reduced SOR for the study of the intermediates of superoxide reduction. The initial conditions for the superoxide dismutase activity were: 0.1 M phosphate, 50 mM formate and 10 µM EDTA, pH 7.4. For the studies of the intermediates on superoxide reduction, the conditions were: 2 mM Tris-HCl, 6.6 mM NaCl and as the $OH^{\cdot}$ radical scavenger 50 mM of formate or 0.5 M of ethanol. The pulses of superoxide were in the range of 0.6 - 3.6 µM. The oxidation of the SORs by superoxide was measured at 500-700 nm by following the absorbance changes as a function of time from the microsecond to the second time scales. The data were analyzed using the BNL Pulse Radiolysis Program, Prwin.

6.2 - Results and Discussion

Aminoacid sequence comparisons

The SOR from the hyperthermophilic *I. hospitalis* was chosen for further studies of this enzyme family by aminoacid sequence comparisons with other SORs, because it is lacking a residue, conserved among almost all the members of this protein family: lysine 13 (*A. fulgidus* SOR numbering), which is substituted by a threonine (T24 in *I. hospitalis* numbering) (Figure 6.1 and Table III.I). This residue has been thought to have an important catalytic role either by attracting the anionic substrate or by stabilizing catalytic intermediates, or even to act as a direct proton donor to an intermediate species (*168, 234*).

A blast search using *I. hospitalis* SOR sequence as query revealed that this is not the only example lacking that lysine residue: eight other protein sequences were found to have this residue substituted by a serine or a threonine residue (Figure 6.1 and 6.2); seven of these proteins belong to organisms of the Crenarchaeota phylum: *Staphylothermus hellenicus*, *Staphylothermus marinus*, *Hyperthermus*

butylicus, *Thermofilum pendens*, *Desulfuroccus mucosus*, *Thermosphaera aggregans*, *Desulfuroccus kamchatkensis,* while the eighth is from *Archaeoglobus profundus,* which belongs to the Euryarchaeota phylum. It should be noted that these are all hyperthermophilic organisms. The aminoacid sequence alignment suggests that there are some other small differences that will probably reflect some structural alterations but the ligands coordinating the iron are all conserved. The aminoacid sequence similarities and identities of *I. hospitalis* SOR to the other SOR sequences are approximately 78% and 63%, respectively for the Lys lacking SORs, and 45% and 34% respectively for the remaining SORs (Figure 6.1). This group of 8 enzymes lacking a Lys residue forms a subgroup of SORs in this varied family of enzymes (see Chapter 8, figure 8.4). Interestingly, no other residue considered relevant was found to be modified or absent apart from the above noted glutamate and lysine.

Although these enzymes lack the Lys residue in the E_{23}**K**H**V**P_{27} motif, there is another Lys residue conserved among them that occupies the 21st position (Figure 6.1) (for *I. hospitalis*) and conserved in the majority of SORs (*e.g. A. fulgidus* SOR). This residue may replace the missing Lys, thus conferring the positive charge to the surface that is important for the first step of the mechanism (see Chapter 7).

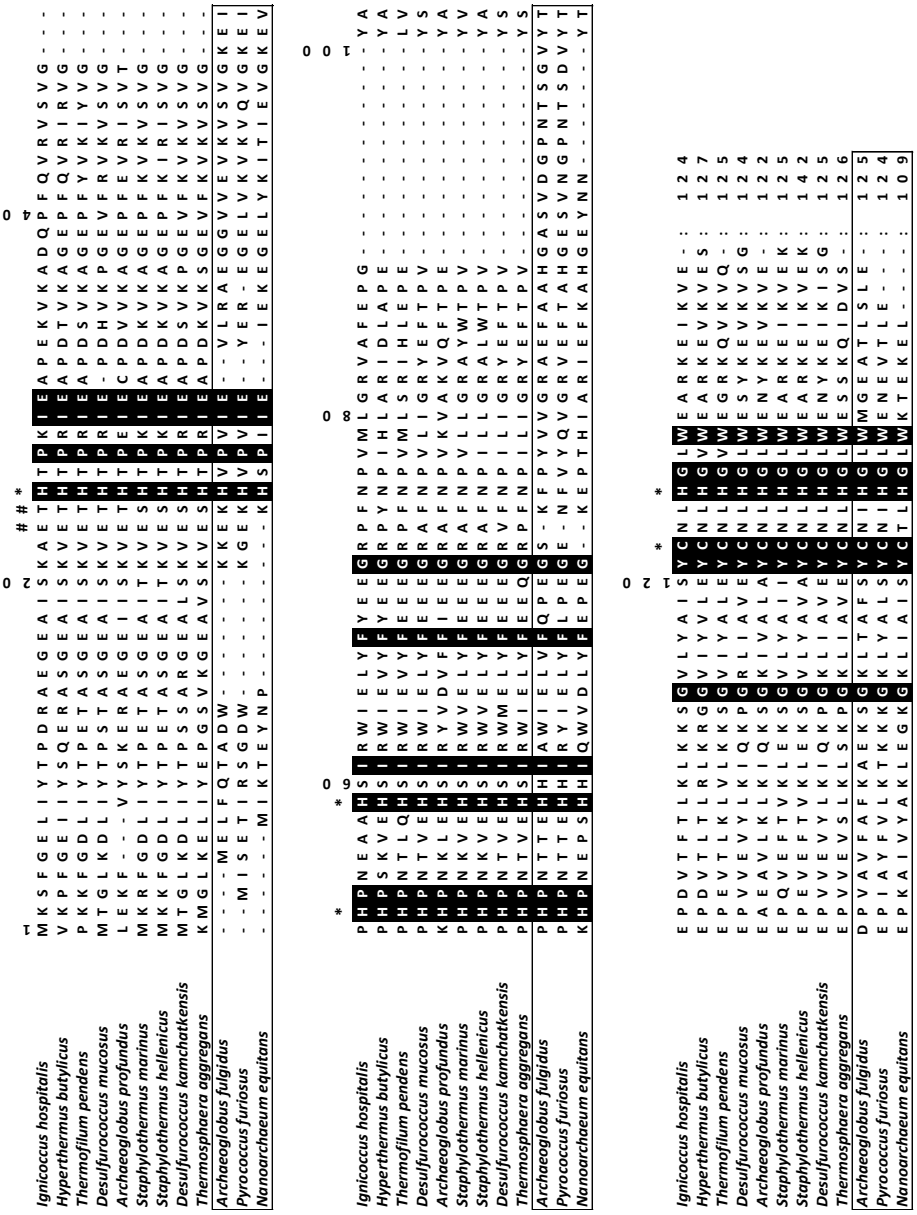

Figure 6.1 – Aminoacid sequence alignment of SORs, using ClustalX (*148*). Residues that bind the catalytic center are indicated by an asterisk (*); the residues indicated by cardinal (#) correspond to the positions of the "conserved" residues Lysine and Glutamate; the strictly conserved residues in all SORs are shaded in black. Aminoacid identities towards the aminoacid sequence of the SOR from *I. hospitalis*, are presented between ( ).The SORs from *A. fulgidus*, *P. furiosus* and *N. equitans* are enclosed in a box. 1Fe-SORs: *Ignicoccus hospitalis* (gi|156938135); *Hyperthermus butylicus* (gi|124028022,

66%); *Thermofilum pendens* (gi|119720733, 67%); *Desulfurococcus mucosus* (gi|320101022, 62%)*; Archaeoglobus profundus* (gi|284161748, 55%); *Staphylothermus marinus* (gi|126464958, 74%); *Staphylothermus hellenicus* (gi|297526761, 64%); *Desulfurococcus kamchatkensis* (gi|218883740, 60%); *Thermosphaera aggregans* (gi|296242328, 59%); *Archaeoglobus fulgidus* (gi|3914137, 35%); *Pyrococcus furiosus* (gi|6066244, 37%); *Nanoarchaeum equitans* (gi|41614807, 31%).

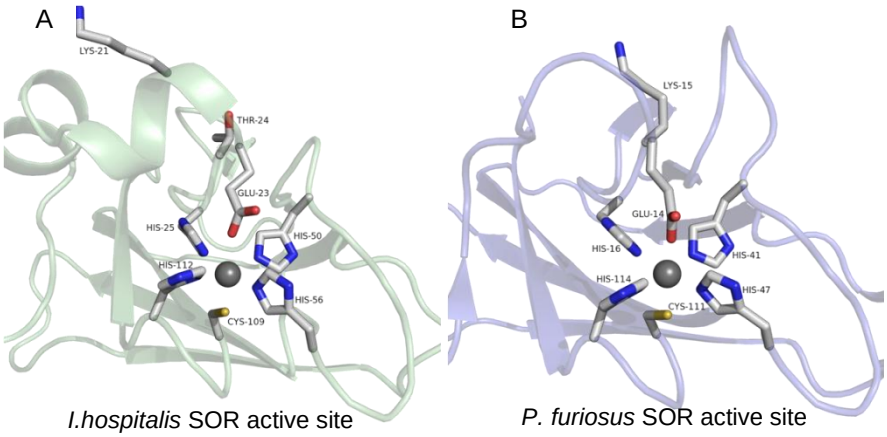

Figure 6.2 –Active center in the oxidized state of A) 1Fe-SOR *Ignicoccus hospitalis* (see chapter 7) and B) 1Fe-SOR *Pyrococcus furiosus* (pdb: 1DQI; chain C). These pictures were created using PyMOL (*63*).

Protein characterization

The SOR from *I. hospitalis* is a 1Fe-SOR, and the wt protein and the two mutants E23A and T24K were overexpressed successfully in *E. coli* and isolated as homotetramers as determined by gel filtration, with each monomer having a molecular mass of ~14kDa, determined by SDS-PAGE, in agreement with the value predicted from the aminoacid sequence. The iron content of each SOR was determined as 1.0 ± 0.1 atoms of Fe per monomer for the wt protein and T24K mutant and 0.90 ± 0.1 for the E23A mutant. These results correspond to an almost full occupancy of the active site by iron. The ferric forms of these SORs have characteristic visible spectra that derive from the charge transfer from the Cys ligand to the Fe^{3+} (*158*). This charge transfer reflects on

the color of the protein: wt and T24K proteins were isolated with a blue color (pH 7.5) and E23A mutant was isolated with a violet color (pH 7.5).

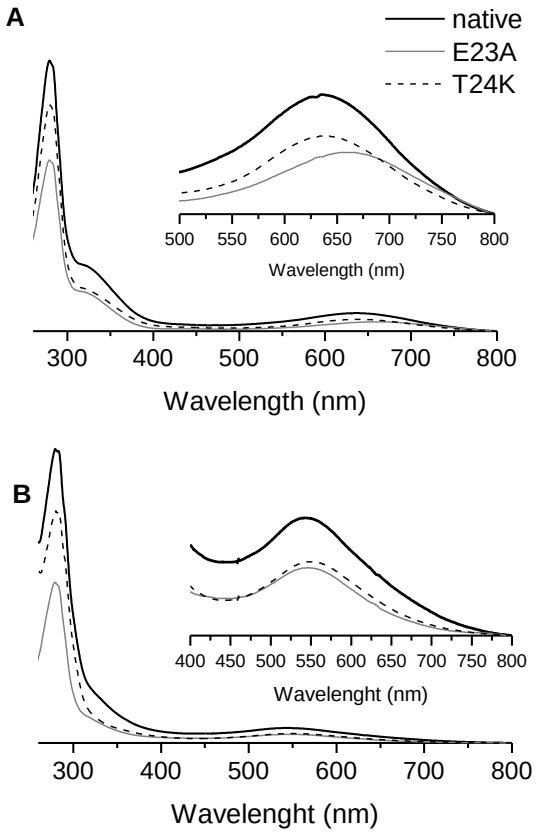

Figure 6.3 – UV-Visible spectra of wt *I. hospitalis* 1Fe-SOR (40 µM), and the E23A (20 µM) and T24K (40 µM) mutants. A) Spectra at low pH values in 100 mM Bis-Tris propane and MES buffer: pH 7 for wt and T24K proteins and pH 5 for E23A protein; B) Spectra at high pH values in 100 mM Bis-Tris propane and CAPS buffer: pH 11.5 for wt and T24K proteins and pH 7 for E23A protein. Wild-type protein (solid black line), E23A mutant (solid grey line) and T24K mutant (dashed line). The spectra are offset vertically. Insets magnified 5 times.

The charge transfer band is red-shifted upon pH increase as in other SORs (Figure 6.3). For the wt and T24K mutant protein the acidic form has absorption maxima at 640 nm and 325 nm, while for E23A the

maximum absorption is at 665 nm and 325 nm. For the basic forms these SORs have an absorption maximum at *c.a.* 550 nm.

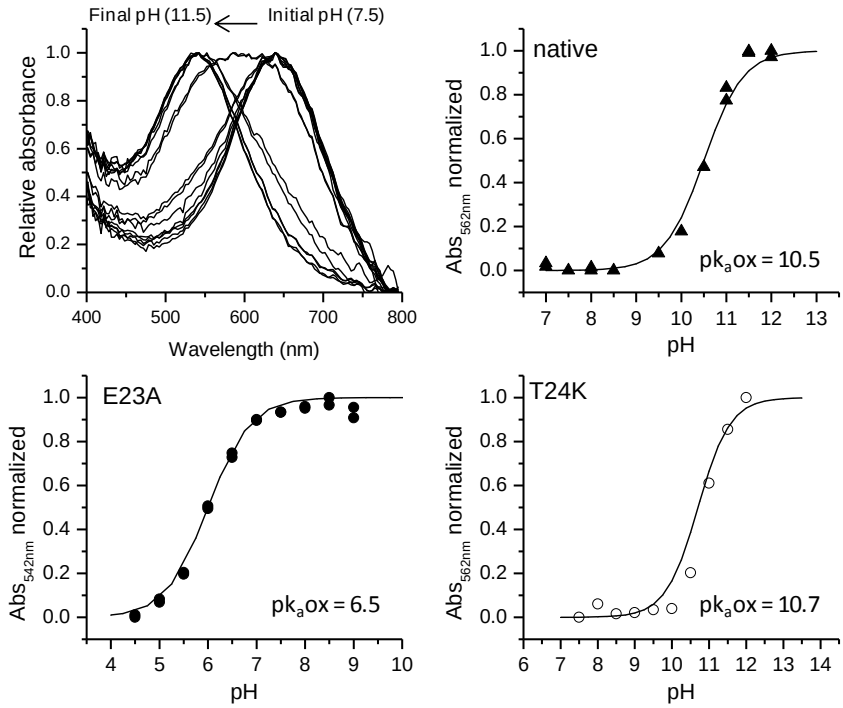

Figure 6.4 – pH Titration curves for wt and T24K proteins following the increase of absorbance at 562 nm and for E23A protein at 542 nm upon pH increase. The solid lines were obtained assuming single protonation equilibria with the indicated associated pK_a. The first panel shows an example of raw data obtained for the wt enzyme.

Apparent pK_a of 10.5 and 10.7 were determined for the wt protein and for the T24K mutant, respectively. These values show that the residue at position 24 has virtually no effect on the pH-linked ligand exchange of the oxidized form, possibly due to its distance from the center (Figures 6.2 and 6.4). On the contrary, the substitution of the glutamate 23 by an alanine leads to a decrease of the apparent pK_a by almost 4 units (Table 6.3), as observed in other enzymes (*160*) and reflecting the increased facility of binding the hydroxide anion in the absence of the

carboxylate ligand. This pK_a is associated, as shown by Resonance Raman spectroscopy (*158-159*), to the binding of an OH^- group upon dissociation of glutamate/H_2O at basic pH (*158*).

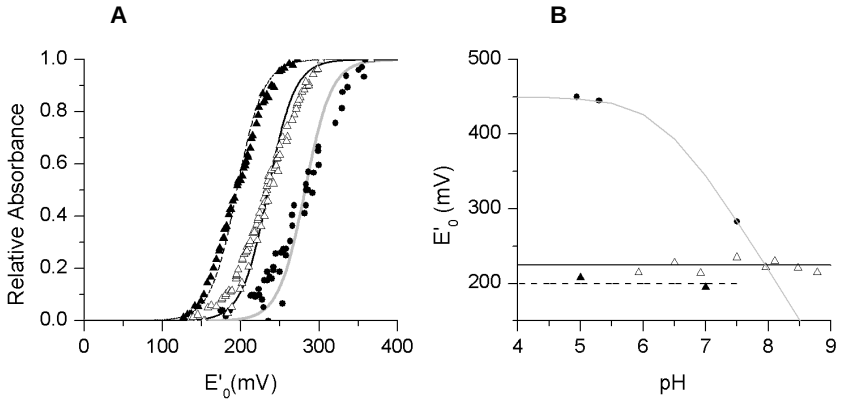

Figure 6.5 – A) Redox titration of wt (open triangle), E23A (black circle) and T24K (black triangle) proteins from *I. hospitalis*. The titration curves were obtained measuring the absorbance at 636 nm for wt and T24K (pH 7), and at 580 nm for E23A (pH 7.5); the solid lines correspond to a Nernst equation with n=1; E'_0 (wt) = + 230 mV; E'_0 (E23A) = +283 mV; E'_0 (T24K) = + 195 mV. B) E'_0 (mV) *versus* pH for wt (open triangle), E23A (black circle) and T24K protein (black triangle) proteins, The solid line correspond to the equation: $E = E'_0 + (nF/RT)\ \log[(K_{red} + [H^+])/(K_{ox} + [H^+])]$; E– standard redox potential; n– number of moles of electrons; F- Faraday constant; R– Universal gas constant; T- temperature; $K_{red} = 10^{-pka(red)}$; $K_{ox} = 10^{-pka(ox)}$.

The reduction potentials (E'_0) of each SOR were determined to be +235 mV (pH 7.5), + 283 mV (pH 7.5) and +195 mV (pH 7.1) (*vs*. SHE), for the wt, E23A, and T24K enzymes, respectively (Figure 6.5), which are in the range of values found for the other SORs (+190 to +365 mV) (Table 6.3). The E'_0 of the wt enzyme and the T24K mutant remain constant between pH 5 and pH 7; on the contrary, for the E23A mutant the E'_0 has a huge increase to +450 mV at pH 5 (Table 6.2), decreases to +283 mV at pH 7.5. The preliminary data leads to an estimated value for the pK_a of the oxidized form of 6.3, which is comparable to the pK_a for the red-shift for the H_2O/OH^- exchange (Figure 6.5). In E23A the pH

dependence of the E'_0 is related with the change of iron coordination and reflects the effect of the binding of the small strong anionic ligand OH^-. A similar pH dependence of the redox potential was observed by Niviére et al, 2004 (*160*), for the 2 Fe-SOR from *Desulfoarculus baarsii*.

Table 6.2 – Reduction potential for *I. hospitalis* SORs at two pH values (5 and ~7.5)

***I. hospitalis* SOR**	**E'_0 (pH 5)**	**E'_0 (pH 7.5)**
wt	+215 mV	+ 235 mV
E23A mutant	+450 mV	+ 283 mV
T24K mutant	+208 mV	+195 mV (pH 7.1)

Kinetics studies

The reaction of the wt protein and the two mutants with superoxide was studied by fast kinetics using pulse radiolysis.

- *Superoxide dismutase activity*

Initial experiments were carried out by monitoring the decrease in the concentration of superoxide anion monitored at 260 nm, in the presence or absence of the enzyme due to the reaction with SOR (eq 6.1 and 6.2) or to the bimolecular auto-disproportionation process (eq 6.3).

$$SOR^{3+} + O_2^{\cdot -} \rightarrow SOR^{2+} + O_2 \qquad \text{(eq 6.1)}$$

$$SOR^{2+} + O_2^{\cdot -} + 2H^+ \rightarrow SOR^{3+} + H_2O_2 \qquad \text{(eq 6.2)}$$

$$O_2^{\cdot -} + HOO^{\cdot} + H^+ \rightarrow O_2 + H_2O_2 \qquad \text{(eq 6.3)}$$

The traces can be fitted to a model involving two simultaneous first order and second order processes. In the presence of the wt enzyme, the rate for the dismutation of superoxide was 5 s^{-1} at 17ºC (4 µM of SOR) at pH 7.1, and the rate of auto-dismutation of superoxide (2.6 µM) in buffer of 5 x 10^5 $M^{-1}s^{-1}$. The plot of the two traces is shown in Figure 6.6A. With the increase of the temperature to 65ºC the rate of wt SOR increased to 19 s^{-1}, and is now better separated from the spontaneous

dismutation of $O_2^{\cdot-}$ in buffer. That the rate is clearly measurable at 65ºC strongly suggests that there is a real catalytic rate of superoxide dismutation by SOR. The same behavior is observed for the E23A and T24K mutants (Figure 6.6B). At pH 7.4, the rate for the catalytic consumption of $O_2^{\cdot-}$ by E23A increases from 8.7 s^{-1} to 20 s^{-1} as the temperature goes from 17ºC to 65ºC. In the case of T24K the rates vary from 6.5 s^{-1} to 17.7 s^{-1} over the same temperature range.

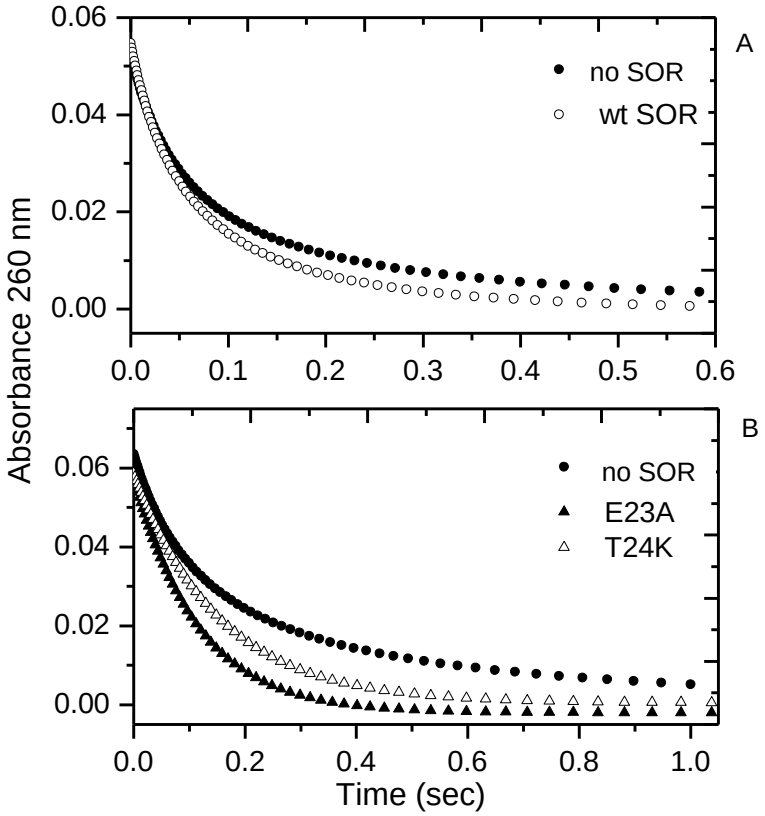

Figure 6.6 – Pulse Radiolysis assay for the catalytic dismutation of superoxide anion ($O_2^{\cdot-}$) followed at 260 nm. The assays were performed in 0.1 M phosphate buffer, pH 7.1 for wt protein and pH 7.4 for mutant proteins, in the presence of 50 mM formate and 10 µM EDTA, in an aerobic atmosphere. A) Consumption of superoxide (2.6 µM), at 25º C, in the presence of 4 µM wt *I. hospitalis* 1Fe-SOR (-○-) and in the absence of SOR (-●-). B) Consumption of superoxide (2.6 µM), at 25º C, in the presence of 4 µM E23A *I. hospitalis* 1Fe-SOR (-▲-), in the presence of 4 µM T24K *I. hospitalis* 1Fe-SOR (-Δ-) and in the absence of SOR (-●-).

For these two mutants, the consumption of superoxide has predominantly a first-order component as the spontaneous disproportionation is slower at 17ºC whereas the catalytic rate is faster.
In comparison with the 1Fe-SOR from *A. fulgidus*, the SOD activity of these SORs are comparable; for *I. hospitalis* the SOD activity at 65ºC and pH 7.1 for the wt protein is 7 x 10^6 $M^{-1}s^{-1}$ and at pH 7.4 for the mutants E23A and T24K is 8 x10^6 $M^{-1}s^{-1}$ and 7 x 10^6 $M^{-1}s^{-1}$, respectively, while for the 1Fe-SOR from *A. fulgidus* a rate of 5 x 10^6 $M^{-1}s^{-1}$ at pH 7.1 and 83ºC was obtained (*235*). In comparison with canonical SODs, the catalytic activity is still two to three orders of magnitude lower (10^{-9} $M^{-1}s^{-1}$).

- *Superoxide reduction activity*

The mechanism of the reaction was investigated by pulsing the reduced enzyme (40-80 µM) with substoichiometric amounts of $O_2^{\cdot-}$ (1.4-2.4 µM). The resultant absorbance changes for both the wt protein and the two mutants are similar. Upon pulsing the reduced wt enzyme with $O_2^{\cdot-}$, an intermediate T_1 is formed in a pseudo first-order process with rates approaching diffusion limit, analogous to that observed so far for all SORs (Figure 6.7A, Table 6.3). This first transient species has a visible spectrum (Figure 6.7C) with a maximum at 590 nm and an extinction coefficient of 3800 $M^{-1}cm^{-1}$ that is characteristic of the (hydro)peroxo-bound ferric species (see Chapter 8). The formation of the T1 species is pH independent and it decays directly into the final species, the Glu-bound Fe^{3+} form or a presumably H_2O-bound form, for the E23A mutant (Figure 6.7B, C). This process is pH-dependent at lower pH and is pH independent at higher pH and the rates can be fitted to the following equation: k_2(obs) = k_2' $[H^+]$ + k_2'' (*234*). At acidic pH values the decay of T_1 is proportional to proton concentration and presumably occurs with a rate-dependent protonation process with a second-order rate of 1.5 x 10^9 $M^{-1}s^{-1}$ (k_2'). At basic pH the first-order process is pH-independent and occurs at a rate of 30 s^{-1} (k_2''), likely involving a proton from a water molecule (Figure 6.7D).

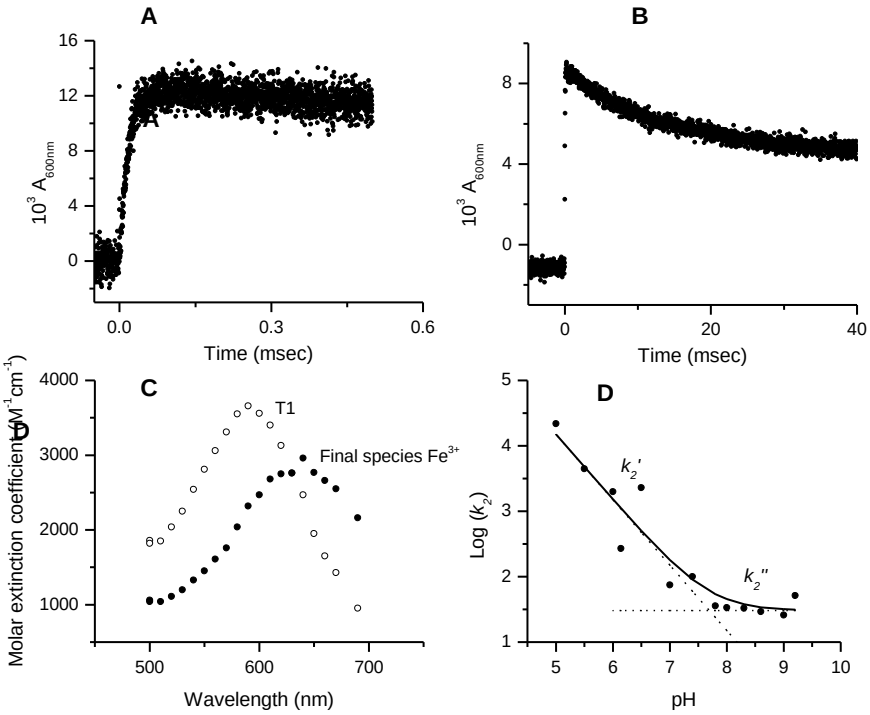

Figure 6.7 – Formation (A) and decay (B) of the T1 intermediate at 600nm following the pulse radiolysis of 40 µM 1Fe-SOR (wt) with 2.6 µM $O_2^{\cdot-}$. In A) the formation of T1 in a range of less than 0.1 ms is a pseudo first-order process and in B) the decay into the final species is a 40 ms process. In C) are the reconstructed Visible spectra of the two species formed, T1 (○) and final oxidized species (●). Molar absortivities were calculated assuming a 1:1 molar stoichiometry of superoxide versus reacted ferrous [$Fe(His)_4(Cys)$] sites. In D) the pH dependence of rate constant k_2 for wt 1Fe-SOR is shown and it was observed upon the decay of T1 in a range of pH from 5 to 9. The black curve corresponds to the fitting of the data to the equation k_2 (obs) = k_2' [H+] + k_2''. All solutions were aerobic in 2 mM Tris-HCl, 6.6 mM NaCl, 50 mM of formate.

The pH independent process was only properly measured for the T24K mutant leading to a k_2'' = 64 s-1, due to a higher stability of this mutant in comparison with the wt and E23A mutant proteins, that have not achieved a proper plateau region. The final species for these enzymes are equivalent to their ferric form or resting state and is generated in stoichiometric amounts, in relation to the amount of superoxide used.

6.3 - Final Conclusion

In *I.hospitalis*, the encoded SOR does not have the conserved motif **EKHVPV**, but rather a motif, **$E^{23}T^{24}HTP^{27}$**, where the Lys residue is absent making it a good naturally-occurring example for studying the role of this residue in the mechanism. By analyzing the sequences in the databases (Figure 6.2) we found out that there are 8 more "Lys lacking"- SORs encoded in Archaea, namely from the Crenarchaeota phylum, and they all have an extra-motif, **$G^{16}EAISK^{21}$** (*I. hospitalis* numbering). These "Lys lacking"- SORs cluster in a specific group, according to Lucchetti-Miganeh *et al.*, (*143*), that may represent a differentiation of a SOR subfamily. In order to understand if these SORs are still effective enzymes, we characterized the *I. hospitalis* SOR and two site-directed mutants. The expected spectroscopic features for the oxidized enzyme were obtained for the wt protein, the T24K and E23A mutants, as well as the pH-equilibrium related to the glutamate unbinding/binding and OH^- binding at basic pH. For E23A the proton equilibrium has a pK_a of 6.5 which is associated with Glu-lacking and Glu-mutant SORs, where a H_2O/OH^- equilibrium is observed. The replacement of the threonine residue by a lysine, maintained the pK_a of the wt protein (10.7) which may mean that the pK_a associated with the Glu-substitution and OH- binding is not dependent on specific charged residues near the active site.

The initial reaction in the superoxide reduction between the ferrous center and the superoxide occurs at a virtually diffusion-controlled rate ($\sim 10^9\ M^{-1}s^{-1}$). In this step, the active center is a pentacoordinated Fe^{2+} and upon superoxide binding forms a Fe^{3+}- hydroperoxo or a Fe^{3+} -peroxo that rapidly protonates to form the hydroperoxo form. This intermediate (T1) is formed in all SORs studied so far, since it has very similar spectroscopic features and the rate of formation is always pH independent. However, its full characterization is still not known since it is too short lived (see [1]footnote pag. 141). Some assumptions about its

structure come from density functional theory (DFT) calculations (*166*), Mössbauer and Resonance Raman spectroscopies (*165, 167, 236*), and a combined X-ray diffraction and Resonance Raman spectroscopy study of SOR crystals incubated with H_2O_2 (*168*). The general assumption that T1 is a ferric end-on (hydro) peroxo rather than a side-on peroxo was proposed by Silaghi-Dumitrescu and co-workers (*166*) by modeling the SOR active site and different iron peroxo adducts. The work published by Katona and co-workers, based on X-ray diffraction data at 1.95 Å resolution and Raman spectra recorded for a SOR E114A mutant from *D. baarsii* incubated with H_2O_2 revealed an iron-(hydro)peroxo intermediate with the (hydro)peroxo group bound end-on (*168*). The same authors also performed DFT calculations proposing a high-spin ferric hydroperoxo species protonated at the distal oxygen. The proton dependent decay of T1 is also indicative that the release of the H_2O_2 product occurs upon proton transfer, which suggests that the first proton is already bound to $O_2^{\cdot-}$ when T1 is formed. The diffraction data of the oxidized enzyme incubated with H_2O_2, showed the formation of the hydroperoxo-Fe^{3+} species with the involvement of a hydrogen bond network (*168*). Near the active site there is also a Lys residue, that upon superoxide binding changed conformation, and it is facilitating the hydrogen bond network around the distal oxygen (Fe^{3+}-OOH) due to electrostatic interaction of this positively charged residue with the hydroperoxo ligand (Figure 6.8) (*168*). It was then proposed the importance of this residue in the catalytic mechanism of superoxide reduction by creating a positive patch around the active site attracting the substrate, as well as possibly stabilizing the hydroperoxo species.

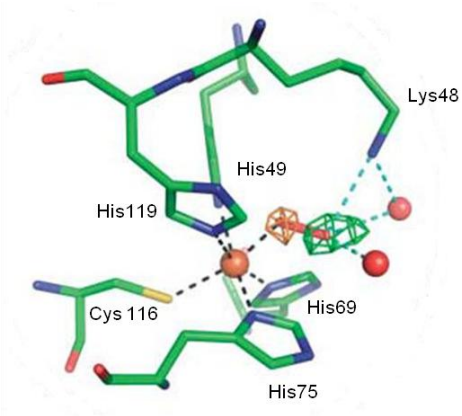

Figure 6.8 - The active site of the SOR-E114A from *D. baarsii* upon incubation of the reduced form with H_2O_2. The residues coordinating the iron are represented as sticks. The bound peroxide ligand is shown as a red stick. Water molecules are shown as red balls. From (*168*).

The pulse radiolysis studies showed that, as for the 1Fe-SOR from *A. fulgidus*, these enzymes also have a superoxide dismutase activity, although 10^2 to 10^3 lower than that of SODs. The catalytic activity of SORs can compete with superoxide auto-dismutation at higher concentrations of enzyme *in vivo*. Increasing the temperature to 65ºC also increased the rate for superoxide dismutation, being the most efficient, the mutant E23A enzyme, probably due to the more solvent exposed active center. These results are relevant since *I. hospitalis* and *A. fulgidus* are hyperthermophiles.

In contrast to *A. fulgidus* SORs, these *I. hospitalis* enzymes reduce superoxide to hydrogen peroxide in an apparent two-step mechanism with the detection of only one intermediate, T1, the hydroperoxo-Fe^{3+} species. This intermediate shows the same spectroscopic characteristics as in the other SORs, and is generated with a rate (k_1 = 0.7 x 10^9 M^{-1} s^{-1}) of the same order of magnitude of the SOR from *A. fulgidus* (k_1 = 1.2 x 10^9 M^{-1} s^{-1}), for example, in contrast with the low rate obtained for the SOR Lys mutant from *D. baarsii* (k_1 = 0.04 x 10^9 M^{-1} s^{-1}) but comparable with that of SOR *D. vulgaris* Lys mutant (k_1 = 0.21 x 10^9 M^{-1} s^{-1}) (Table 6.3). A comparable rate and a characteristic T1

intermediate let us think that the Lys21 residue can be replacing Lys24, present in aminoacid sequences of other SORs. This Lys21 should be contributing to the positive patch around the active site and could be located in a flexible structural region that would allow the construction of the proposed hydrogen bond that is stabilizing the (hydro) peroxo-Fe^{3+} T1 intermediate (see chapter 7).

The T1 decay rate, related to the release of the product, 1 molecule of H_2O_2 per 1 $O_2^{\cdot-}$, with the subsequent binding of glutamate (final resting state), shows the same pH profile dependence for acidic pH with a slope of -1, corresponding to the transfer of 1 H^+. This process is essentially pH independent at basic pH values. The k_2 rate constant for the decay of the T1 intermediate, is associated with the disruption of the hydrogen bonding network supported by the lysine residue and protonation of the (hydro)peroxo-Fe^{3+}, T1 intermediate. At acid pH values the protonation is fast, probably from a protonated residue or a solvent species, and dependent of the proton concentration that will help disrupting the hydrogen bonding bridge between the Lys and the hydroperoxo species. At basic pH the protonation is probably due to water attack, and for that reason slower. For the wt protein the decay rate into the final species is around 75 s^{-1} (at pH 7), which is low and comparable to the 2Fe-SOR family but on the other hand the two mutants, E23A and T24K, have much higher rates, 320 and 500 s^{-1}, meaning that these mutations lead to some rearrangements that affected the enzyme reactivity. The increased rate also shows an apparent lack of importance of Glu in the release of H_2O_2, as deduced also from the studies of the *Nanoarchaeum equitans* enzyme that lacks this residue (*162*).

The design of the mutant T24K was an attempt of reproducing the canonical enzymes that did not lead to the initially expected results, *i.e.*, an increase of the rate of T1 formation (0.4×10^9 $M^{-1}s^{-1}$); furthermore, the T1 release rate is higher (Table 6.3). This suggests that the mutation may have perturbed the Fe-S(Cys) bond, but the positive patch around the active site was not modified or the electrostatic

surface potential was already efficient enough to attract the anionic substrate.

Table 6.3 – Spectroscopic and Kinetic properties of SORs (nd – not detected, T1 decays directly to the final species).

	Oxidized λmax of Fe^{3+}-Glu/$H_2$0 (nm)		E'_0	pK_a Fe^{3+}-(Glu/H_2O)-(OH-) species	T1- Fe^3 "hydroperoxo" λmax	k_1 (T1 formation)	k_2 (T1 decay)	k_3 (final species)	Ref
	Low pH	High pH	*(mV) center II*		*(nm)*	(x 10^9 $M^{-1}s^{-1}$)	(s^{-1})	pH7 (s^{-1})	
D. baarsii 2Fe-SOR	644	550	350	9	600	1	255	110	(*237-238*)
D. baarsii 2Fe-SOR K48I	635	550	520	7.6	600	0.04	nd	300	(*160, 237-238*)
D. vulgaris 2Fe-SOR	647	560	250	-	590	1.5	nd	84	(*234*)
D. vulgaris 2Fe-SOR K48A	~640	-	-	-	600	0.21	nd	25	(*234*)
A. fulgidus 2Fe-SOR	630	540	365	8.5	580	0.8	57	29	(*171*)
A.fulgidus 1Fe-SOR	666	590	250	9.6	620	1.2	3800	25	(*163*)
G. intestinalis 1Fe-SOR	647	560	-	8.7	600	1	nd	~320	(*94*)
N. equitans 1Fe-SOR	655	550	350 (pH 8.0)	6.5	590	1	-	<10	(*162*)
I. hospitalis 1Fe-SOR	640	550	230	10.5	590	0.7	nd	~75	This work
I. hospitalis 1Fe-SOR E23A	665	550	283 (pH 7.0)	6.5	590	1.2	-	~320	This work
I. hospitalis 1Fe-SOR T24K	640	550	195	10.7	590	0.4	-	~500	This work

The efficiency of this SOR from *I. hospitalis* illustrates that the Lys residue conserved in the majority of SORs aminoacid sequences, is not essential. But it also illustrates the natural variability of this enzyme family, in which multiple solutions arose throughout its evolution. Lys21 is then thought to play the same role as the other lysine residue does, in other SORs. Most organisms that contain the same type of SOR studied here belong to the same phylum and should present the same efficiency towards superoxide anion reduction, and also the same structural flexibility that will allow the Lys 21 residue to promote superoxide binding and T1 stabilization.

[1]Footnote

While this thesis was being written, a paper was published on *D. baarsii* 2Fe-SOR (*237*), which clarified several discrepancies in the literature on this enzyme: due to instrumental problems, part of the data published for this enzyme was wrong (*238-239*). This last work published showed finally that *D. baarsii* SOR behaves like *A. fulgidus* 1Fe-SOR and 2Fe-SOR (*163, 171*), *i.e.*, after the initial formation of the common intermediate T1, this species decays in two sequential first-order processes to the oxidized form. In this paper it is also proposed, following an earlier hypothesis by the same authors, that T1 is in fact a Fe^{2+}-superoxide species that very rapidly is transformed into a second intermediate, not detected, which will be the Fe^{3+}-hydroperoxo species.

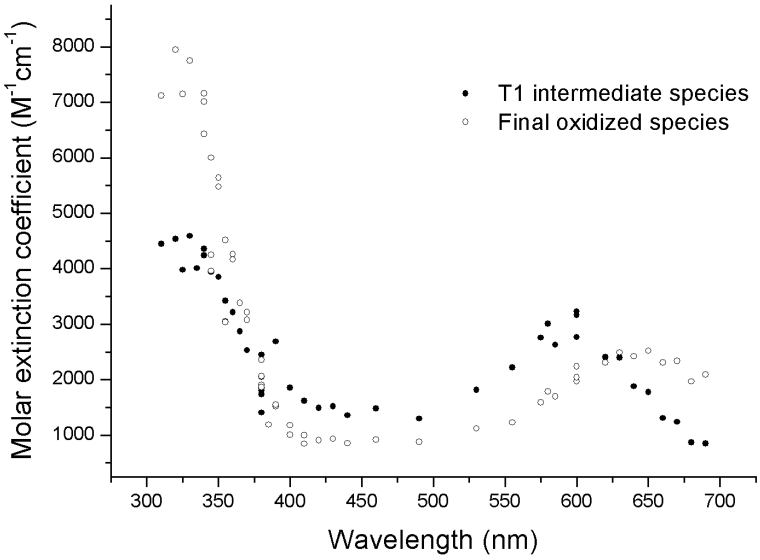

Figure 6.9 – Full spectra of the detected intermediates during the superoxide reduction cycle for the SOR from *I. hospitalis*, obtained by pulse radiolysis.

The supporting data results from DFT calculations of the visible spectrum of a Fe^{2+}-superoxide species that shows absorption bands at ~420 nm and ~620 nm, this last one similar to that observed for the T1 intermediate. However, no theoretical data was presented for the other possibility, the Fe^{3+}-hydroperoxo species, and it also contradicts the theoretical calculations by D. Kurtz and co-workers (*166*). Finally, our own experimental data suggests that this interpretation is wrong: the full experimental spectrum of T1 for the *I. hospitalis* SOR does not show the predicted band at ~420 nm (Figure 6.9).

Further experimental and theoretical data is needed to solve these issues.

Chapter 7

Summary

The hyperthermophile organisms *Ignicoccus hospitalis* and *Nanoarchaeum equitans* are quite unique due to their symbiotic nature, and both encode for 1Fe-SOR lacking residues that have been previously considered important for the catalytic cycle: a glutamate residue in the SOR from *Nanoarchaeum equitans* and a lysine residue in the SOR from *Ignicoccus hospitalis*.

In this chapter we describe the 3D crystal structure determination of these two atypical SORs, as well as *Ignicoccus hospitalis* SOR mutant E23A, where the glutamate is also absent as in the SOR from *Nanoarchaeum equitans*. The results here presented provide us with a structural model for the interpretation of the properties of these SORs.

This Chapter includes material published and to be published

"Insights on the superoxide reductase structures from two symbiotic organisms: *Ignicoccus hospitalis* and *Nanoarchaeum equitans* reveals differences on the catalytic site", Romão CV, **Pinto AF**, Pinho FG, Barradas AR, Matias PM, Teixeira M, Bandeiras TM, manuscript under preparation.

"Superoxide reductase from *Nanoarchaeum equitans*: expression, purification, crystallization and preliminary X-ray crystallographic analysis.", Pinho FG, **Pinto AF**, Pinto LC, Huber H, Romão CV, Teixeira M, Matias PM, Bandeiras TM. 2011Acta Crystallogr Sect F; 67: 591-5

"Cloning, purification, crystallization and X-ray crystallographic analysis of *Ignicoccus hospitalis* neelaredoxin" Pinho FG, Romão CV, **Pinto AF**, Saraiva LM, Huber H, Matias PM, Teixeira M, Bandeiras TM, 2010 Acta Crystallogr Sect F; 66: 605-7

Pinto AF is responsible for gene cloning and protein purification and is also involved in structural analysis, paper discussion and preparation.

7 - Function and Structure of SORs

7.1 - Experimental Procedures

Cloning and protein overproduction of Ignicoccus hospitalis *SOR*

Amplification of the complete gene (375 bp) encoding the wt 1Fe-SOR from *Ignicoccus* (*I.*) *hospitalis* and the site-directed mutagenesis for the selected aminoacid residue (E23) are described in Chapter 6. The wt protein and the E23A mutant were overexpressed in *Escherichia* (*E.*) *coli* as described also in chapter 6.

Purification of SOR from I. hospitalis *and its E23A mutant*

The purification protocol is described in Chapter 6 (see 6.1 section). The collected fractions were analyzed and judged to be pure based on the results from SDS–PAGE (*e.g.* Figure 7.1 represents the SDS-PAGE for a pure fraction of the wt *I. hospitalis* SOR). After the final purification step, the wt and the E23A proteins were concentrated to 15 $mgmL^{-1}$ using a 10 kDa cutoff Centricon (Vivaspin), in 20 mM Tris-HCl, 150 mM NaCl, pH 7.2.

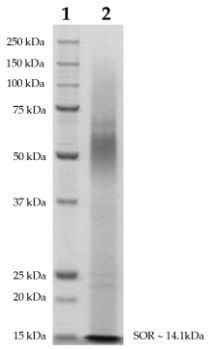

Figure 7.1 - 10% SDS-PAGE of purified recombinant *Ignicoccus hospitalis* SOR. Lane 1, BioRad Un-stained Protein Markers, 161-0363, and correspondent molecular mass (kDa). Lane 2, *Ignicoccus hospitalis* SOR. The band at ~14 kDa corresponds to the monomeric form and the band at ~55 kDa to the tetrameric form, as usually observed for other SORs.

Cloning and overproduction of SOR from Nanoarchaeum equitans

The cells BL21-Gold (DE3) from *E. coli* (Stratagene) containing the plasmid pT7NNlr, previously described (*162*) were grown aerobically at 37 ºC in M9 minimal medium (*240*) supplemented with 30 µg/mL kanamycin and enriched with 400 µM $FeSO_4.7H_2O$, until the OD_{600nm} reached 0.3. At this stage, 400 µM IPTG was added, the temperature was lowered to 30 ºC and growth continued for 20 h. The cells were then harvested by centrifugation at 10 000 g for 10 min at 4 ºC.

Purification of Nanoarchaeum equitans *SOR*

Harvested cells were resuspended in a buffer containing 20 mM Tris–HCl pH 7.6, 1 mM phenylmethanesulfonyl fluoride (PMSF) and 20 μgmL^{-1} DNase I (Sigma), and broken in a large cell French Press at 19000 psi. All subsequent purification steps were performed at pH 7.6 and 4 ºC. After ultracentrifugation at 186 000 g for 1 h, the soluble extract was dialyzed overnight against 20 mM Tris–HCl plus 1 mM PMSF (buffer A), and centrifuged at 20 400g for 15 min. The soluble fraction was subsequently loaded onto a Q-Sepharose Fast Flow column (XK 26/10; GE Healthcare) previously equilibrated with buffer A. The fraction containing *Nanoarchaeum* (*N.*) *equitans* SOR was eluted around 0 mM of NaCl and was concentrated by ultra filtration (Amicon, 10 kDa cutoff), and loaded onto a Superdex 75 column (XK 26/60; GE Healthcare) previously equilibrated with 20 mM Tris–HCl and 150 mM NaCl. The collected fractions were analyzed and judged to be pure on the basis of SDS–PAGE gels. In order to determine the correct molecular mass of the *N. equitans* SOR, the pure protein solution was loaded onto a size-exclusion column (Superdex 200 column, HR3.2/300; GE Healthcare) using appropriate molecular-mass standards in parallel. The buffer used was 20 mM Tris–HCl pH 7.6, 150 mM NaCl with a flow rate of 0.5 mL min^{-1}. The elution profile revealed a protein solution containing a tetramer with a molecular mass of around 56 kDa. The protein concentration and total iron content were

determined using the BCA protein assay kit (*212*) and the TPTZ method (*213*), respectively. Finally, the protein was concentrated to 15 mg mL^{-1} using a 10 kDa cutoff Centricon (Vivaspin).

Crystallization, data collection and data refinement

Crystallization trials were done at the nL scale with the Classic Screen (Nextal) using a Cartesian Crystallization Robot Dispensing System (Genomics Solutions) and round-bottom Greiner 96-well CrystalQuick™ plates (Greiner Bio-One). Crystal optimization was performed by the sitting-drop vapour diffusion technique. The final crystallization conditions for *I. hospitalis* (*Ih*) wt SOR and E23A mutant were 85mM Tris-HCl pH 8.5, 8.5 mM $NiCl_2$, 20% (v/v) PEG 2000 monomethyl ether (MME); and 20% PEG 2000 MME for *N. equitans* (*Ne*) SOR. The *Ih* and *Ne* SOR crystals were cryoprotected, in the crystallization condition supplemented with 17.5% xylitol and 40% (v/v) PEG 2000 MME, respectively. Datasets were collected at European Synchrotron Radiation Facility at 100 K for *Ih* SOR at a resolution of 1.85 Å, and for *Ne* SOR at a resolution of 1.88 Å. For *Ih* SOR E23A a 2.05 Å dataset was measured at room temperature using the *in-house* (ITQB) equipment Bruker AXS Proteum Pt135 CCD detector system coupled to a Bruker AXS Microstar-I rotating-anode X-ray generator with Montel mirrors. The *Ih* SOR dataset had an overall $R\text{-}_{merge}$ of 10.1%, 6.2 % for *Ih* SOR E23A and 5.4 % for *Ne* SOR. The *Ih* wt and E23A SORs protein structures were solved by molecular replacement using PHASER and an initial *Ih* wt SOR low-resolution model (2.4 Å) (*241*). *Ne* SOR crystal structure was determined by the Molecular Replacement method with PHASER (*242*) and using as a search model one monomer from the *Pyrococcus furiosus* SOR (PDB 1DQI). *Ih* SOR structure was refined with REFMAC (*229*) while E23A *Ih* and *Ne* SOR were refined with Phenix (*243*). During refinement, the models were periodically inspected and corrected with Coot (*230*) against sigmaA-weighted $2|F_o|-|F_c|$ and $|F_o|-|F_c|$ electron density maps. The final models had $R\text{-}_{fractor}$ and $R\text{-}_{free}$ of: *Ih* SOR 21.2% and 23.6%; *Ih* SOR E23A 17.7% and 21.4%, *Ne* SOR

19.9% and 25.9%. Full details on data processing and refinement will be presented in the manuscript in preparation.

7.2 – Results and Discussion

For *Ih* wt SOR hexagonal bipyramid-shaped blue crystals with maximum dimensions of 350 x 200 x 200 µm were obtained (Figure 7.2a); for the E23A mutant, the crystals were pink with maximum dimensions of 100 x 70 x 30 µm (Figure 7.2b). For *Ne* SOR were also obtained blue crystals with maximum dimensions of 100 x 80 x 40 mm (Figure 7.2c).

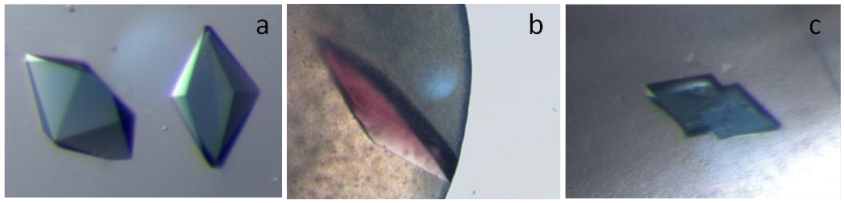

Figure 7.2 – a) Crystals of *I. hospitalis* 1Fe-SOR; b) Crystal of *I. hospitalis* E23A 1Fe-SOR; c) Crystals of *N. equitans* 1Fe-SOR.

SOR overall structure

The crystal structures of the *Ih* wt and mutant SORs and of *Ne* SOR were solved and refined. The overall monomer structure and oligomeric organization of all the proteins is similar to the other 1Fe-SORs previously studied (Figure 7.3) (*141*).

The packing of symmetry-related subunits in the crystal structure reveals a tetrameric quaternary structure for all the proteins (Figure 7.3 A), which is in agreement with previous biochemical studies (Chapter 6, (*241, 244*)). The SOR tetramer is a cubic-shaped structure composed by a pair of two anti-parallel subunits related by non-crystallographic symmetry. Each monomer is in contact with two antiparallel subunits, one through the N-terminal regions and the other through the C-terminal

(Figure 7.3 A). The active iron centre is located at the β-barrel loops and is exposed to the solvent. In the tetramer the distance between the two iron atoms from the same side of the protein is 25 Å to 26 Å for all SORs.

The root mean square deviation (rmsd) between *Ih* SOR tetramer and its E23A mutant is *c.a.* 0.8 Å, while for *Ne* SOR tetramer is 1.2Å.

SOR monomer structure

The structural core of these proteins is a seven-stranded anti-parallel β-barrel (3+4) with an immunoglobulin-like β-sandwich fold.

The main difference between *Ih* SOR structures and *Ne* SOR is in the N-terminal region before the start of the structural core, β-barrel: for *Ne* SOR the N-terminal region is shorter and the rmsd between the *Ih* and *Ne* SORs monomers is 1.07Å (Figure 7.3 B). On this region *Ne* SOR has only 11 amino acid residues compared with the 27 amino acid residues in *Ih* SORs (see Chapter 6, Figure 6.2).

It is interesting to note that the N-terminal region contains two of the key residues in SORs, the glutamate and the lysine of the motif**, EKHVP** (*A. fulgidus* 1Fe-SOR N-terminal motif). The flexibility of this region is important for the catalytic mechanism, allowing the glutamate or the lysine to be close to the center depending on the catalytic state.

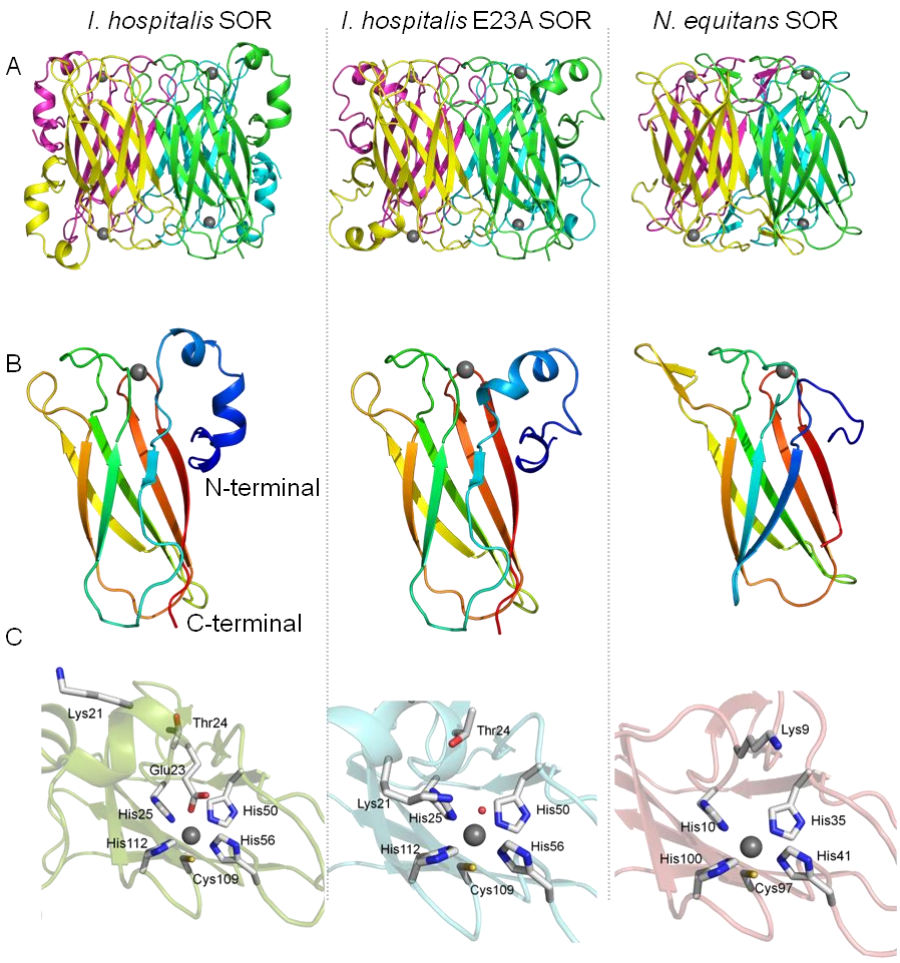

Figure 7.3 – Three-dimensional crystal structures of the SORs from *Ih*, wt and E23A mutant proteins, and of the *Ne* SOR obtained by X-ray crystallography. A) Tetrameric quaternary structure for the three SORs, composed by a pair of two antiparallel subunits; the four subunits are coloured differently; B) SORs monomer structure, each monomer is coloured from blue (N-terminal) to red (C-terminal); C) SORs oxidized active center. Iron ion is represented as gray sphere, a water molecule is in a red sphere, protein secondary structure is represented as in cartoon and the amino acid side-chains are represented as sticks. Figures were generated using PyMOL (*63*).

Iron center

The iron is hexa-coordinated with four histidine-imidazoles in the equatorial plane, a cysteine-sulphur in the axial position, which are

strictly conserved among the family of superoxide reductases, and a sixth axial glutamate residue in most oxidized SORs (Chapter 6, (*245*)). *Ne* SOR does not contain the "sixth ligand" glutamate; instead in this position contains a proline, so the sixth axial position is vacant. The *Ih* SOR iron ligands are H25, H50, H56, H112, C109 (and E23 for the wt SOR), and for *Ne* SOR H10, H35, H41, H100, C97 (Figure 7.3 C). All histidine residues coordinate the metal atom through their $N^{\varepsilon 2}$ atom except for H112 (*Ih* SOR) and H100 (*Ne* SOR) which is done through the $N^{\delta 1}$atom. This data confirms the earlier prediction based on homology modelling studies, that for *Ne* SOR the glutamate next to the **E**[5]YNP**K**[9]**H**[10]SP motif does not bind to the iron site (*162*) (Figure 7.3 C). The mutant *Ih* SOR E23A does not contain the glutamate residue and the structure of the N-terminal region is different in comparison with the wt *Ih* SOR. There was a rearrangement of the N-terminal region in such a way that the iron atom is even more exposed to the solvent. The *Ih* SOR does not have the standard lysine residue just after the glutamate residue in the motif $E^{23}T^{24}HTP^{27}$; the *Ih* SOR E23A structure reveals that another lysine, Lys21, (see Chapter 6, Figure 6.2), is close to the iron center and may have the same role as proposed for the canonical lysine stabilizing the intermediate species (Figure 7.3 C) (Chapter 6, (*141*)).

Charge surface

It has been proposed that the lysine in the conserved motif –EKHVP plays a key role in the catalytic cycle of superoxide reduction, being involved on the attraction and/or hydroperoxide (catalytic intermediate T1) stabilization (see Chapter 6). As the functional unit is a tetramer, it is important to analyse the charge distribution on the entire functional unit.

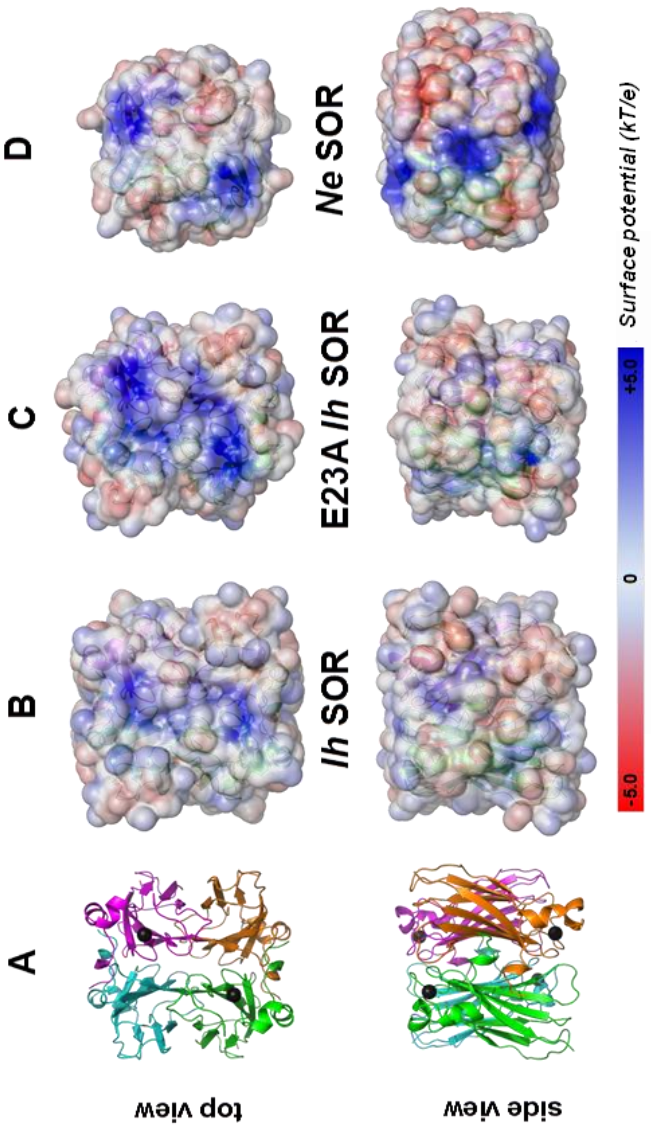

Figure 7.4 – Electrostatic potential surface of *Ih* SOR (B), E23A *Ih* SOR (C) and *Ne* SORs (D) from top and side view. Each monomer is represented in cartoon with a different color and the irons are represented as black spheres. The orientation of each tetramer is the same as represented in A (Ih SOR). The electrostatic potentials were calculated with APSB (247) using a protein and external dielectric of 2.0 and 78.0, respectively, a temperature of 310 K and an ionic strength of 0.15M. The charge for each atom was calculated using PDB2PQR (248), the iron charge (+3.00) and ionic radius (0.65) was manually added. PYMOL (63) was used as an interface to APSB, to analyse the electrostatic surfaces and produce the figures.

An analysis of the charge distribution on the surface of the protein structures (Figure 7.4) from *Ih* SOR shows that there is a positively charged region close to the iron center due to the contribution of histidine residues coordinating the iron but also other positive residues: Arg59 and Asn110 from the same monomer and Arg70 from an adjacent monomer. The Lys21 residue is not close to the iron center instead is pointing out to the surface. These residues could be responsible for directing the substrate to the active center. In the *Ih* E23A SOR structure it is observed that it has a more positive charge on the surface due to the glutamate absence.

In the case of *Ne* SOR, there is a larger positive charge on the top of the iron center due to the absence of the glutamate residue, similarly to *Ih* SOR E23A. Furthermore Lys 9 is also pointing to the iron center and two other Lys residues are on the top, the Lys34 from the same monomer, and Lys 84 from the anti-parallel adjacent monomer. The distribution of positive charges in this protein is different compared with that for *Ih* SOR, since there is a positive region on the side of the "cube", located on the interaction region between two anti-parallel monomers. As a first conclusion, these studies showed the existence of an alternative lysine residue in *Ih* SOR (Lys21), which may explain why the rate constant for the formation of T1 is essentially identical to that of the other SORs. Moreover, it was firmly established that the glutamate close to the "missing" glutamate of *Ne* SOR ($M^{1}IKT\mathbf{E}^{5}YNP\mathbf{K}^{9}\mathbf{H}^{10}SP$) does not substitute it, *i.e.*, oxidized *Ne* SOR is only pentacoordinated.

Part IV – General Discussion and Conclusion

Chapter 8

8 - General Discussion and Conclusion: Reductive pathways for ROS Scavenging

In this thesis two non-heme iron proteins were studied that act as ROS scavengers, widely spread in prokaryotes: Rubrerythrin and Superoxide Reductase.

A multidomain rubrerythrin-like protein, Desulforubrerythrin (DRbr), encoded in *Campylobacter* (*C.*) *jejuni*, contains three iron binding domains. Each iron site was characterized and a NADH linked H_2O_2 reductase activity was determined (Chapter 4). In order to understand the architecture of this multidomain protein, the 3D crystal structure was obtained at a 2.0 Å resolution. The structure allowed us to infer about the possible function of each redox center (Chapter 5).

The superoxide reduction mechanism was evaluated by the study of a superoxide reductase (SOR) from the hyperthermophilic organism, *Ignicoccus* (*I.*) *hospitalis* that lacks a generally conserved positively charged aminoacid residue near the active site, a non-heme pentacoordinated iron. The active site was characterized and the kinetics for superoxide reduction determined by Pulse Radiolysis (Chapter 6). The 3D crystal structures of the wt and of a site-directed mutant (E23A) were solved at a resolution of 1.9 and 2.0 Å, respectively (Chapter 7).

A common theme of these ROS detoxifying proteins (and others such as the flavodiiron proteins) is the presence, in multiple cases, of, apart from the catalytic modules, additional electron-transfer modules (of the rubredoxin and/or desulforedoxin-type) that function, in most cases, as the electron entry point of the enzyme (Figure 8.1).

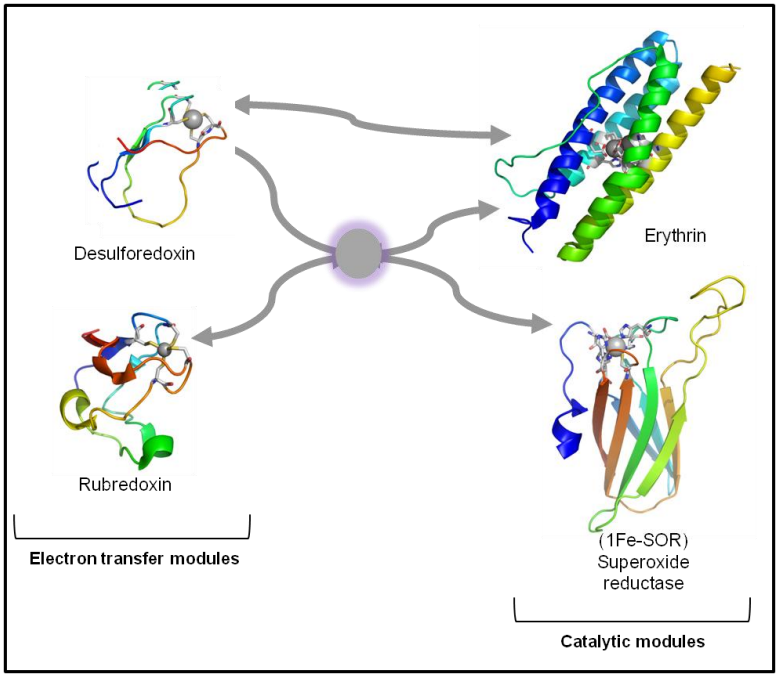

Figure 8.1 – Electron transfer modules and catalytic modules present in ROS scavenging enzymes such as rubrerythrins and superoxide reductases.

8.1 - Rubrerythrin: Structure and Function

The rubrerythrin-like protein encoded in *C. jejuni* ((*115*), Chapter 4), the product of the *cj0012c* gene, has 215 aminoacid residues and a calculated molecular mass of 24 526 Da for the monomer. By sequence homology it was possible to assign two domains: a desulforedoxin-like domain containing a non-heme iron-sulfur center (*15*) found in other proteins, such as rubredoxin: oxidoreductase (*169*) (Rbo, one of the initial names given to a 2Fe-SOR protein), and a rubrerythrin (Rbr) domain, and therefore it was firstly given the name of Rbo/Rbr-like protein from *C. jejuni* (Rrc) (*106*). Due to its building blocks and its homology to the rubrerythrin family, the protein was renamed Desulforubrerythrin (DRbr) ((*115*), Chapter 4).

The three predicted iron sites, $Fe(Cys_4)$ for desulforedoxin (Dx) and rubredoxin (Rd), and the diiron site from the four-helix bundle domain, were shown to be present and studied by a combination of UV-Visible, EPR and Resonance Raman spectroscopies, which allowed the determination of the electronic and redox properties of each site ((*115*), Chapter 4). These centers are in a high-spin configuration in the as isolated ferric form. The diiron center in the oxidized form has a μ-oxo bridged diiron site, as revealed by Resonance Raman spectroscopy using isotope labeling. The reduced protein is rapidly reoxidized by hydrogen peroxide (millisecond timescale) in comparison with oxygen (minute timescale) and has a significant NADH-linked hydrogen peroxide reductase activity of 3.9 ± 0.5 μmol H_2O_2 $min^{-1}mg^{-1}$ ((*115*), Chapter4).

Aminoacid sequence

The 949 aminoacid sequences retrieved from a BLAST search with the desulforubrerythrin aminoacid sequence, using the software Geneious Pro 5.5.6 and the NCBI database, were aligned and analyzed with Clustal X v2.1 (*148*). This established that the large rubrerythrin family contains members composed by a quite diverse combination of structural domains, for example, rubredoxin or desulforedoxin plus the four-helix bundle and other different architectures, as shown in Figure 8.2. The distinctive feature of the family is the presence of the four-helix bundle domain. The simplest family members consist only of this domain, and were initially named erythrins (*246*); more recently, different names were given for orthologues from other organisms- sulerythrin from *S. tokodaii* (*95*), symerythrin from *C. paradoxa* (*88*) and ferriperoxin from *Hydrogenobacter thermophilus* (*247*). These varieties of names are inappropriate and introduce unnecessary confusion, as all these proteins are quite similar, and so in this thesis, the initial name of erythrin were used.

The rubredoxin domain may appear at the N- or at the C-terminus of rubrerythrins or even in both positions (Figure 8.2) while so far the

desulforedoxin-like domain has been found only at the N-terminus. The rubredoxin domains from rubrerythrins can also be distinguished on the basis of the number of aminoacids that separate the two cysteine pairs: in rubredoxin domains from the majority of rubrerythrins, this number is around 12, while for rubredoxin domains in rubrerythrins from cyanobacteria and most isolated rubredoxins, this spacing is higher, about 30 aminoacids.

The dendogram built from the aminoacid sequence alignment, using the neighbour joining method available in Clustal X (*148*) is shown in Figure 8.2. The only well defined monophyletic group in this dendogram is represented by the cyanobacteria. The remaining organisms, from the Bacteria, Archaea or Eukarya domains, are scattered in the dendogram. The sequences cluster mainly according to the subfamilies of rubrerythrins, *i.e.*, to the types of structural domains; in particular, the desulforubrerythrins form a separate cluster, the nigerythrin-like (Ngr) proteins with similarity with the sequence of Ngr from *D. vulgaris*, also cluster and the erythrin-like proteins, as sulerythrin, appear to cluster as well, which further indicates that the use of different names is inappropriate for this subfamily.

Diverse multidomain architectures are found for rubrerythrins in many databases such as *NCBI* or *Pfam* based only on aminoacid sequence similarity. However experimental evidence is still lacking to prove the expression of functional rubrerythrin-like proteins with N-terminal domains such as hydrogenases or flavin reductases-like domains, as proposed in (*128*).

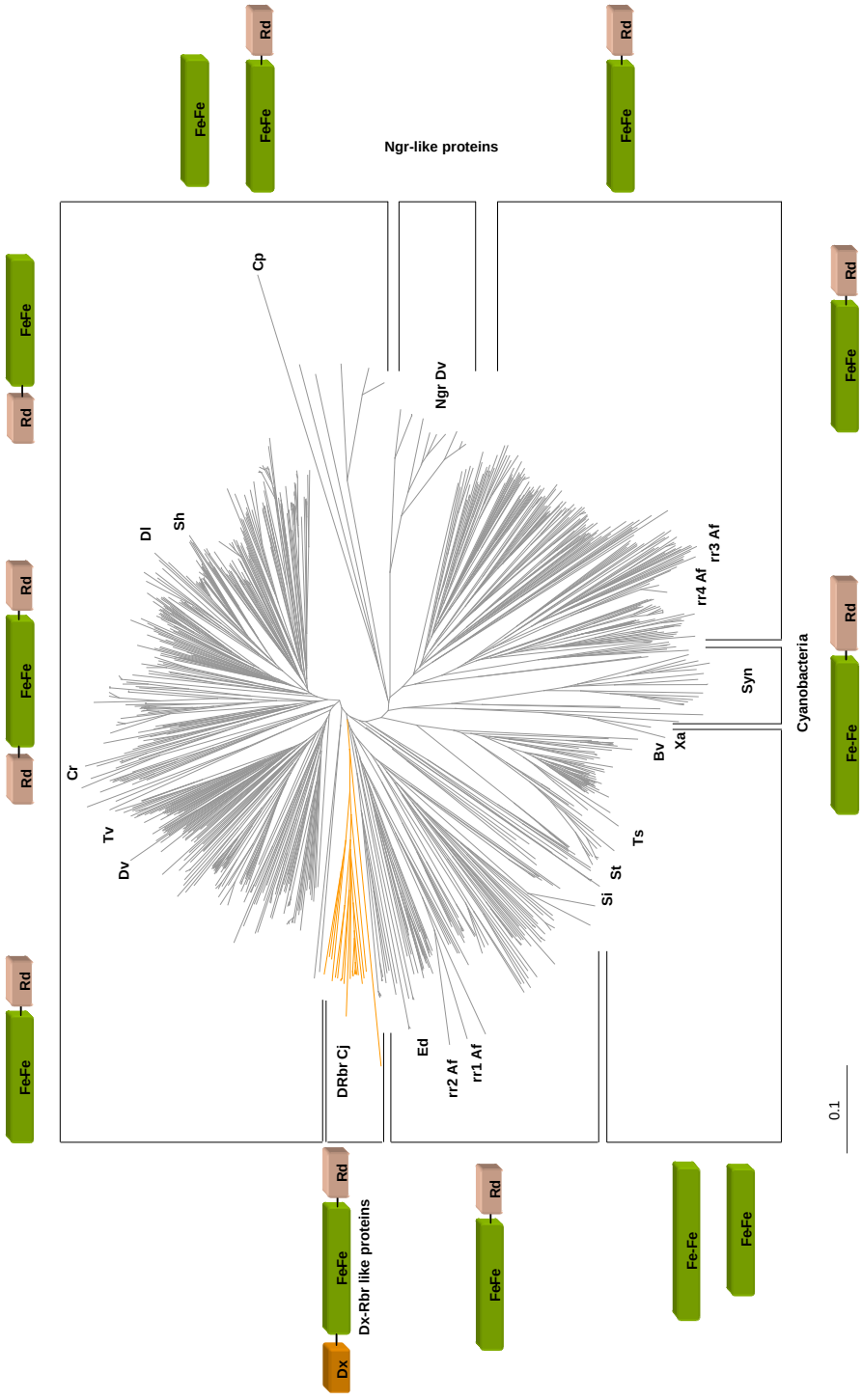
Ngr-like proteins
Cp
Ngr Dv
Dl
Sh
Cr
Tv
Dv
Ed
rr2 Af
rr1 Af
DRbr Cj
Si
St
Ts
Bv
Xa
rr4 Af
rr3 Af
Syn
Cyanobacteria
Dx-Rbr like proteins
Dx
Rd
Fe-Fe
FeFe
0.1

Figure 8.2 - Dendogram of rubrerythrin-like proteins displayed with TreeView (*248*). The highlighted sequences are: DRbr- *C. jejuni subsp. jejuni* NCTC 11168 (gi|218561705|), rr1,2,3,4 Af- *Archaeoglobus fulgidus* (gi|2649783|; gi|2649773|; gi|2648913|; gi|2648207|), Bv- *Burkholderia vietnamiensis* G4 (gi|134291384|), Cp- *Cyanophora paradoxa* (gi|1016189|), Cr- *Clostridium ramosum* DSM 1402 (gi|167754543|), Dl- *Dorea longicatena* DSM 13814 (gi|153853488|), Dv- *Desulfovibrio vulgaris subsp. vulgaris* DP4 (gi|120601988|), Ngr- Nigerythrin from *Desulfovibrio vulgaris subsp. vulgaris str. Hildenborough* (gi|46578436|), Ed- *Entamoeba dispar* SAW760 (gi|165904057|), Sh- *Slackia heliotrinireducens* DSM 20476 (gi|257063907|), Si- *Sulfolobus islandicus* M.16.4 (gi|238382159|), St- *Sulfolobus tokodaii* str. 7 (gi|342306703|), Syn- *Synechococcus sp.* RS9917 (gi|87123471|), Ts- *Thioalkalivibrio sulfidophilus* HL-EbGr7 (gi|220934014|), Tv- *Trichomonas vaginalis* G3 (gi|154420781|) and Xa- *Xanthobacter autotrophicus* Py2 (gi|154243812|). Bv, Cp and Xa – These sequences are preceded by a twin-arginine signal peptide.

Structure

The 3D crystal structure of DRbr is the first example of a rubrerythrin protein with a three domain arrangement and it has a swapped domain configuration, so far only found in rubrerythrins from thermophilic organisms such as *P. furiosus* and *S. tokodaii* (*132-133*) and recently from the mesophilic organism *Burkholderia pseudomallei*. Actually this structural feature was proposed to be important for the protein stability at higher temperatures (*131*). However, around forty 3D protein structures have been found to display this swapping domain structural feature, including proteins from mesophiles and thermophiles (*249*). Whether this structural arrangement is physiologically important is still not known.

The 3D crystal structure of DRbr revealed that the swapped domains allow a tetrameric oligomerization state with a complex domain arrangement where the Rd from different monomers and diiron coordination from different monomers are in the same orientation and distance as in other Rbrs (*104, 133*). This feature is important for the intramolecular electron transfer thought to occur via the rubredoxin site. The electron transfer path occurs directly from the $FeCys_4$ site from the rubredoxin domain to the diiron site from different monomers, where the

catalytic events take place. In Rbr from *D. vulgaris* the intermolecular distance between these two iron sites is *c.a.* 12 Å (*104*) and in the case of DRbr from *C. jejuni*, this distance is *c.a.* 13 Å (Chapter 5). The reduction potential of each center is also in favor of this electron transfer pathway, 230 mV and 185 mV for Rd ($FeCys_4$), and 286-222 mV and 270-235 mV for the diiron site, in rubrerythrins from *D. vulgaris* and *C. jejuni* respectively ((*115*), Chapter 4) (*85, 96, 216*). Furthermore, the Rd center is clearly accessible to an external electron donor. However, in the case of erythrin-like proteins, the direct electron transfer should be dependent on exogenous electron donors.

Some studies (*101*) ((*115*), Chapter 4) have used a rubredoxin and a NADH oxidoreductase to complement the electron transfer pathway (Figure 8.3).

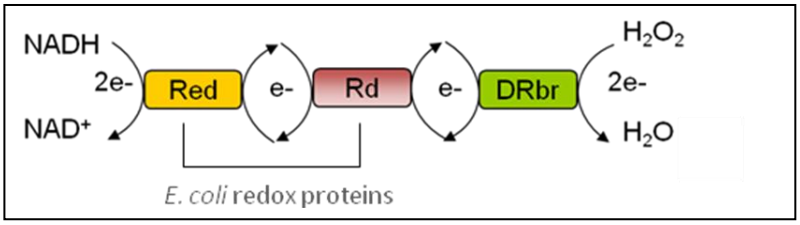

Figure 8.3 – Electron transfer artificial system used for DRbr assays for H_2O_2 reductase activities.

However there is no evidence of these being their physiological electron donors since many organisms do not encode for rubredoxins, *e.g., S. tokodaii* and *C. jejuni*. In this last example, the extra N-terminal domain with a redox center similar to the iron site in rubredoxin, a desulforedoxin-like domain was initially thought to be able to transfer electrons, but due to the distance to the other iron sites (~34 Å from the Dx iron site to the diiron site) and the observed reduction potential (E'_0= 240 mV), this iron site should not be able to participate in the reduction of H_2O_2 (Figure 8.4). Our stopped-flow experiments have shown that the oxidation of this iron site occurs in a different time scale, in comparison with the rubredoxin iron site, which is oxidized in a very fast time scale

(Chapter 4). The desulforedoxin-like domain in DRbr is also very susceptible to oxidative degradation, upon exposure to aerobic conditions or to H_2O_2 (*106*). This phenomenon was also seen for the 2Fe-SOR from *D. vulgaris* (*250*). It is the most solvent accessible redox center in DRbr and so, more prone to oxidative damage relative to the other iron sites. This feature could be part of an auto-regulation process when the concentration of H_2O_2 exceeds the reductive catalytic capacity of desulforubrerythrin, and/or a way of not depleting the NAD(P)H pool or other reducing equivalents in the cell.

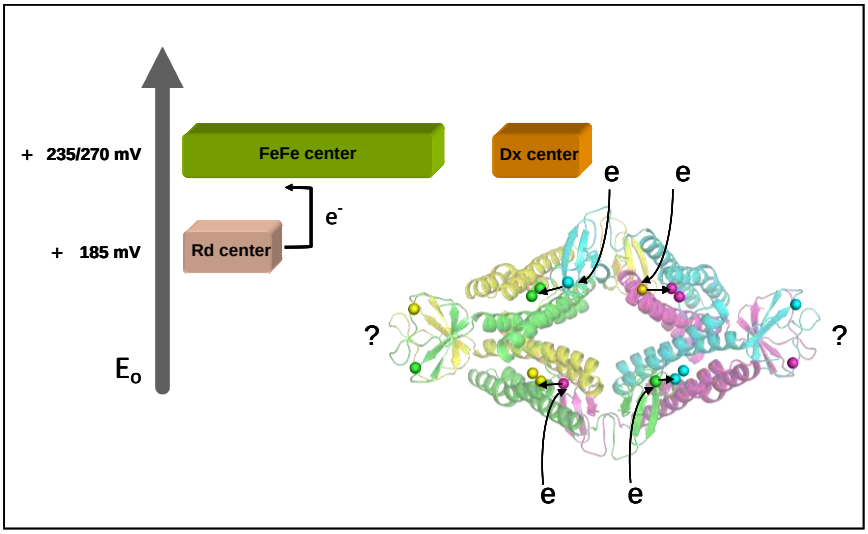

Figure 8.4 – Schematic representation of the reduction potentials (E'_0 mV *vs.* SHE) obtained for each iron center in DRbr protein from *C. jejuni*, and of the four putative electron entry points, the Rd domains. "?" refers to the unknown function of the Dx domains.

Hydrogen peroxide reduction mechanism

Although many activities were attributed to this family of proteins, the H_2O_2 reductase activity linked to the NADH oxidation has been the most reproducible *in vitro* ((*100-101, 251*), Chapter 4). The kinetic characterization of this peroxidase activity *in vitro* has been subjected to the use of non-physiological electron donors or electron redox proteins

as rubredoxin, depending on a NADH: oxidoreductase enzyme and for that reason the turnover rates determined can be underestimated, due to the unknown efficiency of the electron transfer chain.

Rubrerythrin activity is undoubtedly related to oxidative stress response due to the complementation studies and transcriptomic analyses in many organisms, namely in prokaryotes (*e.g.*, (*90, 105*)).

Peroxidase activity is thought to occur as a two-electron reduction of H_2O_2 in a fast and concerted way concomitant with the release of two H_2O molecules and via an intermediate species proposed to be a μ-1, 2-H_2O_2 diferrous species coordinated by a bridging glutamate residue (*104, 131*). The oxidation of the diiron center, the movement of the iron and the carboxylate-shift complete the mechanism and an oxo-bridge is incorporated in the diferric site (Chapter 2, Figure 2.8). This redox-induced movement of the iron plus a symmetrical geometry of the coordination spheres of the reduced state (*104*) are proposed to be reasons for a selective reduction of H_2O_2 and to avoid the formation of high-valence iron intermediates (*86*). The reduction potentials for the diiron and the rubredoxin mono-iron centers, which are the iron sites involved in the catalytic reduction are equal and above 200 mV (E'_0 (Rd domain) ~200 mV and E'_0(Fe-Fe) > 200 mV, *vs.* SHE) (*85, 96, 216*), which under physiological conditions allows them to remain in the all-ferrous state and suitable for the reaction with hydrogen peroxide (E'_0 (H_2O_2/H_2O) = +1.35 V *vs.* SHE (*3*)).

As shown in Figure 8.5, two tyrosine residues, Y27 and Y102 are H-bound to E94 and E20, respectively, in *D. vulgaris* Rbr (or Y59 and Y127 are H-bound to E119 and E52, respectively, in *C. jejuni* DRbr), are strictly conserved among the known members of the Rbr family. In rubrerythrins the conserved symmetric tyrosines close to the diiron site are also thought to be part of the reduction mechanism, having been proposed to help dissipate possible oxidizing species formed, such as a ferryl species. A ferryl center could be quickly re-reduced by oxidation of the hydrogen-bonded tyrosine residue to a tyrosyl radical. A tyrosyl radical can then be re-reduced by exogenous reducing equivalents. The

formation of this radical was seen for Rbr from *D. vulgaris*, but this observation was never published (as cited in (*86*)). For DRbr from *C. jejuni*, we were also able by EPR spectroscopy to observe the presence of a radical species upon incubation of the mixed-valence redox state protein with an excess of H_2O_2.

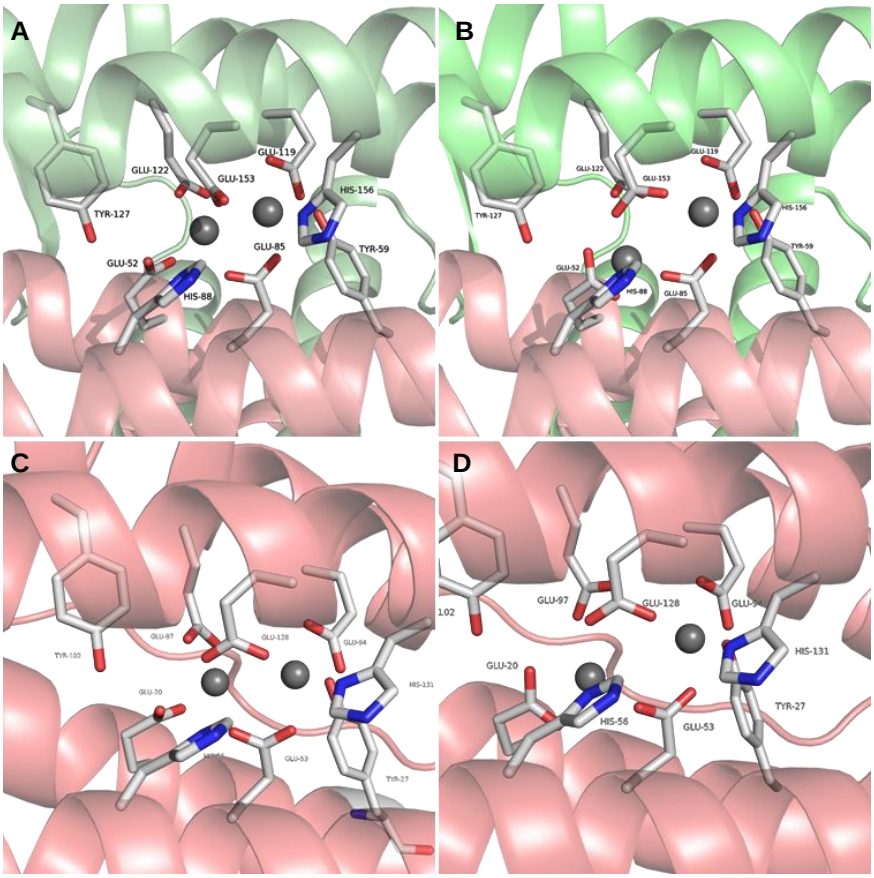

Figure 8.5 – Diiron center and coordinated ligands in the oxidized and reduced state. A) DRbr from *C. jejuni* in the most oxidized redox state; B) DRbr from *C. jejuni* in the most reduced state (chapter 5) Chain A in red and Chain D in green; C) Rbr from *D. vulgaris* in the oxidized state (pdb 1RYT); D) Rbr from *D. vulgaris* in the reduced state (pdb 1LKO) Chain A in red. Figures were generated using PyMOL software (*63*).

8.2 - Superoxide Reductases: Structure and Function

A superoxide reductase enzyme from *I. hospitalis* was found to efficiently reduce superoxide to hydrogen peroxide with kinetic rates similar to other SORs (Chapter 6).

The 1Fe-SOR from *I. hospitalis* lacks the generally conserved positively charged Lys residue in the motif (E^{23}**K(T)**H**V(T)**P^{27}), having in its place a threonine residue. This Lys residue is thought to contribute electrostatically to attract the anionic substrate, and also to contribute to stabilize the first intermediate (T1) of the superoxide reduction mechanism directly through a hydrogen bond. The SOR from *I. hospitalis* showed an efficient k_1 rate (x 10^{9} $M^{-1}s^{-1}$) (Table 8.1) as all other canonical SORs and, contrary to the *A. fulgidus* SOR enzyme, only one intermediate was detected, T1, during the reduction mechanism. The 3D crystal structure of the wt SOR from *I. hospitalis* revealed some structural differences with the other SORs and showed that around the active site the positive charge surface contribution goes beyond that Lys residue. To understand the molecular events of superoxide reduction two mutant proteins, E23A and T24K, were also studied.

Aminoacid sequence

A comprehensive search for superoxide reductase homologues was performed, using more than one type of SOR aminoacid sequence as query and also the database created by Lucchetti-Miganeh *et al.*, in SORGOdb (*143*). As of December 2011, 307 homologues were retrieved. The aminoacid sequences were aligned and an unrooted dendogram (Figure 8.6) was calculated using the neighbor joining methodology of Clustal X (*148*).The aminoacid sequences cluster in two major groups, corresponding to 1Fe- and 2Fe-SORs, and a minor group related to the novel Helix-turn-Helix (HTH) 2Fe-SORs proteins. From the dendogram it is possible to conclude that SORs do not cluster according to the organism phylogeny, as for bacteria or archaea

domains, indicating a high level of lateral gene transfer events throughout evolution.

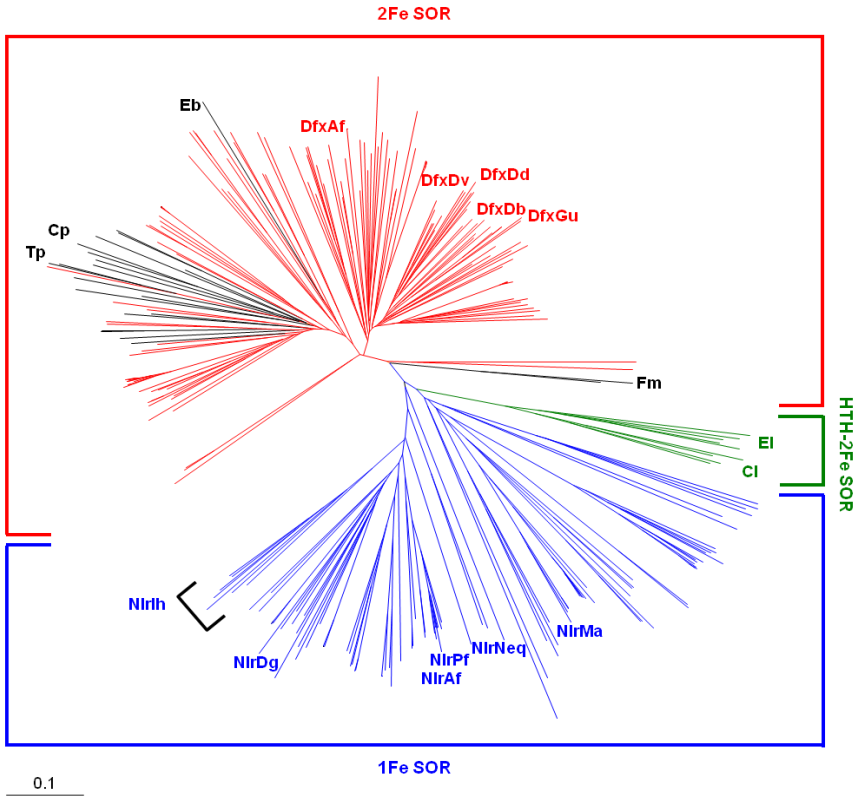

Figure 8.6 – Dendogram of SORs, displayed with TreeView (*248*). 1Fe-SORs are represented in blue, 2Fe-SORs in red, 2Fe-SORs with an Helix-turn-Helix N-terminal domain in green and 1Fe-SORs with the extra N-terminal domain in black. The sequences with a black bracket correspond to SOR sequences from the Crenarchaeota phylum, lacking the canonical lysine residue. Sequences highlighted correspond to 2Fe-SORs: *Archaeoglobus fulgidus* DfxAf gi|11498439|), *Clostridium phytofermentans* (DfxCp gi|160880064|), *Desulfovibrio desulfuricans* (DfxDd gi|157830815|), *Desulfovibrio vulgaris* (DfxDv gi|46581585|), *Desulfoarculus baarsii* (DfxDb gi|3913458|), *Geobacter uraniireducens* (DfxGu gi|148264558|); 1Fe-SORs: *Archaeoglobus fulgidus* (NlrAf gi|11497956|), *Desulfovibrio gigas* (NlrDg gi|4235394|), *Ignicoccus hospitalis* (NlrIh gi|156567119|), *Methanosarcina acetivorans* (NlrMa gi|20092535|), *Nanoarchaeum equitans* (NlrNeq gi|41614807|), *Pyrococcus furiosus* (NlrPfur gi|18977653|), *Thermofilum pendens* (NlrTp gi|119720733|); Class III: *Treponema pallidum* (Tp gi|15639809|), *Fusobacterium mortiferum* ATCC 9817 (Fm gi|237736311|) and *Eubacterium biforme* DSM 3989 (Eb gi|218283678|); and HTH-2Fe-SORs: *Clostridium leptum* (Cl gi|160933365|) and *Eggerthella lenta* (El gi|257474935|).

The extensive number of sequences available revealed some interesting aspects, namely on what concerns the variability of N-terminal domains. In a recent study a database was created and the enzymes classified in a more specific way regarding the N-terminus characteristics (*143*). The authors of this study classified SORs in seven classes:

1) Class I or Dx-SOR – correspond to the 2Fe-SORs proteins, where the N-terminus is a desulforedoxin-like (Dx) domain;

2) Class II – correspond to the 1Fe-SORs, with no extra N-terminal domain;

3) Class III – analogous to Dx-SORs but lacking some or all the iron cysteine ligands ($FeCys_4$) for the desulforedoxin-like iron center and therefore lacking the iron site; designated already by others as a subfamily, being the *T. pallidum* SOR the enzyme studied for this class (*252*);

4) Class IV – SOR with an extra C-terminal domain containing an iron-sulfur center, as in methanoferrodoxin from *Methanosarcina mazei*, a novel type of SOR recently discussed (*253*);

5) HTH-Dx-SOR – correspond to a Dx-SOR (2Fe-SOR) with an extended N-terminal helix-turn-helix (HTH) domain present in transcription regulators;

6) TAT-SOR – this class is only found in a few organisms such as *Desulfuromonas acetoxidans* DSM 684 and *Geobacter sulfurreducens*, whose sequences are preceded by a putative twin-arginine signal peptide, suggesting their periplasmatic localization, in contrast to what is generally believed for the remaining SORs, on the basis of the lack of recognizable translocation signals;

7) “Atypical” SORs – correspond to SORs with a variety of N-terminal domains that range from a metallo-beta-lactamase-like to a NAD(P)H-FMN reductase-like domain. However these more complex structures need experimental verification.

In the dendogram presented in Figure 8.6 the class of “atypical” SORs was not taken into consideration due to the immense variety of N-

terminal domains. Regarding the other minor classes of SORs, only the HTH-Dx-SOR (HTH-2Fe-SOR) protein sequences appear to represent a separate cluster, the class III and TAT-SORs being distributed among the major clusters of 2Fe-SORs and 1Fe-SORs, respectively. The class III SOR shows a scattered distribution in the 2Fe-SOR cluster, suggesting that they may have evolved more than once from 2Fe-SORs, by loss of the cysteine ligands. This classification may trigger new functional studies on these enzymes.

Structure

The 3D crystal structures of three SORs, obtained by X-ray crystallography were described in Chapter 7, one SOR from *N.equitans* and two from *I. hospitalis*, wt and E23A mutant. The structure from wt *I. hospitalis* revealed that the electrostatic potential of the protein surface has a positive path around the active site that include positively charged residues from two different monomers, organized in a head-to-tail arrangement. Most of the contribution to this positively charged surface area comes from Lys, Arg and Asn residues exposed to the solvent.

The Lys 21 residue in *I. hospitalis* 1Fe-SOR showed a major importance as revealed by the 3D structure of *I. hospitalis* E23A SOR: this residue appeared oriented towards the iron atom. In the *N. equitans* 1Fe-SOR structure was also observed a Lys 9 residue side-chain directed toward the iron atom.

These observations led us to conclude that the binding of $O_2^{\cdot -}$ to the ferrous-SOR is dependent and assisted by a number of residues that confer a positively charged surface around the active site. The Lys residue should be the residue contributing to direct the substrate as well as to stabilize the first catalytic intermediate, possibly by further contributing to hold water molecules to promote the necessary protonation steps. In *I. hospitalis* SOR and in other *Crenarchaeota* (Chapter 6), the Lys 21 residue is conserved throughout the phylum and should be the aminoacid residue responsible for those steps, *i.e.*, it

appears that throughout evolution several solutions were found to maintain an efficient mechanism for superoxide reduction.

Superoxide reduction mechanism

The superoxide reduction mechanism has been the scope of various studies mainly by using pulse radiolysis, *e.g.,* (*94, 162-163, 171, 234, 238, 254*), an approach that allows the production of quantified amounts of $O_2^{\cdot -}$ in a very fast time scale (*164*). This technique allowed the study of the oxidative cycle of superoxide reduction, from the ferrous-SOR to ferric-SOR and to detect intermediate species. The nature and the number of intermediates of this mechanism have been in the center of discussion, as well as the molecular events that occur at the active site during catalysis, and which aminoacid residues may participate. The superoxide reduction is initiated by the binding of $O_2^{\cdot -}$ to a pentacoordinated Fe^{2+}, previously reduced by an electron donor (*e.g.*, rubredoxins), with a second-order rate constant near the diffusion rate limit (~10^9 $M^{-1}s^{-1}$). This first step is consensual and the first intermediate (T1) fingerprint consists of a characteristic electronic absorption spectrum with a maximum at 580-620 nm with an extinction coefficient of 3000-4000 $M^{-1}cm^{-1}$ (Figure 8.7, Table 8.1). Due to its electronic absorption spectrum this T1 species is identified as a ferric ion bound to a peroxo species, but due to its fast formation and decay rates (Table 8.1) the exact nature of this species is still under investigation (see Chapter 6, footnote 1). There is however, some evidence for the formation of a hydroperoxo-Fe^{3+}. For example, Silaghi-Dumitrescu *et al.* (*166*) by Density Functional theory (DFT) geometry optimizations of various models for the ferrous and ferric pentacoordinated center, as well as peroxo and hydroperoxo ferric-SOR complexes, determined that a low-spin ferric end-on (hydro)peroxo model is the best suited T1 intermediate. It is proposed that the binding of $O_2^{\cdot -}$ to ferrous-SOR primarily generates a ferric-peroxo SOR complex that is protonated on the terminal oxygen [Fe-O-OH] in a concerted proton-electron transfer step. A second protonation occurs at the iron coordinated oxygen to

form an unstable complex [Fe-O(H)-OH]$^{3+}$, that will promote H_2O_2 release and the formation of a ferric-SOR Glu-bound or H_2O-bound (Figure 8.7) (*166*).

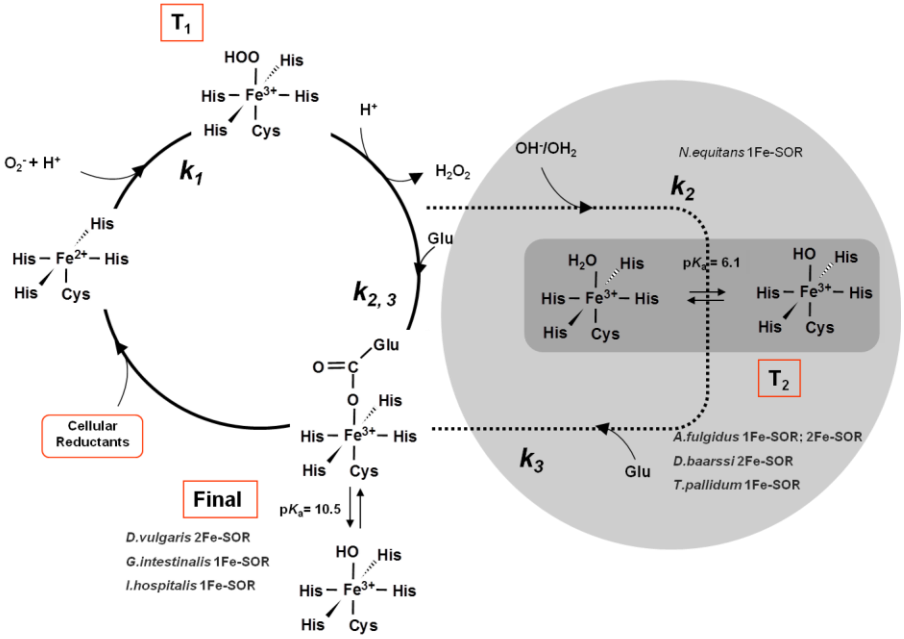

Figure 8.7 – Mechanism of the catalytic reduction of superoxide proposed for different SORs studied, evidencing the detected intermediates for each case. The *N.equitans* SOR appears inside the grey circle, due to the absence of the glutamate residue. Adapted from (*142*).

Kinetically, the T1 formation is the only process in the superoxide reduction mechanism that does not show a detectable pH dependence rate and isotopic effect. The protonation step should then have to exceed the second-order rate verified for T1 formation, as expected for proton transfer in such a solvent-exposed site. Also, in the X-ray crystallography-Resonance-Raman spectroscopy coupled experiment with the 2Fe-SOR E114 mutant from *D. baarsii* (*168*), an end-on ferric-(hydro) peroxo intermediate species was detected, by incubating a ferric pentacoordinated SOR with an excess of H_2O_2. A hydroperoxo species was found to be coordinated by various water molecules and to interact

with a lysine residue in the loop situated above the active site. In a different monomer from the SOR of *D. baarsii*, where the loop containing the Lys residue is displaced, the 3D structure revealed that a water molecule is moved towards the Fe-coordinated oxygen (*168*). Also, DFT calculations from the same authors, proposed that the configuration of this hydroperoxo intermediate is contributing to a weak iron-oxygen bond (*168*). More experiments are still needed to confirm the nature of this intermediate, namely by correlating data with the pulse radiolysis results and the electronic spectra obtained for T1 species (Chapter 6, footnote 1).

All these studies pointed to a ferric-(hydro)peroxo species stabilized by the presence of a hydrogen bonded Lys residue that belongs to a mobile loop that also contains the Glu residue that acts as a 6th ligand in the resting state. Site-directed mutants of this Lys residue in *D.vulgaris* (*234*) and in *D. baarsii* 2Fe-SORs (Table 8.1) (*238*), revealed a 6 and 25*x* decrease in the k_1 rate in comparison to the wt protein, indicating that the absence of this positive charge affected the binding of the substrate, more strongly in the SOR from *D. baarsii*. The 1Fe-SOR from *I. hospitalis* lacking that Lys residue showed, by pulse radiolysis (chapter 6), the formation of a first intermediate with the same electronic absorption characteristics as seen for other T1 intermediates, indicating that this same species is formed and the k_1 rate is only 1.7*x* lower than that for 1Fe-SOR from *A. fulgidus* (Table 8.1). By aminoacid sequence analysis and with the 3D structure of *I. hospitalis* SOR, we were able to see that another Lys residue, number 21, conserved in the majority of SORs (Chapter 6), is part of a mobile loop and is pointing out to the surface. Therefore, due to the flexibility of this loop, the 21st residue can move towards the active site and stabilize the first intermediate, making it a still efficient SOR.

For the E23A mutant, the absence of the Glu residue, that acts as a 6th ligand in the ferric-SOR state was seen not to affect the T1 formation, even increasing its rate by completely exposing the active site to the solvent, including the His ligands, inducing a more positively charged

surface (Table 8.1 for SORs from *N.equitans*, *I. hospitalis* and *D.vulgaris*).

The decay process of the first intermediate is the only process that is pH dependent. In this step, the protonation of the (hydro) peroxo-ferric intermediate occurs by inducing the release of the product and the formation of a ferric-SOR that can be a T2 intermediate (Fe^{3+}-H_2O/OH) and/or a final ferric-SOR state (Fe^{3+}-Glu) (Figure 8.7).

The rate of decay (k_2; k_3) of T1 to T2/Tfinal is pH-dependent in the pH range 5 to 8.5; above pH 8.5 the rate is pH independent or increases with pH. This increase with pH may be related to the substitution of the product by the OH^- anion, which is expected to be faster at higher OH^- concentration. The pH-independent process at higher pH values may be explained by a direct interaction of T1 with a water molecule, a pseudo-first order process (*163, 234*). At low pH values the pH dependence probably results from a process with a diffusion-limited protonation step. For SORs such as *I.hospitalis* (wt and mutants) and *A. fulgidus* (wt), this process has an associated pK_a that is around 6 for all enzymes, regardless of the presence of the Glu residue, supporting the notion that this residue is not involved in proton transfer at lower pH. The role of the Glu residue could be that of preventing the access by adventious ligands to the ferric-SOR that could block the access to the active site by the substrate.

Besides the importance of some residues in the reduction of superoxide, there are other intriguing questions related to the number of intermediates. For the 1Fe-SOR from *I. hospitalis* the superoxide reduction occurred through the formation of only one detectable intermediate, T1 that decays into the final resting ferric species (Figure 8.7). On the contrary, for *A. fulgidus* 1Fe-SOR and 2Fe-SOR, as well as more recently for *D. baarsii* 2Fe-SOR, pulse radiolysis studies revealed the presence of two intermediates, T1 and T2, (Figure 8.7). A fast-scale process that is not detectable by the techniques used may explain this

difference. Structurally, there may be an arrangement of the flexible loop or of other motif that occurs in a different time-scale.

Table 8.1 – Kinetic parameters of SORs in superoxide reduction

	T1- Fe^{3+} hydroperoxo λmax (nm)	***k_1 T1 (x 10^9 $M^{-1}s^{-1}$)***	***k_2 T2 (s^{-1}) pH7***	***k_3 Tfinal (s^{-1}) pH7***	***Ref***
2Fe-SOR					
A. fulgidus	580	0.8	57	29	(*171*)
D.vulgaris	590	1.4		84	(*234*)
D.vulgaris E47A	600	2.2		65	(*234*)
D.vulgaris K48A	600	0.21		25	(*234*)
D.baarsii	610	1.0	255	110	(*239*)
D.baarsii E47A	630	1.0		440	(*160, 238*)
D.baarsii K48I	600	0.04		300	(*160, 238*)
1Fe-SOR					
T.pallidum	610	0.6		4800	(*254*)
T.pallidum E48A	~600	0.6		2080	(*167*)
A.fulgidus	620	1.2	3800	25	(*163*)
A.fulgidus E12V	620	0.22		~360	(*163*)
A.fulgidus E12Q	620	0.9		~600	(*163*)
N.equitans	590	1		<10	(*162*)
G. intestinalis	600	1		~320	(*94*)
I. hospitalis	590	0.7		~75	Chap. 6
I. hospitalis E23A	590	1.2		~320	Chap. 6
I. hospitalis T24K	590	0.4		~500	Chap. 6

8.3 - Conclusions/Final Remarks

This thesis focused on the study of two examples from two protein families involved in the scavenging of ROS operating only in a reductive pathway: rubrerythrin by reducing hydrogen peroxide and superoxide reductase by reducing superoxide. These systems are widely distributed in anaerobes, microaerobes and even some aerobes,

showing the importance of maintaining a low level of ROS in the cell. The same scavenging function of both protein families is found in other enzymes. For rubrerythrins, catalases are the most well known and efficient enzymes acting on the disproportionation of hydrogen peroxide and for SORs, SODs efficiently dismutate superoxide anion. However, a higher distribution of the reductive systems in anaerobes or microaerobes could mean that there is an advantage over enzymes such as SOD and catalase.

The steady state levels of superoxide and hydrogen peroxide in the cell have been estimated to be in the nanomolar range 10^{-9} and 10^{-7} M, respectively. The enzymes SOD and catalase have K_M in the millimolar range and catalyze the disproportionation of those species more efficiently at higher concentrations. For example, in *E. coli* peroxide reductases as AhpC are proposed to reduce hydrogen peroxide to lower levels instead of catalase (*255*). The same should happen for rubrerythrins, functioning as peroxidases. Another reason can be related to the pool of reducing equivalents in the cell. The NAD(P)H /$NAD(P)^+$ ratio reflects the redox status of the cell and may activate transcription factors that will modulate its metabolic activity (*256*). The levels of NADPH /$NADP^+$ have been shown to regulate the expression of the redox regulator, SoxR (*48*). SORs and Rbrs are dependent on this pool of reducing equivalents as a source of electrons and can therefore influence this ratio. At low levels of ROS, the need for NAD(P)H is not very demanding but at higher concentrations of ROS the pool may be depleted, and so the dismutase enzymes should be preferable. Furthermore, and in contrast with those enzymes, the reduction of superoxide or hydrogen peroxide coupled to the consumption of reducing equivalents leads to a decrease on the levels of reduced compounds that could react with O_2 and produce ROS.

In anaerobes or microaerobes the concentration of ROS are maintained at a low level and so the action of these reductive enzymes corresponds to a rapid response for scavenging those reactive species in the cell.

References

1. Severinghaus, J. W. (2003) Fire-air and dephlogistication. Revisionisms of oxygen's discovery, *Adv Exp Med Biol 543*, 7-19.
2. Sternbach, G. L., and Varon, J. (2005) The discovery and rediscovery of oxygen, *J Emerg Med 28*, 221-224.
3. Sawyer, D. T. (1991) *Oxygen Chemistry*, Oxford Univeristy Press, New York.
4. Cassebaum, H., and Schufle, J. A. (1975) Scheele's Priority for the discovery of Oxygen, *Journal of Chemical Education 52*, 442-444.
5. Gerschman, R., Gilbert, D. L., Nye, S. W., Dwyer, P., and Fenn, W. O. (1954) Oxygen poisoning and x-irradiation: a mechanism in common, *Science 119*, 623-626.
6. Williams, R. J. (2012) Iron in evolution, *FEBS Lett 586*, 479-484.
7. Williams, R. J. P., and Fraústo da Silva, J. J. R. (1999) *Bringing Chemistry to Life - from Matter to Man*, Oxford University Press, Oxford.
8. Bharara, M. S., and Atwood, D. A. (2005) Oxygen: Inorganic Chemistry, In *Encyclopedia of Inorganic Chemistry* (R. Bruce King, Ed.) 2 ed., p 6696
9. Crichton, R. (2009) *Iron Metabolism - From Molecular Mechanism to Clinical Consequences*, 3rd ed., John Wiley & Sons, Ltd.
10. Bertini, I., Gray, H. B., Lippard, S. J., and Valentine, J. S. (1994) Dioxygen Reactions, In *Bioinorganic Chemistry* (University Science Books, Ed.), Mill Valley, California.
11. Imlay, J. A. (2003) Pathways of oxidative damage, *Annu Rev Microbiol 57*, 395-418.
12. Halliwell, B., and Gutteridge M.C. John (1999) *Free radicals in biology and medicine*, 3 ed., Oxford University Press.
13. Sawyer, D. T., and Valentine, J. S. (1981) How Super is Superoxide, *Acc. Chem. Res 14* 393-400.
14. McCord, J. M., and Fridovich, I. (1969) Superoxide Dismutase. An Enzymic Function for Erythrocuprein *J. Biol. Chem. 244*, 6049-6055.
15. Tripathy, B. C., and Rieske, J. S. (1985) Antimycin-Resistant Alternate Electron Pathway to Plastocyanin in Bovine-Heart Complex III, *Journal of Bioenergetics and Biomembranes 17*, 142-150.

16. Gutteridge, J. M. (1984) Lipid peroxidation initiated by superoxide-dependent hydroxyl radicals using complexed iron and hydrogen peroxide, *FEBS Lett 172*, 245-249.
17. Henle, E. S., and Linn, S. (1997) Formation, prevention, and repair of DNA damage by iron/hydrogen peroxide, *J Biol Chem 272*, 19095-19098.
18. Valentine, J. S., Wertz, D. L., Lyons, T. J., Liou, L. L., Goto, J. J., and Gralla, E. B. (1998) The dark side of dioxygen biochemistry, *Curr Opin Chem Biol 2*, 253-262.
19. Carlioz, A., and Touati, D. (1986) Isolation of superoxide dismutase mutants in *Escherichia coli*: is superoxide dismutase necessary for aerobic life?, *EMBO J 5*, 623-630.
20. Geary, L. E., and Meister, A. (1977) On the mechanism of glutamine-dependent reductive amination of alpha-ketoglutarate catalyzed by glutamate synthase, *J Biol Chem 252*, 3501-3508.
21. Grinblat, L., Sreider, C. M., and Stoppani, A. O. (1991) Superoxide anion production by lipoamide dehydrogenase redox-cycling: effect of enzyme modifiers, *Biochem Int 23*, 83-92.
22. Imlay, J. A. (1995) A metabolic enzyme that rapidly produces superoxide, fumarate reductase of *Escherichia coli*, *J Biol Chem 270*, 19767-19777.
23. Kussmaul, L., and Hirst, J. (2006) The mechanism of superoxide production by NADH:ubiquinone oxidoreductase (complex I) from bovine heart mitochondria, *Proc Natl Acad Sci U S A 103*, 7607-7612.
24. Massey, V., Strickland, S., Mayhew, S.G., Howell, L.G., Engel, P.C., Matthews, R.G., Schuman, M., Sullivan, P.A. (1969) The production of superoxide anion radicals in the reaction of reduced flavins and flavoproteins with molecular oxygen., *Biochem Biophys Res Commun. 36*, 891-897.
25. Messner, K. R., and Imlay, J.A. (1999) The identification of primary sites of superoxide and hydrogen peroxide formation in the aerobic respiratory chain and sulfite reductase complex of *Escherichia coli*., *J Biol Chem. 274*, 10119-10128.
26. Messner, K. R., and Imlay, J. A. (2002) Mechanism of superoxide and hydrogen peroxide formation by fumarate reductase, succinate

dehydrogenase, and aspartate oxidase, *J Biol Chem 277*, 42563-42571.

27. Imlay, J. A. (2002) How oxygen damages microbes: oxygen tolerance and obligate anaerobiosis, *Adv Microb Physiol 46*, 111-153.
28. Imlay, J. A., and Fridovich, I. (1991) Assay of metabolic superoxide production in *Escherichia coli*, *J Biol Chem 266*, 6957-6965.
29. Gort, A. S., and Imlay, J. A. (1998) Balance between endogenous superoxide stress and antioxidant defenses, *J Bacteriol 180*, 1402-1410.
30. Storz, G., and Imlay, J. A. (1999) Oxidative stress, *Curr Opin Microbiol 2*, 188-194.
31. Boehme, E. D., Vincent, K., and Brown, O. R. (1976) Oxygen and toxicity inhibition of amino acid biosynthesis, *Nature 262*, 418 - 420.
32. Brown, O. R., Smyk-Randall, E., Draczynska-Lusiak, B., and Fee, J. A. (1995) Dihydroxy-acid dehydratase, a [4Fe-4S] cluster-containing enzyme in *Escherichia coli*: effects of intracellular superoxide dismutase on its inactivation by oxidant stress, *Arch Biochem Biophys 319*, 10-22.
33. Flint, D. H., Tuminello, J. F., and Emptage, M. H. (1993) The inactivation of Fe-S cluster containing hydro-lyases by superoxide, *J Biol Chem 268*, 22369-22376.
34. Gardner, P. R., and Fridovich, I. (1992) Inactivation-reactivation of aconitase in *Escherichia coli*. A sensitive measure of superoxide radical, *J Biol Chem 267*, 8757-8763.
35. Hausladen, A., and Fridovich, I. (1994) Superoxide and peroxynitrite inactivate aconitases, but nitric oxide does not, *J Biol Chem 269*, 29405-29408.
36. Crichton, R. (2001) *Inorganic Biochemistry of Iron Metabolism: From Molecular Mechanisms to Clinical Consequences*, 2 ed., John Wiley & Sons Ltd.
37. Seaver, L. C., and Imlay, J. A. (2001) Hydrogen peroxide fluxes and compartmentalization inside growing *Escherichia coli*, *J Bacteriol 183*, 7182-7189.
38. Graf, E., Mahoney, J. R., Bryant, R. G., and Eaton, J. W. (1984) Iron-catalyzed Hydroxyl Radical Formation, *J Biol Chem 259*, 3620-3624.

39. Nunoshiba, T., Obata, F., Boss, A. C., Oikawa, S., Mori, T., Kawanishi, S., and Yamamoto, K. (1999) Role of iron and superoxide for generation of hydroxyl radical, oxidative DNA lesions, and mutagenesis in *Escherichia coli*, *J Biol Chem 274*, 34832-34837.
40. Liochev, S. I., and Fridovich, I. (2011) Is superoxide able to induce SoxRS?, *Free Radic Biol Med 50*, 1813.
41. Hassan, H. M., and Fridovich, I. (1977) Regulation of the synthesis of superoxide dismutase in *Escherichia coli*. Induction by methyl viologen, *J Biol Chem 252*, 7667-7672.
42. Privalle, C. T., Kong, S. E., and Fridovich, I. (1993) Induction of manganese-containing superoxide dismutase in anaerobic *Escherichia coli* by diamide and 1,10-phenanthroline: sites of transcriptional regulation, *Proc Natl Acad Sci U S A 90*, 2310-2314.
43. Imlay, J. A. (2008) Cellular defenses against superoxide and hydrogen peroxide, *Annu Rev Biochem 77*, 755-776.
44. Ding, H., and Demple, B. (2000) Direct nitric oxide signal transduction via nitrosylation of iron-sulfur centers in the SoxR transcription activator, *Proc Natl Acad Sci U S A 97*, 5146-5150.
45. Gallegos, M. T., Schleif, R., Bairoch, A., Hofmann, K., and Ramos, J. L. (1997) Arac/XylS family of transcriptional regulators, *Microbiol Mol Biol Rev 61*, 393-410.
46. Zheng, M., and Storz, G. (2000) Redox sensing by prokaryotic transcription factors, *Biochem Pharmacol 59*, 1-6.
47. Watanabe, S., Kita, A., Kobayashi, K., and Miki, K. (2008) Crystal structure of the [2Fe-2S] oxidative-stress sensor SoxR bound to DNA, *Proc Natl Acad Sci U S A 105*, 4121-4126.
48. Krapp, A. R., Humbert, M. V., and Carrillo, N. (2011) The soxRS response of *Escherichia coli* can be induced in the absence of oxidative stress and oxygen by modulation of NADPH content, *Microbiology 157*, 957-965.
49. Choi, H., Kim, S., Mukhopadhyay, P., Cho, S., Woo, J., Storz, G., and Ryu, S. E. (2001) Structural basis of the redox switch in the OxyR transcription factor, *Cell 105*, 103-113.
50. Maddocks, S. E., and Oyston, P. C. (2008) Structure and function of the LysR-type transcriptional regulator (LTTR) family proteins, *Microbiology 154*, 3609-3623.

51. Lee, J. W., and Helmann, J. D. (2007) Functional specialization within the Fur family of metalloregulators, *Biometals 20*, 485-499.

52. Sheikh, M. A., and Taylor, G. L. (2009) Crystal structure of the *Vibrio cholerae* ferric uptake regulator (Fur) reveals insights into metal co-ordination, *Mol Microbiol 72*, 1208-1220.

53. Mills, S. A., and Marletta, M. A. (2005) Metal binding characteristics and role of iron oxidation in the ferric uptake regulator from *Escherichia coli*, *Biochemistry 44*, 13553-13559.

54. Masse, E., and Gottesman, S. (2002) A small RNA regulates the expression of genes involved in iron metabolism in *Escherichia coli*, *Proc Natl Acad Sci U S A 99*, 4620-4625.

55. Park, S. J., and Gunsalus, R. P. (1995) Oxygen, iron, carbon, and superoxide control of the fumarase fumA and fumC genes of *Escherichia coli*: role of the arcA, fnr, and soxR gene products, *J Bacteriol 177*, 6255-6262.

56. Tseng, C. P. (1997) Regulation of fumarase (fumB) gene expression in *Escherichia coli* in response to oxygen, iron and heme availability: role of the arcA, fur, and hemA gene products, *FEMS Microbiol Lett 157*, 67-72.

57. Andrews, S. C., Robinson, A. K., and Rodriguez-Quinones, F. (2003) Bacterial iron homeostasis, *FEMS Microbiol Rev 27*, 215-237.

58. Zheng, M., Doan, B., Schneider, T. D., and Storz, G. (1999) OxyR and SoxRS regulation of fur, *J Bacteriol 181*, 4639-4643.

59. Lee, J. W., and Helmann, J. D. (2006) The PerR transcription factor senses H_2O_2 by metal-catalysed histidine oxidation, *Nature 440*, 363-367.

60. van Vliet, A. H., Baillon, M. L., Penn, C. W., and Ketley, J. M. (1999) *Campylobacter jejuni* contains two fur homologs: characterization of iron-responsive regulation of peroxide stress defense genes by the PerR repressor, *J Bacteriol 181*, 6371-6376.

61. Mongkolsuk, S., and Helmann, J. D. (2002) Regulation of inducible peroxide stress responses, *Mol Microbiol 45*, 9-15.

62. Jacquamet, L., Traore, D. A., Ferrer, J. L., Proux, O., Testemale, D., Hazemann, J. L., Nazarenko, E., El Ghazouani, A., Caux-Thang, C., Duarte, V., and Latour, J. M. (2009) Structural characterization of the

active form of PerR: insights into the metal-induced activation of PerR and Fur proteins for DNA binding, *Mol Microbiol 73*, 20-31.

63. Schrödinger, L. The PyMOL Molecular Graphics System, Version 1.5.0.4 ed.
64. Roos, D., van Bruggen, R., and Meischl, C. (2003) Oxidative killing of microbes by neutrophils, *Microbes Infect 5*, 1307-1315.
65. Bedard, K., and Krause, K. H. (2007) The NOX family of ROS-generating NADPH oxidases: physiology and pathophysiology, *Physiol Rev 87*, 245-313.
66. Winterbourn, C. C. (2002) Biological reactivity and biomarkers of the neutrophil oxidant, hypochlorous acid, *Toxicology 181-182*, 223-227.
67. MacMicking, J., Xie, Q. W., and Nathan, C. (1997) Nitric oxide and macrophage function, *Annu Rev Immunol 15*, 323-350.
68. Miller, A. F. (2004) Superoxide dismutases: active sites that save, but a protein that kills, *Curr Opin Chem Biol 8*, 162-168.
69. Abreu, I. A., and Cabelli, D. E. (2010) Superoxide dismutases-a review of the metal-associated mechanistic variations, *Biochim Biophys Acta 1804*, 263-274.
70. Miller, A. F. (2003) *Superoxide Processing in Comprehensive Coordination Chemistry II*, Vol. 8, Elsevier/Pergamon Oxford UK.
71. Miller, A. F. (2012) Superoxide dismutases: ancient enzymes and new insights, *FEBS Lett 586*, 585-595.
72. Perry, J. J., Shin, D. S., Getzoff, E. D., and Tainer, J. A. (2010) The structural biochemistry of the superoxide dismutases, *Biochim Biophys Acta 1804*, 245-262.
73. Barondeau, D. P., Kassmann, C. J., Bruns, C. K., Tainer, J. A., and Getzoff, E. D. (2004) Nickel superoxide dismutase structure and mechanism, *Biochemistry 43*, 8038-8047.
74. Koua, D., Cerutti, L., Falquet, L., Sigrist, C. J., Theiler, G., Hulo, N., and Dunand, C. (2009) PeroxiBase: a database with new tools for peroxidase family classification, *Nucleic Acids Res 37*, D261-266.
75. Margis, R., Dunand, C., Teixeira, F. K., and Margis-Pinheiro, M. (2008) Glutathione peroxidase family - an evolutionary overview, *FEBS J 275*, 3959-3970.

76. Parsonage, D., Karplus, P. A., and Poole, L. B. (2008) Substrate specificity and redox potential of AhpC, a bacterial peroxiredoxin, *Proc Natl Acad Sci U S A 105*, 8209-8214.

77. Maria J Maté, G. M., Jerónimo Bravo, William Melik-Adamyan, Peter C Loewen and Ignacio Fita. (2006) Heme-catalases, In *Handbook of Metalloproteins* (Ltd. John Wiley & Sons, Ed.).

78. Chelikani, P., Fita, I., and Loewen, P. C. (2004) Diversity of structures and properties among catalases, *Cell Mol Life Sci 61*, 192-208.

79. McCord, J. M., Keele, B. B., Jr., and Fridovich, I. (1971) An enzyme-based theory of obligate anaerobiosis: the physiological function of superoxide dismutase, *Proc Natl Acad Sci U S A 68*, 1024-1027.

80. Dolla, A., Fournier, M., and Dermoun, Z. (2006) Oxygen defense in sulfate-reducing bacteria, *J Biotechnol 126*, 87-100.

81. Fareleira, P., Legall, J., Xavier, A. V., and Santos, H. (1997) Pathways for utilization of carbon reserves in *Desulfovibrio gigas* under fermentative and respiratory conditions, *J Bacteriol 179*, 3972-3980.

82. Santos, H., Fareleira, P., Xavier, A. V., Chen, L., Liu, M. Y., and LeGall, J. (1993) Aerobic metabolism of carbon reserves by the "obligate anaerobe" *Desulfovibrio gigas*, *Biochem Biophys Res Commun 195*, 551-557.

83. Lobo, S. A., Melo, A. M., Carita, J. N., Teixeira, M., and Saraiva, L. M. (2007) The anaerobe *Desulfovibrio desulfuricans* ATCC 27774 grows at nearly atmospheric oxygen levels, *FEBS Lett 581*, 433-436.

84. Hillmann, F., Fischer, R. J., Saint-Prix, F., Girbal, L., and Bahl, H. (2008) PerR acts as a switch for oxygen tolerance in the strict anaerobe *Clostridium acetobutylicum*, *Mol Microbiol 68*, 848-860.

85. LeGall, J., Prickril, B. C., Moura, I., Xavier, A. V., Moura, J. J., and Huynh, B. H. (1988) Isolation and characterization of rubrerythrin, a non-heme iron protein from *Desulfovibrio vulgaris* that contains rubredoxin centers and a hemerythrin-like binuclear iron cluster, *Biochemistry 27*, 1636-1642.

86. Kurtz, D. M., Jr. (2006) Avoiding high-valent iron intermediates: superoxide reductase and rubrerythrin, *J Inorg Biochem 100*, 679-693.

87. Alban, P. S., Popham, D. L., Rippere, K. E., and Krieg, N. R. (1998) Identification of a gene for a rubrerythrin/nigerythrin-like protein in *Spirillum volutans* by using amino acid sequence data from mass

spectrometry and NH_2-terminal sequencing, *J Appl Microbiol 85*, 875-882.

88. Cooley, R. B., Arp, D. J., and Karplus, P. A. (2011) Symerythrin structures at atomic resolution and the origins of rubrerythrins and the ferritin-like superfamily, *J Mol Biol 413*, 177-194.

89. Kawasaki, S., Ishikura, J., Watamura, Y., and Niimura, Y. (2004) Identification of O_2-induced peptides in an obligatory anaerobe, *Clostridium acetobutylicum*, *FEBS Lett 571*, 21-25.

90. Lumppio, H. L., Shenvi, N. V., Summers, A. O., Voordouw, G., and Kurtz, D. M., Jr. (2001) Rubrerythrin and rubredoxin oxidoreductase in *Desulfovibrio vulgaris*: a novel oxidative stress protection system, *J Bacteriol 183*, 101-108.

91. May, A., Hillmann, F., Riebe, O., Fischer, R. J., and Bahl, H. (2004) A rubrerythrin-like oxidative stress protein of *Clostridium acetobutylicum* is encoded by a duplicated gene and identical to the heat shock protein Hsp21, *FEMS Microbiol Lett 238*, 249-254.

92. Putz, S., Gelius-Dietrich, G., Piotrowski, M., and Henze, K. (2005) Rubrerythrin and peroxiredoxin: two novel putative peroxidases in the hydrogenosomes of the microaerophilic protozoon *Trichomonas vaginalis*, *Mol Biochem Parasitol 142*, 212-223.

93. Sztukowska, M., Bugno, M., Potempa, J., Travis, J., and Kurtz, D. M., Jr. (2002) Role of rubrerythrin in the oxidative stress response of *Porphyromonas gingivalis*, *Mol Microbiol 44*, 479-488.

94. Testa, F., Mastronicola, D., Cabelli, D. E., Bordi, E., Pucillo, L. P., Sarti, P., Saraiva, L. M., Giuffre, A., and Teixeira, M. (2011) The superoxide reductase from the early diverging eukaryote *Giardia intestinalis*, *Free Radic Biol Med 51*, 1567-1574.

95. Wakagi, T. (2003) Sulerythrin, the smallest member of the rubrerythrin family, from a strictly aerobic and thermoacidophilic archaeon, *Sulfolobus tokodaii* strain 7, *FEMS Microbiol Lett 222*, 33-37.

96. Pierik, A. J., Wolbert, R. B., Portier, G. L., Verhagen, M. F., and Hagen, W. R. (1993) Nigerythrin and rubrerythrin from *Desulfovibrio vulgaris* each contain two mononuclear iron centers and two dinuclear iron clusters, *Eur J Biochem 212*, 237-245.

97. Bonomi, F., Kurtz, D. M. Jr., and Cui, X. (1996) Ferroxidase activity of recombinant *Desulfovibrio vulgaris* rubrerythrin, *J Biol Inorg Chem 1*, 67-72.

98. Lehmann, Y., Meile, L., and Teuber, M. (1996) Rubrerythrin from *Clostridium perfringens*: cloning of the gene, purification of the protein, and characterization of its superoxide dismutase function, *J Bacteriol 178*, 7152-7158.

99. Coulter, E. D., and Kurtz, D. M., Jr. (2001) A role for rubredoxin in oxidative stress protection in *Desulfovibrio vulgaris*: catalytic electron transfer to rubrerythrin and two-iron superoxide reductase, *Arch Biochem Biophys 394*, 76-86.

100. Coulter, E. D., Shenvi, N. V., and Kurtz, D. M., Jr. (1999) NADH peroxidase activity of rubrerythrin, *Biochem Biophys Res Commun 255*, 317-323.

101. Riebe, O., Fischer, R. J., Wampler, D. A., Kurtz, D. M., Jr., and Bahl, H. (2009) Pathway for H_2O_2 and O_2 detoxification in *Clostridium acetobutylicum*, *Microbiology 155*, 16-24.

102. Weinberg, M. V., Jenney, F. E. J., Cui, X., and Adams, M. W. (2004) Rubrerythrin from the hyperthermophilic archaeon *Pyrococcus furiosus* is a rubredoxin-dependent, iron-containing peroxidase, *J Bacteriol 186*, 7888-7895.

103. deMare, F., Kurtz, D. M., Jr., and Nordlund, P. (1996) The structure of *Desulfovibrio vulgaris* rubrerythrin reveals a unique combination of rubredoxin-like FeS4 and ferritin-like diiron domains, *Nat Struct Biol 3*, 539-546.

104. Jin, S., Kurtz, D. M., Jr., Liu, Z. J., Rose, J., and Wang, B. C. (2002) X-ray crystal structures of reduced rubrerythrin and its azide adduct: a structure-based mechanism for a non-heme diiron peroxidase, *J Am Chem Soc 124*, 9845-9855.

105. Fournier, M., Aubert, C., Dermoun, Z., Durand, M. C., Moinier, D., and Dolla, A. (2006) Response of the anaerobe *Desulfovibrio vulgaris* Hildenborough to oxidative conditions: proteome and transcript analysis, *Biochimie 88*, 85-94.

106. Yamasaki, M., Igimi, S., Katayama, Y., Yamamoto, S., and Amano, F. (2004) Identification of an oxidative stress-sensitive protein from

Campylobacter jejuni, homologous to rubredoxin oxidoreductase/ rubrerythrin, *FEMS Microbiol Lett 235*, 57-63.

107. Mydel, P., Takahashi, Y., Yumoto, H., Sztukowska, M., Kubica, M., Gibson, F. C., 3rd, Kurtz, D. M., Jr., Travis, J., Collins, L. V., Nguyen, K. A., Genco, C. A., and Potempa, J. (2006) Roles of the host oxidative immune response and bacterial antioxidant rubrerythrin during *Porphyromonas gingivalis* infection, *PLoS Pathog 2*, e76.
108. Kato, S., Kosaka, T., and Watanabe, K. (2008) Comparative transcriptome analysis of responses of *Methanothermobacter thermautotrophicus* to different environmental stimuli, *Environ Microbiol 10*, 893-905.
109. Meyer, J., and Moulis, J.M. (2006) Rubredoxin, In *Handbook of Metalloproteins* (A. Messerschmidt, Huber,R., Poulos, T., and Wieghardt, K., Ed.), John Wiley & Sons, Ltd.
110. Wastl, J., Duin, E. C., Iuzzolino, L., Dorner, W., Link, T., Hoffmann, S., Sticht, H., Dau, H., Lingelbach, K., and Maier, U. G. (2000) Eukaryotically encoded and chloroplast-located rubredoxin is associated with photosystem II, *J Biol Chem 275*, 30058-30063.
111. LeGall, J., Liu, M. Y., Gomes, C. M., Braga, V., Pacheco, I., Regalla, M., Xavier, A. V., and Teixeira, M. (1998) Characterisation of a new rubredoxin isolated from *Desulfovibrio desulfuricans* 27774: definition of a new family of rubredoxins, *FEBS Lett 429*, 295-298.
112. Moura, I., Bruschi, M., Le Gall, J., Moura, J. J., and Xavier, A. V. (1977) Isolation and characterization of desulforedoxin, a new type of non-heme iron protein from *Desulfovibrio gigas*, *Biochem Biophys Res Commun 75*, 1037-1044.
113. Archer, M., Huber, R., Tavares, P., Moura, I., Moura, J. J., Carrondo, M. A., Sieker, L. C., LeGall, J., and Romao, M. J. (1995) Crystal structure of desulforedoxin from *Desulfovibrio gigas* determined at 1.8 A resolution: a novel non-heme iron protein structure, *J Mol Biol 251*, 690-702.
114. Gomes, C. M., Vicente, J. B., Wasserfallen, A., and Teixeira, M. (2000) Spectroscopic studies and characterization of a novel electron-transfer chain from *Escherichia coli* involving a flavorubredoxin and its flavoprotein reductase partner, *Biochemistry 39*, 16230-16237.

115. Pinto, A. F., Todorovic, S., Hildebrandt, P., Yamazaki, M., Amano, F., Igimi, S., Romao, C. V., and Teixeira, M. (2011) Desulforubrerythrin from *Campylobacter jejuni*, a novel multidomain protein, *J Biol Inorg Chem 16*, 501-510.

116. Moura, I., Tavares, P., Moura, J. J., Ravi, N., Huynh, B. H., Liu, M. Y., and LeGall, J. (1990) Purification and characterization of desulfoferrodoxin. A novel protein from *Desulfovibrio desulfuricans* (ATCC 27774) and from *Desulfovibrio vulgaris* (strain Hildenborough) that contains a distorted rubredoxin center and a mononuclear ferrous center, *J Biol Chem 265*, 21596-21602.

117. Silaghi-Dumitrescu, R., Coulter, E. D., Das, A., Ljungdahl, L. G., Jameson, G. N., Huynh, B. H., and Kurtz, D. M. J. (2003) A flavodiiron protein and high molecular weight rubredoxin from *Moorella thermoacetica* with nitric oxide reductase activity, *Biochemistry 42*, 2806-2815.

118. Vicente, J. B., and Teixeira, M. (2005) Redox and spectroscopic properties of the *Escherichia coli* nitric oxide-detoxifying system involving flavorubredoxin and its NADH-oxidizing redox partner, *J Biol Chem 280*, 34599-34608.

119. Kok, M., Oldenhuis, R., van der Linden, M. P., Meulenberg, C. H., Kingma, J., and Witholt, B. (1989) The *Pseudomonas oleovorans* alkBAC operon encodes two structurally related rubredoxins and an aldehyde dehydrogenase, *J Biol Chem 264*, 5442-5451.

120. da Costa, P. N., Romao, C. V., LeGall, J., Xavier, A. V., Melo, E., Teixeira, M., and Saraiva, L. M. (2001) The genetic organization of *Desulfovibrio desulphuricans* ATCC 27774 bacterioferritin and rubredoxin-2 genes: involvement of rubredoxin in iron metabolism, *Mol Microbiol 41*, 217-227.

121. Rodrigues, J. V., Abreu, I. A., Saraiva, L. M., and Teixeira, M. (2005) Rubredoxin acts as an electron donor for neelaredoxin in *Archaeoglobus fulgidus*, *Biochem Biophys Res Commun 329*, 1300-1305.

122. Hillmann, F., Riebe, O., Fischer, R. J., Mot, A., Caranto, J. D., Kurtz, D. M., Jr., and Bahl, H. (2009) Reductive dioxygen scavenging by flavo-diiron proteins of *Clostridium acetobutylicum*, *FEBS Lett 583*, 241-245.

123. Chen, L., Liu, M. Y., Legall, J., Fareleira, P., Santos, H., and Xavier, A. V. (1993) Purification and characterization of an NADH-rubredoxin oxidoreductase involved in the utilization of oxygen by *Desulfovibrio gigas*, *Eur J Biochem 216*, 443-448.

124. Kawasaki, S., Sakai, Y., Takahashi, T., Suzuki, I., and Niimura, Y. (2009) O_2 and reactive oxygen species detoxification complex, composed of O_2-responsive NADH:rubredoxin oxidoreductase-flavoprotein A2-desulfoferrodoxin operon enzymes, rubperoxin, and rubredoxin, in *Clostridium acetobutylicum*, *Appl Environ Microbiol 75*, 1021-1029.

125. Ma, K., and Adams, M. W. (2001) NAD(P)H:rubredoxin oxidoreductase from *Pyrococcus furiosus*, *Methods Enzymol 334*, 55-62.

126. Kurtz , M. D. J. (2005) Iron proteins with dinuclear active sites, In *Encyclopedia of Inorganic Chemistry* (R. Bruce King, Ed.) 2nd ed.

127. Sazinsky, M. H., and Lippard, S. J. (2006) Correlating structure with function in bacterial multicomponent monooxygenases and related diiron proteins, *Acc Chem Res 39*, 558-566.

128. Andrews, S. C. (2010) The Ferritin-like superfamily: Evolution of the biological iron storeman from a rubrerythrin-like ancestor, *Biochim Biophys Acta 1800*, 691-705.

129. Jin, S., Kurtz, D. M., Jr., Liu, Z. J., Rose, J., and Wang, B. C. (2004) X-ray crystal structure of *Desulfovibrio vulgaris* rubrerythrin with zinc substituted into the [Fe(SCys)4] site and alternative diiron site structures, *Biochemistry 43*, 3204-3213.

130. Sieker, L. C., Holmes, M., Le Trong, I., Turley, S., Liu, M. Y., LeGall, J., and Stenkamp, R. E. (2000) The 1.9 A crystal structure of the "as isolated" rubrerythrin from *Desulfovibrio vulgaris*: some surprising results, *J Biol Inorg Chem 5*, 505-513.

131. Dillard, B. D., Demick, J. M., Adams, M. W., and Lanzilotta, W. N. (2011) A cryo-crystallographic time course for peroxide reduction by rubrerythrin from *Pyrococcus furiosus*, *J Biol Inorg Chem 16*, 949-959.

132. Fushinobu, S., Shoun, H., and Wakagi, T. (2003) Crystal structure of sulerythrin, a rubrerythrin-like protein from a strictly aerobic archaeon, *Sulfolobus tokodaii* strain 7, shows unexpected domain swapping, *Biochemistry 42*, 11707-11715.

133. Tempel, W., Liu, Z. J., Schubot, F. D., Shah, A., Weinberg, M. V., Jenney, F. E., Jr., Arendall, W. B., 3rd, Adams, M. W., Richardson, J. S., Richardson, D. C., Rose, J. P., and Wang, B. C. (2004) Structural genomics of *Pyrococcus furiosus*: X-ray crystallography reveals 3D domain swapping in rubrerythrin, *Proteins 57*, 878-882.

134. Li, M., Liu, M. Y., LeGall, J., Gui, L. L., Liao, J., Jiang, T., Zhang, J. P., Liang, D. C., and Chang, W. R. (2003) Crystal structure studies on rubrerythrin: enzymatic activity in relation to the zinc movement, *J Biol Inorg Chem 8*, 149-155.

135. Iyer, R. B., Silaghi-Dumitrescu, R., Kurtz, D. M., Jr., and Lanzilotta, W. N. (2005) High-resolution crystal structures of *Desulfovibrio vulgaris* (Hildenborough) nigerythrin: facile, redox-dependent iron movement, domain interface variability, and peroxidase activity in the rubrerythrins, *J Biol Inorg Chem 10*, 407-416.

136. Das, A., Coulter, E. D., Kurtz, D. M., Jr., and Ljungdahl, L. G. (2001) Five-gene cluster in *Clostridium thermoaceticum* consisting of two divergent operons encoding rubredoxin oxidoreductase- rubredoxin and rubrerythrin-type A flavoprotein- high-molecular-weight rubredoxin, *J Bacteriol 183*, 1560-1567.

137. Lumppio, H. L., Shenvi, N. V., Garg, R. P., Summers, A. O., and Kurtz, D. M., Jr. (1997) A rubrerythrin operon and nigerythrin gene in *Desulfovibrio vulgaris* (Hildenborough), *J Bacteriol 179*, 4607-4615.

138. www.ncbi.nlm.nih.gov/.

139. Chen, L., Sharma, P., Le Gall, J., Mariano, A. M., Teixeira, M., and Xavier, A. V. (1994) A blue non-heme iron protein from *Desulfovibrio gigas*, *Eur J Biochem 226*, 613-618.

140. Coelho, A. V., Matias, P ., Fülöp, V. A., Gonzalez, A. Thompson, and Carrondo, M.A. . (1997) Desulfoferrodoxin structure determined by MAD phasing and refinement to 1.9 Å resolution reveals a unique combination of a tetrahedral FeS_4 center with a square pyramidial $FeSN_4$, *J Biol Inorg Chem 2*, 680-689.

141. Yeh, A. P., Hu, Y., Jenney, F. E., Jr., Adams, M. W., and Rees, D. C. (2000) Structures of the superoxide reductase from *Pyrococcus furiosus* in the oxidized and reduced states, *Biochemistry 39*, 2499-2508.

142. Pinto, A. F., Rodrigues, J. V., and Teixeira, M. (2010) Reductive elimination of superoxide: Structure and mechanism of superoxide reductases, *Biochim Biophys Acta 1804*, 285-297.

143. Lucchetti-Miganeh, C., Goudenege, D., Thybert, D., Salbert, G., and Barloy-Hubler, F. (2011) SORGOdb: Superoxide Reductase Gene Ontology curated DataBase, *BMC Microbiol 11*, 105.

144. Pianzzola, M. J., Soubes, M., and Touati, D. (1996) Overproduction of the rbo gene product from Desulfovibrio species suppresses all deleterious effects of lack of superoxide dismutase in *Escherichia coli*, *J Bacteriol 178*, 6736-6742.

145. Lombard, M., Fontecave, M., Touati, D., and Niviere, V. (2000) Reaction of the desulfoferrodoxin from *Desulfoarculus baarsii* with superoxide anion. Evidence for a superoxide reductase activity, *J Biol Chem 275*, 115-121.

146. Jovanovic, T., Ascenso, C., Hazlett, K. R., Sikkink, R., Krebs, C., Litwiller, R., Benson, L. M., Moura, I., Moura, J. J., Radolf, J. D., Huynh, B. H., Naylor, S., and Rusnak, F. (2000) Neelaredoxin, an iron-binding protein from the syphilis spirochete, *Treponema pallidum*, is a superoxide reductase, *J Biol Chem 275*, 28439-28448.

147. Silva, G., LeGall, J., Xavier, A. V., Teixeira, M., and Rodrigues-Pousada, C. (2001) Molecular characterization of *Desulfovibrio gigas* neelaredoxin, a protein involved in oxygen detoxification in anaerobes, *J Bacteriol 183*, 4413-4420.

148. Thompson, J. D., Gibson, T. J., and Higgins, D. G. (2002) Multiple sequence alignment using ClustalW and ClustalX, *Curr Protoc Bioinformatics Chapter 2, Unit 2.3*.

149. Fridovich, I. (1997) Superoxide anion radical ($O_2^{\cdot-}$), superoxide dismutases, and related matters, *J Biol Chem 272*, 18515-18517.

150. Voordouw, J. K., and Voordouw, G. (1998) Deletion of the rbo gene increases the oxygen sensitivity of the sulfate-reducing bacterium *Desulfovibrio vulgaris* Hildenborough, *Appl Environ Microbiol 64*, 2882-2887.

151. Kawasaki, S., Watamura, Y., Ono, M., Watanabe, T., Takeda, K., and Niimura, Y. (2005) Adaptive responses to oxygen stress in obligatory anaerobes *Clostridium acetobutylicum* and *Clostridium aminovalericum*, *Appl Environ Microbiol 71*, 8442-8450.

152. Le Fourn, C., Fardeau, M. L., Ollivier, B., Lojou, E., and Dolla, A. (2008) The hyperthermophilic anaerobe *Thermotoga Maritima* is able to cope with limited amount of oxygen: insights into its defence strategies, *Environ Microbiol 10*, 1877-1887.

153. McHardy, I., Keegan, C., Sim, J. H., Shi, W., and Lux, R. (2010) Transcriptional profiles of *Treponema denticola* in response to environmental conditions, *PLoS One 5*, e13655.

154. Williams, E., Lowe, T. M., Savas, J., and DiRuggiero, J. (2007) Microarray analysis of the hyperthermophilic archaeon *Pyrococcus furiosus* exposed to gamma irradiation, *Extremophiles 11*, 19-29.

155. Zhang, W., Culley, D. E., Hogan, M., Vitiritti, L., and Brockman, F. J. (2006) Oxidative stress and heat-shock responses in *Desulfovibrio vulgaris* by genome-wide transcriptomic analysis, *Antonie Van Leeuwenhoek 90*, 41-55.

156. Tavares, P., Ravi, N., Moura, J. J., LeGall, J., Huang, Y. H., Crouse, B. R., Johnson, M. K., Huynh, B. H., and Moura, I. (1994) Spectroscopic properties of desulfoferrodoxin from *Desulfovibrio desulfuricans* (ATCC 27774), *J Biol Chem 269*, 10504-10510.

157. Clay, M. D., Jenney, F. E., Jr., Hagedoorn, P. L., George, G. N., Adams, M. W., and Johnson, M. K. (2002) Spectroscopic studies of *Pyrococcus furiosus* superoxide reductase: implications for active-site structures and the catalytic mechanism, *J Am Chem Soc 124*, 788-805.

158. Mathe, C., Niviere, V., and Mattioli, T. A. (2005) Fe3+-hydroxide ligation in the superoxide reductase from *Desulfoarculus baarsii* is associated with pH dependent spectral changes, *J Am Chem Soc 127*, 16436-16441.

159. Todorovic, S., Rodrigues, J. V., Pinto, A. F., Thomsen, C., Hildebrandt, P., Teixeira, M., and Murgida, D. H. (2009) Resonance Raman study of the superoxide reductase from *Archaeoglobus fulgidus*, E12 mutants and a 'natural variant', *Phys Chem Chem Phys 11*, 1809-1815.

160. Niviere, V., Asso, M., Weill, C. O., Lombard, M., Guigliarelli, B., Favaudon, V., and Houee-Levin, C. (2004) Superoxide reductase from *Desulfoarculus baarsii*: identification of protonation steps in the enzymatic mechanism, *Biochemistry 43*, 808-818.

161. Berthomieu, C., Dupeyrat, F., Fontecave, M., Vermeglio, A., and Niviere, V. (2002) Redox-dependent structural changes in the superoxide reductase from *Desulfoarculus baarsii* and *Treponema pallidum*: a FTIR study, *Biochemistry 41*, 10360-10368.

162. Rodrigues, J. V., Victor, B. L., Huber, H., Saraiva, L. M., Soares, C. M., Cabelli, D. E., and Teixeira, M. (2008) Superoxide reduction by *Nanoarchaeum equitans* neelaredoxin, an enzyme lacking the highly conserved glutamate iron ligand, *J Biol Inorg Chem 13*, 219-228.

163. Rodrigues, J. V., Abreu, I. A., Cabelli, D., and Teixeira, M. (2006) Superoxide reduction mechanism of *Archaeoglobus fulgidus* one-iron superoxide reductase, *Biochemistry 45*, 9266-9278.

164. Schwarz, H. A. (1981) Free radicals generated by radiolysis of aqueous solutions, *J Chem Educ 58*, 101-105.

165. Mathe, C., Mattioli, T. A., Horner, O., Lombard, M., Latour, J. M., Fontecave, M., and Niviere, V. (2002) Identification of iron(III) peroxo species in the active site of the superoxide reductase SOR from *Desulfoarculus baarsii*, *J Am Chem Soc 124*, 4966-4967.

166. Silaghi-Dumitrescu, R., Silaghi-Dumitrescu, I., Coulter, E. D., and Kurtz, D. M., Jr. (2003) Computational study of the non-heme iron active site in superoxide reductase and its reaction with superoxide, *Inorg Chem 42*, 446-456.

167. Mathe, C., Niviere, V., Houee-Levin, C., and Mattioli, T. A. (2006) Fe(3+)-eta(2)-peroxo species in superoxide reductase from *Treponema pallidum*. Comparison with *Desulfoarculus baarsii*, *Biophys Chem 119*, 38-48.

168. Katona, G., Carpentier, P., Niviere, V., Amara, P., Adam, V., Ohana, J., Tsanov, N., and Bourgeois, D. (2007) Raman-assisted crystallography reveals end-on peroxide intermediates in a nonheme iron enzyme, *Science 316*, 449-453.

169. Brumlik, M. J., and Voordouw, G. (1989) Analysis of the transcriptional unit encoding the genes for rubredoxin (rub) and a putative rubredoxin oxidoreductase (rbo) in *Desulfovibrio vulgaris* Hildenborough, *J Bacteriol 171*, 4996-5004.

170. Emerson, J. P., Coulter, E. D., Phillips, R. S., and Kurtz, D. M., Jr. (2003) Kinetics of the superoxide reductase catalytic cycle, *J Biol Chem 278*, 39662-39668.

171. Rodrigues, J. V., Saraiva, L. M., Abreu, I. A., Teixeira, M., and Cabelli, D. E. (2007) Superoxide reduction by *Archaeoglobus fulgidus* desulfoferrodoxin: comparison with neelaredoxin, *J Biol Inorg Chem 12*, 248-256.

172. Auchere, F., Sikkink, R., Cordas, C., Raleiras, P., Tavares, P., Moura, I., and Moura, J. J. (2004) Overexpression and purification of *Treponema pallidum* rubredoxin; kinetic evidence for a superoxide-mediated electron transfer with the superoxide reductase neelaredoxin, *J Biol Inorg Chem 9*, 839-849.

173. Speed, B., Kaldor, J., and Cavanagh, P. (1984) Guillain-Barre syndrome associated with *Campylobacter jejuni* enteritis, *J Infect 8*, 85-86.

174. Young, K. T., Davis, L. M., and Dirita, V. J. (2007) *Campylobacter jejuni*: molecular biology and pathogenesis, *Nat Rev Microbiol 5*, 665-679.

175. De Wood, P. (2008) Photo by De Wood; digital colorization by Chris Pooley, Agricultural Research Service (ARS) is the U.S. Department of Agriculture's chief scientific research agency.

176. Gundogdu, O., Bentley, S. D., Holden, M. T., Parkhill, J., Dorrell, N., and Wren, B. W. (2007) Re-annotation and re-analysis of the *Campylobacter jejuni* NCTC11168 genome sequence, *BMC Genomics 8*, 162.

177. Parkhill, J., Wren, B. W., Mungall, K., Ketley, J. M., Churcher, C., Basham, D., Chillingworth, T., Davies, R. M., Feltwell, T., Holroyd, S., Jagels, K., Karlyshev, A. V., Moule, S., Pallen, M. J., Penn, C. W., Quail, M. A., Rajandream, M. A., Rutherford, K. M., van Vliet, A. H., Whitehead, S., and Barrell, B. G. (2000) The genome sequence of the food-borne pathogen *Campylobacter jejuni* reveals hypervariable sequences, *Nature 403*, 665-668.

178. Kaakoush, N. O., Miller, W. G., De Reuse, H., and Mendz, G. L. (2007) Oxygen requirement and tolerance of *Campylobacter jejuni*, *Res Microbiol 158*, 644-650.

179. Hodge, J. P., and Krieg, N. R. (1994) Oxygen tolerance estimates in Campylobacter species depend on the testing medium, *J Appl Bacteriol 77*, 666-673.

180. Hoffman, P. S., George, H. A., Krieg, N. R., and Smibert, R. M. (1979) Studies of the microaerophilic nature of *Campylobacter fetus* subsp. jejuni. II. Role of exogenous superoxide anions and hydrogen peroxide, *Can J Microbiol 25*, 8-16.

181. Juven, B. J., and Rosenthal, I. (1985) Effect of free-radical and oxygen scavengers on photochemically generated oxygen toxicity and on the aerotolerance of *Campylobacter jejuni*, *J Appl Bacteriol 59*, 413-419.

182. Smith, M. A., Finel, M., Korolik, V., and Mendz, G. L. (2000) Characteristics of the aerobic respiratory chains of the microaerophiles *Campylobacter jejuni* and *Helicobacter pylori*, *Arch Microbiol 174*, 1-10.

183. Atack, J. M., Harvey, P., Jones, M. A., and Kelly, D. J. (2008) The *Campylobacter jejuni* thiol peroxidases Tpx and Bcp both contribute to aerotolerance and peroxide-mediated stress resistance but have distinct substrate specificities, *J Bacteriol 190*, 5279-5290.

184. Baillon, M. L., van Vliet, A. H., Ketley, J. M., Constantinidou, C., and Penn, C. W. (1999) An iron-regulated alkyl hydroperoxide reductase (AhpC) confers aerotolerance and oxidative stress resistance to the microaerophilic pathogen *Campylobacter jejuni*, *J Bacteriol 181*, 4798-4804.

185. Day, W. A., Jr., Sajecki, J. L., Pitts, T. M., and Joens, L. A. (2000) Role of catalase in *Campylobacter jejuni* intracellular survival, *Infect Immun 68*, 6337-6345.

186. Purdy, D., and Park, S. F. (1994) Cloning, nucleotide sequence and characterization of a gene encoding superoxide dismutase from *Campylobacter jejuni* and *Campylobacter coli*, *Microbiology 140 (Pt 5)*, 1203-1208.

187. van Vliet, A. H., Baillon, M. A., Penn, C. W., and Ketley, J. M. (2001) The iron-induced ferredoxin FdxA of *Campylobacter jejuni* is involved in aerotolerance, *FEMS Microbiol Lett 196*, 189-193.

188. Wainwright, L. M., Elvers, K. T., Park, S. F., and Poole, R. K. (2005) A truncated haemoglobin implicated in oxygen metabolism by the microaerophilic food-borne pathogen *Campylobacter jejuni*, *Microbiology 151*, 4079-4091.

189. Holmes, K., Mulholland, F., Pearson, B. M., Pin, C., McNicholl-Kennedy, J., Ketley, J. M., and Wells, J. M. (2005) *Campylobacter*

jejuni gene expression in response to iron limitation and the role of Fur, *Microbiology 151*, 243-257.

190. Palyada, K., Threadgill, D., and Stintzi, A. (2004) Iron acquisition and regulation in *Campylobacter jejuni*, *J Bacteriol 186*, 4714-4729.
191. van Vliet, A. H., Wooldridge, K. G., and Ketley, J. M. (1998) Iron-responsive gene regulation in a *Campylobacter jejuni* fur mutant, *J Bacteriol 180*, 5291-5298.
192. Ridley, K. A., Rock, J. D., Li, Y., and Ketley, J. M. (2006) Heme utilization in *Campylobacter jejuni*, *J Bacteriol 188*, 7862-7875.
193. Stetter, K. O. (2006) Hyperthermophiles in the history of life, *Philos Trans R Soc Lond B Biol Sci 361*, 1837-1842.
194. Takai, K., Nakamura, K., Toki, T., Tsunogai, U., Miyazaki, M., Miyazaki, J., Hirayama, H., Nakagawa, S., Nunoura, T., and Horikoshi, K. (2008) Cell proliferation at 122 degrees C and isotopically heavy CH_4 production by a hyperthermophilic methanogen under high-pressure cultivation, *Proc Natl Acad Sci U S A 105*, 10949-10954.
195. Paper, W., Jahn, U., Hohn, M. J., Kronner, M., Nather, D. J., Burghardt, T., Rachel, R., Stetter, K. O., and Huber, H. (2007) *Ignicoccus hospitalis* sp. nov., the host of '*Nanoarchaeum equitans*', *Int J Syst Evol Microbiol 57*, 803-808.
196. König, H., R. Rachel, and H. Claus (2007) *Proteinaceous surface layers of Archaea: ultrastructure and biochemistry*, ASM Press, Washington, DC.
197. Junglas, B., Briegel, A., Burghardt, T., Walther, P., Wirth, R., Huber, H., and Rachel, R. (2008) *Ignicoccus hospitalis* and *Nanoarchaeum equitans*: ultrastructure, cell-cell interaction, and 3D reconstruction from serial sections of freeze-substituted cells and by electron cryotomography, *Arch Microbiol 190*, 395-408.
198. Jahn, U., Gallenberger, M., Paper, W., Junglas, B., Eisenreich, W., Stetter, K. O., Rachel, R., and Huber, H. (2008) *Nanoarchaeum equitans* and *Ignicoccus hospitalis*: new insights into a unique, intimate association of two archaea, *J Bacteriol 190*, 1743-1750.
199. Giannone, R. J., Huber, H., Karpinets, T., Heimerl, T., Kuper, U., Rachel, R., Keller, M., Hettich, R. L., and Podar, M. (2011) Proteomic characterization of cellular and molecular processes that enable the

Nanoarchaeum equitans--Ignicoccus hospitalis relationship, *PLoS One 6*, e22942.

200. Poly, F., and Guerry, P. (2008) Pathogenesis of Campylobacter, *Curr Opin Gastroenterol 24*, 27-31.

201. Bury-Mone, S., Kaakoush, N. O., Asencio, C., Megraud, F., Thibonnier, M., De Reuse, H., and Mendz, G. L. (2006) Is *Helicobacter pylori* a true microaerophile?, *Helicobacter 11*, 296-303.

202. Fernie, D. S., and Park, R. W. (1977) The isolation and nature of campylobacters (microaerophilic vibrios) from laboratory and wild rodents, *J Med Microbiol 10*, 325-329.

203. Weingarten, R. A., Grimes, J. L., and Olson, J. W. (2008) Role of *Campylobacter jejuni* respiratory oxidases and reductases in host colonization, *Appl Environ Microbiol 74*, 1367-1375.

204. Jackson, R. J., Elvers, K. T., Lee, L. J., Gidley, M. D., Wainwright, L. M., Lightfoot, J., Park, S. F., and Poole, R. K. (2007) Oxygen reactivity of both respiratory oxidases in *Campylobacter jejuni*: the cydAB genes encode a cyanide-resistant, low-affinity oxidase that is not of the cytochrome bd type, *J Bacteriol 189*, 1604-1615.

205. Purdy, D., and Park, S. F. (1994) Cloning, nucleotide sequence and characterization of a gene encoding superoxide dismutase from *Campylobacter jejuni* and *Campylobacter coli*, *Microbiology 140* 1203-1208.

206. Pesci, E. C., Cottle, D. L., and Pickett, C. L. (1994) Genetic, enzymatic, and pathogenic studies of the iron superoxide dismutase of *Campylobacter jejuni*, *Infect Immun 62*, 2687-2694.

207. Palyada, K., Sun, Y. Q., Flint, A., Butcher, J., Naikare, H., and Stintzi, A. (2009) Characterization of the oxidative stress stimulon and PerR regulon of *Campylobacter jejuni, BMC Genomics 10*, 481.

208. Pinto, A. F., Rodrigues, J. V., and Teixeira, M. (2009) Reductive elimination of superoxide: Structure and mechanism of superoxide reductases, *Biochim Biophys Acta 1804*, 285-297.

209. Klippenstein, G. L., Holleman, J. W., and Klotz, I. M. (1968) The primary structure of *Golfingia gouldii* hemerythrin. Oder of peptides in fragments produced by tryptic digestion of succinylated hemerythrin. Complete amino acid sequence, *Biochemistry 7*, 3868-3878.

210. http://www.neb.com/nebecomm/products/productE8000.asp.

211. Laemmli, U. K. (1970) Cleavage of structural proteins during the assembly of the head of bacteriophage T4, *Nature 227*, 680-685.

212. Smith, P. K., Krohn, R. I., Hermanson, G. T., Mallia, A. K., Gartner, F. H., Provenzano, M. D., Fujimoto, E. K., Goeke, N. M., Olson, B. J., and Klenk, D. C. (1985) Measurement of protein using bicinchoninic acid, *Anal Biochem 150*, 76-85.

213. Fischer, D. S., and Price, D. C. (1964) A Simple Serum Iron Method Using the New Sensitive Chromogen Tripyridyl-S-Triazine, *Clin Chem 10*, 21-31.

214. Nicholas, K. B., and Nicholas, Hugh B. Jr. (1997) GeneDoc: Analysis and Visualization of genetic variation, *EMB New 4*, 14.

215. Gomes, C. M., Giuffre, A., Forte, E., Vicente, J. B., Saraiva, L. M., Brunori, M., and Teixeira, M. (2002) A novel type of nitric-oxide reductase. *Escherichia coli* flavorubredoxin, *J Biol Chem 277*, 25273-25276.

216. Gupta, N., Bonomi, F., Kurtz, D. M., Jr., Ravi, N., Wang, D. L., and Huynh, B. H. (1995) Recombinant *Desulfovibrio vulgaris* rubrerythrin. Isolation and characterization of the diiron domain, *Biochemistry 34*, 3310-3318.

217. Dave, B. C., Czernuszewicz, R. S., Prickril, B. C., and Kurtz, D. M., Jr. (1994) Resonance Raman spectroscopic evidence for the FeS_4 and Fe-O-Fe sites in rubrerythrin from *Desulfovibrio vulgaris*, *Biochemistry 33*, 3572-3576.

218. Kurtz, D. M. (1990) Oxo- and hydroxo-bridged diiron complexes: a chemical perspective on a biological unit, *Chem. Rev. 90*, 585-606.

219. Fox, B. G., Shanklin, J., Ai, J., Loehr, T. M., and Sanders-Loehr, J. (1994) Resonance Raman evidence for an Fe-O-Fe center in stearoyl-ACP desaturase. Primary sequence identity with other diiron-oxo proteins, *Biochemistry 33*, 12776-12786.

220. Sanders-Loehr, J., Wheeler, W. D., Shiemke, A. K., Averill, B. A., and Loehr, T. M. (1989) Electronic and Raman spectroscopic properties of oxo-bridged dinuclear iron centers in proteins and model compounds, *J. Am. Chem. Soc. 111*, 8084-8093.

221. Ravi, N., Prickril, B. C., Kurtz, D. M., Jr., and Huynh, B. H. (1993) Spectroscopic characterization of ^{57}Fe-reconstituted rubrerythrin, a

non-heme iron protein with structural analogies to ribonucleotide reductase, *Biochemistry 32*, 8487-8491.

222. Shiemke, A. K., Loehr, T.M., Sanders-Loehr, J. (1986) Resonance Raman study of oxyhemerythrin and hydroxyhemerythrin. Evidence for hydrogen bonding of ligands to the Fe-O-Fe center., *J Am Chem Soc 108*, 2437-2443.

223. Todorovic, S., Justino, M. C., Wellenreuther, G., Hildebrandt, P., Murgida, D. H., Meyer-Klaucke, W., and Saraiva, L. M. (2008) Iron-sulfur repair YtfE protein from *Escherichia coli*: structural characterization of the di-iron center, *J Biol Inorg Chem 13*, 765-770.

224. Maralikova, B., Ali, V., Nakada-Tsukui, K., Nozaki, T., van der Giezen, M., Henze, K., and Tovar, J. (2010) Bacterial-type oxygen detoxification and iron-sulfur cluster assembly in amoebal relict mitochondria, *Cell Microbiol 12*, 331-342.

225. Luo, Y., Ergenekan, C. E., Fischer, J. T., Tan, M. L., and Ichiye, T. The molecular determinants of the increased reduction potential of the rubredoxin domain of rubrerythrin relative to rubredoxin, *Biophys J 98*, 560-568.

226. Kabsch, W. (1993) Automatic processing of rotation diffraction data from crystals of initially unknown symmetry and cell constants. , *J. Appl. Cryst. 26*, 795-800.

227. Collaborative Computational Project. (1994) The CCP4 suite: programs for protein crystallography., *Acta Crystallogr D Biol Crystallogr 50*, 760-763.

228. Perrakis, A., Morris, R., and Lamzin, V. S. (1999) Automated protein model building combined with iterative structure refinement. , *Nat Struct Biol 6*, 458-463.

229. Murshudov, G. N., Vagin, A. A., and Dodson, E. J. (1997) Refinement of macromolecular structures by the maximum-likelihood method, *Acta Crystallogr D Biol Crystallogr D 53*, 240-255.

230. Emsley, P., and Cowtan, K. (2004) Coot: model-building tools for molecular graphics., *Acta Crystallogr D Biol Crystallogr 60*, 2126-2132.

231. Laskowski, R. A., MacArthur, M.W., Moss, D.S., Thornton, J.M. (1993) PROCHECK: a program to check the stereochemical quality of protein structures, *J Appl Cryst 26*, 283-291.

232. Goto, J. J., Gralla, E. B., Valentine, J. S., and Cabelli, D. E. (1998) Reactions of hydrogen peroxide with familial amyotrophic lateral sclerosis mutant human copper-zinc superoxide dismutases studied by pulse radiolysis, *J Biol Chem 273*, 30104-30109.

233. Buxton, G. U., Greenstock, C.L., Helman, W.P., and Ross, A.B. (1988) Critical review of rate constant for reactions of hydrated electrons, hydrogen atoms and hydroxyl radicals ($HO^{\cdot}/O^{\cdot-}$) in aqueous solution, *J Phys Chem 17*, 513-759.

234. Emerson, J. P., Coulter, E. D., Cabelli, D. E., Phillips, R. S., and Kurtz, D. M., Jr. (2002) Kinetics and mechanism of superoxide reduction by two-iron superoxide reductase from *Desulfovibrio vulgaris*, *Biochemistry 41*, 4348-4357.

235. Abreu, I. A., Saraiva, L. M., Carita, J., Huber, H., Stetter, K. O., Cabelli, D., and Teixeira, M. (2000) Oxygen detoxification in the strict anaerobic archaeon *Archaeoglobus fulgidus*: superoxide scavenging by neelaredoxin, *Mol Microbiol 38*, 322-334.

236. Horner, O., Mouesca, J. M., Oddou, J. L., Jeandey, C., Niviere, V., Mattioli, T. A., Mathe, C., Fontecave, M., Maldivi, P., Bonville, P., Halfen, J. A., and Latour, J. M. (2004) Mossbauer characterization of an unusual high-spin side-on peroxo-Fe^{3+} species in the active site of superoxide reductase from *Desulfoarculus baarsii*. Density functional calculations on related models, *Biochemistry 43*, 8815-8825.

237. Bonnot, F., Molle, T., Menage, S., Moreau, Y., Duval, S., Favaudon, V., Houee-Levin, C., and Niviere, V. (2012) Control of the evolution of iron peroxide intermediate in superoxide reductase from *Desulfoarculus baarsii*. Involvement of lysine 48 in protonation, *J Am Chem Soc 134*, 5120-5130.

238. Lombard, M., Houee-Levin, C., Touati, D., Fontecave, M., and Niviere, V. (2001) Superoxide reductase from *Desulfoarculus baarsii*: reaction mechanism and role of glutamate 47 and lysine 48 in catalysis, *Biochemistry 40*, 5032-5040.

239. Bonnot, F., Houee-Levin, C., Favaudon, V., and Niviere, V. (2010) Photochemical processes observed during the reaction of superoxide reductase from *Desulfoarculus baarsii* with superoxide: re-evaluation of the reaction mechanism, *Biochim Biophys Acta 1804*, 762-767.

240. Ausubel, F. M., Brent, R., Kingston, R. E., Moore, D. D., Seidman, J. G., Smith, J. A., and Struhl, K. (1995) *Current Protocols in Molecular Biology*, Greene Publishing Associates and Wiley-Interscience, New York.

241. Pinho, F. G., Romao, C. V., Pinto, A. F., Saraiva, L. M., Huber, H., Matias, P. M., Teixeira, M., and Bandeiras, T. M. (2010) Cloning, purification, crystallization and X-ray crystallographic analysis of *Ignicoccus hospitalis* neelaredoxin, *Acta Crystallogr Sect F Struct Biol Cryst Commun 66*, 605-607.

242. McCoy, A. J., Grosse-Kunstleve, R. W., Storoni, L. C., and Read, R.J. . (2005) Likelihood-enhanced fast translation functions, *Acta Cryst D 61*, 458-464.

243. Adams, P. D., Afonine, P. V., Bunkóczi,G., Chen,V. B., Davis, I. W., Echols, N., Headd, J. J., Hung, L.W., Kapral, G. J., Grosse-Kunstleve, R. W.,McCoy, A. J., Moriarty, N. W., Oeffner, R., Read, R. J., Richardson, D. C., Richardson, J. S.,Terwilliger, T. C., and Zwart, P. H. (2010) PHENIX: a comprehensive Python-based system for macromolecular structure solution, *Acta Cryst D 66*, 213-221.

244. Pinho, F. G., Pinto, A. F., Pinto, L. C., Huber, H., Romao, C. V., Teixeira, M., Matias, P. M., and Bandeiras, T. M. (2011) Superoxide reductase from *Nanoarchaeum equitans*: expression, purification, crystallization and preliminary X-ray crystallographic analysis, *Acta Crystallogr Sect F Struct Biol Cryst Commun 67*, 591-595.

245. Pinto, A. F., Rodrigues, J. V., and Teixeira, M. (2009) Reductive elimination of superoxide: Structure and mechanism of superoxide reductases, *Biochim Biophys Acta*.

246. Andrews, S. C. (1998) Iron storage in bacteria, *Adv Microb Physiol 40*, 281-351.

247. Sato, Y., Kameya, M., Fushinobu, S., Wakagi, T., Arai, H., Ishii, M., and Igarashi, Y. (2012) A novel enzymatic system against oxidative stress in the thermophilic hydrogen-oxidizing bacterium *Hydrogenobacter thermophilus*, *PLoS One 7*, e34825.

248. http://taxonomy.zoology.gla.ac.uk/rod/treeview.html.

249. Liu, Y., and Eisenberg, D. (2002) 3D domain swapping: as domains continue to swap, *Protein Sci 11*, 1285-1299.

250. Fournier, M., Zhang, Y., Wildschut, J. D., Dolla, A., Voordouw, J. K., Schriemer, D. C., and Voordouw, G. (2003) Function of oxygen resistance proteins in the anaerobic, sulfate-reducing bacterium *Desulfovibrio vulgaris* hildenborough, *J Bacteriol 185*, 71-79.

251. Zhao, W., Ye, Z., and Zhao, J. (2007) RbrA, a cyanobacterial rubrerythrin, functions as a FNR-dependent peroxidase in heterocysts in protection of nitrogenase from damage by hydrogen peroxide in *Anabaena sp.* PCC 7120, *Mol Microbiol 66*, 1219-1230.

252. Santos-Silva, T., Trincao, J., Carvalho, A. L., Bonifacio, C., Auchere, F., Raleiras, P., Moura, I., Moura, J. J., and Romao, M. J. (2006) The first crystal structure of class III superoxide reductase from *Treponema pallidum*, *J Biol Inorg Chem 11*, 548-558.

253. Kratzer, C., Welte, C., Dorner, K., Friedrich, T., and Deppenmeier, U. (2011) Methanoferrodoxin represents a new class of superoxide reductase containing an iron-sulfur cluster, *FEBS J 278*, 442-451.

254. Niviere, V., Lombard, M., Fontecave, M., and Houee-Levin, C. (2001) Pulse radiolysis studies on superoxide reductase from *Treponema pallidum*, *FEBS Lett 497*, 171-173.

255. Seaver, L. C., and Imlay, J. A. (2001) Alkyl hydroperoxide reductase is the primary scavenger of endogenous hydrogen peroxide in *Escherichia coli*, *J Bacteriol 183*, 7173-7181.

256. Lin, S. J., and Guarente, L. (2003) Nicotinamide adenine dinucleotide, a metabolic regulator of transcription, longevity and disease, *Curr Opin Cell Biol 15*, 241-246.